Characterization of Synphilin-1/alpha-Synuclein Double Transgenic Mice

Dissertation

zur Erlangung des Grades eines
Doktors der Naturwissenschaften

der Mathematisch-Naturwissenschaftlichen Fakultät
und
der Medizinischen Fakultät
der Eberhard-Karls-Universität Tübingen

vorgelegt
von

Nicolas Casadei
aus Belfort , Frankreich

07-2014

Tag der mündlichen Prüfung: 09 Oktober 2014

Dekan der Math.-Nat. Fakultät: Prof. Dr. W. Rosenstiel
Dekan der Medizinischen Fakultät: Prof. Dr. I. B. Autenrieth

1. Berichterstatter: Prof. Dr. O. Riess
2. Berichterstatter: Prof. Dr. R Krüger

Prüfungskommission: Prof. Dr. D. Berg
                                     Prof. Dr. P. Kahle

I hereby declare that I have produced the work entitled: "*Characterization of Synphilin-1/alpha-Synuclein Double Transgenic Mice*",

submitted for the award of a doctorate, on my own (without external help), have used only the sources and aids indicated and have marked passages included from other works, whether verbatim or in content, as such. I swear upon oath that these **statements** are true and that I have not concealed anything. I am aware that making a false declaration under oath is punishable by a term of imprisonment of up to three years or by a fine.

Tübingen,   09th October 2014

Date   **Signature**

"We are beginning to understand aging, not as a single inexorable progression but as a group of related processes. Strategies are emerging for fully reversing each of these aging progressions, using different combinations of biotechnology techniques." — Ray Kurzweil

Table of Contents

Abstract

Parkinson's disease (PD) is a sporadic and progressive neurodegenerative disease characterized by dopaminergic neuronal cell death in the substantia nigra pars compacta and by the presence of characteristic Lewy bodies (LB) and Lewy neuritic (LN) inclusions. These inclusions are mainly constituted of the alpha-synuclein (a-syn) protein, suggesting a role of a-syn in the neuropathophysiology of PD. Synphilin-1 (sph1) is described as an interacting partner of a-syn, present in LBs and sharing the same intracellular compartments as a-syn. Sph1 was shown to induce the formation of a-syn positive inclusions *in vivo* and *in vitro* as well as to promote clearance of protein inclusions by autophagy. But the impact of sph1 in a-syn-mediated toxicity is inconsistent, presumably due to the variety of models used to model synucleinopathy, the variety of toxicity markers analyzed and the poor description of aggregates found in these studies. Furthermore, the normal function of sph1 needs still to be explored.

The overall aim of this study is to characterize the effects of sph1 on a-syn aggregation and on the development of synucleinopathy *in vivo*. Therefore, we cross-bred mice overexpressing the human sph1 under the mouse PrP promoter with a synucleinopathy mouse model overexpressing the human A30P mutated a-syn under the Thy-1 promoter.

Using different fractionation protocols of brain lysates, we did not observe in mice coexpressing sph1 an increased amount of soluble a-syn nor detergent-insoluble a-syn. At the histological level, we observed that the coexpression of sph1 drastically decreased levels of proteinase K resistant a-syn inclusions as well as thioflavin S positive structures. These changes were accompanied by the formation of aggresome-like structures positive for a-syn, K63 polyubiquitinated proteins and gamma-tubulin in double transgenic animals. We also observed in double transgenic mice a reduced neuropathology reflected by a decreased neuroinflammation and suggesting a protective role of sph1 in synucleinopathy.

Accordingly, we demonstrated that sph1 reduces the accumulation of soluble full-length and truncated species of a-syn with aging. Similarly, we also shown that sph1 decreases levels of fibrillar forms of a-syn. Moreover, we also reported increased levels of ubiquitinated proteins in double transgenic mice without measuring an impairment of the ubiquitin-proteasome system activity. Interestingly, we observed an increased autophagic flux in double transgenic mice, suggesting a possible role of the autophagy-lysosome pathway in the reduction of a-syn species.

We tracked the evolution of neuropathology and associated behavioral alterations over 18 months. We found that sph1 coexpression in transgenic mice overexpressing the human mutated A30P alpha-synuclein led to a delayed motor phenotype in rotarod when compared to single transgenic mice overexpressing A30P a-syn. A motor phenotype was also observed in single transgenic sph1 mice when using challenging beam walk. Interestingly, mouse gait analysis suggested a different origin in motor impairment in sph1 and A30P single transgenic mice.

Introduction

1) *Parkinson´s disease*

Parkinson's disease (PD) was described possibly for the first time under the name of Kampavata in the ancient Indian medical text (5000 B.C.) (Stern 1989). PD was also reported in the first Chinese medical text (Nei Jing Chinese medicine 500 B.C.) (Zheng 2009). During the ancient Rome, the Greek physician Galen (129-200) also described symptoms related to PD [tremors of the hand at rest, exhibited tremor and decline in control motion of limbs with aging] (Stern 1989). Nevertheless, the first description of all four cardinal signs [tremor, bradykinesia, rigor, and postural instability] was made by the Hungarian doctor Ferenc Pápai Páriz in 1690 in his medical text Pax Corporis (Bereczki 2010).

During modern time, James Parkinson reported a medical condition termed "shaking palsy" observed in six patients presenting most of the typical clinical features of PD (Parkinson 1817). This description was completed later in the nineteenth century by the French physician Jean-Martin Charcot which fully detailed the PD symptoms (Charcot 1877) [Historical description of PD reviewed in (Pearce 1989; Goetz 2011)].

2) *Epidemiology*

Despite numerous epidemiological studies, a high variation exists on the prevalence and incidence of PD (Muangpaisan et al. 2011) probably due to difficulties of diagnostic criteria, methodology or population studied.

It is commonly accepted that the incidence and prevalence of PD is increasing with aging, affecting approximately 1% of the population older than 60 years and 0.3% of the general population [reviewed in (de Lau & Breteler 2006; Hirtz et al. 2007; Driver et al. 2009)]. Although PD is not a primary or direct cause of death (Phillips et al. 1999), life expectancy (Driver et al. 2008; Forsaa et al. 2010) and quality of life are decreased in PD [reviewed in (Welsh 2004)].

2.1 Clinical features

Clinical symptoms of PD are dominated by four cardinal motor signs: 1) tremor at rest, 2) rigidity (permanently increased muscle tone), 3) bradykinesia (slowness of movement), and 4) postural instability. However, these manifestations of the disease are also accompanied by the presence of non-motor symptoms which can be present before diagnosis and which emerge with disease progression. Treatment side effects could also be observed in some patients. These symptoms (Table 1-01) could be categorized under four main classes: neuropsychiatric, autonomic, sensory, and sleep disorders [reviewed in (Chaudhuri et al. 2006; Chaudhuri & Odin 2010; Lyons & Pahwa 2011)].

| Introduction

Lack of diagnostic tests, and especially of reliable biomarkers, is making diagnosis of PD relying on clinical observation. In this context, the clinical diagnosis of PD is based on the combination of motor signs including bradykinesia, rigidity, tremor, or postural instability [reviewed in (Jankovic 2008; Reichmann 2010)]. Dopamine replacement therapy, which is well known to improve motor symptoms, may be used to confirm PD diagnosis (D'Costa et al. 1995). Most recent advancement in neuroimaging, and especially in diffusion-weighted magnetic resonance imaging, ultrasonography and radiotracer-based imaging, could also be used to confirm and to follow the degeneration of the nigrostriatal and basal ganglia systems [reviewed in (Piccini & Brooks 2006)].

Table 1-01: Symptoms of Parkinson's disease

Table adapted from (Chaudhuri et al. 2006)

Neuropsychiatric disorders	Autonomic disorders
Depression, apathy, anhedonia	Urinary dysfunction
Anxiety	Constipation, fecal incontinence
Impulse behavior	Dysphagia, drooling
Cognitive impairment	Orthostatic hypotension
Attention deficit	Nausea, vomiting
Dementia, delirium, confusion	Sexual dysfunction

Sleep disorders	Sensory disorders
Insomnia	Pain / paresthesia
Fragmented sleep	Olfactory deficit
Excessive daytime sleepiness	Taste deficit
Vivid dreaming	

2.2 Etiology

PD is a neurodegenerative disorder with no identifiable cause. The definition of PD does not include parkinsonism, a nomenclature used for syndromes where the etiology is known. This includes parkinsonian signs due to stroke, infection, neuroleptic drugs, and toxic agents. Parkinsonism also includes signs from other neurodegenerative disorders, such as multiple system atrophy, progressive supranuclear palsy, and nigrostriatal degeneration.

Numerous etiologic studies pointed out possible genetic and environmental components on the risk to developing PD [reviewed in (Wirdefeldt et al. 2011; Noyce et al. 2012)]. Aging, gender, and family history are the strongest risk factors associated with PD diagnosis. Further risk factors correlated with PD and putative premotor symptoms are summarized in table 1-02.

Table 1-02: Risk factors of Parkinson's disease

Table adapted from (Noyce et al. 2012)

Positive correlation	Negative correlation
Age	Coffee drinking, smoking, alcohol
Gender	Anti-inflammatory drugs
Family history of Parkinson's disease	Exercise
Head injury	Cholesterol, use of statins
Rural living, pesticide exposure	Hormonal therapy, oral contraceptive
Metal/solvent exposure	Calcium channel blockers
Depression, constipation, anxiety	Hypertension
Beta-blockers	Gastric ulcers
	Acetaminophen/paracetamol

2.3 Neuropathology

2.3.1 Loss of dopaminergic neurons and related lesion pattern

PD is characterize at the histological level by a severe loss of A9 dopaminergic pigmented neurons in the substantia nigra, leading to a pale appearance of this region when compared with healthy controls could be observed. The loss of pigmented neurons in the substantia nigra was already reported in the 1920s in brains of patients affected with PD [reviewed in (Goetz 2011)]. It was estimated that at the onset of symptoms 60% of the nigral dopaminergic neurons were lost (Pakkenberg et al. 1991) and can increase up to 94% in latest stages (Damier et al. 1999).

The substantia nigra is a layer of large pigmented nerve cells located in the midbrain (mesencephalon) and playing a critical role on the motor system control of the basal ganglia (Hodge & Butcher 1980) [represented in Fig. 1-01 and reviewed in (Bergman & Deuschl 2002; Groenewegen 2003; Santens et al. 2003)]. Loss of these neurons leads to an increased inhibition of the thalamocortical projection and impairs balancing between direct excitation and indirect inhibition pathways of cortex inducing an abnormal activation of upper motor neurons in the motor cortex and subsequently reducing excitation of cortical motor areas.

Dopaminergic neuronal cell loss in the substantia nigra is reported to be the central pathology in PD. In addition to the loss of the nigrostriatal dopaminergic neurons, a variety of other neuronal systems (such as a mild degeneration of the cholinergic, noradrenergic, and serotonergic systems) are also known to be affected in several brain regions including brainstem, olfactory bulb, cerebral cortex, spinal cord, or peripheral autonomic system of patients (Jellinger 1991; Forno 1996; Braak et al. 2003). Degeneration of these centers may lead to diverse clinical symptoms of PD including depression, constipation, rapid eye movement behavior sleep disorder, cognitive, and affective changes.

Direct pathway / Indirect pathway

Cortex

Glu / Glu

SNc — Striatum — SNc
DA — ACh — ACh — DA

GABA, Enk

GPe — GABA

GABA, SP

STN

Glu

GPi SNr — GPi SNr

GABA / GABA

Thalamus (VA, VL)

Glu / Glu

To cortical motor areas
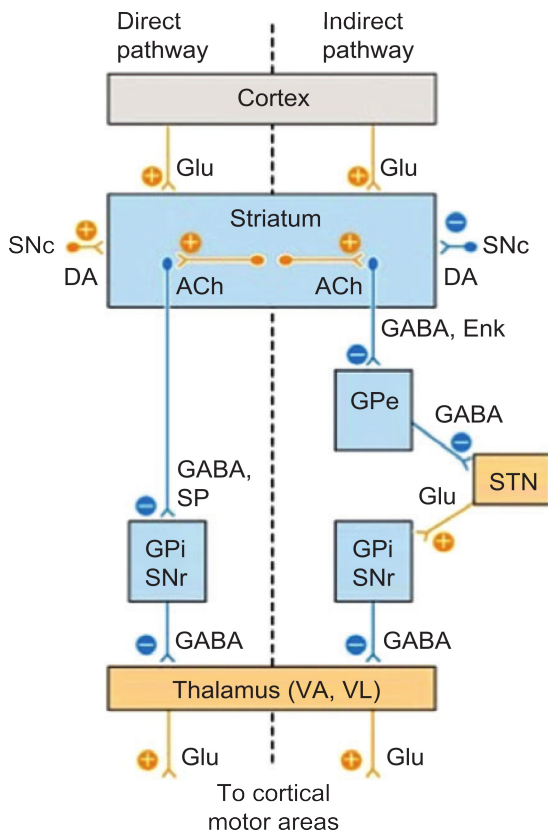
Figure 1-01: Architecture of the basal ganglia

Figure copied from (Leisman & Melillo 2013)

The motor system control of the basal ganglia is extensively interconnected to subcortical structures such as the striatum [composed of the putamen and the caudate nucleus], the globus pallidus [composed of the internal and external segment], the subthalamic nucleus and the substantia nigra [composed of the pars compacta and the pars reticulata]. Main inputs of the basal ganglia are the glutamatergic projection of the cerebral cortex neurons [including sensory, motor, association, and limbic areas] to the striatum and the dopaminergic projection of the substantia nigra pars compacta (SNc). Striatum projects then direct and indirect inhibitory GABAergic output signals to the globus pallidus internal, to the substantia nigra reticulata complex (GPi/SNr) and to the globus pallidus external (GPe). The direct pathway involves the inhibition of the GPi/SNr GABAergic neuron projection onto the thalamus and reducing the inhibition of the thalamus. This disinhibition of the thalamus promotes excitatory outputs to the cortex, to the brain stem and to the muscle fibers via projection of glutamatergic neurons. The indirect pathway involves the inhibition of the GPe GABAergic neurons projection to the subthalamic nucleus (STN) and reduces the inhibition of the STN. The disinhibition of the STN promotes the inhibitory outputs of the GPi/SNr complex to the thalamus via GABAergic neurons. This inhibition of the thalamus decreases the excitatory outputs to the cortex, to the brainstem results in a reduced muscle activity. ACh, acetylcholine; DA, dopamine; Glu, glutamate; Enk, enkaphalin; SP, substance P.; SNc, substantia nigra pars compacta; GPe, globus pallidus pars externa; VL, ventrallateral nucleus; VA, ventral anterior nucleus.

2.3.2   *Lewy bodies and Lewy neurites*

Lewy bodies (LBs) were first described by Friedrich Heinrich Lewy a century ago in brains of PD patients (Lewy 1913; Lewy 1921) in which atrophic cells with fibrillar changes and cellular loss were described mainly in the nucleus basalis [discovery of LB reviewed in (Holdorff 2002)]. Lewy neurites can also be detected in axons of affected neurons. A large variety of neurons are vulnerable to LBs as monoaminergic neurons (in the substantia nigra pars compacta and the locus coeruleus) or cholinergic neurons (in the basal forebrain, dorsal raphe, and subpeduncular nuclei of the pons). LBs are also common in hypothalamus (posterior and lateral), brainstem reticular formation, olfactory bulb, and spinal cord (neurons of the intermediolateral cell). Interestingly, some regions do not develop LBs such as the basal ganglia, thalamus, pontine basis, or cerebellar cortex [reviewed in (Braak et al. 2004)].

LBs are circular intracytoplasmic inclusions, 8–30 nm in diameter, observable using hematoxylin and eosin staining. Two major components can be distinguished: a granular dense core of protein and a clearer peripheral halo of large filaments radially oriented (Duffy & Tennyson 1965). At the ultrastructural level, LBs as composed of a 7–20 nm large central core containing densely packed filaments and of dense granular material at the periphery surrounded by 10 nm filaments radially arranged (Roy & Wolman 1969).

Lewy neurites (LNs) are elongated neuronal processes presenting various structures commonly regrouped under a thick and rounded form or under an elongated thread-like structures (Braak et al. 1999; Kanazawa et al. 2008). In the earlier forms of the disease, LNs could be observed before LBs in the medulla oblongata and in the olfactory bulb, suggesting an early aberrant neuritic pathology preceding the formation of LBs (Braak et al. 2003).

LBs are constituted of a mixture of lipids, neurofilaments and proteins [(Goldman et al. 1983), reviewed in (Licker et al. 2009)]. In the large variety of proteins present in LBs, ubiquitin (Kuzuhara et al. 1988; Lennox et al. 1989) and alpha-synuclein (a-syn) (Spillantini et al. 1998) are constituting the major protein components. Other protein subgroups can be distinguished such as structural elements, a-syn binding partners, ubiquitin-proteasome system components, cellular response proteins, phosphorylation and signal transduction proteins, cytoskeletal proteins, cell cycle proteins and cytosolic proteins that passively diffuse into LBs. The exact link between a-syn and these complex inclusions is unclear, but based on a-syn immunohistochemistry, a model of LB formation involving five successive stages of complex aggregation (Fig. 1-02) was proposed (Wakabayashi et al. 2007).
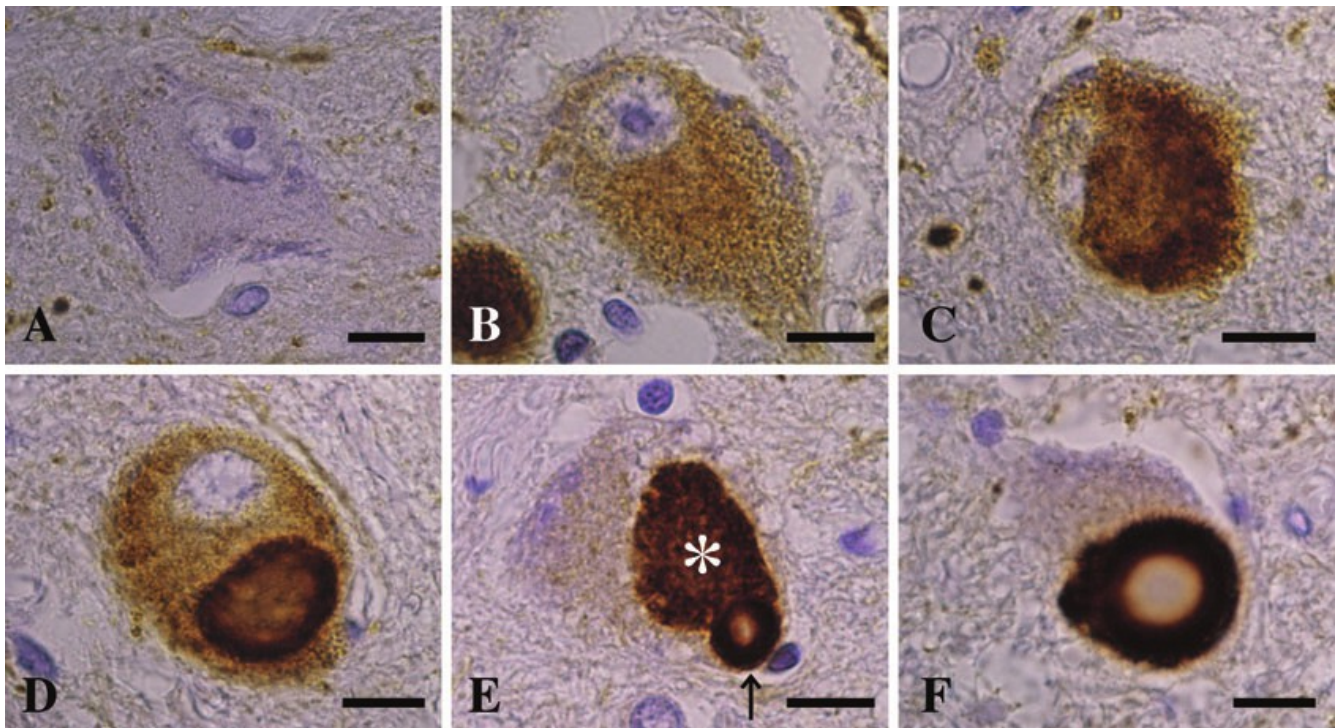
Figure 1-02: Lewy bodies formation

Figure copied from (Wakabayashi et al. 2007)

Immunohistology of LBs at different maturation stages in the substantia nigra using a-syn antibody. **A)** *No a-syn could be normally observed under normal conditions in neuronal cytoplasm.* **B)** *Stage 1: diffuse, pale cytoplasmic staining.* **C)** *Stage 2: irregularly shaped and uneven staining of moderate intensity.* **D)** *Stage 3: pale body, displaying peripheral condensation.* **E)** *Stage 4: one or more small LBs occasionally located within the periphery of pale bodies and developing into typical LBs.* **F)** *Stage 5: LB, composed of ring-like staining presenting a central core and a surrounding halo; scale-bar=10 µm.*

In this classification, healthy neurons do not present cytoplasmic a-syn staining. Neurons containing pale a-syn cytoplasmic staining, considered to start protein accumulation, are regrouped under the first stage of LB formation. Neurons presenting both a moderate a-syn staining intensity and showing an irregular shape are grouped on the stage 2 of LB formation. In the stage 3, peripheral condensations can be observed in neurons and are termed pale bodies. Neurons displaying both pale bodies and containing at their periphery one or several small LBs are considered as stage 4. During the final stage, pale bodies disappear and leave a donuts-shaped structure.

The biological significance of these cytoplasmic inclusions and especially the toxicity of LBs is still actively debated. They have been considered to be toxic, protective or even innocuous [reviewed in (Hartmann 2004; Shults 2006)]. LBs are usually found in brain regions with high neuronal cell loss suggesting their involvement in neuronal cell loss (Braak et al. 2004). Supporting these results, it was shown that LBs retain iron and promote oxidative stress (Castellani et al. 2000). It is also likely that LBs, via space-occupying lesions, are interfering on the long term with metabolic activity or cellular transport within the neuron (Goedert 2001) and can reflect a proteolytic degradation dysfunction.

Observation that most of aggregated a-syn in PD is forming small deposits located at the presynapses, and of synaptic pathology with almost complete loss of dendritic spines at the postsynaptic area (Kramer & Schulz-Schaeffer 2007) suggests a neurotransmitter deprivation and raised the notion that not cell death but rather a-syn aggregate-related synaptic dysfunction causes the neurodegeneration [reviewed in (Schulz-Schaeffer 2010)].

On the other hand, LBs are also found in patients without any clinical signs of parkinsonism (Hughes et al. 1992). Interestingly, LBs do not disturb nerve cell metabolism or predispose them to undergo apoptosis (Gertz et al. 1994; Tompkins & Hill 1997), suggesting that the dendritic abnormalities seen in PD are not LB dependent (Patt et al. 1991). Finally, LBs have also been proposed to represent a survival effort of neurons by sequestering the toxic soluble proteins in an insoluble form (McNaught, Shashidharan, et al. 2002; Olanow et al. 2004).

2.3.3 Evolution of the disease

Because only few and very well defined neurons are containing LBs and are damaged during PD, a model of PD development was created based on the distribution and evolution of a-syn lesions in different stages of PD observed in a large bank of brain samples. A six-stage model has been proposed by (Braak et al. 2003) as displayed in Fig. 1-03, and was confirmed by other large studies (Braak et al. 2004; Dickson et al. 2010).

In this model, stages 1 and 2 are characterized by the presence of pathological events in neurons of the dorsal vagal nucleus, olfactory bulb, and lower brainstem (including reticular and raphe nuclei), corresponding well to the early and frequent pre-motor symptoms (depression, impaired smell and autonomous function). In these early stages, the presence of LNs in the brainstem and the few LBs and cell death observed in these brain regions is suggesting that LNs are the first impaired structures which precede intraneuronal inclusions development and neuronal degeneration (Jellinger 2003; Jellinger 2004; Dickson et al. 2010).
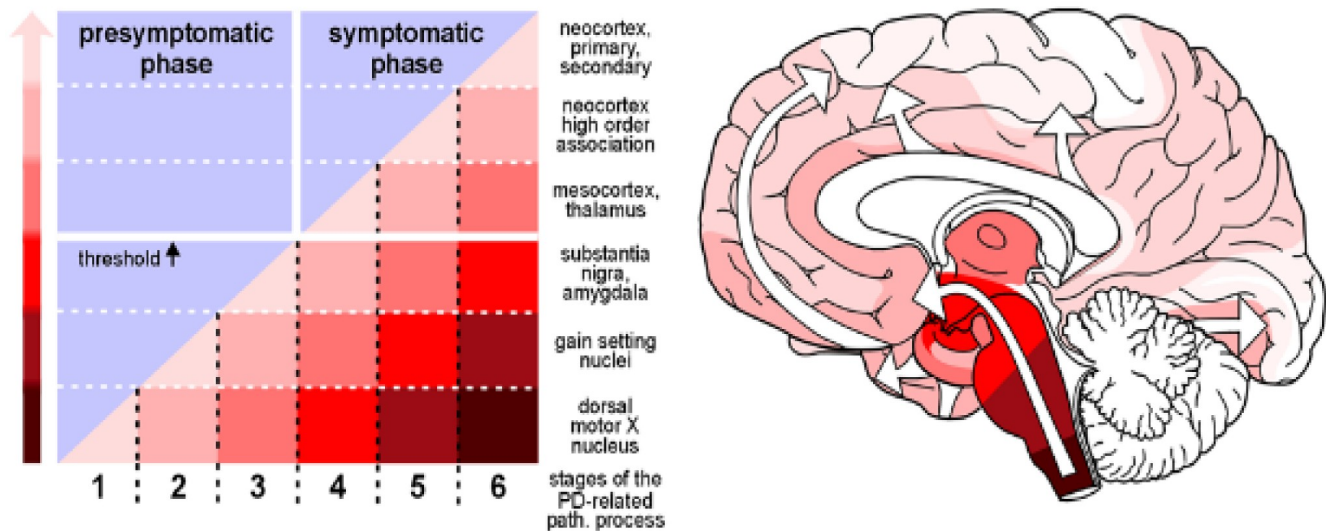
Figure 1-03: Lewy bodies spread

Figure copied from (Braak et al. 2004)

A) Presymptomatic phase, marked by the appearance of LBs and LNs in brains of asymptomatic persons. In symptomatic phase neuropathological threshold is exceeded and an increasing pathology in an increasing variety of brain regions is represented by colored areas below the diagonal line. B) Diagram representing the ascending pathological process (white arrows) using the similar shading intensity that in A.

The stage 3 is characterized by Lewy pathology reaching the brainstem as well as the amygdala and basal portions of the midbrain as well as the forebrain. During the stage 3 LBs can be observed first in the substantia nigra without cell depletion. In stage 4, the disease reaches the limbic circuit and starts spreading to the mesocortex and to the entorhinal cortex. Stages 3 and 4 are correlated with typical clinical PD symptoms.

In terminal stages 5 and 6, LBs reach telencephalic cortex, sensory association cortex and prefrontal areas. The spread of the disease leads to a widespread presence of LB involving almost the complete neocortex. In these late stages, cognitive and psychiatric symptoms accompany severe motor deficits.

This theory is criticized in literature due to the fact that the substantia nigra is only affected in stage 3 (Milber et al. 2012) and does not coincide with the age of onset observed in pre- and early-symptomatic stages (Burke et al. 2008). As mentioned before, the role of lesions in neurodegeneration process is not clear. Thus, analysis of lesion spread to study the disease progression has to be reconsidered.

A model of the spread of pathology was developed, where pathology spreads from the brainstem to the midbrain involving downstream the limbic circuit and the neocortex. Since even in an asymptomatic case LBs or/and LNs could be observed [reviewed in (Burke et al. 2008)], the symptomatic stage is defined when a neuropathological threshold is exceeded.

2.4 Genetics

As described previously, PD is classically reported as a sporadic disease and may result from a combination of environmental factors (rare cases of intoxication) and brain aging. Nonetheless, these factors do not completely explain other forms of disease such as young-onsets of PD. With the development of genomic technologies, an increasing number of genes, mutations and polymorphisms have been implicated in the PD pathogenesis, suggesting that PD is rather a multifactorial disorder arising from a combination of genetic and environmental factors [reviewed in (Klein & Westenberger 2012; Scholz et al. 2012; Cooper-Knock et al. 2012; Houlden & Singleton 2012; Trinh & Farrer 2013)].

Monogenic forms of PD demonstrate usually a positive family history and provide robust study cases accounting for approximately 10% of PD patients. These are related to more than 18 distinct chromosomal regions (also called chromosomal loci) termed PARK and numbered in the chronological order of their identification (Table 1-03).

The most recent classifications of PARK loci are incomplete systems with a number of inconsistencies (*i.e.* several loci could not be replicated, some loci do not have an identified gene or locus, loci PARK4 and PARK1 are identical). However, despite inconsistencies, the following list contains the six most established heritable monogenic forms unequivocally linked to PD:

[1] *SNCA* is the first discovered and the most studied gene associated with PD. *SNCA* encodes a-syn, a key component of LBs and hallmark of PD, as previously described. Five point mutations were reported in individuals who developed these rare autosomal dominant PD forms, with all mutations situated on the amino-terminus domain of a-syn (Thomas & Beal 2007). Interestingly, point mutations were also reported to increase the propensity of a-syn to aggregate, suggesting a possible toxic gain of function (Polymeropoulos et al. 1997; Krüger et al. 1998; Zarranz et al. 2004; Kiely et al. 2013; Lesage et al. 2013; Proukakis et al. 2013; Appel-Cresswell et al. 2013). Moreover, specific mutations of the *SNCA* gene (such as A30P or A53T) provide unique modifications of a-syn folding and aggregation rate (Conway et al. 1998). Duplication and triplication in the *SNCA* gene have been reported to lead to an early onset of the disease with prominent dementia (Singleton et al. 2003; Ibáñez et al. 2004; Miller et al. 2004)].

[2] *LRRK2* gene mutations [reviewed (Biskup & West 2009; Corti et al. 2011; Houlden & Singleton 2012; Trinh & Farrer 2013)] have been reported to be the most frequent known causes of autosomal dominant and sporadic PD [reviewed in (Nuytemans et al. 2010)]. *LRRK2* (leucine-rich repeat kinase 2) is a large gene composed of 51 exons and encodes a 2527 amino acids cytoplasmic protein. The protein contains a leucine-rich repeat on the amino-terminus and a kinase domain on the carboxy-terminus with various conserved domains in between. More than 50 different missense mutations are reported and interestingly most of the pathogenic changes are clustered in 10 exons, the majority encoding the protein's carboxy-terminal region. The increasing importance of *LRRK2* in the regulation of protein homeostasis highlights the importance of protein degradation in PD, probably via the regulation of the autophagy-lysosomal system (Orenstein et al. 2013). High levels of LRRK2 in peripheral monocytes and macrophages also suggest a role for LRRK2 in the

immune system [reviewed in (Dzamko & Halliday 2012)]. A role of LRRK2 in host response to pathogen and microglial inflammatory response has also been suggested (Moehle et al. 2012; Gardet et al. 2010). *LRRK2* forms of PD usually show similarities with idiopathic forms of PD including, (1) slow disease progression, (2) mid to late disease onset, and (3) a response to levodopa. Neuropathological findings are variable within *LRRK2* mutation carriers, showing both LBs pathology and nigral degeneration without LBs (Giasson et al. 2006).

Table 1-03: Monogenic forms of Parkinson's disease

PARK loci	Gene position	Disease onset	Inheritance	Gene	Protein function Cellular function
PARK1	4Q21-22	Early and late onset	Dominant	SNCA	Exact function unknown Synaptic transmission
PARK2	6q25.2-q27	Early onset	Recessive	PRKN	E3 ubiquitin ligase Mitophagy regulator
PARK3	2p13	Late onset	Recessive	Unknown	-
PARK4	4q21-q23	Early onset	Dominant	SNCA	Exact function unknown Synaptic transmission
PARK5	4p13	Late onset	Dominant	UCHL1	Ubiquitin-protein hydrolase Proteasomal protein degradation
PARK6	1p35-p36	Early onset	Recessive	PINK1	Serine-threonine kinase Mitophagy regulator
PARK7	1p36	Early onset	Recessive	DJ-1	Redox sensor Redox-sensitive chaperone
PARK8	12q12	Late onset	Dominant	LRRK2	GTPase, kinase Role in protein degradation?
PARK9	1p36	Early onset	Recessive	ATP13A2	Apoptosis Lysosomal ATPase
PARK10	1p32	Late onset	Risk factor	Unknown	-
PARK11	2q36-27	Late onset	Dominant	GIGYF2	Tyrosine kinase receptor signaling?
PARK12	Xq21-q25	Late onset	Risk factor	Unknown	-
PARK13	2p12	Late onset	Risk factor	HTRA2	Serine protease Mitochondrial protein release
PARK14	22q13	Early onset	Recessive	PLA2G6	A2 phospholipase Free fatty acids and lysophospholipids generation
PARK15	22q12-q13	Early onset	Recessive	FBX07	Proteasomal protein degradation E3 ubiquitin-protein ligase
PARK16	1q32	Unclear	Risk factor	Unknown	-
PARK17	16q11.2	Late onset	Dominant	VPS35	Adapter protein Endosome retrograde transport
PARK18	3q27.1	Late onset	Dominant	EIF4G1	Scaffolding protein mRNA recruitment to ribosome

| Introduction

[3] *PARK2* was the second identified monogenic form of PD and a common autosomal recessive form of PD. *PARK2* codes for parkin, a 465 amino acids protein with an E3 ubiquitin ligase activity. Structurally, parkin contains an amino-terminus ubiquitin-like domain (UBL) sharing a high homology with ubiquitin and four consecutive RING domains ("really interesting new gene") (Riley et al. 2013). Of the large number of identified *PARK2* mutations, about half affect the region spanning exons 2–4 (coding for the UBL domain, the very beginning of the RING0 domain and the linker region) highlighting their relevance to parkin's normal function [reviewed in detailed in (Klein & Westenberger 2012)]. Mutations in *PARK2* are the most frequent known cause of the early onset form of PD, characterized by its slow development (Lücking et al. 2000) and sharing similar clinical symptoms with idiopathic PD patients (Lohmann et al. 2003). *Post mortem* findings indicate variable levels of LBs and neurofibrillary tangle pathology depending on the *PARK2* mutation, highlighting its atypical development when compared with IPD (Hayashi et al. 2000; Pramstaller et al. 2005).

[4] Mutations in *PINK1* [phosphatase and tensin homologue (PTEN)-induced putative kinase 1] gene are the second most common cause of early onset autosomal recessive forms of PD (Rogaeva et al. 2004; Y. Li et al. 2005; Bonifati et al. 2005)]. PINK1 protein is a 581 amino acids ubiquitously expressed protein kinase containing a mitochondrial targeting motif at the amino-terminus, a serine-threonine kinase domain and a carboxy-terminal autoregulatory domain. PINK1 has been shown to control the outer mitochondrial membrane integrity and mitophagy, thus playing a protective role against oxidative-stress-induced apoptosis [mechanisms of PINK1 function reviewed in (Deas et al. 2009; Corti & Brice 2013). The importance of the PINK1 kinase activity is highlighted by the loss of kinase function observed in patients (Valente et al. 2004). The clinical phenotype of *PINK1* mutation carriers is relatively similar to idiopathic PD, but earlier symptoms onset and less severe pathology progression could be observed (Bonifati et al. 2005).

[5] Mutations in DJ-1 represent a less common form of PD and despite the few patients reported in literature, more than 10 different point mutations and exonic deletions have been described (Pankratz et al. 2006). DJ-1 is a 189 amino acids protein that is ubiquitously expressed, functioning as a cellular sensor of oxidative stress which regulates its translocation to the outer mitochondrial membrane (Canet-Avilés et al. 2004; Martinat et al. 2004; Junn et al. 2005). Mutated DJ-1 proteins are frequently reported to be improperly folded, unstable, and rapidly degraded thus reducing its antioxidant and neuroprotective function (Malgieri & Eliezer 2008; Anderson & Daggett 2008). Patients carrying DJ-1 mutations that result in PD present an early onset with slow disease progression, which closely resembles to the disorder caused by *PARK2* or *PINK1* mutations.

[6] Mutations in *ATP13A2* have been found to cause an autosomal recessive and atypical form of PD named Kufor Rakeb syndrome (Ramirez et al. 2006). *ATP13A2* is a large gene comprised of 29 exons coding for an 1180 amino acids protein. The ATP13A2 protein is normally located in the lysosomal membrane, consisting of 10 transmembrane domains and an ATPase domain. About 10 different pathogenic mutations have been found, directly or indirectly affecting transmembrane domains resulting in an unstable and truncated protein. This syndrome has a juvenile onset with rapid disease progression, accompanied by dementia, supranuclear gaze palsy, and pyramidal signs (Ramirez et al. 2006).

The rest of the PARK loci listed have been hypothesized to be linked to the development of PD condition, whereas their involvement as monogenic form of PD has not been confirmed yet. More precisely, some monogenic forms of PD were observed only in one patient (such as *EIF4G1*, *UCHL1*, and *GIGYF2*), other gene mutations provide minor features in a complex phenotype (like *FBXO7*, *PLA2G6*), and finally the *HTRA2* gene was involved as a risk factor and not as a monogenic form of PD [reviewed in (Corti et al. 2011; Houlden & Singleton 2012; Klein & Westenberger 2012; Trinh & Farrer 2013)].

Several genetic risk factors have been related in developing idiopathic PD. Variants in several PARK loci (*SNCA*, *UCHL1* and *LRRK2*) and a few other genes (*MAPT*, *GBA*, *NAT2*, *INOS2A*, *GAK*, *HLA-DRA*, and *APOE*) have been associated with an increased risk of developing PD. Most significant risk factors identified are 1) polymorphisms or mutations in *SNCA*, 2) missense single-nucleotide polymorphisms (SNPs) in the *LRRK2* gene (G2385R and R1628P), and 3) *GBA* loss-of-function mutations (Gaucher's Disease).

Finally, a last group of genes (including *SNCAIP*, *NR4A2/Nurr1*, *POLG*, *HSPA9*, and *PARL*) could be considered pathogenic based on their translated proteins functions and interactomes. However, further detailed studies did not validate a major contribution of these genes in the development of PD.

To conclude, discovery and detailed analysis of monogenic forms and risk factors of PD allowed a partial clarification of the complex etiology of the disease, highlighting pathways critically involved in the process. Understanding the function and the involvement of these genes in PD is probably the key to find out links between poorly understood neuropathological mechanisms, cell loss and the spectrum of clinical features observed in PD.

3)   Physiopathological pathways

Genetic components of PD, as suggested by the PARK loci table, seem to converge on three inter-connected cellular processes: 1) synaptic exocytosis and endocytosis, 2) lysosome-mediated autophagy, and 3) mitochondrial quality control and stress response. This sequence of pathological events (Fig. 1-04) is reviewed in detailed in (Hardy et al. 2006). However, it is still unknown whether alterations of these pathways lead to different entities or whether they finally converge at a common pathogenic denominator.
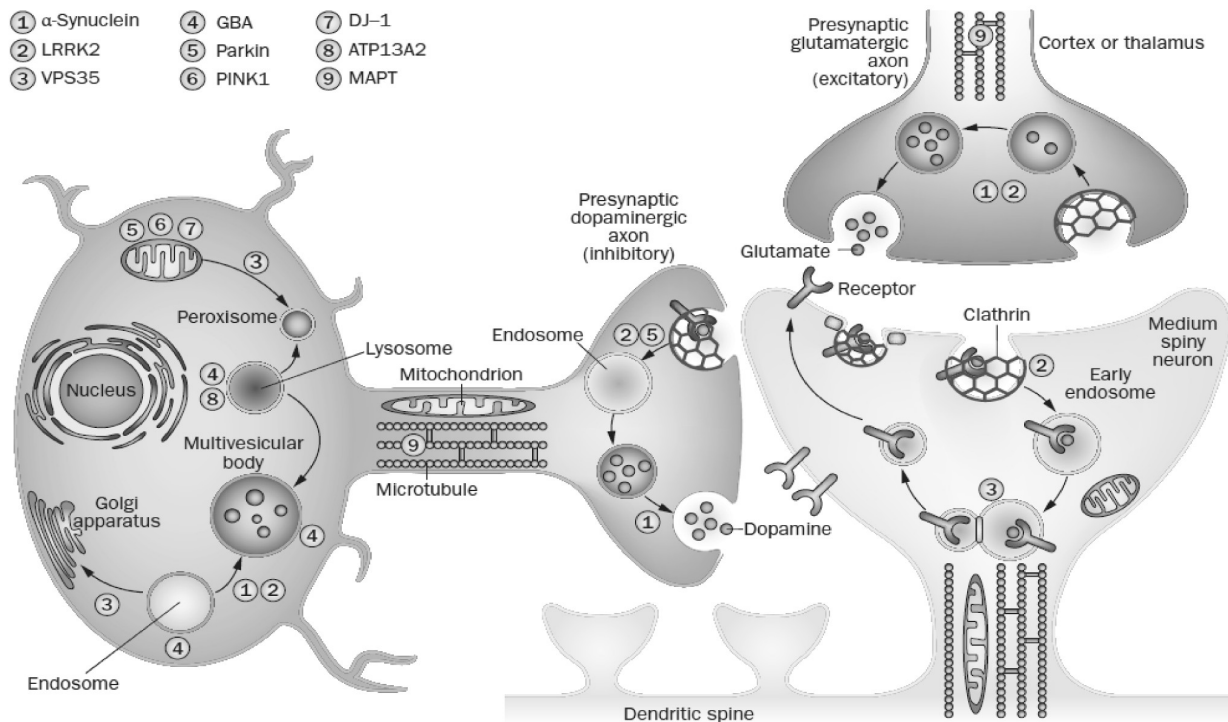
Figure 1-04: Extrapolation of genetic findings to model Parkinson's disease process

Figure copied from (Trinh & Farrer 2013)

In presynaptic terminals, 1) high levels of a-syn inhibits exocytosis, a-syn promote the formation of early endosomes. Postsynaptically, 2) LRRK2 regulates the release of vesicles, neuronal polarity and arborization. LRRK2 also play a role in chaperone-mediated autophagy, MAPT phosphorylation and microtubule stabilization. 3) VPS35 plays an essential role in the retromer complex and especially in the cargo recognition complex. These cargoes have several destinations such as lysosomal degradation, exosome secretion, and endosome recycling by the Golgi apparatus or peroxisome. 4) Lysosomal acid hydrolases, including GBA, require retromer complexes for receptor recycling. 5–7) Loss-of-function mutations in PARK2, PINK1 and DJ-1 affect mitochondrial biogenesis and induction of autophagy. Parkin is involved in ubiquitination and proteasomal function, PINK1 and parkin are involved in mitochondrial maintenance. 8) ATP13A2 plays a role in lysosome-mediated autophagy. 9) MAPT helps to regulate cargo trafficking and delivery, primarily in axons.

3.1   Synaptic dysfunction

Expression analysis of key genes involved in the disease pathogenesis reveals that encoded proteins are particularly concentrated at synaptic terminals (such as a-syn (Iwai et al. 1995) or LRRK2 (Biskup et al. 2006)). Moreover, functional analysis also showed their association with synaptic vesicles in animals lacking a-syn (Abeliovich et al. 2000) or overexpressing mutated G2019S LRRK2 protein (Xianting Li et al. 2010) [reviewed in (Picconi et al. 2012) and detailed in the section describing animal models of PD].

Accordingly to the synaptic dysfunction hypothesis, damage to axons and axonal terminals are preceding dopaminergic neuronal cell loss, suggesting that pathology may start at the axon terminal level [reviewed in (Cheng et al. 2010)]. It is noticeable that an increase of dopamine turn-over has been described in presymptomatic PD patients (Whone et al. 2003), but origins and consequences of this observation are not completely understood. Altogether, changes of nigrostriatal excitability may have a profound influence on striatal synaptic transmission efficacy and hint at a synaptic dysfunction in early PD [reviewed in (Picconi et al. 2012)].

3.2   Protein degradation

The presence of abnormal accumulations and aggregates, forming characteristic inclusions in PD, suggests that impairment of protein degradation pathways might play a primary role in the physiopathology of the disease (Soto 2003; Ross & Poirier 2004). Maintenance of the cellular proteome (entire pool of proteins located inside the cell and its membrane) involves a complex and dynamic equilibrium, regulated on the one hand by the synthesis and on the other hand by the degradation of proteins. Synthesis and usage of proteins lead to the generation of unwanted proteins including incomplete, mutant, misfolded, mislocalized, denatured, oxidized, and otherwise damaged proteins. These modified proteins, if they are not removed by the quality control system, could induce cytotoxicity due to their tendency to aggregate, interfering with cellular processes by loss or gain of function [reviewed in (Dobson 2003; Balch et al. 2008)]. Impairment of the cellular protein quality-control system may lead to partial degradation of damaged proteins. This impairment can result not only from one single severe condition, but also from combination of different moderate conditions, which cannot overwhelm the system on their own. Conditions leading to a reduced effectiveness of the quality-control system can be categorized in four classes: mutations, protein biogenesis, environmental stress, and aging [reviewed in detail in (Tyedmers et al. 2010)].

Protein quality control has three main parallel strategies: 1) refolding of misfolded proteins by molecular chaperones, 2) degradation of proteins via the ubiquitin-proteasome system or the autophagy-lysosomal pathway, and 3) sequestration of misfolded proteins in inclusions or large aggregates [reviewed in (Takalo et al. 2013)]. More recently, exosomal release has been shown as a fourth alternative degradation pathway for the cell [reviewed in (Schneider & Simons 2013)].

3.2.1   Molecular chaperones

To be functional, most proteins must adopt a defined three-dimensional structure representing a specific tertiary structure termed native fold. This structure is determined by the folding of intermediate elements (secondary structure constituted of small numbers of closed amino acids interacting with each other) into a 3D structure presenting functional regions (Anfinsen 1973). Incompletely folded proteins can be trapped in non-productive intermediates, such as misfolded conformers, consequence of free energy minimal conformation.

As a small energy barriers usually separate native and non-native conformations, even native proteins are at permanent risk of unfolding, especially under environmental stress (Shortle 1996). Misfolded conformers and folding intermediates typically expose hydrophobic residues, which are prone to aggregation and normally buried in the native structure (Dobson 2003).

| Introduction

Chaperones and co-chaperones are the first line of defense against misfolded proteins, binding to unfolded proteins or aggregation-prone folding intermediates and playing several roles: 1) stabilizing proper protein folding, 2) refolding proteins in their native state, 3) preventing unwanted interactions between hydrophobic regions with their neighboring proteins, 4) dis-assembling larger protein aggregates, and 5) targeting proteins which cannot be refolded for degradation [reviewed in (Goloubinoff & De Los Rios 2007; Witt 2010; Wolff et al. 2014)].

The relevance of this defense mechanism's failure in PD pathogenesis is highlighted by the observation in LBs of abnormally high levels of molecular chaperones and co-chaperones [reviewed in (Licker et al. 2009)]. This is suggesting a mechanism involving massive protein misfolding, exceeding the refolding capability of the molecular chaperones, leading to the depletion of chaperones in cells and resulting in a widespread aggregation (Kalia et al. 2010).

3.2.2   *Proteolytic degradation*

The ubiquitin-proteasome system and the autophagy-lysosomal pathway are the two major cellular proteolytic systems participating in protein turn-over and removal of altered proteins.

Ubiquitin-proteasome system

Ubiquitin-proteasome system (UPS) is a molecular mechanism responsible for the selective degradation of most short-lived intracellular and plasma membrane proteins, as well as misfolded or damaged proteins in the cytosol, nucleus or endoplasmic reticulum (ER) (Ciechanover 2005)]. Clearance of proteins by the UPS involves an elaborate sequence of events, extensively reviewed in (Glickman & Ciechanover 2002), schematized in Fig. 1-05 and resumed below:

[1] The process is initiated by the ubiquitin-activating enzyme (E1), linking its cysteine residue to the ubiquitin terminal glycine in an ATP-dependent manner. Activated ubiquitin is then transferred to a cysteine residue of the ubiquitin-conjugating enzyme (E2). Final binding of ubiquitin to its target protein is driven by a specific ubiquitin-protein ligase (E3). Ubiquitin can be attached to substrate proteins in several ways, generating a broad repertoire of signals with different topologies and lengths, leading to various functional outcomes for the tagged substrate protein.

[2] A single ubiquitin molecule attached to a target protein (termed monoubiquitinated) could be extended to several sites (termed multi-monoubiquitinated), or could form an ubiquitin chain (termed polyubiquitinated) via the appropriate E2/E3 pair or through ubiquitin-elongating enzymes (E4). Polyubiquitination is the most frequent ubiquitination signal found on proteins, and can occur on several different lysine residues of ubiquitin (seven lysine residues at positions 6, 11, 27, 29, 33, 48, 63 and the N-terminal methionine). Polyubiquitination presents a large repertoire of signals depending on the position of the ubiquitin-ubiquitin chain elongation and on the length of the polyubiquitin chain. Thus, ubiquitin-dependent signaling affects almost all cellular processes [reviewed in (Pickart & Fushman 2004; Kulathu & Komander 2012; Kravtsova-Ivantsiv & Ciechanover 2012)].
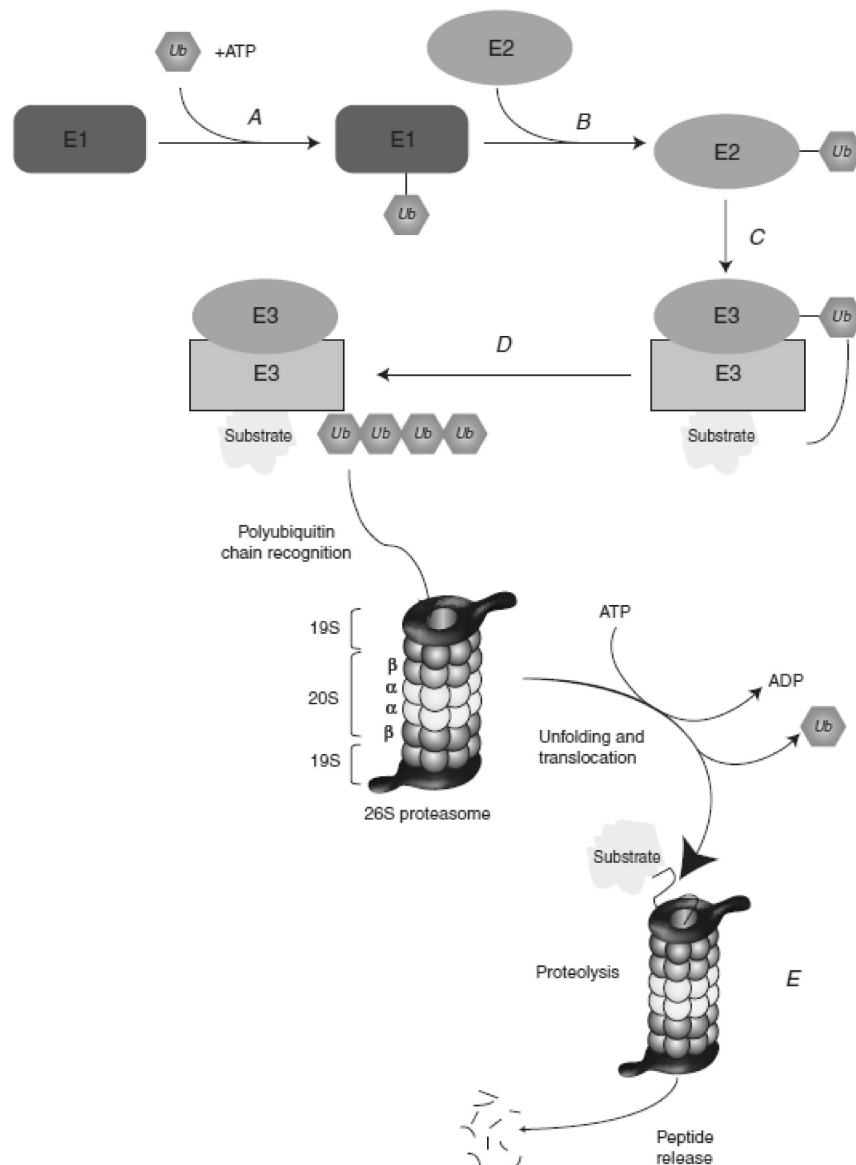
Figure 1-05: 26S ubiquitin-proteasome degradation system

Figure copied from (Cook et al. 2012)

A) Activation of ubiquitin protein by ubiquitin-activating enzyme E1 in an ATP-dependent manner. B) Transfer of activated ubiquitin to the E2. C) Ubiquitin transfer from the E2 to the substrate driven by specific E3 either prior or after E3 conjugation to the substrate. D) Additional ubiquitin molecules can be added to the internal lysine residues of ubiquitin to form polyubiquitin chain on the substrate. E) Ubiquitinated substrate is recognized and degraded by the 26S proteasome complex, leading to the release of short peptides. Ubiquitin can be then recycled via the activity of deubiquitinases.

| Introduction

[3] Degradation of the vast majority of intracellular proteins is performed by the proteasome [reviewed in (Lamark & Johansen 2012; Kish-Trier & Hill 2013)]. The proteasome refers to a variety of complexes, classically composed of the 20S proteasome (as catalytic core) and regulatory subunits (forming "lid" or "cap" at the end of the 20S to regulate the entry and catalytic function of the core). The 20S element forms a barrel-shaped structure and is constituted of 28 protease subunits, two copies of seven different outer α-subunits and two copies of seven different inner β-subunits. Three catalytic active subunits (β1, β2, and β5) possess caspase-, trypsin-, and chymotrypsin-like activities, respectively. Regulation of complexes containing the 20S element is still poorly understood, but two main mechanisms (ATP-dependent and ATP-independent) are emerging. In the ATP-dependent regulation, a 19S complex is attached at one or both ends of the 20S to form the 26S proteasome. In this structure, 19S forms a regulatory lid and selects appropriate targets by binding to ubiquitinated proteins via Rpn10 and Rpn13. The selected substrate is then unfolded and translocated into the 20S in an ATPase dependent manner. In the ATP-independent regulation, several protein complexes (such as 11S (or PA28), Blm10 (or PA200) as well as PI31) can interact at one or both ends of the 20S to form alternative isoforms of the proteasome able to regulate ubiquitin-independent substrate degradation [reviewed in (Kish-Trier & Hill 2013)].

The involvement of ubiquitin-mediated processes has been suspected in the physiopathology of PD since immunoreactivity against ubiquitin was detected in Lewy bodies from samples of sporadic PD patients (Lennox et al. 1989). Accordingly, origin of the disorder has been hypothesized to be a consequence of an age-related decrease of UPS function (Gray et al. 2003). This hypothesis is supported by 1) decreased 20S proteasome alpha-subunits observed in patients (McNaught, Belizaire, et al. 2002), 2) reduced 20S proteasomal enzymatic activities in *post mortem* brain tissue extracted from PD patients (McNaught et al. 2001), 3) existence of rare genetic forms of PD affecting components and substrates of the UPS (*i.e. PARK2* coding for parkin which is an E3 ligase or *UCH-L1* coding for a deubiquitinase), and 4) numerous *in vivo* and *in vitro* studies based on administration of proteasome inhibitors (hypothetically modeling and accentuating the natural decrease of UPS observed with aging) also showing the importance of the UPS function in the formation of cellular inclusions and neurodegeneration (McNaught, Mytilineou, et al. 2002; McNaught et al. 2004; Bedford et al. 2008).

Autophagy-lysosome pathway

The autophagy-lysosome pathway (ALP) is the general term used to describe the degradation pathway of intracellular proteins and organelles in lysosomes (Fig. 1-06). According to the different pathways by which cargo is delivered to the lysosome, autophagy can be divided into three main types: macroautophagy, microautophagy, and chaperone-mediated autophagy. Lysosomes are cellular organelles composed of a single membrane vesicle, which maintain an acidic pH through ATP-dependent proton pumps, and contain an assortment of soluble acid-dependent hydrolases including proteases, lipases, and glycosidases.
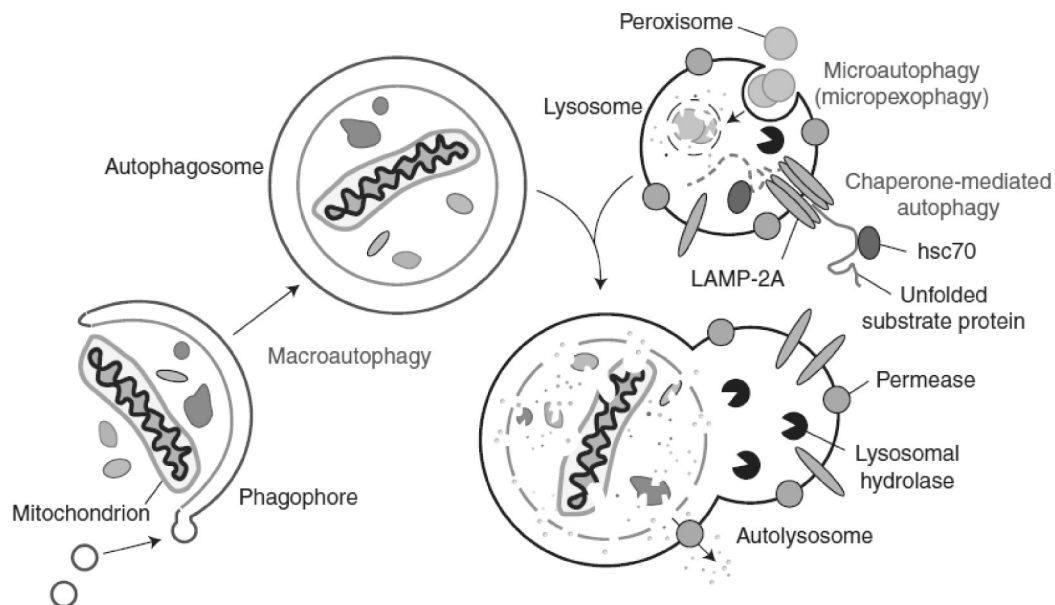
Figure 1-06: Autophagy-lysosomal degradation pathway

Figure copied from (Lynch-Day et al. 2012)

Schematic model of the three main autophagy types. Chaperone-mediated autophagy involves recognition of substrates by HSC70 chaperones, translocating them across lysosomal membrane via interaction with LAMP-2A oligomer. Various types of microautophagy-like processing selectively degrade organelles (such as peroxisomes and mitochondria) via their sequestration into lysosomal membranes. Macroautophagy involves a double membrane phagophore to sequester cargo consisting of cytoplasmic component, expanding into an autophagosome and fusing with the lysosome to allow the cargo to be degraded.

Macroautophagy

Macroautophagy [reviewed extensively in (Lynch-Day et al. 2012; Lamark & Johansen 2012) is a tightly regulated process consisting of several sequential steps: 1) initiation of the process by the formation of a double-membrane structure (termed phagophore), 2) elongation of the phagophore resulting in its closure (forming the autophagosome) and sequestering a portion of the cytoplasm, 3) autophagosome transported along microtubules from the cell periphery to the microtubule-organizing center area, 4) fusion of the outer membrane of the autophagosome with the lysosome (forming the autophagolysosome) and resulting in the degradation of their content by its acidic environment and by lysosomal proteases.

Although macroautophagy has commonly been described as a cellular adaptive response to nutrient starvation, an important role has emerged in intracellular quality control to protect cells against microbial infection, oxidative stress, proteasome inhibition, or protein aggregation (Mizushima et al. 2008; Deretic 2010). Oxidative stress to organelles is an interesting example illustrating the critical role of selective autophagy in the intracellular quality control. In the particular mitochondrial case, damaged mitochondria will accumulate in the cell and lead to neuronal cell death (Chen & Chan 2009) if not processed by the autophagy (so called mitophagy) (de Vries & Przedborski 2013).

| Introduction

In contrast to starvation-induced autophagy, quality control autophagy requires specific mechanisms allowing the selection and disposal of aberrant protein aggregates and damaged organelles. Selective macroautophagy is driven by autophagic adapter proteins (such as p62 or NBR1) acting as autophagy cargo receptors due to their ability to bind to ubiquitinated substrates and to be recruited for degradation by phagophores (Pankiv et al. 2007; Kirkin et al. 2009; Johansen & Lamark 2011).

Microautophagy

Microautophagy is a non-selective lysosomal degradation process involving the direct delivery and rapid digestion of cellular constituents (including organelles, lipids, or proteins) through lysosomal membrane invagination engulfing complete regions of the cytosol [reviewed in detail in (Mijaljica et al. 2011; Li et al. 2012)]. Despite the complexity and variety of microautophagy mechanisms, a general mechanism can be observed: 1) initiation of microautophagy by the formation of a spontaneous pit on a localized area of the lysosomal membrane and its extension leading to a characteristic tubular shape (termed autophagic tube), 2) formation of a vesicle at the bottom of the tube, 3) vesicle expansion by specialized enzymes binding to the inside of the nascent spherical structure, 4) vesicle pinch-off into the lumen from the tube via an enzyme or a mechanic excision and, 5) vesicle degradation and recycling by lysosomal hydrolases.

Microautophagy could be induced by starvation and rapamycin, but also occurs constitutively (Dubouloz et al. 2005) and simultaneously or in synergy with other types of selective autophagy stabilizes intracellular environment and sequestering specific organelles with arm-like protrusions (Todde et al. 2009).

Chaperone-mediated autophagy

Chaperone-mediated autophagy (CMA) involves the identification of specific unfolded cytosolic proteins and their delivery to the lysosomal membrane. This mechanism is based on the recognition of the specific KFERQ motif via the chaperone hsc70 (70 kDa heat-shock cognate protein). The substrate/chaperone complex is targeted to the surface of the lysosomes via its binding to the lysosome-associated membrane protein type 2A (LAMP-2A). Assembly of a high molecular weight complex is promoted at the lysosomal membrane and results in the substrate's translocation into the lysosomal lumen [reviewed extensively in (Majeski & Dice 2004; Kaushik & Cuervo 2012)].

A selectivity activation of protein degradation via CMA arises after nutrient deprivation and cellular stress (Cuervo et al. 1995), underlining its importance to the maintenance of the protein quality control.

Involvement of proteolytic degradation in Parkinson's disease

They are increasing evidences that autophagy is deregulated in the physiopathology of PD. At the histological level, accumulation of abnormal autophagic vacuoles was observed in neurons of PD patients (Anglade et al. 1997; Zhu et al. 2003). At the genetic level, genes linked to autosomal dominant PD are also playing an important role in autophagy. For instance, the mutated a-syn protein was shown to inhibit the CMA (Cuervo et al. 2004),

LRRK2 mutations were also shown to regulate both CMA and macroautophagy (Alegre-Abarrategui et al. 2009; Tong et al. 2010; Orenstein et al. 2013) and mutated ATP13A2 protein was described to provoke lysosomal dysfunction (Ramirez et al. 2006). Accordingly, the selective deletion of Atg proteins in mouse models (either Atg5 or Atg7 which both play a critical role in autophagy) was reported to induce neurodegeneration and formation of ubiquitin-positive cytoplasmic aggregates (Hara et al. 2006; Komatsu et al. 2006).

Moreover, the progressive impairment of specific and selective protein degradation mechanisms with aging (such as proteasomal pathway and CMA) [reported in (Gray et al. 2003; Cuervo & Dice 2000) respectively] is reported to lead to an upregulation of the macroautophagy (Massey et al. 2006; Pandey et al. 2007). This excessive activation of a less selective in-bulk degradation mechanism (macroautophagy) is on the one hand compensating the reduced protein degradation, but on the other hand also associated with a lower capacity to respond to stress conditions and can itself induce stress to cells (Massey et al. 2006). Thus, autophagosome formation can exert toxicity regardless whether it leads to protein degradation or accumulation [reviewed in (Maiuri et al. 2007)]. This could be illustrated at the histological level by the presence of autophagic vacuoles in the brains of PD patients, which are usually rarely detected (Anglade et al. 1997; Zhu et al. 2003). In this context, maintaining a proper level of autophagy to reduce protein aggregation and damaged organelles could be apply as a strategy to reduce neuronal damage (Lynch-Day et al. 2012).

3.2.3   *The aggresome*

Aggresomes are a specialized form of inclusion bodies found in the cytoplasm of mammalian cells (Johnston et al. 1998) and characterized by their localization in the centrosome at the perinuclear site (Fig. 1-07). Their overall structure and size is variable, depending on cell type and aggregating substrate. Aggresomes appear usually as a single sphere of 1 to 3 µm diameters or as an extended ribbon and are composed mainly of a core of aggregated ubiquitinated proteins surrounded by a cage-like shell composed of vimentin intermediate filaments [reviewed in (Kopito 2000)]. Aggresomes are not permanently present in cells, but are induced by cellular stress as in the case of large amounts of unfold proteins (such as proteasome inhibition).

These dynamic structures are able to recruit various cytosolic components such as chaperones, ubiquitination enzymes or proteasome components [generation of aggresomes detailed in (Garcia-Mata et al. 2002)]. The formation of aggresome is initiated by the retrograde transport of small and dispersed cytoplasmic aggregates to the centrosome to form enlarged inclusions of aggregated-ubiquitinated proteins (Johnston et al. 2002; McNaught, Shashidharan, et al. 2002). This transport mechanism is driven mainly by the histone deacetylase 6 (HDAC6), binding to polyubiquitinated-proteins so that the dynein motor complex can transport them along microtubules (Kawaguchi et al. 2003). Aggresomes are finally degraded by macroautophagy via autophagosome, underlining the role of aggresomes in the promotion of specific and efficient clearance of aggregation-prone proteins (Fortun et al. 2003; Tanaka et al. 2004; Iwata et al. 2005).

| Introduction

In many ways, LBs could be considered as a form of aggresome. First, LBs have an aggresome appearance (presence of a centrosome as well as aggresome-specific proteins such as gamma-tubulin and pericentrin). Second, numerous discrete ubiquitinated aggregates are transported from peripheral sites to the centrosome, where aggresomes are forming, similarly to LBs which are also containing large quantity of ubiquitinated proteins. Finally, LBs contain heat shock proteins as well as components of the UPS, which are also typically found in the aggresomes [reviewed in (Olanow et al. 2004)].
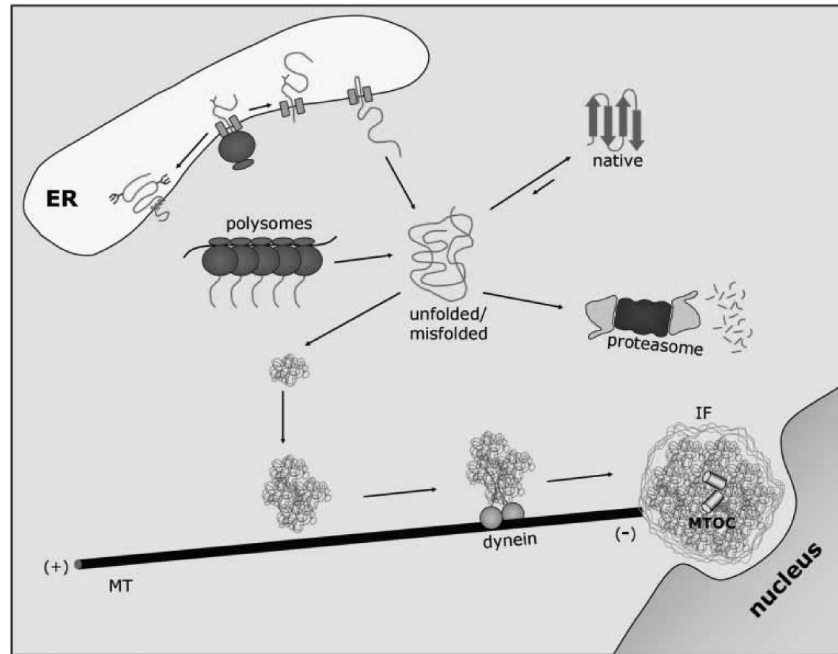
Figure 1-07: Aggresome formation

Figure modified from (Garcia-Mata et al. 2002)

Proteins unfolding (or misfolding) may occur during polysome translation, proteins retrotranslocation from the ER to the cytosol or during cellular stress. These abnormal proteins may then present reduced degradation efficiency by the proteasome, and therefore form aggregates throughout the cells. Such aggregates can be transported in a microtubule- dependent manner to the microtubule organizing center (MTOC) in a process requiring dynein/dynactin complex.

3.3 Mitochondrial dysfunction, oxidative stress and inflammation

3.3.1 Mitochondrial dysfunctions

The concept of mitochondrial dysfunction in the physiopathology of PD was first seriously investigated after the discovery of 1-methyl-4-phenyl-1,2,3,6-tetrahydropyridine (MPTP) toxicity mechanism. MPTP is a synthetic heroin analog, discovered accidentally in drug users who injected themselves this homemade compound; these subjects developed parkinsonism within days consequence of irreversible lesions of dopaminergic neurons in the substantia nigra pars compacta [reviewed in detail in (Hauser & Hastings 2013)].

MPTP toxicity comes from its ability to cross the blood-brain barrier, penetrating into glial cells and being converted into the neurotoxin 1-methyl-4-phenylpyridinium (MPP+). MPP+ is transported by the dopamine transporter into monoaminergic neurons, getting concentrated into mitochondria where it specifically inhibits the complex I of the respiratory chain and leads to ATP depletion, oxidative stress and apoptotic cell death.

Following this discovery, analysis of mitochondrial complex I activity in patients with sporadic PD revealed a moderate deficit in several brain regions including substantia nigra, frontal cortex but also peripheral tissues like skeletal muscle [reviewed in (Winklhofer & Haass 2010; Hauser & Hastings 2013)]. Confirming the previous findings, the administration of the complex I inhibitor rotenone was reported to cause many of the pathological and behavioral hallmarks of PD (Betarbet et al. 2000). Therefore, this strategy provides an elegant animal model allowing a better understanding of the physiopathology of PD.

3.3.2   *Oxidative stress*

Mitochondria are involved in various cell functions, but are well known as an important source of energy by generating ATP energy via oxidative phosphorylation. This metabolic pathway is driven by the transport of electrons through mitochondrial complexes I–IV in the inner mitochondrial membrane via series of coupled redox reactions providing the energy to create a proton gradient across the inner mitochondrial membrane and driving ATP synthesis from ADP as protons re-enter the matrix. Under normal conditions, molecules and free radicals derived from molecular oxygen participate in oxidative phosphorylation, providing the major source of reactive oxygen species (ROS) (Chance et al. 1979). ROS levels are regulated under normal conditions by a battery of protective systems sequentially reducing ROS to water by the electron transport chain complexes (Brand 2000). Certain situations (such as mitochondrial dysfunctions) can cause ROS production to surpass the antioxidant capacity of a cell (Trifunovic & Larsson 2008).

In this specific condition, termed oxidative stress, irreversible damage are caused to cellular macromolecules (such as protein oxidation, lipid peroxidation, DNA and RNA oxidation) and can lead ultimately to cell death. Several markers of oxidative stress, including high levels of oxidatively modified lipids, proteins and DNA, have all been found in brain samples of PD patients (Dexter et al. 1989; Floor & Wetzel 1998).

Thus, mitochondria are at the same time essential to produce energy and potentially dangerous. Therefore, several mitochondrial quality control pathways have evolved to efficiently protect mitochondria from molecular damage and to maintain an overall healthy population [reviewed in (Fischer et al. 2012; Andreux et al. 2013)]. As reported previously in this thesis, mutations in genes involved in monogenic PD (*PARK2*, *PINK1* and *DJ-1*) were shown to impair key function in the control of mitochondrial morphology and integrity [reviewed in (de Vries & Przedborski 2013)] via the degradation of damaged mitochondria by macroautophagy [also termed mitophagy and reviewed in (Youle & Narendra 2011)]. These observations suggest that the autophagic pathway is also essential for the turn-over of dysfunctional mitochondria and its failure seems definitely involved in pathogenic mechanisms of PD (Hirsch & Hunot 2009).

3.3.3 Abnormal inflammation

Chronic inflammation is associated with a broad spectrum of neurodegenerative diseases (McGeer & McGeer 2004). Accordingly, in postmortem PD patient brains, an increased inflammatory response is suggested to increase levels of 1) glial activation (resulting in microglial activation as well as an increase in astroglia cells), 2) lymphocyte infiltration, 3) pro-inflammatory mediators (such as tumor necrosis factor alpha (TNFα), interleukin1 beta (IL-1β) or interferon gamma (IFNγ)), and 4) inflammation-inducible enzymes (such as cyclooxygenase 2 (COX2) as well as nitric oxide synthase (iNOS)) [reviewed in detail in (Hirsch & Hunot 2009)].

Unfortunately, the exact origin and role of the neuroinflammation is still unknown yet, despite an increasing number of studies pointing to its relevance in the progression of the disease in both animal models and clinical studies [reviewed in (Collins et al. 2012)]. In this context, the involvement of the neuroinflammation process as a cause of the disease or as a consequence of neuronal degeneration is still highly debated.

4) Animals models

PD is a complex disorder in which causes, mechanisms and neurodegeneration progression are still unclear. Due to their interdependence, studying these aspects simultaneously is probably the best strategy to achieve significant advances. However, this proposes a challenge concerning the methodology as it requires a parallel analysis at physiological, cellular, molecular and biochemical levels.

Analysis of limited post-mortem material from patients implies methodology limitations that *in vivo* model cannot emphasis. For example, the large variety of neuronal and non-neuronal cell types implies that the complex physiopathology of PD cannot be modeled in cellular models. These considerations lead to the frequent use of animal models, and especially mouse models because of their similarity with human neuronal network as well as their well-known genome and behavior (Waterston et al. 2002). Therefore, in the next chapter concerning animal models of PD, we will mainly focus on mouse models, and provide an overview of the most studied PD mouse models (Table 01-04).

Two main strategies are commonly applied to generate these models: 1) neurotoxins to destroy the striatonigral system, 2) genetic modifications to model monogenic forms of the disease by deleting (knock-out) or replacing (knock-in) or inserting (transgenic) gene(s) involved in familial forms of PD.

Ideally, a PD mouse model should reproduce all the disease features: dopaminergic cell degeneration, presence of LB inclusions, microglial activation and non-motor symptoms. Despite the variety of methods existing to generate animal models, no single model reproduced so far the combination of slow and progressive degeneration of dopaminergic cells, presence of LBs and inflammation.

Table1-04: Examples of Parkinson's disease mouse models

	Method	Injection/ expression	Dopaminergic cell loss	Alpha-synuclein aggregates	Progressive pathology	Motor deficit	Reference
Toxin	MPTP	IP injection	Yes	Conflicting	No	Yes	Heikkila 1984 Fornai 2005
	6-OHDA	Intracranial injection	Yes	No	No	Yes	Faull 1969
	Rotenone	IP injection	Yes	Conflicting	Yes	Weak	Heikkila 1985 Betarbet 2000
	Paraquat	IP injection	Conflicting	No	No	No	Brook 1999
Transgenetic	TH WT, A30P or A53T a-syn	Catecholamine neurons	No	Yes	Yes	No	Matsuoka 2001
	Thy-1 WT a-syn	Neuron specific	No	Yes	Yes	Mild	Kahle 2000
	Thy-1 A30P a-syn	Neuron specific	No	Yes	Yes	Mild	Kahle 2000
	Thy-1 A53T a-syn	Neuron specific	No	Yes	Yes	Sever	van der Putten 2000
	PrP WT a-syn	Majority of neurons	No	Conflicting	Conflicting	No	Giasson 2002 Lee 2002
	PrP A30P a-syn	Majority of neurons	Conflicting	Conflicting	Conflicting	Mild	Lee 2002 Gomez-Isla 2003
	PrP A53T a-syn	Majority of neurons	No	Conflicting	Yes	Sever	Lee 2002 Gispert 2003
	PDGF WT a-syn	Majority of brain neurons	No	Yes	Yes	Yes	Masliah 2000 Lee 2002
	Complete human SNCA	Widespread	No	Yes	Yes	Mild	Kuo 2010 Hansen 2013
	PDGFβ G2019S LRRK2	Majority of brain neurons	Yes	No	Yes	Yes	Ramonet 2011
	DAT promoter truncated parkin Q311X	Catecholamine neurons	Yes	Yes	Yes	Yes	Lu 2009
KO	Parkin KO	_	No	No	No	No	Itier 2003 Goldberg 2003
	Pink KO	_	No	Conflicting	Conflicting	Mild	Kitada 2007 Gispert 2009
	DJ1 KO	_	Conflicting	Conflicting	Conflicting	Mild	Goldberg 2005 Rousseaux 2012

| Introduction

4.1   Neurotoxin-based model of Parkinson's disease

Administration of neurotoxic agents to inducing the degeneration of neurons is the classical approach to model PD and to reproduce pathological and behavioral changes observed in patients. The most common neurotoxins used to induce dopaminergic neurodegeneration include1-methyl-5-phenyl-1,2,4,6-tetrahydropyridine (MPTP), 6-hydroxydopamine (6-OHDA), rotenone, paraquat and maneb. A common feature of these neurotoxins is their effect on mitochondria, either by inhibiting mitochondrial complex I or by complex III, resulting in the production of ROS, which induces microglia-mediated inflammation. Alternatively, the use of lipopolysaccharides (LPS) to selectively activate microglial cells also leads to an effective degeneration of dopaminergic cells.

All of these models lead to a rapid and age-independent degeneration of dopaminergic cells in rodents over a period of a few days. Unfortunately, this rapid progression represents the major drawback in these models, known to inadequately translate neuroprotective or regenerative strategies to human patients [reviewed in (Hirsch & Hunot 2009)].

Systemic administration of MPTP

MPTP was discovered in a group of drug users having consumed synthetic meperidine contaminated with MPTP and showing a severe parkinsonism responsive to L-dopa treatment, suggesting for the first time a direct relationship between environment and PD [reviewed in (Davis et al. 1979; Langston et al. 1983)].

Toxicity of MPTP results from its lipophilicity, allowing MPTP to cross the blood-brain barrier [reviewed in (Dauer & Przedborski 2003)]. When inside the brain, MPTP is metabolized in astrocytes to an active toxic cation termed 1-methyl-4-phenylpyridinium (MPP+) which is then released into the extracellular space through the organic cation transporter 3 and taken up by dopaminergic neurons and terminals through the dopamine transporter (Cui et al. 2009). Once accumulated in dopaminergic neurons, MPP+ inhibits complex I of the mitochondrial electron transport chain, resulting in ATP depletion and increased oxidative stress (Forno et al. 1993; Dauer & Przedborski 2003).

In mice, MPTP intoxication by intraperitoneal injections leads to a specific and reproducible degeneration of the nigrostriatal dopaminergic pathway [reviewed in (Nicklas et al. 1985; Mizuno et al. 1987)]. Generally, MPTP injection in mice does not lead to the presence of intraneuronal inclusions, except in some models receiving chronically low dose of MPTP (Fornai et al. 2005). Behavioral motor deficits induced by MPTP are reversible by L-dopa or dopamine agonists (Ogawa et al. 1985; Fredriksson & Archer 1994; Rozas et al. 1998).

6-OHDA

6-OHDA is a hydroxylated derivate of dopamine that is inducing a selective degeneration of sympathetic adrenergic nerve terminals (Thoenen & Tranzer 1968; Tranzer & Thoenen 1973). The high affinity of 6-OHDA to dopaminergic and noradrenergic transporters (Luthman et al. 1989) induces an accumulation of the molecule into the neuronal cytosol and leads to an oxidative stress-related cytotoxicity (Saner & Thoenen 1971; Graham et al. 1978).

6-OHDA is usually stereotactically injected unilaterally into the substantia nigra, medial forebrain bundle, or striatum and leading to the degeneration of dopaminergic neurons within 12 hours followed by a loss of striatal terminals occurring 2 to 3 days later (Faull & Laverty 1969; Jeon et al. 1995). 6-OHDA cannot efficiently pass the blood-brain barrier, probably because of its polar structure. Therefore neurodegeneration following 6-OHDA injection lacks the progressive, age-dependent and aggregated structures typically found in PD.

Paraquat

Paraquat (N,N'-dimethyl-4-4'-bipiridinium) is a herbicide with a molecular structure similar to MPP+ (Snyder & D'Amato n.d.). Relevance of paraquat intoxication for modeling and studying PD is highlighted by several epidemiological studies, suggesting an increased risk for PD after paraquat exposure (Hertzman et al. 1990; Liou et al. 1997; Kamel et al. 2007).

The exact mechanism leading to neurotoxicity in dopaminergic neurons is not well known because despite structural similarity to MPP+, paraquat does not cross the blood-brain barrier (Shimizu et al. 2001; McCormack & Di Monte 2003) and does not bind to the dopamine transporter (Richardson et al. 2005). Paraquat is not a complex I inhibitor (Richardson et al. 2005), but leads to a strong oxidative stress consequence of its redox cycling (Day et al. 1999).

Paraquat injection leads to motor deficits and to a moderate, but specific loss of nigral dopaminergic neurons in a dose- (McCormack et al. 2002) and age- (McCormack et al. 2002; Thiruchelvam et al. 2003) dependent manner without affecting striatal dopamine levels (Thiruchelvam et al. 2000; McCormack et al. 2002). Furthermore, paraquat treatment induces a-syn positive aggregates (Manning-Bog et al. 2002; Fernagut et al. 2007).

Rotenone

Rotenone is a pesticide with a high lipophilicity, able to cross the blood-brain barrier, but also to penetrate cells without any transporter mechanism. Toxicity of rotenone is linked to its inhibition of the mitochondrial complex I.

High doses of rotenone via intravenous injections lead to widespread lesions beyond the nigrostriatal system in mice (Heikkila et al. 1984; Heikkila et al. 1985; Ferrante et al. 1997). Rotenone in low doses, via chronic intraperitoneal injections, induces a more selective nigrostriatal neurodegeneration with cytoplasmic inclusions positive for a-syn (Betarbet et al. 2000; Cannon et al. 2009).

Other nigrostriatal neurotoxic models

Other models have also been used to deplete striatal dopamine and to induce neurotoxicity in the nigrostriatal pathway such as reserpine (depletion of monoamines), α-methyl-p-tyrosine (inhibitor of tyrosine hydroxylase), amphetamine derivates (neurotoxin), isoquinoline derivates (same neurochemical properties as MPTP) and lipopolysaccharides (activation of microglia through the toll-like receptor-4 receptor). These models are not commonly used, mainly because of their non-specific effects [reviewed in detail in (Tieu 2011)].

4.2 Transgenic mouse models of Parkinson's disease

Since the discovery of familial forms of PD, pathological similarities and shared genetic backgrounds in monogenic and sporadic forms of PD suggested an excellent potential of monogenic PD animal models (Blandini & Armentero 2012).

Accordingly, the generation of animal models expressing these genes has been already expanding the comprehension of PD pathogenesis (Bezard & Przedborski 2011). The major strength of the genetic models is their association with identified potential mechanisms known to cause PD in humans (Meredith et al. 2008). But unfortunately at the present time, the major weakness of these models is their relative mild phenotype and a low dopaminergic cell loss.

4.2.1 Alpha-synuclein

To date, various a-syn transgenic mice have been developed using 1) different promoters to regulate the location of transgene overexpression, 2) different point mutations and/or truncations to modulate its aggregation. These different strategies were shown to have an important impact on the age of onset and pathology (such as motor dysfunctions and non-motor dysfunctions including gastrointestinal alterations or olfactory deficits). These models, developing usually a mild neurodegeneration, are an important tool to understand molecular mechanisms leading to *in vivo* a-syn aggregation and neurodegeneration.

Alpha-synuclein expression under the tyrosine hydroxylase promoter

Tyrosine hydroxylase (TH) promoter allows the selective expression of transgenic proteins in catecholaminergic neurons. Transgenic mice expressing a-syn under the TH promoter show a down regulation of TH expression without evidence of neuronal cell death, an increased sensitivity to MPTP toxicity as well as a specific accumulation of a-syn within dopaminergic cell bodies and in striatal terminals (Matsuoka et al. 2001; Rathke-Hartlieb et al. 2001; Maskri et al. 2004). Moreover, expression of mutant forms of a-syn leads to an exacerbated sensitivity to MPTP as well as a more pronounced age-related neuropathology when compared to wild-type a-syn (Richfield et al. 2002). Similarly, expression of a C-terminal truncated a-syn form (1-120) leads to relatively strong phenotype presenting a-syn accumulation in the substantia nigra, axonal pathology in the striatum and the olfactory bulb, reduced striatal dopamine levels and a locomotor impairment (Michell et al. 2007).

Alpha-synuclein expression under the thymus cell antigen 1 promoter

Expression of wild-type, A30P and A53T a-syn under the brain neuron specific Thy-1 promoter is sharing the formation of somatodendritic accumulations of detergent insoluble a-syn throughout the brain and the spinal cord as well as the development of a severe motor phenotype (Kahle et al. 2000; van der Putten et al. 2000; Kahle et al. 2001; Rockenstein et al. 2002). Moreover, a time dependent decrease of striatal dopaminergic content, a reduced TH expression in the striatum, movement slowness and an increased susceptibility to MPTP toxicity could also be observed (Song et al. 2004; Chesselet et al. 2012). It is interesting that expression of the murine a-syn under the Thy-1 promoter shows a phenotype similarity with expression of the human wild-type or mutant a-syn (Rieker et al. 2011).

Alpha-synuclein expression under the prion protein promoter

Similarly to the Thy-1 promoter, transgenic mice overexpressing the A53T mutated a-syn under the prion protein (PrP) promoter do not replicate the typical dopaminergic neurodegeneration observed in PD. However, these mice exhibit neurotoxic fibrillization of transgenic a-syn in the brainstem and spinal cord, inducing a fatal motor phenotype with advanced age which is responsive to dopaminergic treatment (Giasson et al. 2002; M. K. Lee et al. 2002). Mice overexpressing wild-type human a-syn or A30P mutated a-syn present a relatively similar phenotype to mice overexpressing the A53T mutated a-syn, with a milder neuronal cell loss and a later onset of motor phenotype (Gomez-Isla et al. 2003).

Alpha-synuclein expression under the platelet-derived growth factor promoter

Expression of wild-type a-syn under the CMV-enhanced human platelet-derived growth factor β chain platelet derived growth factor (CMVE-PDGFβ) promoter leads to a reduction of TH positive terminals in the striatum without a loss of dopaminergic cells in the substantia nigra. At the histological level, these mice develop electron dense inclusion bodies immunoreactive for ubiquitin and a-syn. Inclusions are localized in brain structures usually affected in PD in which amorphous non-filamentous a-syn could be detected (Masliah et al. 2000). Moreover, a lysosomal pathology (Rockenstein et al. 2005) and a reduced neurogenesis (Winner et al. 2004; Winner et al. 2008) were reported in the whole brain and the olfactory bulb respectively.

Alpha-synuclein expression under the full human *SNCA* promoter

Models based on bacterial artificial chromosome (BAC) and P1-derived artificial chromosome (PAC) technology were used to integrate the entire human *SNCA* gene to the mouse genome in order to humanized mouse (carrying the human gene but lacking the endogenous one).

Transgenic mice overexpressing wild-type, but also A30P and A53T mutated a-syn, were generated using PAC and crossed into *SNCA* KO background (Kuo et al. 2010). All lines show robust abnormalities in the enteric nerve system, but only A53T mice develop motor abnormalities, however without inclusions in the central nervous system.

Another transgenic mouse model overexpressing GFAP tagged human a-syn using BAC was created, presenting a slow aggregation of a-syn, a reduced striatal dopamine release and a modest motor and olfactory impairment (Hansen et al. 2013).

Inducible and conditional models

The molecular "switch" provided by inducible models allows the creation of tissue-specific and/or time-specific expression. Two systems have been used to control SNCA expression:

1) tet-OFF system, based on tetracycline transactivator (tTa) fusion protein, binding to DNA present on specific tetracycline repressor (TetR) sequence, (Gossen & Bujard 1992)).

2) The Cre-ER system, which is an amelioration of the Cre-loxP system. In the Cre-loxP system, Cre recombinase excises DNA sequences flanked by two loxP sequences (Sauer 1987). In Cre-ER system, Cre is fused to a modified human oestrogen receptor which control Cre activity depending of receptor ligand concentration (Feil et al. 1997).

Mice overexpressing wild-type human a-syn protein under the CaMKII promoter develop a nigral and hippocampal neuropathology, as well as cognitive and motor decline (Nuber et al. 2008). In this model, drastic decrease of the transgene expression using tet-OFF system is stopping the disease progression without reversing symptoms.

Cre-loxP based transgenic mouse models were also generated to induce specific expression of E46K, A53T or truncated 119 a-syn in nigral neurons (Daher et al. 2009). These mice do not present a dopaminergic neuronal cell loss or a-syn positive aggregates.

4.2.2   LRRK2

Familial forms of PD resulting from *LRRK2* mutations suggest that LRRK2 loss or gain of function may play an important role in neuronal degeneration. But surprisingly, LRRK2 knockout mice present an intact dopaminergic system without displaying an increased susceptibility to MPTP (Andres-Mateos et al. 2009; Hinkle et al. 2012).

Overexpression of wild-type LRRK2 in BAC transgenic mice is inducing an increased dopamine release in the striatum and a motor hyperactivity. Overexpression of the G2019S mutated protein leads to an age-dependent reduction of the striatal content without nigral cell loss (Xianting Li et al. 2010). Similarly, BAC transgenic mice overexpressing R1441G mutant LRRK2 protein are presenting an age-dependent and a progressive reduction of dopamine release as well as pathology of nigrostriatal dopaminergic projection resulting in motor-activity deficits, which could be reversed by dopaminergic agents (Li et al. 2009). Remarkably, mice overexpressing G2019S mutated LRRK2 under the CMV-enhanced human platelet-derived growth factor β chain platelet derived growth factor (CMVE-PDGFβ) develop a mild age-dependent degeneration of dopaminergic nigral neurons; and mice overexpressing R1441G mutated LRRK2 under the CMVE-PDGFβ develops a more mild motor phenotype (Ramonet et al. 2011).

4.2.3   Parkin

Familial PD forms resulting from the loss of parkin E3 ubiquitin ligase activity are highlighting the critical function of parkin in neuron survival. Accordingly, several parkin KO mice were generated, but no degeneration of nigral dopaminergic neurons was observed despite a dysregulation of the dopaminergic system (Itier et al. 2003; Goldberg et al. 2003). Parkin KO mice show a strong reduction of mitochondrial respiratory chain proteins and stress response proteins which is accompanied by the accumulation of several parkin substrates (Ko et al. 2006; Shin et al. 2011). But despite mitochondrial abnormalities present in parkin KO mice, MPTP intoxication does not acerbate neuronal toxicity in these animals, whereas parkin overexpression provides a protection against MPTP (Perez et al. 2005; Paterna et al. 2007; Thomas et al. 2007).

BAC mice expressing C-terminal truncated human mutant *PARK2* (Parkin-Q311X) via the murine dopaminergic transporter promoter (Slc6a3) exhibit an age-dependent degeneration of nigral dopaminergic neurons accompanied by dopaminergic loss in striatum, formation of a-syn positive inclusions, and development of a progressive motor deficit (Lu et al. 2009).

4.2.4   *Pink1*

PINK1 loss of function mutations are leading to autosomal recessive PD. However, PINK1 KO mice do not exhibit major abnormalities except a mild mitochondrial and nigrostriatal neurotransmission deficit (Kitada et al. 2007; Gispert et al. 2009). PINK1 KO mice show also an increased susceptibility to oxidative stress and ROS production (Gautier et al. 2008).

4.2.5   *DJ-1*

Heritable PD forms resulting from mutations impairing DJ-1 function also lead to a higher neuronal sensibility to oxidative stress. Similarly to parkin and to PINK1 KO mice, DJ-1 KO mice also develop a mild dopamine neurotransmission deficit and mitochondrial dysfunction without nigral dopaminergic neuron loss (Goldberg et al. 2005).

Consistent with its protective role against stress, dopaminergic neurons with DJ-1 deletion are presenting an increased susceptibility for MPTP and 6-OHDA (Kim et al. 2005; Lev et al. 2013). Recently, a novel DJ-1 KO was generated showing a dramatic early-onset loss of nigral dopaminergic neurons and an age-dependent mild motor behavior (Rousseaux et al. 2012).

4.3   Viral transfection

Generation of animal models using viral vectors offer various advantages, they are an easier and also faster alternative to KO and transgenic approach, and they do not present developmental morbidity. Unfortunately, viral vector injection leads to a limited expression in time but also in space.

The most striking difference between transgenic and viral models is the strongest neurodegeneration observed in viral induced models of PD (Kirik et al. 2002; Kirik et al. 2003). This suggests that the viral vector procedure is inducing a typical inflammatory response that may synergize with the effect of the misfolded protein and promotes neurodegeneration [reviewed extensively in (Löw & Aebischer 2012)].

4.3.1   *Alpha-synuclein*

PD mouse models generated by using viral a-syn expression are presenting a slower and a milder dopaminergic neuronal cell degeneration than rat models. Therefore, a large number of rat models overexpressing human or rat a-syn, with a large panel of mutations or of post transcriptional modifications were generated [reviewed in (Löw & Aebischer 2012)].

Despite this limitation, lentivirus-mediated overexpression of human A30P mutant a-syn in the mouse substantia nigra under hCMV promoter results in a 10–25% loss of dopaminergic neurons. Dystrophic morphology of striatal neurons and presence of inclusions was observed 10 to 12 months after viral injections (Lauwers et al. 2003).

AAV2/2 overexpression of wild-type human a-syn using CBA promoter and directly injected in the substantia nigra resulted in a 25% nigral dopaminergic neuronal cell loss 24 weeks after injection, accompanied by a decreased density of dopaminergic fibers in the striatum, but without a-syn positive inclusions (St Martin et al. 2007).

4.3.2 LRRK2 models

To reproduce LRRK-2 linked PD in mice, herpes simplex virus was used to deliver wild-type, G2019S, D1994A (kinase dead) or G2019S/D1994A LRRK-2 under the immediate-early gene 4/5 promoter (Lee et al. 2010). Expression of LRRK-2 G2019S is inducing a 50% loss of nigral dopaminergic neurons, whereas wild-type, D1994A or EGFP expressing viruses caused a 20% cell loss and suggesting that pathogenesis of LRRK2 is likely to result from aberrant kinase activity.

5) Alpha-synuclein

5.1 Discovery

The synuclein protein family was discovered in a screening performed in electromotor nuclei of the Torpedo californica stingray by using an antiserum against cholinergic vesicles and by expressing vector cDNA library from the isolated mRNA (Maroteaux et al. 1988). Synuclein's name reflects the original observation of the protein's nuclear envelope localization in neurons as well as at presynaptic nerve terminals. Different synuclein isoforms were first reported in the rat brain after the discovery that the synuclein gene hybridizes to several clones in a rat brain cDNA library (Maroteaux & Scheller 1991). The alpha isoform was purified later from amyloid depositions isolated from Alzheimer's disease patients and termed non-amyloid β component precursor (NACP); this study involved for the first time the synuclein family in the neurodegenerative disease process (Uéda et al. 1993). In the meantime, beta-synuclein was purified in a screening aiming to characterize specific brain proteins and their function based on their structure. Synuclein was isolated from bovine brain as a phosphorylated 14 kDa protein and designated as phosphoneuroprotein 14 (PNP 14) (Nakajo et al. 1990; Nakajo et al. 1993). NACP and phosphoneuroprotein 14 become respectively alpha-synuclein and beta-synuclein based on their amino acid sequence homology revealed by monoclonal homology affinity (Jakes et al. 1994). The third and last synuclein member, gamma-synuclein, was discovered independently by several laboratories several years later during the study of different forms of cancer, neurodegenerative disorder or ocular pathology (Ji et al. 1997; Lavedan et al. 1998; Buchman et al. 1998; Surguchov et al. 1999).

PD and a-syn were associated after the discovery of different *SNCA* genetic defects leading to familial forms of parkinsonism (Polymeropoulos et al. 1997), including *SNCA* single-nucleotide polymorphisms enhancing the propensity of a-syn to aggregate (Conway et al. 1998) as well as *SNCA* multiplication resulting in increased expression and accumulation of a-syn (Singleton et al. 2003). The importance of a-syn was confirmed by the observation that it is a major constituent of LBs (Spillantini et al. 1997), becoming rapidly the hallmark of PD despite that the mechanisms underlying a-syn-dependent LB formation are still elusive.

5.2 Expression

SNCA maps to chromosome 4q21.3-q22 (Campion et al. 1995; Chen et al. 1995; Shibasaki et al. 1995). Its expression was shown to be increased by nerve growth factor (NGF) or basic fibroblast growth factor (bFGF) via the MAP/ERK and PI3 kinase pathway (Clough & Stefanis 2007) and to be decreased by poly-ADP-ribose transferase/polymerase-1 (PARP-1) (Chiba-Falek et al. 2005).

The a-syn protein is expressed in the central nervous system and in numerous neuronal cells of the peripheral nervous systems. Lower concentrations of a-syn are also detectable in various peripheral tissues including adult heart, lungs, kidneys, skeletal muscles, pancreas, liver or red blood cells (Ltic et al. 2004; Barbour et al. 2008). It is interesting to note that a-syn amounts are elevated when compared to the pool of soluble proteins in adult brain [up to 0.1% of total brain proteins] (Shibayama-Imazu et al. 1993).

Originally, a-syn was described in most nerve cells of the human nervous system, with highest concentration at synaptic terminals and nucleus (Jakes et al. 1994; Uéda et al. 1994; Iwai et al. 1995; Irizarry et al. 1996). Detailed localization studies suggest a greater presence of a-syn in nerve terminals rather than in the cell body, and more precisely in dendrites and extrasynaptic sites along the axon (Mori et al. 2002). Presence of a-syn in cell nucleus has been confirmed (McLean et al. 2000; Mori et al. 2002; Gonçalves & Outeiro 2013). However, as the size of a-syn is lower than the molecular weight cut-off of the nuclear pore (at around 40 kDa) it is likely that a-syn enters the nucleus based on simple diffusion [suggested in (Kontopoulos et al. 2006)].

Within the cell, a-syn is commonly reported to be distributed between soluble and vesicle-bound pools (Maroteaux & Scheller 1991). However, high mobility of a-syn and its weak association with synaptic vesicles suggest that the disruption of a-syn binding to synaptic vesicles may occur during biochemical procedures. Therefore, the amount of soluble forms usually measured may be artificially increased. Furthermore, the absence of intravesicular a-syn suggests a dynamic function of a-syn at the surface of vesicles (Shibayama-Imazu et al. 1993).

5.3 Structure

The a-syn protein is 140 amino acids long and unusually well conserved among vertebrates [reviewed in (Clayton & George 1998)]. Human and mouse a-syn are highly identical and differ only of seven amino acids in their whole sequence: A53T, S87N, L100M, N103G, A107V, D121G, and N122S. Interestingly, the threonine 53 in murine a-syn is a mutation observed in a familial form of PD (Polymeropoulos et al. 1997), and asparagine 87 in mice prevents the phosphorylation found at serine 87 in humans.

Three different domains were identified on a-syn:

(1) The positively charged N-terminus (residues 1–64) contains repeats of 11 residues (XKTKEGVXXXX) including 7 imperfectly repeated hexamer (KTKEGV) motifs. This domain forms 5 amphipathic helices similar to apolipoproteins, and plays an important role in lipid binding (Segrest et al. 1992; George et al. 1995; Davidson et al. 1998). The N-terminal part contains all mutations known to lead to autosomal dominant forms of PD (A30P, E46K, H50Q, G51D, and A53T).

(2) The non-amyloid beta component domain (residues 65–90), abbreviated NAC, is the most hydrophobic portion of the protein and is critical for the aggregation of a-syn (Yoshimoto et al. 1995; Bodles et al. 2001; Lin et al. 2006). The NAC domain enables a-syn to form beta-sheet structures and furthermore to form amyloid-like protofibrils and fibrils (Giasson et al. 2001; el-Agnaf & Irvine 2002).

| Introduction

(3) The less conserved and ordered C-terminus (residues 91–140), generally exhibiting an acidic nature due to glutamate residues, is proposed to regulate amyloid aggregation (I. V. J. Murray et al. 2003). This domain is relatively resistant to proteolytic degradation (Kim et al. 2006; de Laureto et al. 2006) and is also important for the chaperone-like activity of a-syn (Souza, Giasson, Lee, et al. 2000).

Interestingly, the structure of the three isoforms of synuclein is relatively similar (Fig. 1-08). Beta-synuclein is lacking one third of the NAC domain and gamma-synuclein C-terminus is shorter than in the other isoforms. These slight modifications result in a quasi-absence of amyloid fibril formation by beta-synuclein and in a strong reduction of amyloid fibril formation of gamma-synuclein; moreover, presence of one of these isoforms inhibits a-syn fibril formation *in vitro* (Uversky, Li, et al. 2002).

SNCA is composed of six exons but only the five last are translated. Three isoforms were described: a-syn140 the longest isoform, and two splicing variants a-syn126 and a-syn112 [(Fig. 1-09) and reviewed in detail in (Beyer 2006)].
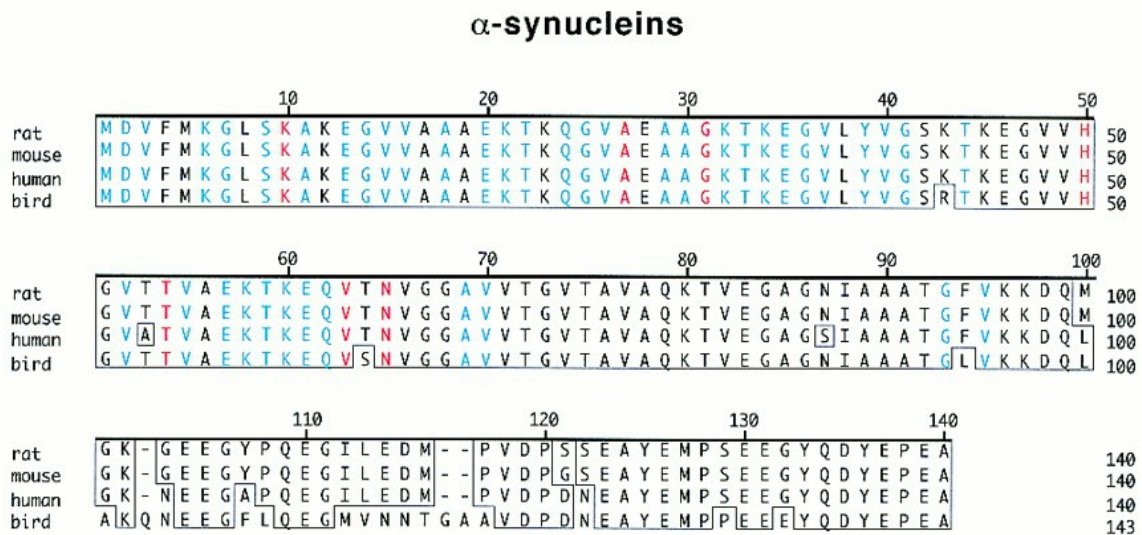
Figure 1-08: Alignment of alpha-synuclein

Figure modified from (Lavedan 1998)

Alignment of the a-syn proteins by species using the human protein as reference. Residues conserved in all three classes of synuclein proteins throughout the species are shown in blue. Residues specific to a particular class of synuclein proteins are marked in red.
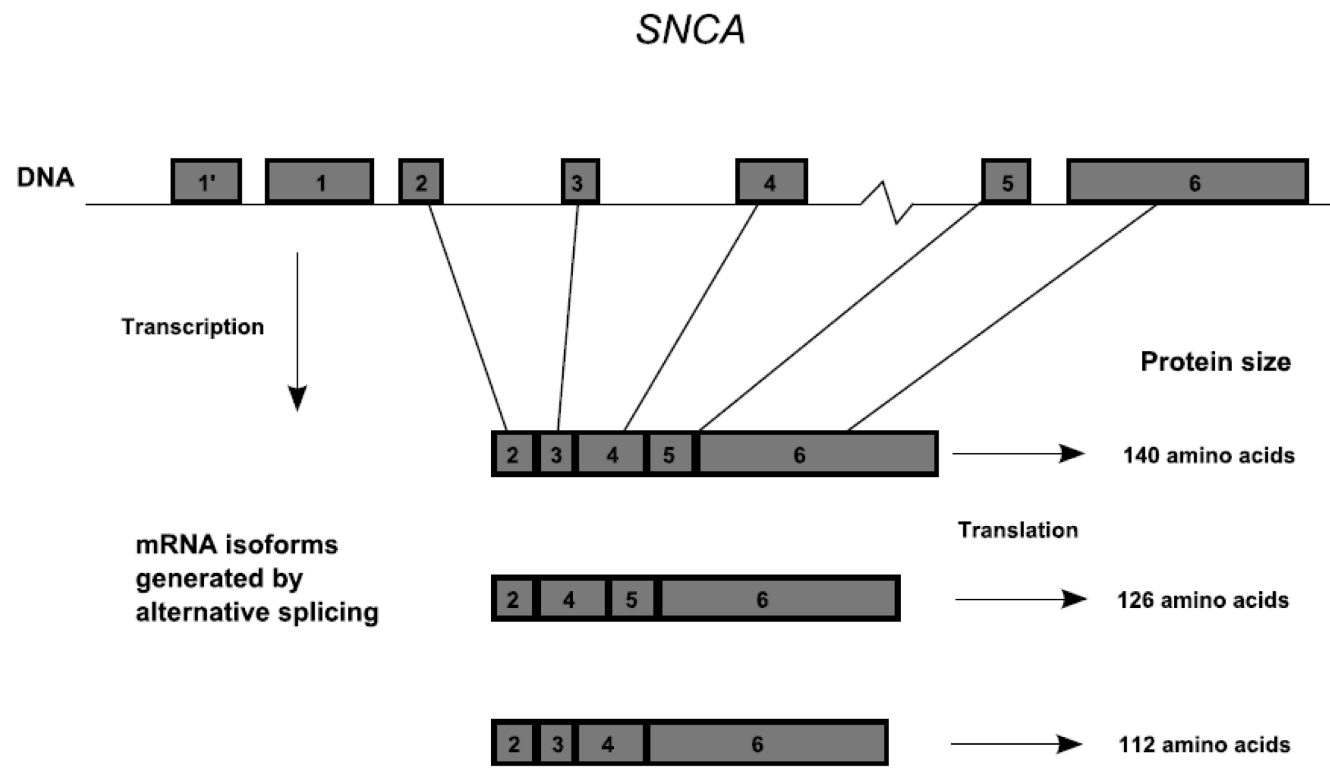
Figure 1-09: Alpha-synuclein isoforms

Figure modified from (Pihlstrøm & Toft 2011)

Representation of a-syn isoforms. Isoform a-syn126 results from the in-frame deletion of the exon 3 from the amino acids 41–53 located in the N-terminal of a-syn. Isoform a-syn112 results from an in-frame deletion of the amino acids 103–140 in exon 5 located in the C-terminal of a-syn.

5.4 Conformation

Monomeric a-syn is reported to exist in two different fractions: 1) bound to plasma membranes or vesicles, involving an alpha-helix composed of the 11-residue imperfect repeats distributed among the N-terminal and the NAC domain regions (Davidson et al. 1998; Eliezer et al. 2001) and 2) soluble in the cytoplasm as an intrinsically disordered protein potentially allowing the formation of more ordered structures due to its dynamic and flexible conformation (Weinreb et al. 1996; Eliezer et al. 2001).

Several long-range interactions within the a-syn protein were reported including 1) C-terminus interaction with the NAC domain (Bernadó et al. 2005), 2) N-terminal interaction with the NAC domain (Wu et al. 2009), and 3) C-terminal region interaction with the N-terminus (Ullman et al. 2011). Long-range interactions between NAC domain and protein termini have been suggested to protect the NAC domain from other interactions, thereby minimizing a-syn (Bertoncini et al. 2005; Bernadó et al. 2005; Wu et al. 2009), however long-range contacts between the N- and C-termini were also suggested to place the NAC domain in a more solvent exposed conformation (Ullman et al. 2011). Consequently, the potential role of a-syn long-range interactions to regulate a-syn aggregation is not clear.

| Introduction

As a natively unfolded protein, a-syn was shown to be able to adopt a large variety of conformers (Fig. 1-10), including monomers, oligomers, spherical and linear protofibrils, and fibrils [reviewed in (Bendor et al. 2013)]. Therefore, a model of a-syn aggregation kinetics was proposed based on a nucleation dependent polymerization mechanism [reviewed in detail in (Lashuel et al. 2012)]. This mechanism consists of an initial lag phase (nucleation) followed by a growth phase (elongation) until a thermodynamic equilibrium between aggregates and monomers is reached.
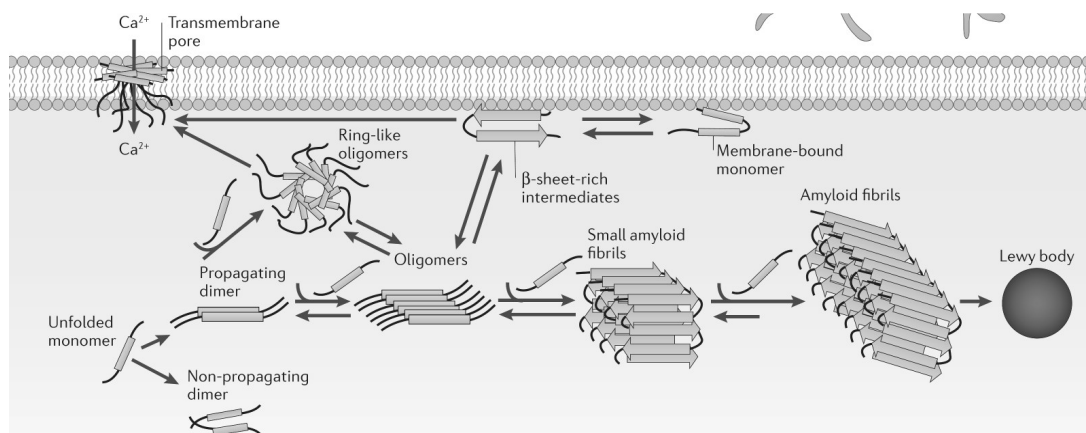
Figure 1-10: Mechanisms of alpha-synuclein aggregation

Figure modified from (Lashuel et al. 2012)

Aggregation of a-syn is taking place either in the cytoplasm or associated with the cellular membrane. In the cytosol, unfolded a-syn monomers form unstable dimers and slowly grow to generate oligomers of varying morphologies that eventually convert to fibrils. Oligomers of a-syn are following equilibrium with monomers and are converted to fibrils by monomer addition via a nucleated polymerization mechanism. Accumulation of amyloid a-syn fibrils leads to the formation of LBs. Monomeric a-syn bound to the membrane is adopting predominantly an alpha-helical conformation, but high concentrations of a-syn undergo a conformational change to form membrane-bound beta-sheet rich structures self-associating to oligomers, including trans-membrane amyloid pores and fibrils.

5.5 Functions

Despite numerous efforts to understand the normal function of a-syn, many hypotheses have been suggested but none have been generally accepted [schematized in Fig. 1-11 and reviewed in (Bendor et al. 2013)]. A role in presynaptic function is suggested by its purification from cholinergic vesicles (Maroteaux et al. 1988), its abundance in presynaptic terminals (Kahle et al. 2000) and a high association mobility to presynaptic vesicles depending on neuronal activity (Fortin et al. 2005). Interestingly, the overexpression of a-syn is impairing synaptic vesicle exocytosis and leads to a reduction of neurotransmitter release (Yavich et al. 2004; Larsen et al. 2006; Scott et al. 2010). Moreover, a-syn knockout mice present an impaired refilling and trafficking of synaptic vesicles confirming a role of a-syn in neurotransmitter release (Abeliovich et al. 2000; Cabin et al. 2002). Therefore, a-syn may play a role in synaptic function [reviewed in (Chua & Tang 2011; Bendor et al. 2013)] and more precisely in synaptic vesicle pool size regulation in mature neurons (Murphy et al. 2000) or in synaptic vesicle mobilization at nerve terminals (Cabin et al. 2002; Larsen et al. 2006).
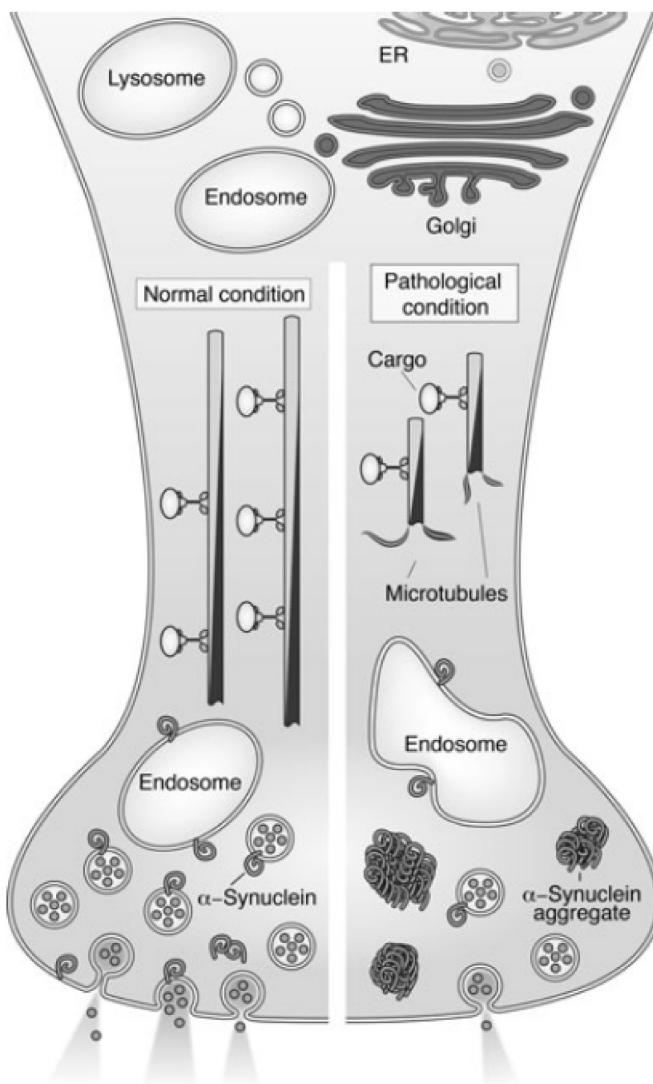
Figure 1-11: Alpha-synuclein functions

Figure modified from (Eisbach & Outeiro 2013)

*Under normal homeostatic conditions, native a-syn species play a role in axonal trafficking and vesicle formation. Several discrete trafficking steps are impaired in synucleinopathies including **1)** Golgi fragmentation, probably resulting from the inhibition of ER-to-Golgi trafficking and impairing transport of newly synthesized proteins inside the cell, **2)** impairment of axonal transport (and especially microtubule-dependent trafficking), impairing proteins transport, vesicle pool size, and cell shape integrity, and **3)** disturbance of SNARE complexes impairing vesicle endo- and exocytosis.*

The a-syn chaperone-like activity was shown to play an important role in assembly, maintenance and distribution of the presynaptic SNARE (sensitive factor attachment protein receptor) complex (Chandra et al. 2005; Burré et al. 2010). SNARE is a large protein family required for facilitating membrane fusion events-like neurotransmission [reviewed in (Südhof & Rizo 2011)]. Accordingly, the binding of a-syn to VAMP2 (vesicle-associated membrane protein 2) was shown to drive vesicle fusion with plasma membrane and is implicated in the release of neurotransmitters including dopamine (Chandra et al. 2004; Burré et al. 2010). Additionally, a-syn was shown to protect nerve terminals by enhancing SNARE proteins cooperation with CSPα, a synaptic vesicle protein acting as a co-chaperone, essential for neurotransmitter release (Chandra et al. 2005).

Furthermore, the interactions of a-syn with several other non-SNARE proteins reinforce its important role in vesicle endocytosis or exocytosis [reviewed in (Chua & Tang 2011)]. For example, a-syn interacts with phospholipase D2 (PSD2) and reduces its activity [(Jenco et al. 1998; Ahn et al. 2002) reviewed in (Bendor et al. 2013)] leading to a decreased number of endosomes and resulting in a reduced release of dopamine. Another example is the sequestration of proteins important for the transport of vesicle such as Rab GTPase [reviewed in (Eisbach & Outeiro 2013)] which can be observed in a-syn inclusions both in DLB patients and a-syn transgenic mice (Dalfó, Barrachina, et al. 2004; Dalfó, Gómez-Isla, et al. 2004). However, it is yet unclear if this dysregulation is the origin or the consequence of this impairment.

It is interesting to note that a-syn and fatty acid-binding proteins are sharing similarities in the primary structure (Sharon et al. 2001), allowing the modulation of fatty acid metabolism or transport via their binding. For example, recruitment of fatty acids from the aqueous environment to synaptic vesicles is promoted by a-syn and leads to the formation of early endosomes (Castagnet et al. 2005; Golovko et al. 2005).

Finally, a-syn was observed to directly reduce dopamine release by interfering with dopamine reuptake and synthesis in dopaminergic neurons. For example, dopaminergic transporter (DAT) was shown to be inhibited by a-syn, reducing the mediated uptake of synaptic dopamine (Sidhu et al. 2004). Moreover, the catalytic activity of tyrosine hydroxylase (TH), the rate limiting enzyme in dopamine synthesis, was shown to be regulated by a-syn phosphorylation (Perez et al. 2002; Drolet et al. 2006).

5.6 Toxicity

The discovery of fibrillar a-syn structures in LBs and in LNs (Spillantini et al. 1998; Trojanowski & Lee 1998) suggested a potential neurotoxic role of these specific a-syn aggregate species (Hashimoto et al. 1998; Conway et al. 1998; Giasson 1999). Nowadays, this hypothesis is challenged by multiple studies reporting that toxic forms of soluble a-syn drive oxidative damage [reviewed in (Lotharius & Brundin 2002a)], proteolysis [reviewed in (Ebrahimi-Fakhari et al. 2012)] and vesicle transport impairment [reviewed in (Cheng et al. 2011)], and thus relaying a-syn aggregation to a potential consequence of a-syn toxicity.

5.6.1   Conformational gain of function

The toxicity of LBs in PD is a highly debated topic, the propensity of a-syn to form structured species (Hashimoto et al. 1998) as well as the presence of a-syn filamentous inclusions in LBs (Spillantini et al. 1997) has generated a strong interest on highly ordered a-syn species and on mechanisms involved in the generation of these structures (Conway et al. 1998; Giasson 1999). Intense efforts spent in studying the formation and the toxicity of highly ordered a-syn species highlighted complex and divergent mechanisms leading to neuron dysregulation but not always to a direct cell toxicity [reviewed in (Bendor et al. 2013)]. The most common observation is the strong tendency of a-syn to aggregate spontaneously (Hashimoto et al. 1998) leading to the formation of various higher structured species, including oligomers, protofibrils and fibrils (Fink 2006). Interestingly, only small oligomers (Lashuel et al. 2002) and protofibrils (Bucciantini et al. 2002) were reported to induce toxicity.

It is important to note that many parameters were shown to modulate a-syn fibril formation: 1) *in vitro* culture parameters, such as low pH, high temperature, presence of detergents/organic solvents/metal ions (Hashimoto et al. 1999), and concentration of fatty acids (Perrin et al. 2001; Sharon et al. 2003; Karube et al. 2008); 2) presence of beta- or gamma-synuclein, (Uversky, Li, et al. 2002), a-syn concentration, a-syn species (such as oligomers, fibrils), missense mutations (Conway et al. 1998; El-Agnaf et al. 1998; Conway et al. 2000), post-translational modifications (such as phosphorylation (Fujiwara et al. 2002; Sato et al. 2013) or ubiquitination (Nonaka et al. 2005)); and 3) cellular stress such as oxidative stress (Hashimoto et al. 1999) and proteolysis (Crowther et al. 1998; Serpell et al. 2000; I. V. J. Murray et al. 2003; Dufty et al. 2007).

Oligomers

Oligomers are complex structures abundantly found in the cell and composed of identical (termed homo-oligomeric proteins) or different polypeptide chains (termed hetero-oligomeric proteins). Most proteins have the potential to form oligomers (Klotz et al. 1970). It has been suggested that protein oligomerization may be an advantageous feature from the perspective of protein evolution (Ali & Imperiali 2005), leading to a subtle control of protein functions via allosteric regulation or via complex formation [reviewed in (Hlavacek et al. 2003)].

The exact purpose of oligomerization has not been established for numerous proteins, consequence of the complexity of oligomer structures. To illustrate this complexity, numerous oligomerization analyzes have shown a critical role of pH, ionic strength, protein constituent and their respective concentration levels on their formation mechanisms. These parameters do not only vary between different cell types, but also locally within the cell and its compartments. Even within the same protein family, different members can exhibit different oligomeric properties (Weitzman & Kinghorn 1978). Fortunately, most prevalent oligomers are rather small homo-oligomer (Jones & Thornton 1996; Goodsell & Olson 2000) which can be classified by their subunit type, subunit association kinetics and folding resulting from subunit associations.

Most interestingly, the assembly formation and folding of oligomers allow the prediction and modeling of polypeptide interactions (Chothia & Janin 1975). These analysis highlighted the fundamental differences between 'transient' oligomers (equilibrium based on kinetic) and 'permanent' oligomers (single unstable proteins without formation of a stable oligomer structure) (Nooren & Thornton 2003).

Very little is known about the conformational state(s) of a-syn in the different compartments of the living cell. Classically, a-syn extracted from biological samples migrates as a 14 kDa protein in denaturing gels, and as a 57–60 kDa protein when evaluated by non-denaturing gels or size exclusion chromatography columns (El-Agnaf et al. 1998; Luk et al. 2009). These data suggest the possible formation of a-syn tetramers as a native equilibrium between different conformational and/or oligomeric states of a-syn. This hypothesis is highly controversial [reviewed in (Lashuel et al. 2012)] as a-syn has a natively unfolded conformation (Weinreb et al. 1996; Fauvet et al. 2012) which may impact the measurement of its molecular weight.

However, detergent resistant a-syn oligomers are a consistent pathological hallmark of PD (Campbell et al. 2001; Pountney et al. 2005) which could be easily isolated from *post mortem* brain of PD patients (Sharon et al. 2003). In general, SDS resistant oligomers can be divided into small (~2–5 mers), medium (~5–15 mers), and large (~15–150 mers) oligomers (Danzer et al. 2007; Cremades et al. 2012), with the smallest oligomers promoting neuronal degeneration and abnormal calcium currents when added to cultured primary cortical neurons (Danzer et al. 2007). Interestingly, a-syn oligomers may acquire spherical, chain-like, or annular morphologies depending on the *in vitro* conditions and the presence of a-syn mutations (Conway et al. 2000; Ding et al. 2002; Lashuel et al. 2002). Altogether, it is clear that a-syn exists as a monomer without excluding the possibility that it can form stable multimers and/or adopt different structures *in vivo*.

Protofilaments

Experimentally, a-syn molecular crowding *in vitro* was shown to lead to an equilibrium between a-syn monomers and various oligomeric species, resulting in a slow fibrils formation via metastable oligomeric species such as protofibrils (Volles & Lansbury 2002). Accordingly, the existence of a critical a-syn concentration range, in which protofibrils but not fibrils can be formed, confirms the role of a-syn oligomers and protofibril intermediates in the formation of fibrils (Volles & Lansbury 2002). During this assembly, major conformational changes of a-syn are observed and especially in its secondary structure. Most noticeable is the decrease of the helical content resulting from the conversion of spheroidal oligomers (with high helical content) (Apetri et al. 2006) to protofibrils (mainly cross-beta sheet) (Serpell et al. 2000).

It is tempting to speculate that oligomers may contribute to cell toxicity at an early aggregation point whereas fibrillar and amorphous insoluble a-syn aggregates contribute only later to synucleinopathy (Ding et al. 2002).

5.6.2 *Mechanisms of toxicity*

Mechanisms leading to cell toxicity are a complex issue. For example, it may seem obvious that aggregation leads to toxicity via the capture of a-syn and results in decreased levels of native a-syn. However, it is rather unlikely that a lack of a-syn drives the toxic mechanism since a-syn KO mice show a rather increased than decreased resistance to MPTP-induced loss of dopaminergic neurons (Dauer et al. 2002).

Permeabilization of membranes

The formation of oligomers has been shown to increase synthetic lipid vesicle leaking (Volles & Lansbury 2002) and therefore might cause damage to cellular membranes *in vivo* by altering the balance of ions within the cells, thus triggering apoptosis (Danzer et al. 2007).

It has been suggested that a-syn could fold into the membrane structure via anti-parallel arranged alpha-helicoidal regions, able to form pores and permeabilize membranes (Volles & Lansbury 2002). Another hypothesis suggests the capture of some phospholipids by folded a-syn structures on the membrane surface which can induce membrane disruption (Comellas et al. 2012). Protofibrils were also shown to exert a similar toxicity, forming amyloid pores resembling to beta-sheet pore-forming toxins (Varkey et al. 2013).

It is unclear if and how membranes influence the conformation and oligomerization of a-syn in cells. This is illustrated on the one hand by the description that a-syn oligomers form helical conformation on membranes (Ding et al. 2002) and on the other by anionic phospholipid membranes converting helical a-syn into fibrils (Furukawa et al. 2006).

Finally, it was also observed that a-syn-related pathology could result from defective vesicle secretion and recycling (Unni et al. 2010). This hypothesis is confirmed in cell models overexpressing a-syn, in which dopamine release is inhibited while an increase of the number of vesicles docked to the plasma membrane is observed (Larsen et al. 2006). Accordingly, animals overexpressing a-syn present abnormal vesicle clustering as well as unusual non-uniform vesicle sizes (Nemani et al. 2010; Scott et al. 2010).

Dopamine toxic effect

In cell culture, endogenous dopamine production was shown to acerbate drastically a-syn associated toxicity (Conway et al. 2001). This critical role of dopamine was shown to be indirect and to require oxidative stress conditions facilitating dopamine (and other catecholamines) conversion to highly reactive metabolites, such as dopamine quinones (Cadet & Brannock 1998). When reactive dopaminergic metabolite levels exceed the anti-oxidative buffering capacity of neurons, these species can bind covalently to proteins. *In vivo*, dopamine quinones block a-syn fibril formation, stabilizing toxic a-syn protofibrils at the expense of fibrils (Xu et al. 2002; Petrucelli et al. 2002).

As suggested previously, a possible role of a-syn on vesicles clustering and on permeabilization of membranes (Scott et al. 2010; Nemani et al. 2010; Lundblad et al. 2012) is supported by the localization of oligomers in axons and presynaptic terminals. Therefore, it is likely that a-syn leads to an improper sequestration of dopamine into vesicles (Lotharius & Brundin 2002a) explaining the vicious cycle resulting in the higher sensitivity of dopaminergic neurons to a-syn toxicity.

Transport mechanism disruption

As described previously, the formation of LNs preceding the development of LBs (Eisbach & Outeiro 2013) suggests an early accumulation of a-syn in axons which could result from a disrupted protein transport in neurons. Accordingly, a-syn was reported to inhibit trafficking from the ER to the Golgi in yeast over-expressing a-syn (Jellinger 2003; Jellinger 2004; Dickson et al. 2010), probably via the inhibition of docking or fusion of the ER to Golgi membranes (Cooper et al. 2006).

Thus, the disruption of the newly synthesized proteins' transport by a-syn (Gitler et al. 2008) is critical for synaptic maintenance in neurons. This is especially true in dopaminergic cells in which the dopaminergic machinery (such as the vesicular monoamine transporter) has to be delivered to synaptic sites to avoid accumulation of dopamine and its by-products. Accordingly, accumulation of dopamine in the synaptic cytoplasm was shown to result in oxidative stress (Thayanidhi et al. 2010).

| Introduction

Protein degradation impairment

Accumulation of a-syn in PD strongly suggests a dysfunction of the protein degradation system [reviewed in (Thayanidhi et al. 2010)]. Whether a-syn aggregation is the cause or the consequence is unclear but numerous reports suggest a direct role of a-syn on protein degradation impairment, for example 1) increased a-syn levels inhibit autophagy via Rab1a (Manzoni & Lewis 2013), 2) a-syn mutations associated with PD decrease lysosomal functionality and reduce the autophagic flux (Winslow et al. 2010) and 3) a-syn mutations are blocking CMA as a consequence of their strong binding to the transporter protein LAMP-2A (Cuervo et al. 2004).

Furthermore, a-syn may itself play an important role in protein degradation. Previous observations pointed to the role of a-syn in the SNARE function which are required for the regulation of vesicle trafficking and fusion. Protein degradation pathways, such as autophagy, are also based on vesicle trafficking and fusion, suggesting a potential link between the physiological role of a-syn and these pathways (Burré et al. 2012).

Cells overexpressing a-syn present lysosomes containing aggregated a-syn species suggesting lysosomal dysfunctions (Gispert et al. 2009). Interestingly, accumulation of a-syn prefibrillar aggregates was shown to disrupt lysosomal activity (Krenz et al. 2009; Smith et al. 2010), initiating a vicious cycle as lysosomal degradation is critical for a-syn turn-over [a-syn degradation is described later in this thesis, and reviewed in (Stefanis et al. 2001)].

Mitochondrial impairment

The first link between high levels of a-syn and mitochondrial dysfunction was proposed soon after the discovery of a-syn's role in PD based on the observation of increased free radical levels which were suspected to trigger a-syn oxidation and aggregation (Hsu et al. 2000). Nowadays, an increasing body of evidence suggests that a-syn has a toxic effect on mitochondria [reviewed in (Mullin & Schapira 2013)]. For example, a-syn knockout mice are resistant to mitochondrial damage caused by complex I inhibitor toxins (Dauer et al. 2002; Klivenyi et al. 2006), and mice overexpressing a-syn are developing a mitochondrial pathology (Song et al. 2004; Martin et al. 2006).

Despite that a-syn is predominantly cytosolic, it has been identified to interact directly with mitochondrial membranes (Li et al. 2007; Parihar et al. 2008; Parihar et al. 2009), probably because of its mitochondria targeting sequence present on the N-terminal domain (Devi et al. 2008). The interaction between a-syn and mitochondrial membranes was shown to inhibit mitochondrial fusion, leading to their fragmentation (Kamp et al. 2010) but only under certain environmental factors (Zhu et al. 2012). Moreover, high levels of a-syn were also suggested to decrease mitochondrial protein transport via reduction of TOMM40, a translocase of the outer mitochondrial membrane (Bender et al. 2013).

Despite the excitement generated in the neurodegenerative diseases field by mitophagy, an autophagy-based mitochondrial control mechanism, (Palikaras & Tavernarakis 2012) involvement of a-syn in this process is controversial (Sampaio-Marques et al. 2012; Watanabe et al. 2012).

5.6.3   Post-translational modifications

Intensive research on a-syn has highlighted the influence of a variety of different factors on its structure. We are going to review only the main modifications of a-syn, as well as their repercussions on a-syn structure/conformation and the resulting modulation of a-syn aggregation at the morphological and kinetic level.

Serine and tyrosine phosphorylation of alpha-synuclein

The most studied modification of a-syn is certainly its phosphorylation (Stefanis 2012), probably because protein phosphorylation is one of the most common post translational modifications regulating protein function. Protein phosphorylation consists of the covalent addition of a phosphate group on a serine, threonine or a tyrosine residue by a protein kinase. The phosphorylation of a-syn was observed early in the history of a-syn discovery (Nakajo et al. 1993). Experimentally both serine and tyrosine phosphorylation of a-syn could be observed in Ser87, Ser129, Tyr125, Tyr133, and Tyr136 (Okochi et al. 2000; Pronin et al. 2000; Fujiwara et al. 2002; Negro et al. 2002). However, only a-syn phosphorylation at Ser87, Ser129, and Tyr125 sites were validated *in vivo*.

The enzymes that modulate a-syn phosphorylation have been of major interest as they may provide a potential therapeutic target [reviewed in (Braithwaite et al. 2012)]. A subset of protein kinases has been shown to phosphorylate a-syn *in vitro* and *in vivo*. Involvement of polo-like kinases (PLKs) in the phosphorylation at Ser129 (Inglis et al. 2009; Mbefo et al. 2010) has been largely demonstrated and multiple stages of a-syn aggregation have been proved to influence its phosphorylation status (Mbefo et al. 2010; Waxman & Giasson 2011). Casein kinases 1 and 2 (CK1 and CK2) have been demonstrated to phosphorylate a-syn at Ser129, and CK1 appears to phosphorylate also Ser87 *in vitro* while CK2 appears to be able to phosphorylate only soluble a-syn species (Okochi et al. 2000; Waxman & Giasson 2008; Waxman & Giasson 2011). Finally, G-protein-coupled receptor kinases can also phosphorylate a-syn at the Ser129 residue (Pronin et al. 2000; Sakamoto et al. 2009).

A possible interplay between a-syn and LRRK2 was suggested [reviewed in (Cookson 2010)], and illustrated by LRRK2 presence in LBs (Alegre-Abarrategui et al. 2008). But unfortunately the exact role of LRRK2 in synucleinopathy remains controversial as illustrated by *in vivo* studies showing conflicting modulation of synucleinopathy by LRRK2 in mouse models (Lin et al. 2009; Daher et al. 2012). In this unclear context, a direct phosphorylation of a-syn by LRRK2 was reported (Qing et al. 2009), but this effect failed to be replicated in other studies or systems.

Several phosphatases were shown to dephosphorylate a-syn *in vitro*. For example, phosphatase 2A (PP2A) dephosphorylates Ser129 (Peng et al. 2005) and was confirmed *in vivo* (Lee et al. 2011). PP2C also dephosphorylates a-syn at Ser129 (Waxman & Giasson 2008).

Tyrosine phosphorylation of a-syn has been less studied than its serine phosphorylation, phosphorylation at Tyr125 could be driven by Src and Fyn (Ellis et al. 2001; Nakamura et al. 2001), as well as by Lyn and Frg (Negro et al. 2002). Furthermore, Syk has also been shown to phosphorylate a-syn at residues Tyr125, Tyr133, and Tyr136 (Negro et al. 2002).

| Introduction

Phosphoserine 129

In *post mortem* human brain studies, a-syn present in LBs has been shown to be hyperphosphorylated at Ser129 (Fujiwara et al. 2002; Anderson et al. 2006). Moreover, this post-transcriptional modification could also be observed in pre-LB stages (including Lewy threads and axons) and seems to progress with advancing disease (Saito et al. 2003). Additionally, transgenic mice overexpressing a-syn (Wakamatsu et al. 2007; Schell et al. 2009; Lee et al. 2011) also present accumulation of Ser129 phosphorylated a-syn (pSer129), confirming that it's accumulation is a common phenomenon during the disease progression.

In vitro studies have suggested that pSer129 a-syn promotes formation of a-syn filaments and oligomers (Fujiwara et al. 2002) as a consequence of change in charge distribution and hydrophobicity in the protein's carboxy-terminal region (McLean & Hyman 2002). But as the levels of pSer129 are not very high in the neuronal cytosol of PD brain samples, it was suggested that a-syn may be phosphorylated after its deposition into LB (Anderson et al. 2006). This hypothesis is supported by the abundant presence of proteinase K resistant pSer129 a-syn in cytoplasmic inclusions but not in presynaptic inclusions (Tanji et al. 2010).

The investigation of pSer129's role in synucleinopathy development is a challenging process as it is technically impossible to track pSer129 levels in brain of PD patients and even difficult to localize and quantify it in living animal models. Therefore, most of studies relied on chromatography and specific antibodies for phosphorylated (Fujiwara et al. 2002; Saito et al. 2003) or unphosphorylated forms of a-syn (Lee et al. 2013) to investigate distribution and levels of pSer129 either *in vitro*, in blood or in *post mortem* tissues. Interestingly, expression of phospho-mimic such as [S129D] a-syn in cell and fly models leads to an enhanced aggregation and cytotoxicity (Smith et al. 2005; Chen & Feany 2005) despite a decreased fibrillation of [S129D] a-syn *in vitro* (Paleologou et al. 2008). Similarly, expression of non-phosphorylable [S129A] a-syn does not present more toxicity than wild-type a-syn *in vivo* (Gorbatyuk et al. 2008; Azeredo da Silveira et al. 2009). However, even if these strategies are debatable (as phospho-mimics [S129E/D] a-syn) were shown to poorly reproduce the effect of phosphorylation on the structural and aggregation properties of a-syn *in vitro)*, and the cellular defense mechanism reported is questioning pSer129's role in synucleinopathy development.

Accordingly, phosphorylation of a-syn reduces its phospholipid-binding properties, suggesting its involvement in the regulation of a-syn binding to synaptic vesicle membranes [reviewed in (Lotharius & Brundin 2002a; Lotharius & Brundin 2002b)]. Furthermore, the phosphorylation of a-syn is inhibiting phospholipase D2 (PLD2) (Pronin et al. 2000; Payton et al. 2004), an enzyme involved in lipid-mediated signaling cascades and vesicle trafficking. However, PLD2 mechanisms and functions are still unclear. Therefore a direct link between a-syn phosphorylation and dysregulation of dopamine neurotransmission is still hypothetical.

Phosphoserine 87

Phosphorylation of a-syn Ser87 (pSer87 a-syn) is one of the few differences between the human and the mouse a-syn and might carry an important function in the development of synucleinopathy present in human, but not in mouse.

Ser87 is located in the hydrophobic NAC region of a-syn, expanding its hydrophobic structure, increasing its conformational flexibility, blocking its fibrillization *in vitro* and reducing its binding to membranes (Paleologou et al. 2010). An increasing body of evidence suggests that pSer87 a-syn may also play an important role in the regulation of synucleinopathies, as suggested by the presence of pSer87 a-syn in LBs (Paleologou et al. 2010). Interestingly, rat injected with adenovirus expressing phospho-deficient [S87A] a-syn were showing a synucleinopathy similar to the expression of human wildtype a-syn, but no change could be observed for phospho-mimic Ser87 [S87E] a-syn expression. This suggests that mimicking pSer87 inhibits a-syn aggregation and protects against a-syn induced toxicity *in vivo* (Oueslati et al. 2012).

Phosphotyrosine 125

As previously noticed, tyrosine phosphorylations are less studied than serine phosphorylation. However, it was shown that phosphorylated Tyr125 a-syn (pTyr125) prevents potential nitrosylation of this residue (Nakamura et al. 2002). Furthermore, the observation of Tyr125 nitration inducing the formation of a-syn oligomers (Takahashi et al. 2002) suggests a neuroprotective function of pTyr125 a-syn, especially under nitrative stress. Accordingly, decreased levels of pTyr125 a-syn could be observed during the normal aging process in humans, and notably in cortical tissue from PD patients (Chen et al. 2009).

Oxidation

Presence of nitrotyrosine immunoreactivity in LBs is reflecting an oxidative cellular injury leading to the nitration of protein tyrosine residues by peroxynitrite (Good et al. 1998), and suggesting a link between oxidative and nitrative damage and synucleinopathies (Duda et al. 2000; Giasson et al. 2000). Although mechanisms leading to a-syn oxidation are not well understood, covalent modifications of a-syn by quinones (derived from dopamine) have been observed (Conway et al. 2001), and one main nitrated residue has been identified on the Tyr125 (Giasson et al. 2000).

Nitration of a-syn has been observed robustly *in vivo* using antibodies specific for nitrated a-syn: 1) in PD patients (Giasson et al. 2000), 2) in toxin-based PD animal models (Ara et al. 1998) and 3) in transgenic mice developing PD (Neumann et al. 2002; Papay et al. 2002). Interestingly, presence of a-syn aggregates lacking nitrotyrosine immunoreactivity suggests that a-syn nitration is not required for its deposition and may occur after the fibrillization process (Gómez-Tortosa et al. 2002). Accordingly, it was observed that soluble and nitrated a-syn species do not fibrillize unless preformed fibrils are treated with nitrating agents. Fibrillization in presence of nitrated agents leads to the stabilization of nitrated fibrils through dityrosine cross-linking, resulting in the formation of SDS and heat stable dimers (Souza, Giasson, Chen, et al. 2000; Takahashi et al. 2002; Yamin et al. 2003; Hodara et al. 2004) which limits a-syn fibrillogenesis (Conway et al. 2001) and blocks a-syn folding rendering it resistant to proteasomal degradation [reviewed in (Malkus et al. 2009)].

Relevance of a-syn's methionine oxidation (four methionine residues for a-syn), reported to inhibit fibrillization of unmodified a-syn (Uversky, Yamin, et al. 2002), was challenged in a more recent study focusing on oxidative stress induced by dopamine (Norris et al. 2005).

| Introduction

Glycosylation and glycation

Glycosylation is an important protein post-translational modification, attaching enzymatically different glycans to proteins in the endoplasmic reticulum (ER) before they are targeted to their action sites [reviewed in (Moremen et al. 2012)]. Glycosylation of a-syn *in vitro* results in a 22 kDa protein (Shaikh & Nicholson 2008) mainly occurring in the Golgi apparatus (Tompkins et al. 2003) and indicating a possible processing of a-syn before its localization into the synapse and nucleus. Furthermore, *PARK2* mutations leading to autosomal recessive forms of PD present an accumulation of soluble glycosylated a-syn (Shimura et al. 2001) and the role and function of glycosylated a-syn species in idiopathic forms of PD is unclear.

Binding of a glucose molecule in a non-enzymatic manner (so called glycation) may rather result from normal metabolism, aging or oxidative stress (Ahmed 2005). Rearrangement of proteins following the binding of a glucose molecule undergoes multiple and diverse irreversible modifications such as dehydration, condensation, fragmentation, oxidation or cyclization. These reactions are leading to the disruption of the protein structure as well as to an accumulation of reactive species [reviewed in (Takeuchi & Yamagishi 2009)]. Immunoreactivity for glycated proteins was reported at the periphery of LBs (Castellani et al. 1996). Moreover, PD patients report an abnormal increase of glycated protein levels (so called advance glycation end products (AGEs)) (Dalfó et al. 2005). Glycation of a-syn *in vitro* via its 15 lysine residues leads to the formation of smaller globular-like aggregates instead of the typical fibrils formed by native a-syn, suggesting a potential role in the nucleation of aggregates (Padmaraju et al. 2011) and in the chemical crosslinking and proteolytic resistance of the protein deposits [reviewed in (Vicente Miranda & Outeiro 2010)].

Glycation of a-syn *in vitro* was also described to alter DNA integrity, probably via conformational changes of DNA stabilizing the uncoil scDNA (Padmaraju et al. 2011). As a-syn oligomers are suspected to form pores in membranes, it has been hypothesized that glycated a-syn could enter the nucleus leading to an increased oxidative stress and direct DNA damage inside the nucleus (Guerrero et al. 2013).

Ubiquitination of a-syn

Presence of ubiquitinated proteins in LBs from PD patients (Kuzuhara et al. 1988; Lennox et al. 1989; Gai et al. 1995) highlighted a potential role of ubiquitination pathways in the aggregation pathway. This hypothesis was confirmed later in LBs (Wakabayashi et al. 1997; Spillantini et al. 1997) involving single or multiple ubiquitinated lysine residues of a-syn such as ubiquitination at K12, K21 and K23 (Anderson et al. 2006) which are also found in inclusions from animal models (Hasegawa et al. 2002; Lee & Lee 2002; Giasson et al. 2002). More precisely, a-syn harbors 15 lysine residues located mostly at its N-terminus. Ubiquitination assays of soluble a-syn *in vitro* showed ubiquitination of multiple lysine residues K21, K23, K32, and K34 (and in lower extend K10, K43, K96). Interestingly, recombinant a-syn fibrils were also shown to be ubiquitinated at K6, K10 and K12 (Nonaka et al. 2005).

Ubiquitinated a-syn in LBs is predominantly phosphorylated at Ser129 but is absent in the soluble fraction in PD brain lysates despite a high levels of phosphorylated a-syn, suggesting that the observed ubiquitination may occur after the deposition of phosphorylated a-syn into LBs (Sampathu et al. 2003; Anderson et al. 2006). Another hypothesis is that N-terminus ubiquitination of a-syn stabilizes the monomeric form of the protein and thus prevents its oligomerization and fibrillogenesis *in vitro* (Oueslati et al. 2010).

Three different enzymes have been identified to play an important role in the ubiquitination of a-syn *in vitro* and *in vivo:* parkin (E3 ubiquitin ligase), UCH-L1 (deubiquitinase) and SIAH (seven in absentia homologue, E3 ubiquitin ligase) (Liani et al. 2004; Lee et al. 2008; Rott et al. 2008). It is noticeable that both, parkin and UCH-L1 were described previously to be linked genetically to familial forms of PD [reviewed in (Nuytemans et al. 2010)].

In two transgenic animal models developing a-syn pathology (drosophila (Yang et al. 2003; Haywood & Staveley 2004) and rat (Lo Bianco et al. 2004)), parkin was shown to play a protective effect without modifying a-syn levels. In transgenic mice overexpressing a-syn but lacking endogenous parkin a potential protective effect on pathology development is debated (Fournier et al. 2009; von Coelln et al. 2006). Therefore, parkin may not directly modulate a-syn levels, and its protective role in a-syn deposition *in vivo* need to be resolved.

In cell culture, endogenous SIAH colocalizes with a-syn and is, in part, responsible for its mono- and di-ubiquitination (Lee et al. 2008; Rott et al. 2008). SIAH also enhances a-syn aggregation, leading to the formation of a-syn positive inclusions. These observations suggest that ubiquitination by SIAH may enhance a-syn aggregation (Rott et al. 2008).

UCH-L1 monomer catalyzes the recycling of free ubiquitin by cleaving ubiquitinated peptides produced by proteasomal degradation of polyubiquitinated proteins (Larsen et al. 1998; Ciechanover & Schwartz 1998). Unlike monomers, UCH-L1 dimers display ubiquitin ligase activity that elongates K63- rather than K48-linked ubiquitin-chains (Liu et al. 2002). Therefore UCH-L1 dimers can polyubiquitinate mono- or di- but not non-ubiquitinated a-syn. It is still unclear whether S18Y mutation in UCH-L1 results in a gain or loss of function, resulting from observations of PD-related pathology in transgenic mice overexpressing the human mutated protein (Setsuie et al. 2007) and in mice naturally lacking UCH-L1 (Saigoh et al. 1999), but surprisingly not in engineered KO mouse models (Shimshek et al. 2012).

Interestingly, coexpression of ubiquitin and a-syn is reducing synucleinopathy in a fly model (Lee et al. 2009). Furthermore, this effect is driven by expression of the K48R, and not K63R ubiquitin mutants, suggesting that the ubiquitin-mediated neuroprotective effect is potentially dependent on the K48 polyubiquitin linkage, highlighting complex roles of a-syn polyubiquitination in PD.

5.6.4 *Degradation*

As a-syn accumulation have been linked to toxicity, a better understand of the degradation of a-syn in neurons may lead to the generation of novel therapeutics [schematized in Fig. 1-12 and reviewed in (Ebrahimi-Fakhari et al. 2012; Xilouri et al. 2013)]. Therefore, much effort has been applied to reduce a-syn levels by increasing its clearance using a pharmacological approach, but has resulted in a large body of controversial results.
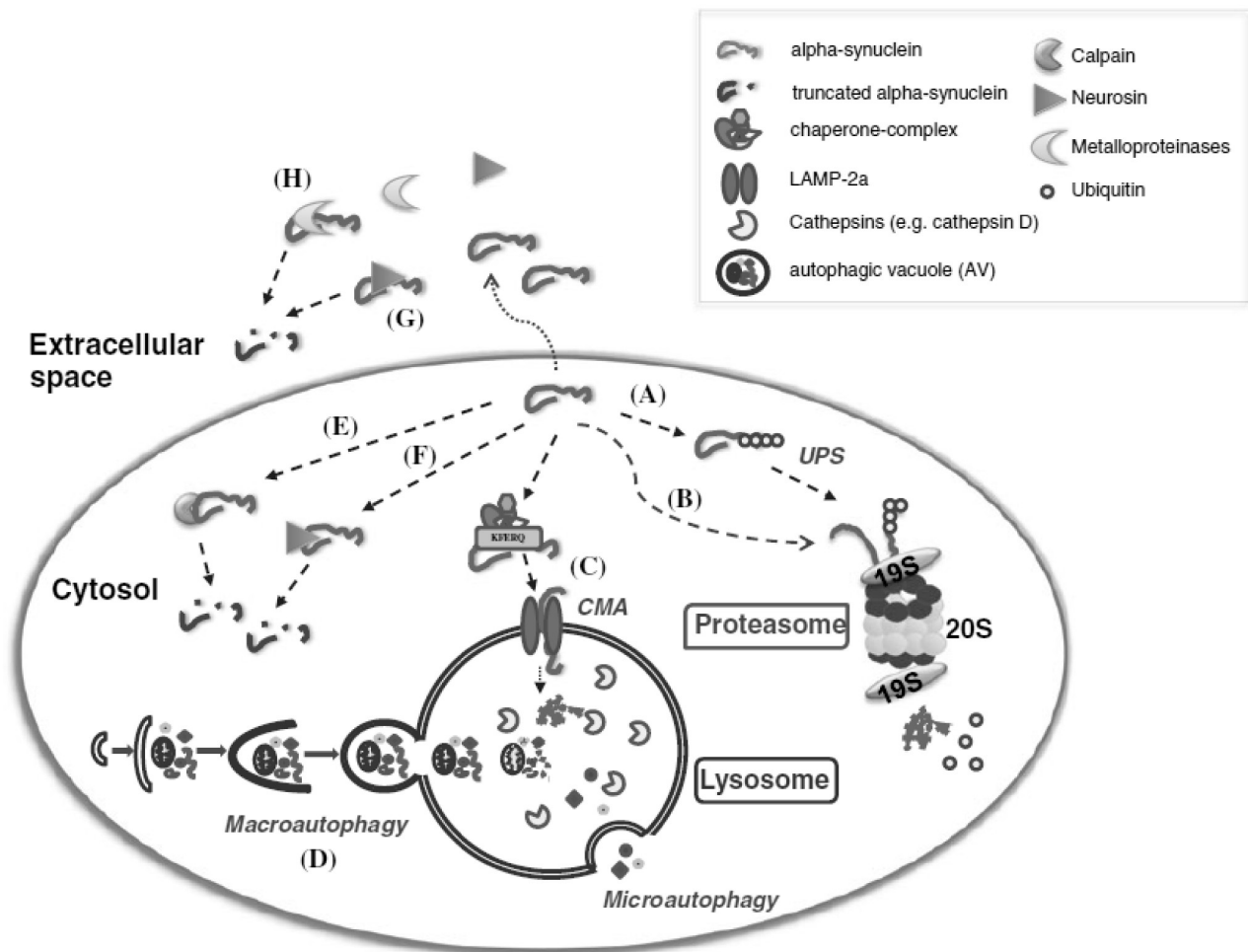
Figure 1-12: Proteolytic pathways involved in alpha-synuclein processing

Figure copied from (Xilouri et al. 2013)

*Proteasome and lysosomal pathways play a major role in the final degradation of a-syn. The ubiquitin-proteasome system (UPS) is degrading **A)** ubiquitin-tagged a-syn and **B)** non-ubiquitinated a-syn. Three different lysosomal pathways have been described to also degrade a-syn, **C)** chaperone-mediated autophagy (CMA) selectively target a-syn (presenting a KFERQ-like motif) into the lysosomes after binding to the lysosomal receptor LAMP-2A, **D)** macroautophagy sequesters intracellular constituents (including various forms of a-syn such as oligomers) by a double membrane (phagophore) that finally generates the autophagic vacuole, which then fuses with the lysosome; and microautophagy in which substrates are directly delivered into the lumen through invaginations of the lysosomal membrane. Moreover, other proteases such as **E)** calpains or **F)** neurosin have been implicated in the cleavage of normal or aggregated forms of intracellular a-syn. Interestingly, **G)** secreted neurosin and **H)** metalloproteases have been found to cleave extracellular a-syn.*

Ubiquitin-proteasome system

Despite many evidences suggesting an important role of the UPS in the degradation of a-syn, altered UPS degradation involvement in the initiation of synucleinopathy is controversial. Moreover, it is still unclear whether a-syn can modulate UPS activity.

More precisely, a general impairment of UPS is observed in PD and is reflected by a decreased proteasomal function (McNaught & Jenner 2001) as well as by a decrease of proteasomal subunit levels (McNaught, Belizaire, et al. 2002; Chu et al. 2009). Accordingly, a-syn possesses a short turn-over which is increased drastically *in vitro* by UPS inhibition (Bennett et al. 1999; Webb et al. 2003).

Accordingly, inhibition of the proteasome leads to intracellular inclusions immunoreactive for a-syn, ubiquitin and the chaperone Hsp70 in apoptotic cells (McNaught, Mytilineou, et al. 2002; Rideout & Stefanis 2002). Similarly, rodent models treated with proteasome inhibitors develop a progressive parkinsonism as well as neuronal degeneration and a-syn positive LBs in different brain regions (McNaught et al. 2004). But it is important to note that other independent studies failed to reproduce these reported effects (Bové et al. 2006; Kordower et al. 2006). Interestingly, the importance of UPS in the initiation of PD is also highlighted in a mouse model expressing a conditional deletion of the Rpt2/PSMC1 subunit (19S ATPase regulatory complex) and developing neurodegeneration as well as a-syn positive inclusion bodies (Bedford et al. 2008).

The presence of ubiquitinated a-syn inclusions is classically associated with an abnormal decrease of a-syn degradation by the UPS (Stefanis et al. 2001; Tanaka et al. 2001; Petrucelli et al. 2002). But accumulation of ubiquitinated a-syn is not invariably associated with a significant impairment of proteasome function (Tofaris et al. 2003), and correlation between the load of ubiquitinated inclusions and the degree of UPS activity is not evident (Giasson et al. 2002; Neumann et al. 2002). Accordingly, a-syn degradation by the proteasome has been shown to be independent of its monoubiquination (Rott et al. 2008) and ubiquitination in general (Tofaris et al. 2001).

In this context, cellular models have shown that expression of high levels of a-syn (or mutated a-syn forms) leads to the formation of oligomers and aggregated structures and result in proteasomal activity inhibition (Stefanis et al. 2001; Tanaka et al. 2001; Snyder et al. 2003). However this effect was not replicated *in vivo* (Dyllick-Brenzinger et al. 2010).

Autophagy

An increasing body of evidence suggests a dysfunction of ALP in brain of PD patients: 1) increased presence of autophagic vacuoles (Anglade et al. 1997), 2) increased autophagosome markers (Crews et al. 2010; Higashi et al. 2011; Tanji et al. 2011), 3) decreased lysosomal markers (Chu et al. 2009; Dehay et al. 2010) and 4) increased selective autophagy substrates (Tanji et al. 2011).

Since aggregates of a-syn are a substrate of autophagy, ALP could be regarded as a complementary system to compensate an overwhelmed UPS, as well as to cope with specific aggregated substrates not targetable by the UPS [reviewed in (Ebrahimi-Fakhari et al. 2012; Xilouri et al. 2013)]. Degradation of a-syn by the lysosome (Paxinou et al. 2001), initially thought to promote the clearance of a-syn aggregates by macroautophagy (Rideout et al. 2004), plays an important role in the degradation of soluble proteins and soluble oligomers under physiological conditions (H.-J. Lee et al. 2004; Mak et al. 2010).

| Introduction

Interestingly, a-syn has been suggested to inhibit macroautophagy at very early stages of autophagosome formation via inhibition of the small GTPase Rab1A (Winslow et al. 2010; Winslow & Rubinsztein 2011). This hypothesis was confirmed in mice lacking a-syn and showing an increased autophagy activity (Corrochano et al. 2012).

Decreased levels of the CMA adapter molecule LAMP-2A and of the lysosomal protease cathepsin D in brain of PD patients suggests a potential function of CMA in the pathogenesis (Alvarez-Erviti et al. 2010; Chu et al. 2009). Interestingly, a-syn is normally internalized in lysosomes for degradation via the adapter molecule LAMP-2A. But as mutant and dopaminergically modified a-syn present a strong binding to LAMP-2 on the surface of lysosomes, these a-syn species have been shown to inhibit the CMA (Cuervo et al. 2004; Martinez-Vicente et al. 2008), resulting from cellular stress due to the alteration of all proteins dependent on CMA degradation (Cuervo et al. 2004; Vogiatzi et al. 2008).

Crosstalk between autophagy and proteasome protein degradation

Depending on a-syn conformational states and on the cellular conditions, both proteasomes and lysosomes were shown to be capable of degrading recombinant a-syn (Liu et al. 2003; Cuervo et al. 2004). However, mechanisms determining a-syn degradation by UPS or ALP are yet to be resolved.

One simplified view is to consider that only less complex soluble forms of a-syn are degraded by UPS because more complex structures may get jammed inside the proteasome and block its activity [proposed in (Lynch-Day et al. 2012)]. These species, as well as more complex soluble forms of a-syn, may also be degraded by the CMA. However, it is likely that the CMA is not a viable long term degradation alternative for a-syn as mutant or modified species of a-syn have a high binding affinity to the CMA receptor, blocking uptake and degradation of CMA substrates (Cuervo et al. 2004; Martinez-Vicente et al. 2008). Finally, UPS and CMA inhibition was shown to promote macroautophagy activation as a potential compensatory mechanism to maintain normal protein degradation levels and also to remove abnormal cytosolic toxic and aggregated proteins (Pandey et al. 2007; Massey et al. n.d.). Unfortunately, the drawback of this cellular strategy is the production of cellular stress as a consequence of the in-bulk non-selective degradation [reviewed in (Cherra & Chu 2008)].

This degradation model is also supported by an increasing body of evidence demonstrating distinct roles of UPS and ALP in a-syn degradation. For example, *in vivo* observation of a-syn turn-over in mouse brain using multiphoton imaging supports 1) the critical role of the UPS both in non-transgenic mice and in mice overexpressing a-syn, 2) a more pronounced age-dependent UPS impairment in transgenic mice overexpressing a-syn than in non-transgenic controls and 3) the optional involvement of autophagy in the degradation of endogenous levels of a-syn and its critical recruitment in transgenic mice overexpressing a-syn to eliminate excess protein levels [reviewed in (Ebrahimi-Fakhari et al. 2012)].

Much effort has been put on explaining molecular mechanisms involved in the shift of a-syn degradation using the process of a-syn ubiquitination. Monoubiquitination of a-syn, for example by USP9X (Rott et al. 2011), promotes its degradation by the UPS whereas deubiquitination, for example by SIAH1 (Rott et al. 2008), inhibits its degradation.

However, either UPS or ALP inhibition in cell models overexpressing a-syn leads to an accumulation of monoubiquitinated a-syn and formation of cytosolic inclusions (Rott et al. 2008), obscuring degradation mechanisms involving a-syn monoubiquitination. Furthermore, polyubiquitination at the residue 63, for example by the E3 ligase Nedd4 (Tofaris et al. 2011), mediates a-syn degradation by the ALP. Accordingly, proteasomal inhibition does not lead to an accumulation of a-syn or polyubiquitinated forms of a-syn (Bennett et al. 1999; Rideout & Stefanis 2002; Ebrahimi-Fakhari et al. 2011) suggesting that the Lys63-linked ubiquitination of a-syn is a possible specific signal for ALP degradation. Finally, several studies suggest that a-syn does not require ubiquitination to be degraded by the proteasome (Tofaris et al. 2001; Kravtsova-Ivantsiv & Ciechanover 2012).

Taken together, no clear mechanism of a-syn degradation can be formulated due to conflicting results described in literature. This may result from the large variety of models used to induce a-syn accumulation as well as the methods used to modulate and measure degradation pathways. However, the elucidation of ubiquitin roles, as well as the functions of UPS and ALP in a-syn degradation, had just began.

Other proteolytic systems

Additionally to the ALP and to the UPS, proteases (such as calpains, neurosin, caspases and metalloproteases) have been observed to process a-syn [reviewed in (Xilouri et al. 2013). Truncation of a-syn by calpain-1 could be observed *in vitro*, in animal models overexpressing a-syn and in LBs (Mishizen-Eberz et al. 2003; Dufty et al. 2007). Calpains are intracellular calcium-dependent cysteine proteases [reviewed in detail in (Ono & Sorimachi 2012)], cleaving mainly a-syn close to its C-terminus (amino acid 120). Interestingly, calpains can also cleave a-syn at its NAC domain (amino acid 57) and this cleavage is blocked by the A53T mutation. Finally, a-syn truncation by calpains leads to a-syn aggregation and to the formation of beta sheet structures (Dufty et al. 2007).

Neurosin (also termed kallikrein-6) is a secreted serine protease, suggesting an enzymatic activity in the extracellular compartment [reviewed in (Wang et al. 2008)]. The main cleavage site of a-syn by neurosin is inside the NAC region (amino acid 80). Interestingly, phosphorylated Ser129 and A30P a-syn are less susceptible to be cleaved. Neurosin was suggested to play a role in PD since LBs are immunoreactive for neurosin (Ogawa et al. 2000), and neurosin inhibition in cell models results in a decrease of a-syn fragments and aggregation (Kasai et al. 2008).

Matrix metalloproteinases (MMPs) are another family of extracellular proteases. These enzymes are zinc-dependent and up-regulated upon oxidative and nitrative stress that accompany various neurodegenerative conditions. MMPs have been shown to cleave recombinant a-syn (Sung et al. 2005; Levin et al. 2009). More precisely, MMP-3 is cleaving a-syn both at its C-terminus and within its NAC regions. Additionally a-syn was also showed, to a lesser extent, a substrate of MMP-14, MMP-2, MMP-1, and MMP-9 (Sung et al. 2005).

Concerning caspases, analysis of a-syn truncation patterns extracted from LBs did not present any possible caspase sequences, and recombinant a-syn digestion by caspase 3 did not present any truncation pattern, suggesting that a-syn is probably not an important substrate for caspase-mediated cleavage (Dufty et al. 2007).

Truncated a-syn

It is interesting to note that LBs are abundant truncated C-terminal a-syn, however, these species were also reported to be increased in the soluble fraction of synucleinopathy brain extract along with full-length a-syn (W. Li et al. 2005). As described previously, several animal models overexpressing truncated forms of a-syn were reported to develop a severe phenotype (Michell et al. 2007), even stronger than in mice overexpressing full-length a-syn (Wakamatsu et al. 2008; Daher et al. 2009).

These observations, coupled with *in vitro* investigations showing that truncation of a-syn C-terminus increases its propensity to form fibrils (Crowther et al. 1998), suggest that the aggregation of a-syn may be initiated or enhanced by the generation of a-syn fragments. Accordingly, expression of C-terminal truncated forms of a-syn increase the aggregation and the toxicity of a-syn when compared to the full-length protein *in vitro* (I. V. J. Murray et al. 2003), suggesting that the C-terminal part of a-syn regulates its aggregation by protecting the hydrophobic NAC domain.

Several further hypotheses were proposed to explain the formation of a-syn C-terminal fragments [reviewed in (Ritchie & Thomas 2012)], including additionally the UPS via 20S subunit truncation (C.-W. Liu et al. 2005) and the ALP via lysosomal protease cathepsin D (Sevlever et al. 2008; Qiao et al. 2008). Finally, it is still unclear whether the formation of C-terminal truncated a-syn species results from an abnormal or incomplete degradation of a-syn, or whether these species are normal intermediates of the a-syn catabolism.

In vitro data also suggests a role of the a-syn N-terminus in a-syn aggregation (Kessler et al. 2003), but relevance of these truncation products were less studied and are therefore less understood.

5.7 Interacting partners

Cellular a-syn has been described to be available for physical interactions, as suggested by its chaperone functions. Accordingly, a-syn conformation or aggregation states could be modified by protein interactions (Chung et al. 2001; Uversky et al. 2001; Hasegawa et al. 2002; Alim et al. 2002; H.-J. Lee et al. 2002). Numerous interactions of a-syn with proteins were already reported [reviewed in (Surguchov 2008)], involving a-syn in several key signaling pathways such as protein degradation system, synaptic functionality, regulation of oxidative stress, mitochondrial function or gene regulation [(Zhou et al. 2004; Woods et al. 2007; Wakabayashi et al. 2007) reviewed in (Dev 2003)].

Briefly, best defined interacting partners are:

1) Synphilin-1, encoded by the *SNCAIP* (*SNCA* interacting partner) gene, present in LBs and enhancing a-syn aggregation (Engelender et al. 1999; Wakabayashi et al. 2000; O'Farrell et al. 2001).

2) Beta- and gamma- synuclein, inhibiting a-syn fibril formation (Biere et al. 2000; Uversky, Li, et al. 2002).

3) Tubulin, a basic structural constituent of microtubules, purified by immunoprecipitation of a-syn (Alim et al. 2002), initiating polymerization of a-syn and resulting in a-syn fibril formation.

4) Cysteine-string protein-a (CSPa), a synaptic vesicle protein with a co-chaperone activity, leading to the binding of a-syn to phospholipids (Chandra et al. 2005) and most likely playing a key role in synaptic function (Bonini & Giasson 2005).

5) 14-3-3, a ubiquitous eukaryotic adapter protein involved in the regulation of cell-cycle control, signal transduction, protein trafficking and apoptosis (Hermeking & Benzinger 2006), forming high molecular weight complexes with a-syn and found in LBs (Xu et al. 2002).

6) Rab, a group of GTP-binding proteins implicated in the targeting of different transport vesicles within the cell (Park 2013), interacting with a-syn (Dalfó et al. 2005). More precisely, Rab3a, Rab5, and Rab8 were shown to interact with a-syn.

7) Agrin, a large proteoglycan playing a major role in the formation of acetylcholine receptors during synaptogenesis (Daniels 2012). Agrin binds to a-syn and induces its aggregation (I.-H. Liu et al. 2005).

8) Histones, affecting histones acetylation and promoting neurotoxicity (Goers et al. 2003; Kontopoulos et al. 2006).

9) Chaperones, such as Hsp27, Hsp70, Hsp90, and aB-crystallin, interact with a-syn and are present in LBs (Outeiro et al. 2006). Chaperones play an important role in a-syn aggregation (Kilpatrick et al. 2013).

10) Tau, modifying both proteins' fibrillization (Giasson et al. 2003; Guo et al. 2013). Tau enhances a-syn aggregation and toxicity in cellular models of synucleinopathy (Badiola et al. 2011).

Unfortunately, a-syn's complex and large interaction range is obscuring the general molecular functions of its interactome, which is further complicated by the change of a-syn properties by post-transcriptional modifications such as ligand binding or truncation. It's interesting to note that a-syn was suggested to be a substrate recognition protein for ubiquitinated substrates such as synphilin-1 (Chung et al. 2001), TH (Perez et al. 2002; Døskeland & Flatmark 2002) or glycosylated forms of a-syn (Guerrero et al. 2013), facilitating their degradation (Dev 2003).

6)   Synphilin-1

6.1 Discovery

Synphilin-1 (sph1) was first identified in a yeast two-hybrid screen aiming to better understand a-syn function and role in LBs formation by elucidating its protein interaction partners (Engelender et al. 1999). Confirmation of the interaction was performed in cell models overexpressing both a-syn and sph1, showing an increase of a-syn inclusions. These data suggest a link between sph1 and a-syn aggregation.

Presence of sph1 in LBs in brains of sporadic PD patients (Wakabayashi et al. 2000), as well the identification of R621C mutation in the sph1 gene (*SNCAIP*) in a PD patient (Marx et al. 2003) pointed out an important functional link between sph1 and neurodegeneration in PD (Jung & Grune 2012).

6.2 Expression

SNCAIP maps to chromosome 5q23.2 and encodes the sph1 protein. Sph1 is expressed in the central nervous system, as well as in various peripheral tissues including heart, lungs, kidneys, liver and blood cells (Safran et al. 2003). During neuronal development, sph1 gradually translocates from neuronal cell bodies to nerve terminals where it accumulates and associates with synaptic vesicles (Ribeiro et al. 2002).

6.3 Structure

Sph1 is a 919 amino acid protein containing six ankyrin-like (ANK) repeats, a coil-coiled domain and an ATP/GTP-binding site (uniprot, protein reference Q9Y6H5). Interestingly, ankyrin repeats suggest a role of sph1 in protein-protein interaction (Crowther et al. 1998; Kim et al. 2002; I. V. J. Murray et al. 2003) and the coiled-coil domain suggests a possible multimerisation of the protein. Furthermore, murine sph1 showed a high homology with human sph1 and particularly in the coiled-coil and ankyrin-like motif domains (Kish-Trier & Hill 2013).

6.4 Conformation

Analysis of human brain extracts revealed sph1 as a predominantly soluble 90 kDa protein, but a less soluble 120 kDa form as well as fragments of 65 kDa and 50 kDa have also been observed, supporting an alternative splicing (or post-translational processing) potentially playing a role in sph1 function or distribution (I. J. Murray et al. 2003). Accordingly, a splicing isoform of synphilin-1, termed synphilin-1A, was associated with an enhanced aggregatory and neurotoxic properties (Eyal et al. 2006).

6.5 Function

The function of sph1 was scarcely investigated. Its presence in nerve terminals as well as its interaction with phospholipids (Takahashi et al. 2006) suggests a potential role of sph1 for maturation or modulation of synapse but also for mediating synaptic roles attributed to a-syn (Ribeiro et al. 2002).

Since its discovery, sph1 was described to promote a-syn aggregation (Engelender et al. 1999). More precisely, aggregates formed by a-syn and sph1 shared morphological and molecular characteristics of aggresomes (Tanaka et al. 2004), including 1) a round structure

with a core and halo organization, 2) a juxtanuclear localization, 3) an active formation of inclusions depending on the microtubular cytoskeleton and 4) a protective effect against a-syn induced toxicity.

The formation of aggresomes, as well as their protective effectiveness, could also be observed *in vivo* (Smith et al. 2010). Accordingly, several studies pointed out that aggresome formation may represent a specific cellular response to a failure of the proteasome/chaperone machinery (Zaarur et al. 2008; Wong et al. 2008; Wong et al. 2012). Accordingly, aggresome-like inclusions generated in cells overexpressing a-syn and sph1 are amenable to clearance by autophagy (Wong et al. 2008). This mechanism was shown to be directly dependent on sph1's ANK1 domain when undergoing K63 ubiquitination, probably reducing the mobility of aggregating proteins in the aggresomes (Wong et al. 2012).

Therefore, K63 polyubiquitination of sph1 may play a critical role on aggresome formation, and several E3 ubiquitinase candidates such as parkin (Chung et al. 2001) and dorphin (Ito et al. 2003) were identified to ubiquitinate sph1. It is predictable that ubiquitin binding proteins are recognizing small aggregates and facilitating their association to motor proteins, promoting their transport to the centrosome and connecting ubiquitination of abnormal polypeptides to their accumulation in aggresomes (Tsai et al. 2012). As an example, microtubule-associated histone deacetylase HDAC6 was shown to interact with aggregates of ubiquitinated proteins via its ubiquitin binding BUZ domain and facilitate their association with the dynein motor protein that drives this cargo to the aggresomes (Meriin et al. 2010). Other ubiquitin binding proteins-like PLIC or ataxin-3 may also target these abnormal complexes to the aggresomes (Heir et al. 2006; Burnett & Pittman 2005). Interestingly, sph1 overexpression in A53T a-syn mouse models promotes the formation of aggresome-like structures that protect neurons against degeneration via multiple cellular pathways including ALP and apoptosis (Smith et al. 2010).

Phosphorylation of sph1 by casein kinase II (CKII) (Tanji et al. 2003) plays an important role in the interaction between a-syn and sph1. This is suggested by the impaired protein binding in presence of CKII inhibitor, but not in the case of the non-phosphorylable [S129A] a-syn (G. Lee et al. 2004). Phosphorylation of sph1 also results from a decreased ubiquitination of sph1 by SIAH (Avraham et al. 2005), inhibiting sph1 degradation by the UPS (Nagano et al. 2003). Moreover, sph1 was reported to interact with the regulatory proteasomal protein S6 ATPase (tbp7) and to reduce proteasomal activity (Marx et al. 2007). In this context, sph1 was shown to inhibit high potassium-induced dopamine release from PC12 cells (Nagano et al. 2003), but it is still unclear if this observation resulted directly from a-syn or sph1 disturbance.

6.6 Toxicity

Originally, toxicity of sph1 was suggested after its discovery in LBs (Wakabayashi et al. 2000) and after observing that sph1 coexpression in a-syn models was increasing aggregation (C.-W. Liu et al. 2005). However, this hypothesis was challenged by the discovery of a point mutation in *SNCAIP* in a PD patient (Marx et al. 2007) as well as the improved cell viability with aggresome formation in models overexpressing a-syn (Tanaka et al. 2004).

6.6.1 Synphilin-1 interaction with alpha-synuclein

Sph1 and a-syn were shown to interact via their C-terminus, but also more weakly via their N-terminus (Kawamata et al. 2001). These data were challenged by a more recent study reporting the interaction of the central coiled-coil domain of sph1 with the N-terminal stretch of a-syn (Xie et al. 2010), inducing the formation and the accumulation of cellular inclusions (represented in Fig. 1-13). Interaction of mutant A53T a-syn with sph1 was described to be higher than with wild-type or the A30P a-syn, but R621C mutated sph1 does not modify its binding to a-syn.
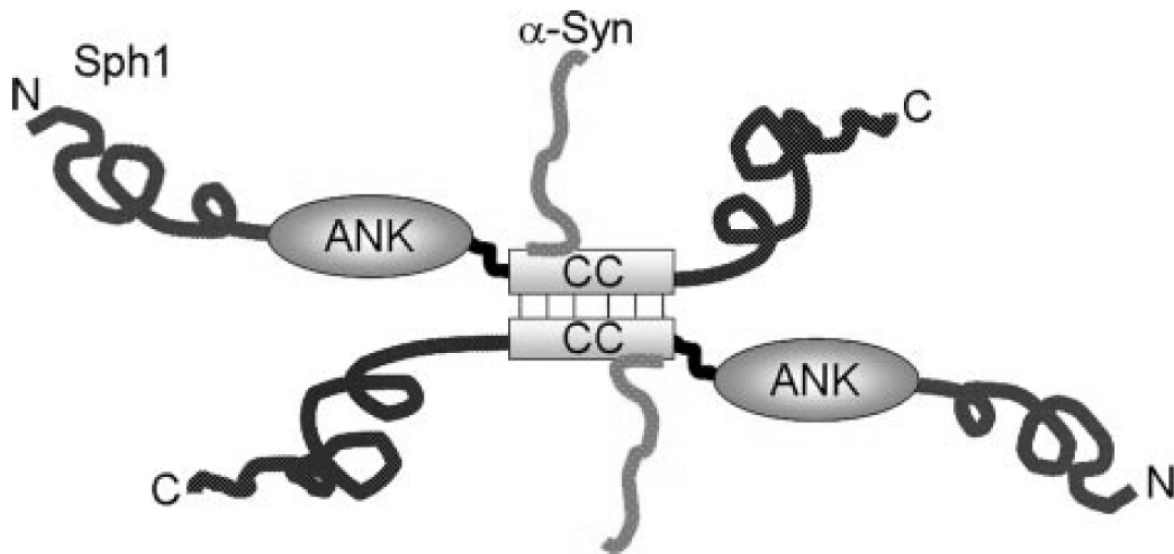
Figure 1-13: Representation of the interaction between synphilin-1 and alpha-synuclein

Figure copied from (Xie et al. 2010)

Formation of a dimer of sph1 interacting via its central coiled-coil domain. Binding of a-syn to the opposite coiled-coils dimerization surface of sph1 via a-syn's N-terminal stretch.

Coexpression of sph1 specifically increases half-life of a-syn by inhibiting its degradation by the UPS, probably by hiding the a-syn sequence necessary for its recognition by the proteasome more than by reducing UPS activity (Alvarez-Castelao & Castaño 2011).

Binding of sph1 to synaptic vesicles has been shown to be negatively modulated by a-syn (Ribeiro et al. 2002). Thus, sph1 seems to be a synaptic partner of a-syn and imply that this interaction mediates the synaptic effects of a-syn.

6.6.2   Synphilin-1 mutation

A mutation in *SNCAIP,* leading to R621C substitution in sph1, was reported in a PD patient (Marx et al. 2003). This mutation was also shown to reduce the number of inclusions as well as the a-syn turn-over by the UPS leading to apoptotic stimuli in cells overexpressing a-syn. Accordingly, mice overexpressing the mutated sph1 showed an enhanced neurotoxic effect and a motor phenotype when compared to mice overexpressing the wild-type sph1 (Nuber et al. 2010). However, frequency of the R621C substitution was reported to be equivalent between PD and control subjects (Myhre et al. 2008), questioning the relevance of this mutation in PD physiopathology.

6.6.3   Synphilin-1A isoform

Synphilin-1A is an alternative splice variant of sph1 lacking exons 3 and 4 and containing the exon 9A of the *SNCAIP* gene, generating a different N-terminus (Eyal et al. 2006). Interestingly, synphilin-1A is also present in LBs and could be detected in detergent insoluble fractions of brain protein samples. These data are supported by the observation of altered mRNA expression levels of sph1 isoforms in PD (Humbert et al. 2007).

Synphilin-1A was also described to be toxic for cells (Eyal et al. 2006), binding to sph1 and forming aggregates containing a-syn. But even more interestingly, synphilin-1A inactivates SIAH ubiquitinase activity and SIAH autoubiquitination, resulting in accumulated sph1 and decreased a-syn monoubiquitination (Szargel et al. 2009). Altogether, these findings suggest that sph-1 isoform expression may play a significant role in PD pathogenesis.

6.6.4   Mouse models

Transgenic mice expressing human sph1 under the mouse prion protein promoter presented a motor phenotype accompanied by ubiquitinated insoluble structures all over the brain (Jin et al. 2008). These findings were confirmed in another transgenic mouse overexpressing wild-type and mutant sph1 under the mouse prion protein promoter. Both sph1 forms showed a motor phenotype and the presence of inclusions; however the effects were more robust in mutant sph1 mice (Nuber et al. 2010).

Transgenic mice generated via injection of viral vectors were also used to study the effects of wild-type and R621C mutated sph1 in dopaminergic neurons. Both sph1 species were reported to lead to an equal neuronal degeneration and an equal increase of inclusion formation in wild-type mice (Krenz et al. 2009).

Finally, a protective effect of sph1 expression was observed in mice overexpressing A53T a-syn (both transgenes expressed under the mouse prion protein promoter). This protection was illustrated by an increased life span, milder motor abnormalities and decreased astroglia reactions accompanied by the formation of aggresome-like structures and increased autophagy. This suggests that sph1 alters multiple cellular pathways to protect against neuronal degeneration (Smith et al. 2010). However, these results were challenged by a study using a viral vector to coexpress human sph1 in mice overexpressing A30P a-syn, in which loss of dopaminergic neurons was increased by sph1 coexpression (Krenz et al. 2009).

7) *Aim of the thesis*

The role of a-syn aggregation in synucleinopathy is controversial. On the one hand a-syn aggregation was clearly shown to lead to cell toxicity and to be involved in PD pathogenesis. On the other hand a protective role of aggregates is emerging in diverse synucleinopathy models and also in PD. The overall aim of this study is to investigate the impact of a-syn aggregation on the development of synucleinopathy using the genetic enhancer of a-syn aggregation sph1.

It is noticeable that similar approaches have already been tested. However, the impact of sph1 in a-syn-mediated toxicity was inconsistent. Several reasons may explain these divergent results, including the variety of models used to induce synucleinopathy, the relevance of methods or biological markers used to analyze pathology and the absence of inclusion characterization in these studies. Therefore, the initial point of this study is to better characterize the impact of sph1 on a-syn aggregation by studying changes in a-syn protein levels, solubility and post transcriptional modifications in detail (including potentially toxic truncated, oligomerized and fibrillized a-syn forms). Hallmarks of neuropathology were be investigated using a-syn aggregation or inflammation markers. The relevance of histological marks of pathology in our model were correlated to the pathology observed at the behavioral levels using motor performances or cognition tests.

Several functions of sph1 in protein degradation were suggested: sph1 was first reported to interact and to impair the UPS, and more recently sph1 was reported to promote inducible autophagy. However, these suggested functions have opposite consequences on proteolysis. Therefore, this study was focusing in a second step on the impact of sph1 overexpression on proteolysis *in vivo*, focusing more particularly on a-syn degradation.

Materials and Methods

1) *Characterization of the double transgenic model at the biochemical level*

1.1 Cross-breeding strategies

Two transgenic mice generated previously were used in this study and described in (Kahle et al. 2000; Nuber et al. 2010). The first mouse model is overexpressing the human A30P mutated a-syn under the Thy-1 promoter (designated as A30P mice in this study), and the other mouse is overexpressing the human synphilin-1 under the PrP promoter (designated as sph1 mice in this study). Mice expressing both transgenes are designated as double transgenic mice in this study.

The breeding strategy is schematized in the Fig. 2-01. We first cross-bred homozygous A30P and sph1 mice (P) to generate a group of hemizygous double transgenic mice (so called F1). The F1 generation, composed exclusively of hemizygous, mice was cross-bred to generate a group of both homozygous and hemizygous sph1, A30P and double transgenic (so called F2) based on Mendelian inheritance.

Hemizygous double transgenic mice, hemizygous A30P mice, hemizygous sph1 mice, and nTg mice, were generate by crossed-breeding homozygous A30P, homozygous sph1 and nTg mice with non-transgenic C57BL/6NCrt littermates (Charles River Laboratories, Wilmington, USA) from the same litter (so called F3).
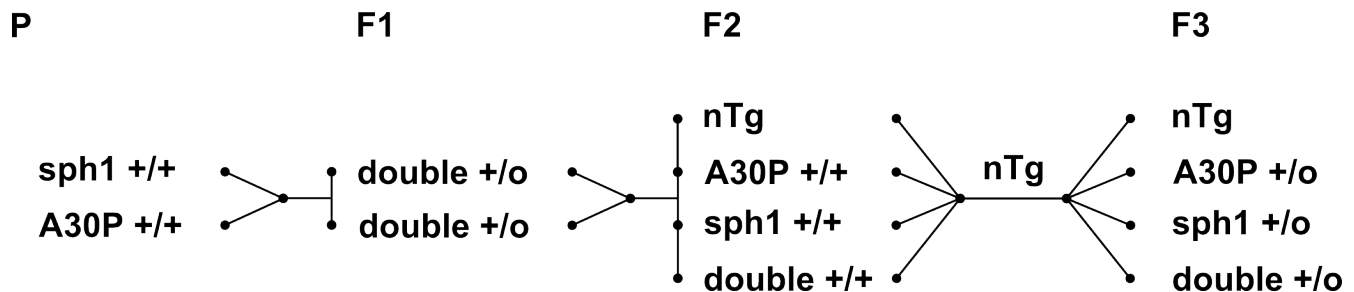
Figure 2-01: Schematic representation of breeding strategy

Homozygous single transgenic mice were crossbred to generate hemizygous double transgenic F1. F1 was cross-bred to generate homozygous A30P, sph1, double transgenic as well as non-transgenic mice F2. F2 was cross-bred to a group of wild-type littermates to generate the experimental groups. +/+: homozygous; +/o hemizygous

1.2 DNA extraction

Animal's genomic DNA was extracted to determine their genotype, using 0.5 cm diameter ear biopsy and the Roche High Pure PCR Template Preparation Kit (Roche Applied Science, Mannheim, Germany). Manufacturer buffers, filters and recommendations were used.

| Materials and Methods

Briefly, tissues were digested with proteinase K overnight at 55°C in microcentrifugation tubes (Eppendorf Safe-Lock Tubes; Eppendorf, Hamburg, Germany) using 40 µl of proteinase K and 200 µl of lysis buffer. After addition of isopropanol and binding buffer, samples were vortexed for 5 sec and centrifuged. Supernatant was filtered through a High Pure Filter Tube. DNA was washed using inhibitor removal buffer, to prevent DNA loss during washing steps, and washed twice with washing buffer. Excess of washing buffer was removed by an extra centrifugation step and DNA was then eluted in 200 µl of 70 °C prewarmed elution buffer. DNA was stored for short time at 4 °C or for longer period at -20 °C.

1.3 Polymerase chain reaction (PCR)

PCR allows the amplification of a target sequence of DNA using polymerase reaction. Briefly, polymerase amplification requires the presence of a DNA template (in our case mouse genomic DNA) and a free 3'-OH (in our case sequence-specific oligonucleotide primers). Reaction could be decomposed in three main steps: denaturation by heating (at 95°C, for 30 sec, to render DNA single-stranded), annealing (temperature and time depending on length and GC content of primers, to allow the binding of primers to the appropriate complementary DNA strand) and the extension (optimal temperature depending of the polymerase, time depending of the length of the amplicon and of the extension speed of the polymerase, to amplify the primers to an amplicon).

Transgenic animals were identified by PCR using DNA polymerase (OneTaq; New England BioLabs, Ipswich, USA) and primers designed to amplify the transgenic PrP or the Thy-1 fragment (Table 2-01; Metabion, Martinsried, Germany).

Table 2-01: Mouse genotyping primers

Transgene	Primer sequence	DNA strand direction	Amplicon size	Annealing temp.
Thy-1 hum SNCA	5′-ATGGATGTATTCATGAAAGG-3′	Forward	400 bp	50 °C
Thy-1 hum SNCA	5′-TTAGGCTTCAGGTTCGTAG-3′	Reverse	400 bp	50 °C
Thy-1 hum SNCA	5′-TGTAGGCTCCAAAACCAAGG-3′	Forward	200 bp	55 °C
Thy-1 hum SNCA	5′-TGTCAGGATCCACAGGCATA-3′	Reverse	200 bp	55 °C
PrP hum SNCAIP	5′-CAGAACTGAACCATTTCAACC-3′	Forward	400 bp	60 °C
PrP hum SNCAIP	5′-GGGCTTCCAAGTCTTCTTC-3′	Reverse	400 bp	60 °C
PrP hum SNCAIP	5′-TTTGGAATATGTTTGCGCTG-3′	Forward	200 bp	55 °C
PrP hum SNCAIP	5′-GTGCCATGTTGGATGATGAG-3′	Reverse	200 bp	55 °C
Mouse ACTB	5′-GATCTGGCACCACACCTTCT-3′	Forward	200 bp	55 °C
Mouse ACTB	5′-TCTTCTCCCGGTTAGCTTTG-3′	Reverse	200 bp	55 °C

A 25 µl reaction mixture was prepared for PCR and composed of 5 pM/µl primers (Metabion, Martinsried, Germany), 10 mM dNTP mix (11814362001; Roche), 25 unit/ml taq polymerase, 1× Standard or GC Reaction Buffer (One Taq; NEB), approximately 100 pg DNA and water to adjusted for 25 µl per reaction (Ampuwa; Fresenius Kabi, Germany). Reaction was performed in a 96 well plate (4ti-0750-5; 4titude, Wotton, UK) or in 0.2 mL microcentrifuge tubes (2-2600; NeoLab, Heidelberg, Germany).

Amplicons generated were visualized using 1% agarose gel (Invitrogen; Karlsruhe, Germany) containing 0.5 µg/ml ethidium bromide (2218; Roth, Karlsruhe, Germany). Specificity of the amplification was confirmed by comparing amplicon size in base pair to a DNA size ladder (100 bp DNA-Ladder; Invitrogen).

1.4 Quantitative PCR genotyping

Zygosity was determined performed by estimating the relative number of gene copies using quantitative real-time polymerase chain reaction (qPCR) on a LightCycler 2.0 (Roche) and FastStart DNA MasterPlus SYBR Green (Roche), a dye becoming fluorescent when binding to double stranded DNA. Reaction mixture used for qPCR contained 10 pmol of each primer, 20 pg of DNA and 1× SYBR Green Mix (Roche) and was adjusted to 10 µl per reaction using water (provided with the kit). Reaction was measured in a 384 well plate (4Ti-0382; 4titude).

Relative quantitative PCR was quantified using ΔΔCp method. Crossing point value (Cp value) of PCR reaction was calculated by the LightCycler software (version 4.0) using the maximum of the second derivative of the amplification curve fluorescence representing fluorescence signal acceleration (method resulting in more consistent results). The ΔCp of the samples was calculated by subtracting the Cp of the transgene of interest from the Cp of the reference gene beta-actin. The ΔΔCp was determined by subtracting the ΔCp of the sample from the ΔCp of hemizygous control animals. Relative gene copy number was calculated using $2^{-\Delta\Delta Cp}$. Specificity of PCR reactions was assessed using melting curve, a method based on the slow warm up of the final PCR product, leading to the formation of double stranded DNA able to bind SYBR and resulting to fluorescence increase. As the temperature resulting to double stranded DNA formation depends of DNA length and GC content, presence of different amplicons results to multiple distinct fluorescence increase at different temperatures.

1.5 Tissue preparation

Single mice were sacrificed by asphyxiation using accumulation of CO_2 in home-cage preferentially and using a low gas pressure (lower as 0.5 bar). A coronal cut approximately at bregma –3 mm was performed on mouse brain to separate forebrain and hindbrain region. Brain region were then prepared and snap frozen in a 2 ml cryotube (126261; Greiner Bio One, Kremmsmuenster, Austria) and stored at -80ºC for future biochemical analysis.

1.6 Tissue lysate

Proteins were lysed from brain tissue in 10 volume of lysis buffer in order to perform gel electrophoresis. Brain tissues were disrupted 30 sec using a homogenizer (T10 ultra turrax; VWR, Radnor, USA) in ice. Lysis buffers were selected depending of the solubility of studied proteins. Cytosolic proteins were extracted using Tris-saline lysis buffer (*10 mM Tris, 150 mM sodium chloride, pH 8.0*), cytosolic and membrane bound proteins were extracted using NP-40 lysis buffer (*50 mM Tris, 150 mM sodium chloride, 1.0% NP-40, pH 8.0*), and whole cell extract including less soluble proteins were extracted using RIPA buffer (*50 mM Tris, 150 mM NaCl, 1.0% NP-40, 0.5% sodium deoxycholate, 0.1% SDS, pH 8.0*). All lysis buffers were supplemented with protease inhibitor (Complete; Roche Diagnostics). After the homogenization, samples were incubated for 30 min at 4 °C and spun for 20 min at 12 000 g for NP-40 or RIPA lysis buffer and 30 min at 120 000 g for Tris-saline lysis buffer. Proteins lysate supernatants were supplemented with 10% glycerol before long storage at -80 °C.

1.7 Sequential protein extraction

A sequential protein extraction based on detergent solubility of these proteins was performed to quantify a-syn aggregation using buffers with different salinity, detergent concentration, and intermittent ultracentrifugation steps as described previously (Tofaris et al. 2003) with minor modifications (Fig. 2-02).

Brain samples were homogenized in 5 volumes of TBS+ (Tris-buffered saline plus complete protease inhibitor (Complete; Roche)) using a homogenizer for 30 sec, incubated for at least 1 h and spun for 30 min at 120 000 g. The resulting supernatant represented the TBS+ soluble fraction. The pellet was then extracted sequentially with 1) 1 ml of TBS+ containing 1% of Triton X-100, 2) TBS+ containing 1 M sucrose, 3) RIPA buffer (*50 mM Tris-HCl, 175 mM NaCl, 5 mM ethylenediaminetetraacetic acid [EDTA], 1% NP-40, 0.5% sodium deoxycholate, 0.1% sodium dodecyl sulfate (SDS), pH 7.4*) and 4) 2 M urea/5% SDS. Pellets were suspended 10 times in buffer using three needles of decreasing diameter (Nr.1, Nr.14, Nr.18; BD).
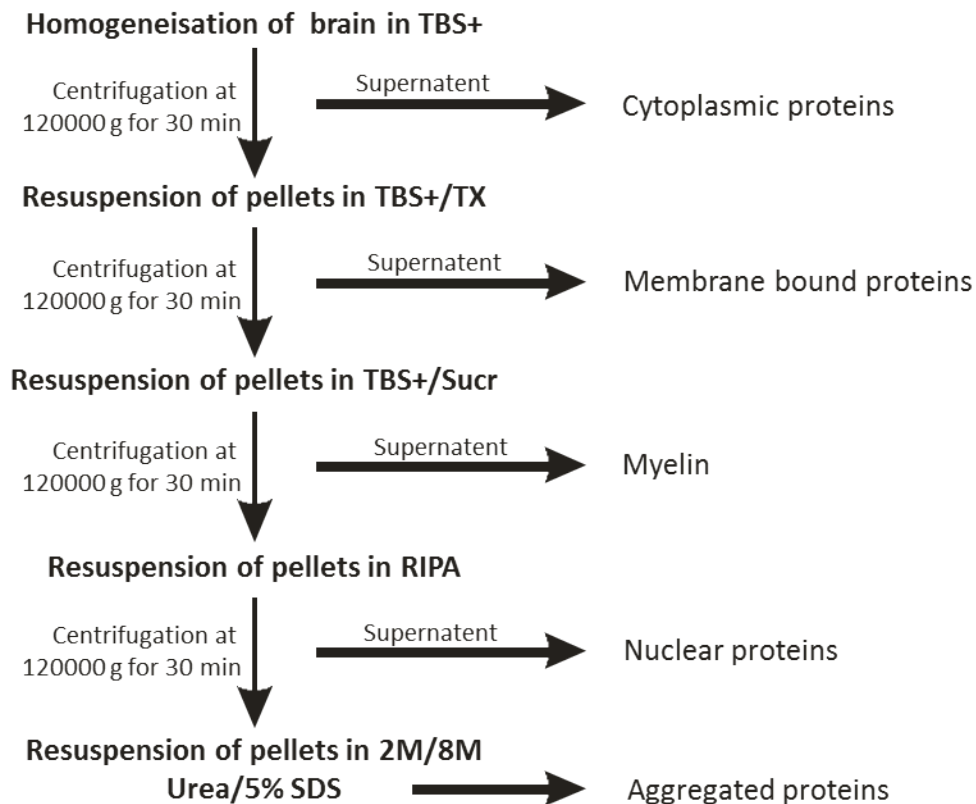

Figure 2-02: Sequential protein extraction protocol

Originally, 8 M of urea was used to suspend RIPA detergent-insoluble proteins (Liang et al. 1999), but we used 2 M of Urea to preserve higher molecular a-syn structures (Paleologou et al. 2009). In all extracts, 10% of glycine was added as cryoprotectant before storage at -80 °C.

1.8 Protein concentration measurement

We determined protein concentration using Bradford method (Protein Assay Dye Reagent Concentrate; Bio-Rad, Munich, Germany). This method is based on the proportional shift of Coomassie dye from red to blue when binding to protein, absorbance of samples at 595 nm was performed and concentration of samples was calculated by standard curve extrapolation. Standard curve of BSA (0, 10, 20, 50, 100, 150 and 200 µg/ml) and sample were diluted in 800 µl of water and 200 µl of Bradford reagent was then added in each tube and incubated for 5 min at room temperature.

1.9 Western blotting

Separation and identification of proteins in tissue lysate or tissue sequentially extracted was performed based on molecular weight using SDS-polyacrylamide gel electrophoresis followed by protein transfer and immunostaining of membrane.

Samples were prepared by diluting protein lysates in PAGE buffer (*0.2 M glycine, 25 mM Tris, 1% SDS*) to a final volume of 15 µl. Samples were denatured at 95 °C for 10 min in loading buffer (*80 mM Tris, 2% SDS, 5% 2-mercaptoethanol, 10% glycerol, 0.005% bromophenol blue, pH 6.8*) to denature proteins and shortly centrifuged for 30 sec at 400 g.

Proteins were separated by electrophoresis using homemade SDS-PAGE gel (Table 2-02) or precast gradient gels (SERVAGel Vertical Tris-Glycin Gel 2D 8-16%; Serva, Heidelberg, Germany). Gels containing proteins were washed for 5 minutes in transfer buffer (*0.2 M glycine, 25 mM Tris, 10–20% methanol*) to remove excess of SDS and transferred to membranes labeled with pencil and equilibrated in transfer buffer for 10 min for a homogenous transfer to the membrane. Transfer was performed for 1h30 to 2 h at 80 V at 4 °C. Several membranes were used to blot protein as nitrocellulose membranes (Optitran or Protran; Millipore, Billerica, USA) or PVDF membranes (Immobilon-P; Millipore). Choice of membranes was done depending of the molecular weight of proteins of interest or of the antibody used for the immunoblot detection. For PVDF membranes, some extra steps were required. Prior equilibration in transfer buffer for 10 min, PVDF membranes were activated 30 sec in methanol and washed with distilled water. After the transfer, membrane PVDF were dried for 15 min to enhance protein binding and re-hydrated in TBS (*10 mM Tris, 0.15 M NaCl, pH 7.5*) before blocking.

Table 2-02: Western blot gel composition

Running gel (5 ml)	8%	10%	12%	15%	17%	Stacking gel (3ml)	5%
H2O	2.3 ml	2 ml	1.65 ml	1.15 ml	0.8 ml	H2O	2.1 ml
30% acrylamide	1.35 ml	1.65 ml	2 ml	2.5 ml	2.35 ml	30% acrylamide	0.5 ml
1.5M Tris (pH 8.8)	1.25 ml	1.25 ml	1.25 ml	1.25 ml	1.25 ml	1.0M Tris (pH 6.8)	380 µl
10% SDS	50 µl	50 µl	50 µl	50 µl	50 µl	10% SDS	30 µl
10% APS	50 µl	50 µl	50 µl	50 µl	50 µl	10% APS	30 µl
TEMED	3 µl	3 µl	3 µl	3 µl	3 µl	TEMED	3 µl

| Materials and Methods

To prevent any antibody non-specific binding to the membrane surface, immunoblot were washed 5 min in TBS buffer and blocked using 5% non-fat milk (Slim Fast; Slim Fast Deutschland, Wiesbaden, Germany) or 5% BSA (Sigma-Aldrich; Steinheim, Germany) in TBS. Membranes were then washed twice 5 min in TBST and incubated with the primary antibody over night at 4 °C, or 2 h at room temperature depending of the antibody specificity (primary antibodies used in this study are listed in table 2-03). After incubation with the first antibody, membranes were washed four times (5 min each) with TBST. Membranes were then incubated for 75 min with the secondary antibody coupled to horseradish peroxidase (GE Healthcare, Freiburg, Germany). After four washing steps with TBST (5 min each), bands were visualized using the enhanced chemiluminescence method (ECL+; GE Healthcare). Light signal was detected using X-ray films (Hyperfilm ECL; GE Healthcare) and a developer (CP100; Agfa, Mortsel, Belgium).

Films were scanned at 300 dpi (HP Scanjet 3970; Hewlett-Packard, Dübendorf, Switzerland) and exported as 8-bit TIFF. Image were then quantified using densitometry (ImageJ; NIH, USA) following (Gassmann et al. 2009) and background correction was done with the default settings of ImageJ (rolling ball radius=50). To define the band profiles, rectangular boxes of the exact same size were defined arbitrarily. Intensity of the signal was quantified using the area under the curve of the gray intensity level plotted by the size of the band.

Table 2-03: Antibodies and staining conditions

Antibody	Epitope	Specie	Reference	Company	Conc. (WB)	Blocking (WB)	Conc. (IHC)
human and mouse alpha synuclein	NAC domain	mouse	610786	Transduction	1:3000	Slim fast 5%	1:1000
human and mouse alpha synuclein	N-terminus	rabbit	SAB4502831	Milipore	1:200	Slim fast 5%	-
human alpha synuclein	C-terminus	rat	804-258-L001	Enzo Life Science	1:50	Slim fast 5%	1:20
myc	mab A14	rabbit	sc-789	Santa Cruz	1:200	Slim fast 5%	1:100
myc	polyclonal	rabbit	2272	Cell Signaling	1:1000	Slim fast 5%	-
myc	mab 9b11	mouse	2276	Cell Signaling	1:1000	Slim fast 5%	1:500
myc	mab 71d10	rabbit	2278	Cell Signaling	1:1000	Slim fast 5%	-
myc	polyclonal	rabbit	9106	Abcam	1:500	Slim fast 5%	-
myc	Mab 9E10	mouse	m4439	Sigma	1:200	Slim fast 5%	-
synphilin-1	N-terminus	rabbit	S5946	Sigma	1:500	Slim fast 5%	1:200
synphilin-1	C-terminus	rabbit	S6071	Sigma	1:500	Slim fast 5%	-
synphilin-1	polyclonal	rabbit	AB6179	Abcam	1:500	Slim fast 5%	-
synphilin-1	polyclonal	mouse	9627-B01	Novus	1:1000	Slim fast 5%	-
synphilin-1	N-terminus	mouse	9627-M01	Novus	1:1000	Slim fast 5%	-
beta-actin	C-terminus	mouse	A4700	Sigma	1:5000	Slim fast 5%	-
alpha-tubulin	mab DM1A	mouse	cp06	Milipore	1:10000	Slim fast 5%	-
GAPDH	mab GA1R	mouse	AB125247	Abcam	1:3000	Slim fast 5%	-

proteasome 20S α5 subunit	unknown	mouse	PW8125	Enzo Life Science	1:1000	Slim fast 5%	1:200
proteasome 20S α1,2,3,5,6,& 7 subunits	unknown	mouse	PW8195	Enzo Life Science	1:1000	Slim fast 5%	1:200
proteasome activator 11S beta subunit	polyclonal	rabbit	PW8240	Enzo Life Science	1:1000	Slim fast 5%	1:200
proteasome activator 11S alpha subunit	polyclonal	rabbit	PW8185	Enzo Life Science	1:1000	Slim fast 5%	1:200
proteasome 19S Rpt2/S4	polyclonal	rabbit	PW8160	Enzo Life Science	1:1000	Slim fast 5%	1:200
proteasome 19S Rpt2/S4	polyclonal	rabbit	PW8305	Enzo Life Science	1:1000	Slim fast 5%	1:200
LC3	polyclonal	rabbit	MBL-PD014	Biozol	1:1000	Slim fast 5%	1:500
LC3	mab 5F10	mouse	0231	Nano Tools	1:500	Slim fast 5%	-
p62	N-terminus	mouse	610497	BD Bioscience	1:200	Slim fast 5%	-
LAMP2	polyclonal	rabbit	5571	Santa Cruz	1:200	Slim fast 5%	-
LAMP2A	polyclonal	rabbit	AB12528	Abcam	1:1000	Slim fast 5%	1:500
beclin-1	N-terminus	mouse	48341	Santa Cruz	1:500	Slim fast 5%	-
beclin-1	polyclonal	rabbit	NB500-249	Novus	1:1000	Slim fast 5%	-
gamma-tubulin	mab GTU-88	mouse	T6557	Sigma	1:200	Slim fast 5%	1:100
ubiquitin	polyclonal	rabbit	Z0458	dako	1:1000	Slim fast 5%	1:500
ubiquitin	mab ubi-1	mouse	MAB1510	milipore	1:1000	Slim fast 5%	-
K63 ubiquitin	mab D7011	rabbit	5621	Cell Signaling	1:1000	Slim fast 5%	1:500
K48 ubiquitin	mab D9D5	rabbit	8081	Cell Signaling	1:1000	Slim fast 5%	1:500
TH	polyclonal	rabbit	657012	Milipore	1:1000	Slim fast 5%	-
DAT	mab DAT-nt	rat	MAB369	Milipore	1:1000	Slim fast 5%	-
GFAP	polyclonal	rabbit	Z0334	Dako	-	Slim fast 5%	1:200
IBA1	polyclonal	rabbit	019-19741	Wako	-	Slim fast 5%	1:100
phospho Ser129 alpha synuclein	Ser129	mouse	014-20281	Wako	1:200	BSA 5%	-
phospho Ser129 alpha synuclein	Ser129	rabbit	AB51253	Abcam	1:500	BSA 5%	-
phospho Ser129 alpha synuclein	Ser129	rabbit	2014-1	Epitomics	1:500	BSA 5%	-
oligomer A11	polyclonal	rabbit	AHB0052	Invitrogen	1:500	Slim fast 5%	-
oligomer Fila1	polyclonal	rabbit		From Pr. Jensen	1:100	Slim fast 5%	-

1.10 AGERA

To analyze high molecular weight ubiquitinated proteins and a-syn species, SDS-PAGE cannot be used as proteins do not migrate in the resolving acrylamide and stay blocked in the stacking gel because of their elevated molecular weight. Therefore, we performed electrophoresis in agarose gel as described previously (Weiss et al. 2008).

| Materials and Methods

Hindbrain and forebrain of mice were homogenized into 10 volumes of Tris-buffered saline (*0.1 M Tris, 0.15 M NaCl, pH 7.4*) completed with protease inhibitor (complete; Roche) using a 1 ml cylinder dounce homogenizer (8530742; Sartorius, Goettingen, Germany) and 40 suspensions on ice. Samples were aliquoted and kept at -80°C.

75 ml agarose gels were prepared by dissolving 1.5 g of agarose (161-3101; Biorad) in Tris-buffered saline (*0.375 M Tris-HCl, pH 8.8*) and SDS was added after agarose dissolution to a final concentration of 0.1%. Samples were heat denatured for 5 min at 95°C into 1:1 non-reducing Laemmli sample buffer (*0.15 M Tris-HCl, 33% glycerol, 1.2% SDS and bromophenol blue, pH 6.8*).

After loading, gels were run in running buffer (*192 mM glycine, 25 mM Tris-base, 0.1% SDS*) at 100 V, and blotted on PDVF membranes (Immobilon-P; Millipore, Zug, Switzerland) at 80 V for 2 h in transfer buffer (*192 mM glycine, 25 mM Tris-base, 0.1% SDS, 15% methanol*). After transfer, immunoblots were detected exactly like in the western blot section.

1.11 Dot blot

Dot blots were used to make semi-quantitative analysis of a-syn oligomers as described previously (Colla et al. 2012). Nitrocellulose membranes (Optitran; Millipore) were washed first with 100 µl of deionized water under vacuum. 10 µg of protein samples extracted for AGERA analysis were diluted in 50 µl of TBS (*10 mM Tris, 0.15 M NaCl, pH 7.5*), spot on the nitrocellulose membrane under vacuum and washed once using 100 µl of TBS.

Immunoblots were detected exactly like in the western blot section. Total amount of protein was estimated by staining membranes with amido black staining solution (*0.1% amido black, 25% isopropanol, 10% acetic acid*) for 5 min and washed twice 5 min with water.

1.12 Proteasome activity measurement

To measure enzymatic activity of the proteasome, substrates specific for different 20S protease activities were used (described in Fig. 2-03). Mouse brain tissue was prepared and directly (without being frozen) homogenized in 10 volume of hypotonic buffer (*10 mM Tris, 5 mM MgCl2, 5 mM ATP, pH 7.0*) using dounce homogenizer and ultrasonicated (Sonopuls; Bandelin, Berlin, Germany) at 40% power for 30 pulses of 0.5 second each (waiting 0.5 second between pulses) to reduce sample viscosity. For storage at -80°C, 10% of glycerol was added to lysate.

Proteasomal activity (Proteasome-Glo 3-Substrate Assay System; Promega, Madison, USA) was measured in 25 µl of detection reagent containing luciferin detection reagent and specific substrate for chymotrypsin-, trypsin- or caspaselike activity of the proteasome. Detection reagent was incubated for 30 min at room temperature before the measurement to reduce free aminoluciferin and reduce background luminescence.

Proteasomal activity was monitored for 15 µg proteins diluted in 25 µl hypotonic buffer in presence or absence of 10 µM of the proteasome inhibitor lactacystin (bml-PI104-0200; Enzo Life Sciences, Lörrach, Germany) in 96 well plate (735-0199; VWR) using microplate reader (Synergy HT; Bio-Tek, Winooski, USA) for 1 h at room temperature.
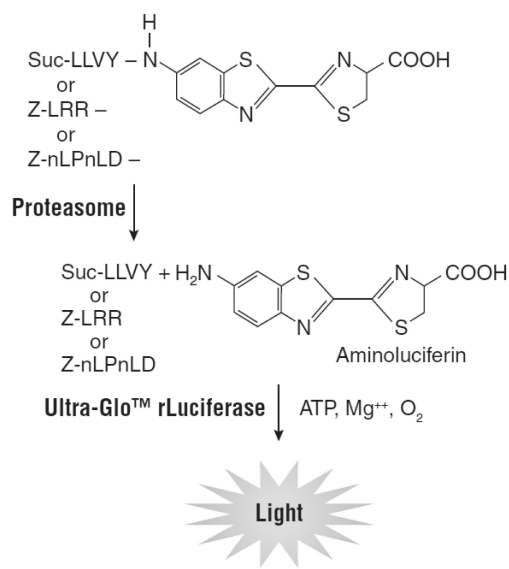
Figure 2-03: Bioluminescent measurement of proteasome activities

Figure copied from (Moravec et al. 2009)

Cleavage of the substrate by the proteasome leads to the release of aminoluciferin serving as the substrate for firefly luciferase. The light produced as a result of the luciferase reaction is then detected using a plate reader.

1.13   Preparation of tissue for histological analysis

Mice were deeply anesthetized by CO2 inhalation and transcardially perfused using a pump first with room temperature PBS (*10 mM phosphate, 150 mM NaCl, pH 7.4*) until most of the blood is flushed, and then using cold 4% paraformaldehyde (PFA) in PBS. Brains were removed carefully from the skull and post-fixed 24 h in 4% PFA, alcohol-dehydrated and embedded in paraffin (Table 2-04) using a tissue processor (TP1020; Leica Instruments, Nussloch, Germany). Samples were embedded in paraffin blocks using a tissue embedding station (EG1160; Leica) and stored at room temperature. Paraffin blocks containing brains were cool on ice block and cut in 7 µm thick sections using a microtome (RM2155; Leica). Section were placed in 45 °C water bath (HI1210; Leica) for flattering, collected on a glass slide (SuperFrost; R. Langenbrinck, Emmendingen, Germany), dried in an incubator at 50 °C for 1 h (Bachoffer, Reutlingen Germany) and stored at room temperature.

Table 2-04: Brain fixation

Buffer	Time
70% ethanol	4 h
96% ethanol	10 h
96% ethanol	14 h
100% ethanol	5 h
100% ethanol	5 h
100% ethanol	6 h
xylene	5 h
xylene	5 h
xylene	6 h
paraffin	2 h
paraffin	2 h
paraffin	4 h

Table 2-05: Section dewaxing and dehydration

Dewaxing	Buffer	Time	Dehydration	Buffer	Time
	xylene	5 min		70% ethanol	5 min
	xylene	5 min		80% ethanol	5 min
	xylene	5 min		96% ethanol	5 min
	100% ethanol	5 min		100% ethanol	5 min
	100% ethanol	5 min		100% ethanol	5 min
	96% ethanol	5 min		xylene	8 min
	96% ethanol	5 min		xylene	8 min
	80% ethanol	5 min		xylene	8 min
	70% ethanol	5 min			
	50% ethanol	5 min			
	30% ethanol	5 min			
	PBS				

1.14 Immunohistochemistry

Sections were deparaffinized in xylene and rehydrated in decreasing ethanol series (Table 2-05) using an automatic slide stainer (Autostainer XL; Leica). Heat antigen retrieval was performed for 15 min using a microwave set at 1000 W and using 10 mM sodium citrate (pH 6.0) and sodium citrate was refilled every 5 min to avoid the slides to dry. Sections were then washed 3 times 3 min in PBS and incubated 20 min in 0.3% hydrogen peroxide to block endogenous peroxidases.

After washing the slides 3 times 3 min in PBS, non-specific binding was blocked for 40 min by treating sections with 5% normal serum of the secondary antibody host animal (goat serum S-1000; Vector, Burlingame, USA) (rabbit serum, S-5000; Vector)(donkey serum 017-000-001; Dianova, Hamburg, Germany) diluted in PBS and supplemented with 0.3% Triton X-100 to permeabilize cell membranes. After washing the slides 3 times 3 min with PBS, sections were incubated overnight with the primary antibody diluted in PBS containing 1% normal serum. The next day, slides were washed 3 times 3 min with PBS Brij (0.005%) and incubated for 1 h with a biotin conjugated secondary antibody (mouse: BA-9200, rabbit: BA-1000, rat: BA-4000; Vector) diluted 1:250 in PBS containing 1% normal serum.

Sections were washed 3 times 3 min with PBS Brij and then incubated with an avidin-biotin enhancer complex coupled with peroxidase (ABC Elite; Vector) at room temperature for 1 h. After washing 3 times 3 min with PBS Brij, sections were detected using 3,3′-diaminobenzidine (DAB; Sigma) providing a brown precipitate when oxidized by the peroxidase linked to the secondary antibody. Reaction was stopped by washing slides in distilled water after 5–15 min. Slides were counterstained with hematoxylin (1.09249.0500; Merck, Darmstadt, Germany), washed 3 times 1 min in 70% ethanol containing 1% HCl and immediately dehydrated in increasing ethanol series (Table 2-06) using an automatic slide stainer. For microscopy, slides were mounted using a coverslipping media (CV mount; Leica), dried overnight, and stored at room temperature.

Similarly, double immunofluorescence staining of paraffin embedded sections was also performed using heat antigen retrieval, but without endogenous peroxidase inhibition. Sections were blocked for 40 min in 10% normal serum diluted in TBS and supplemented with 0.3% Triton X-100. After washing 3 times 3 min with TBS, sections were double stained using two primary antibodies pooled together in TBS supplemented with 0.3% Triton X-100 and 1% normal serum for 2 h at room temperature. After washing the slides 3 times 5 min with TBS, slides were incubated for 1 h with the secondary antibodies (Table 2-06) pooled together and diluted 1:250 in TBS supplemented with 0.3% Triton X-100 and 1% normal serum at room temperature in dark. After washing 3 times 5 min, cell nuclei were stained by incubating sections 5 min with 1 µg/ml DAPI (D1306; Invitrogen) solved in TBS and washed 2 times 3 min in TBS. Sections were cover slipped with an aqueous mounting medium (Mowiol; Merck, Darmstadt, Germany) supplemented with 25 mg/ml of the antifade 1,4-diazabicyclo[2.2.2]octane (DABCO, D27802; Sigma-Aldrich). Slides were stored in dark at 4°C and investigated within 2 weeks.

Staining was visualized using a microscope (Axioplan 2; Carl Zeiss Microimaging, Oberkochen, Germany) equipped with a color camera (Axio-Cam MRc; Zeiss) and imaging software package (AxioVision 4.6; Zeiss). To visualize fluorescence stainings, a fluorescence lamp was used with suitable filter sets and a monochrome camera (Axio-Cam MR; Zeiss) was preferred to the color camera.

Table 2-06: Secondary antibodies and staining conditions

Dye	Specificity	Host specie	Reference	Company
Alexafluor 488	mouse	donkey	715-545-150	Dianova
Alexafluor 488	rabbit	donkey	711-545-152	Dianova
Alexafluor 595	mouse	donkey	715-585-150	Dianova
Alexafluor 595	rabbit	donkey	711-585-152	Dianova
Alexafluor 595	rat	donkey	712-585-150	Dianova

1.15   Proteinase K digestion on nitrocellulose membrane

Aggregate load location was investigated by using proteinase K digestion of paraffin sections blotted on nitrocellulose membranes as described previously (Neumann et al. 2002). Paraffin embedded tissues were cut using a microtome and 5 µm thick sections were placed in 55 °C water bath and collected on a wet 0.45 µm nitrocellulose membrane (162-0116; Bio-Rad), and dried for at least 8 h at 55 °C. Blotted sections were stored at room temperature.

Sections on nitrocellulose membrane were deparaffinized with xylene and rehydrated using a descending ethanol series (Table 2-06). Membranes were washed with TBST (*10 mM Tris-HCl, 100 mM NaCl; 0.05% Tween-20, pH 7.8*), and digestion of sections was performed with 50 µg/ml proteinase K (P-6556; Sigma) in TBSB (*10 mM Tris-HCl, 100 mM NaCl, 0.1% Brij-35, pH 7.8*) for 12 h at 55°C.

After three washing steps using TBST, proteins blotted on sections on the membranes were denatured to allow a better access to epitopes to antibodies for 10 min (*10 mM Tris-HCl, 3 M guanidine isothiocyanate, pH 7.8*). Aspecific antibody bindings to membrane were blocked

| Materials and Methods

using 0.2% casein in TBST for 30 min. Sections were immunostained for 8 h with the monoclonal 15G7 anti-a-syn antibody diluted 1:50 at 4 °C. After three washes in TBST, signal was enhanced using a bridging rabbit anti-rat antibody diluted 1:500 incubated 1 h on membranes at room temperature and were incubated 1 h with alkaline phosphatase coupled to a goat anti-rabbit antibody (DO487, DAKO). After five washes of 10 min in TBST, membranes were adjusted to alkaline pH using two incubations of 5 min in NTM (*100 mM Tris-HCl, 100 mM NaCl; 50 mM MgCl2, pH 9.5*). Detection of the antibody staining was performed using a mixture of formazan and nitrotetrazolium blue/5-bromo-4-chloro-3-indolyl phosphate p-toluidine salt. Membranes were dried overnight at room temperature and stored at room temperature.

1.16 Proteinase K digestions on glass slide

Aggregate load location was also investigated by using proteinase K digestion of paraffin sections on slides as described previously (Tanji et al. 2010). Sections were deparaffinized in xylene, rehydrated in a descending ethanol series (Table 2-06) and washed twice in PBS. Sections were digested with 50 µg/ml proteinase K (P-6556; Sigma) in TBSB (*10 mM Tris-HCl, 100 mM NaCl; 0.1% Brij-35, pH 7.8*) for 30 min at 55 °C and reaction was stopped by washing slides in PBS. Immunohistochemical staining was then performed as described in paragraph 1.14.

1.17 Immunohistological quantification of stained cells and neurites

To avoid bias during the quantification, animal section genotypes were coded prior the analysis. Brain regions of interest were mapped using an overlapping process represented in Fig. 2-04. To avoid over- or under- represented regions, pictures were taken using 10× objective only adjusting mapping pattern and focus. The mean of 8 fields was investigated on 4 to 8 sections per animal. Pictures were saved as high quality color TIFF files and were analyzed using ImageJ (NIH). To increase the reproducibility of the counting, a predetermined threshold (triangle autothreshold) was establish on a positive control section using absorbance for DAB staining (or fluorescence intensity) to highlight the signal.

For most simple and clear stainings, such as proteinase K digestion followed by a-syn staining, a small batch based on size and circularity of signal was used to count automatically the number of cells and processings. Results were manually confirmed on a subset of pictures (around 10% of the complete set). For more complex stainings, such as thioflavin S, original pictures were overlaid with the calculated threshold to determine number of stained cells. For glial cell staining, only cells with more than three clear process were counted.
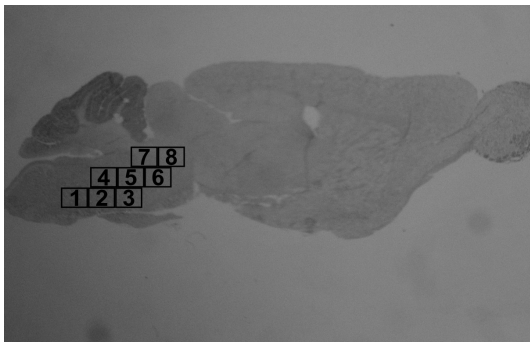

Figure 2-04: Representation of brain region mapping

Picture of mouse brain using macroscope. An example of brainstem mapping is represented by black rectangles numbered from the most caudal and ventral regions to the most cranial and dorsal regions. In our study, the mean of 8 fields was investigated on 4 to 8 sections per animal.

2) *Animal housing*

Mice were housed in a group of maximum five animals per cage on a 12:12 hours light:dark cycle. Cages used for the housing [Eurostandard Type II L cage; 365 × 207 × 140 mm; (1284L, Tecniplast, Italy)] were autoclaved and bedding was added prior to use. Mice received *ad libitum* access to water and to chow.

2.1 Animal marking

In order to identify animals within the same cage ear punch marking was applied to 6 weeks old mice and biopsies were collected to investigate animal genotypes. Prior each marking, preparation tools (ear-punch tools and tweezers) were cleaned with 70% propanol, rinse with distilled water, and dried before the procedure to avoid infection or biopsy cross contamination. Individual mice were selected randomly and exposed for a short time (less than 1 min) to isoflurane (Forene, Abbott, Abbott Park) into an induction chamber to render them unconscious. Ear punching was performed using ear-punch tool to provide a unique number and biopsies were collected in 1.5 ml microcentrifuge tubes (Safe-Lock Tubes, Eppendorf). Mice were returned to their home-cage and observed till the end of the anesthesia.

2.2 Mouse genetic background

To reduce possible effect of genetic background on gene expression [*i.e.* (Coleman & Hummel 1973; Carlson et al. 1997)], all mice were cross-breed to the same inbreed stain C57BL/6NCrl mice (designated as nTg, reference strain: 027, Charles River, USA).

2.3 Mouse breeding

To provide an experimental group within the same age range, females were mated in the same cage couple at least 4 weeks prior starting to breed mice to synchronize hormone cycles (Whitten Effect (WHITTEN 1957)). For optimal breeding setup and to avoid overpopulation, one male and two females at sexual maturity (between 2 and 6 months) were chosen according to their genotype. To increase breeding performances, mice were housed in the male cage 1 h before the end of the light phase. The next day, a plug-check examination was performed on females. To avoid cannibalism, females were isolated as soon as pregnancy was detected (Lane-Petter 1968). Females that were not positive for a plug for 3 consecutive days were separated from the breeding cage. Pups were weaned at 21 days and were marked by ear biopsy as described previously.

2.4 Validation of animal health before behavioral analysis using SHIRPA procedure

In order to assess the general health of animals, a short battery of tests was perform to detect any potential behavioral or neurological abnormalities (Rogers et al. 1997). Mice were placed in a clean transparent plastic tube (20 cm diameter × 20 cm length) and observed. Activity, as well as abnormal behavior like tremors or convulsions, was assessed. Inside the tube, palpebral closure (animal able to close their eyelid), coat appearance (presence of any fur scratch or biting), whiskers appearance (regularity of the hairs), defecation, urination and presence of abnormal lacrimation were recorded. Reflexes were observed by rolling slowly the mouse in the investigation plastic tube.

| Materials and Methods

Mice were then transfer to a metal grid and reactions of the mice to the new environment were examined (duration of freezing behavior). Fluidity of movements was observed (elevation of the pelvis during walking process, position of the tail). To observe reaction to the noise, mice were exposed to a timer alarm located around 30 cm above the arena; stimulation of escape behavior was performed by approaching finger from their nose.

When holding animals by their tail, handling behavior and grasping of front- or hind- limbs was observed. The handling behavior was also studied by holding animals by the neck, allowing the investigation of plantar and digit surface. Vocalization and aggressiveness was recorded.

3) *Phenotyping of double-transgenic mice*

3.1 Behavioral tests

To avoid bias induced by repeated behavioral experiments in a short interval of time (McIlwain et al. 2001), the order of the behavioral tests was determined in regard of stress induced to the animals and a break of at least 48 h was applied between two different experiments. Experimenter was blind to mouse genotype during the behavioral testing to reduce experimenter expectancy effects. Before each experiment, mice were acclimatized for at least 15 min to the experimental room. Experimental group of animals was composed originally of 12 mice.

3.2 Weight investigation

In order to follow the weight gain in every line, mice routinely put in behavioral tests were weighted every 6 weeks. This procedure was performed at the end of the light phase before any behavioral test.

3.3 Motor function evaluation

3.3.1 *Motor skill learning and motor coordination assessment using rotarod*

Motor skill learning and motor coordination were measured using rotarod [represented in Fig. 2-05 (RotaRod Advanced, TSE Systems, Bad Homburg, Germany)]. The rotarod consists of an elevated rotating cylinder with rotation speed programmable by the user (speed expressed in revolutions per min (RPM)).

Mice were placed on the rotating rod and latency to fall was recorded. To optimize rotarod outcome, experiment was performed during dark phase (Hossain et al. 2004) and mice were trained in the apparatus before starting the motor skill performance. During the first training day, animals get used to the system by being placed 3 trials at low and constant speed (4 RPM for 5 min, 10 RPM for 5 min and 20 RPM for 5 min). A second training was made to familiarized mice to higher speed and acceleration (10 RPM for 5 min, 20 RPM for 5 min and 4-40 RPM for 7 min).

During training, animals were placed back on the rotating cylinder after falling. To limit stress, mice were brought back on the rod 5 times maximum. Test was repeated for 3 consecutive days and latency to fall from the rod was measured 4 times per day at constant acceleration (4-40 RPM in 7 min).

Mice falling accidentally before the first 30 sec were put back on the rod. An inter-trial recovery time of at least 1 h was allowed between trials. Assessment of motor ability was first measured in 4 month-old mice and repeated every 6 weeks over a 12 months period.

Motor coordination was investigated by evaluating the progression of latency to fall over using the average of the 16 trials per time point and using two-way ANOVA. Motor skill learning was analyzed by evaluating the progression of latency to fall over the 4 days of testing within an age point using the average of all trials per day and using two-way ANOVA.
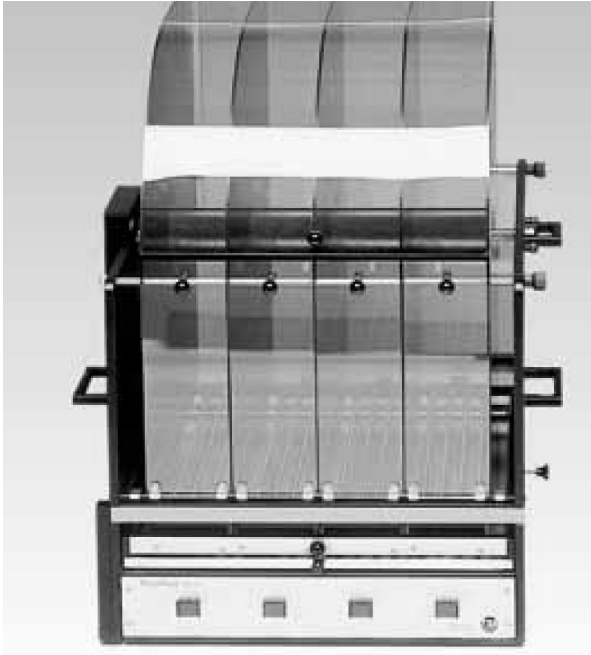
Figure 2-05: Rotarod

Picture copied from TSE System GmbH commercial brochure: RotaRod Advanced 2013

Apparatus consists of a rotating grooved drum to provide animals an optimal grip. Panels divide the drum into separate lane each suited for an individual animal.

3.3.2   *Motor coordination assessment using challenging beam traversal*

To gain more insight on motor coordination and fine movement alterations, mice were tested in challenging beam walk as described previously (Goldberg et al. 2003; Fleming et al. 2006). Mice were trained for two days to traverse a beam without stopping. The beam was constituted of a transparent thermoplastic beam consisting of 4 sections (25 cm each, 1 m total length) of different width (3.5 cm to 0.5 cm by 1 cm increments) and leading to the animals' home-cage.

For the experimental day, a mesh grid of 1 cm squares was placed 1 cm over the beam surface and time to traverse the beam was measured three times.

4, 12, and 18 month-old mice were tested, behavioral test was performed during the dark phase and the mean of the three trials was analyzed using one-way ANOVA.

3.3.3   *Automatized gait analysis using CatWalk*

To assess motor functions and coordination in voluntarily walking mice, gait analysis were performed (Fig. 2-06A and B) using an automatic system (CatWalk, Noldus, Wageningen, The Netherlands). 18 month-old animals were trained to cross the runway without any interruption.

Five runs with a speed variation below 30% and without any abnormal walking pattern resulting of exploration (climbing walls) or abnormal print (prints distorted because of a dirty glass plate) were analyzed. From these data, multiple parameters were calculated via the CatWalk software as intensity of the paw contact, print area, stand (duration of paw contact with the glass plate in a step cycle), swing (duration of no contact with the glass plate in a step cycle), swing speed (speed of the paw during swing), stride length (the distance between successive placements of the same paw), number of steps to cover walk way distance and locomotor speed.

Data were explored using a R script (R Development Core Team 2008) calculating the mean of 3 to 5 runs per animals and analyzed using one-way ANOVA.
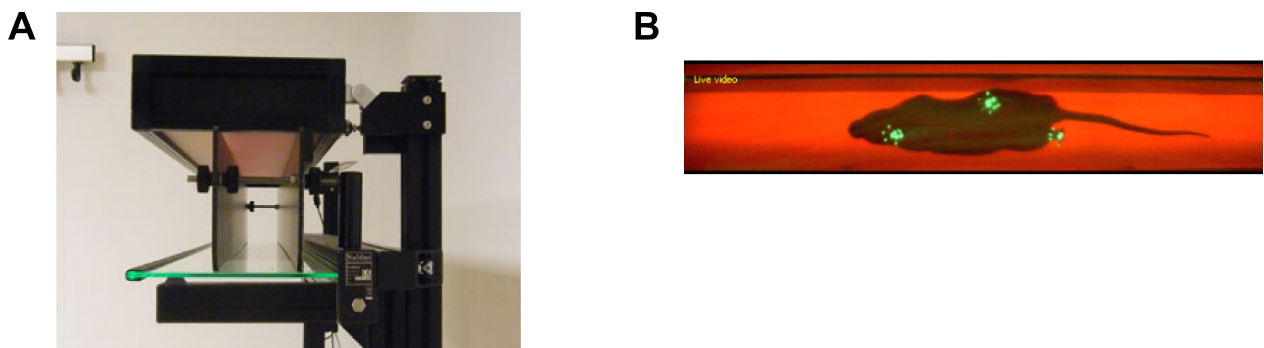
A   **B**

Figure 2-06: CatWalk

Picture copied from CatWalk user manually

CatWalk consists of a horizontal glass runway illuminated by LED light and reflecting footprints captured by a high-speed video camera positioned underneath the walkway. Because an increasing luminosity in the experimental room decreases the contrast of the illuminated footprint, experiment was performed during dark phase and under indirect red light illumination.

3.3.4   *Spontaneous home-cage activity assessment using LabMaster/PhenoMaster*

Spontaneous activity in home-cage environment of 4, 12 and 18 month-old mice was assessed using an automatic system allowing the tracking of single-housed mice represented in Fig. 2-07 (LabMaster/PhenoMaster, TSE). LabMaster/PhenoMaster is a system consisting of infrared beams surrounding a home-cage, recording ambulation of mice using beam breaks. Mice were acclimatized to the experimental room for at least 30 min before being transferred in the automatic system and recorded for three consecutive days. Data analysis was performed by calculating the mean of a parameter of interest for a fixed time interval using a R script (script in annex).

Novelty exploration was defined as the activity during the first 15 min of experiment. Total spontaneous activity (during complete dark or light phase) was assessed by binning data by interval of 30 minutes. Acclimatization to the system was investigated by comparing the mean of a parameter of interest over successive dark or light periods separately.

These data sets were analyzed using two-way ANOVA. Food and water intake was assessed by comparing the total amount of food or of water consumed by animal over three days and analyzed using one-way ANOVA.
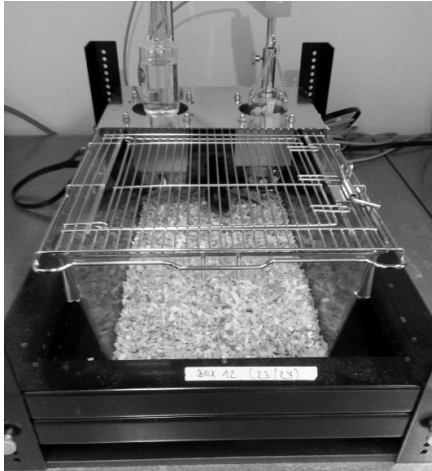

Figure 2-07: Automated cages

LabMaster/PhenoMaster is a system for single housed mice consisting of infrared beam surrounding a home cage, recording ambulation of mice using beam breaks.

3.3.5   *Exploratory and anxiety behavior assessment using open field*

Exploratory and emotional behavior was tested in open field test (represented in Fig. 2-08) in 4, 12, and 18 month-old mice. Mice were placed in a 100 × 100 cm arena with 50 cm high walls and activity was recorded for 10 min using video tracking software (VideoMot2, TSE).
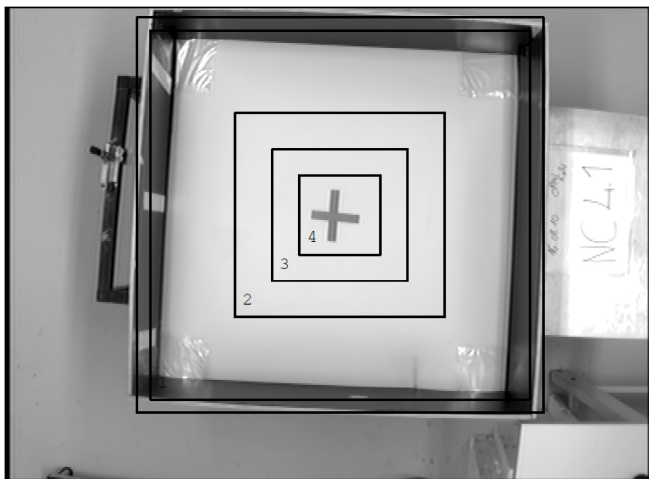

Figure 2-08: Open field

Screen shot of tracking system before the beginning of an experiment. Center of the field was determined in 4 concentric squares of 100, 60, 40 and 20 cm in order to test robustness of data.

| Materials and Methods

Light intensity in the center of the arena was set at l000 lux. Open field was separated in four area: the region 1 is the rim with a width of 8 cm; region 2, 3, and 4 are square of respectively 60, 40, and 25 cm side length and representing 36, 16, and 6% of the overall area respectively.

Mice were acclimatized in a separated room with a luminosity fixed at 25 lux for 15 min minimum prior the analysis. Mice were put in a corner of the open field pseudo-randomly chosen. Total distance, distance and time spend in each areas as well as the latency to reach each regions were analyzed using one-way ANOVA.

3.4 Smell test assessment using olfactory preference test

Olfactory preference tests (represented in Fig. 2-09) were conducted in 18 month-old mice to investigate potential olfactory perception deficit in mice. Mice were put into a rat type IV cage (595 × 380 × 200 mm box) that was separated into two equal compartments. The separating wall had a 6 × 10 cm opening that the mouse could move from one compartment to the other.

Experiment was performed during dark cycle under low light (animals kept at 25 lux, field at 50 lux) and video tracked (VideoMot2, TSE). Before the test, mice were acclimatized at least 30 min to the experimental room.

In a first experiment, one compartment of the cage was filled with 1–2 cm of clean bedding using a dustpan, and the other compartment was filled with 2–3 cm of 2 days old home-cage bedding. Mice were monitored for 10 min and bring back into their home-cage.

After testing all animals of the same home-cage, we added in the compartments containing the clean bedding of the system 1–2 cm of two days old rat bedding. Mice were introduced in the rat bedding and tracked for 10 min. Latency to leave the compartment as well as distance and time spent in each compartment were analyzed using one way ANOVA.

Figure 2-09: Smell test

Screen shot of video tracking system before smell test. Type IV cage was separated into two equal compartments by a plastic wall containing a 6 × 10 cm opening to separated mouse home-cage bedding (here region on the bottom 1) from the experimental region (here bedding from rat cage on the top 2).

3.5 Cognitive function assessment using water maze

To identify any potential cognitive deficits, we used the Morris water maze experiment as described previously (Freichel et al. 2007). A 2 m diameter and 50 cm high water-tank filled with opaque white water (21 °C ± 1 °C) was placed in a room containing extra maze cues (Fig. 2-10). Light intensity in water maze was set at l00 lux and mice were acclimatized to the same room. Mouse swim paths were monitored with a camera connected to the video tracking software (VideoMot2, TSE). Animals were introduce into a closed water tank compartment of the water maze in a pseudo-randomly order. Before opening the compartment and beginning the test, mice were acclimatized to the water for around 5 sec. The maximum trial duration was fixed at 60 sec. At the end of each trial, mice were standing on the platform for 30 sec (or were put on it if they did not found it). An inter-trial interval of 10 min was observed. Mice removed from the water were dried using paper towels and were warmed up in a cage illuminated by a red heat lamp for 5 minutes before putting them back on their home-cage.

Mice were first trained to find a 20 cm in diameter visible platform to escape from the water for 2 days and 4 trials per day. Spatial learning curve was calculated using latency or distance needed to find the platform and was analyzed using two-way ANOVA.

After the training, mice were tested for 2 days and 4 trials per day to find the same platform, located at the same place but hidden under the water. Spatial testing curve was calculated using latency or distance needed to find the platform and was analyzed using two-way ANOVA.

The last day, mice were placed in the pool in the water tank compartment in front of the platform. Platform was removed and mice strategy to find the platform was tracked for 60 sec. Spatial memory was investigated by calculating the percentage of time spent in each quadrant and by comparing the time spend in the quadrant containing previously the platform compared to the other using one-way ANOVA.
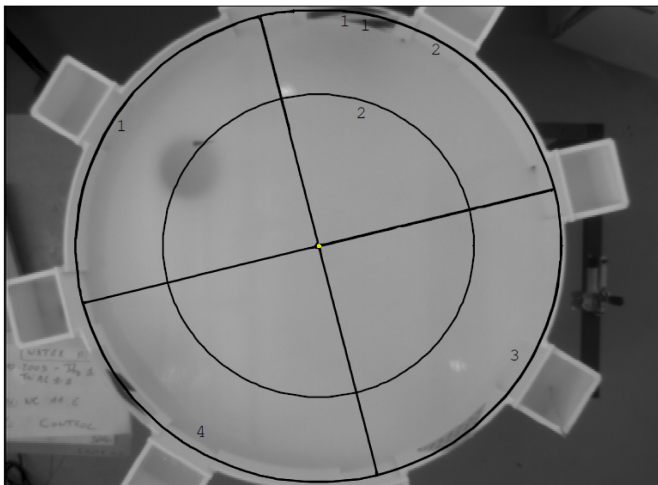

Figure 2-10: water maze

Screen shot of video tracking system during the cued test. Black platform and flag where used in order to facilitate spatial learning. Moreover, cued inside both the experimental room and the water tank were used to improve the spatial learning.

Results

The aim of this work is to investigate the potential effect(s) of the human synphilin-1 (sph1) on the progression of neuropathology in a mouse model of Parkinson's disease (PD). For this purpose, we cross-bred transgenic sph1 mice with mice overexpressing the human A30P mutated alpha-synuclein (a-syn) under the neuron specific promoter Thy-1 and presenting a progressive synucleinopathy extensively characterized (Kahle et al. 2000; Kahle et al. 2001; Neumann et al. 2002; Freichel et al. 2007; Schell et al. 2009).

1)   Generation of the double transgenic animals

Double transgenic mice (designated as double) resulting from cross-breeding homozygous mice expressing the human A30P mutated a-syn (A30P) with mice expressing the human sph1 (sph1) were viable, fertile, normal in size and did not display any gross physical or behavioral abnormalities. To generate a homogeneous group of double transgenic mice, we cross-bred homozygous A30P mice, sph1 mice, double-transgenic mice and non-transgenic (nTg) mice with C57BL/6N littermates.

Mice were genotyped using genomic DNA isolated from ear biopsies and presence of the transgene was investigated using PCR (Fig. 3-01).
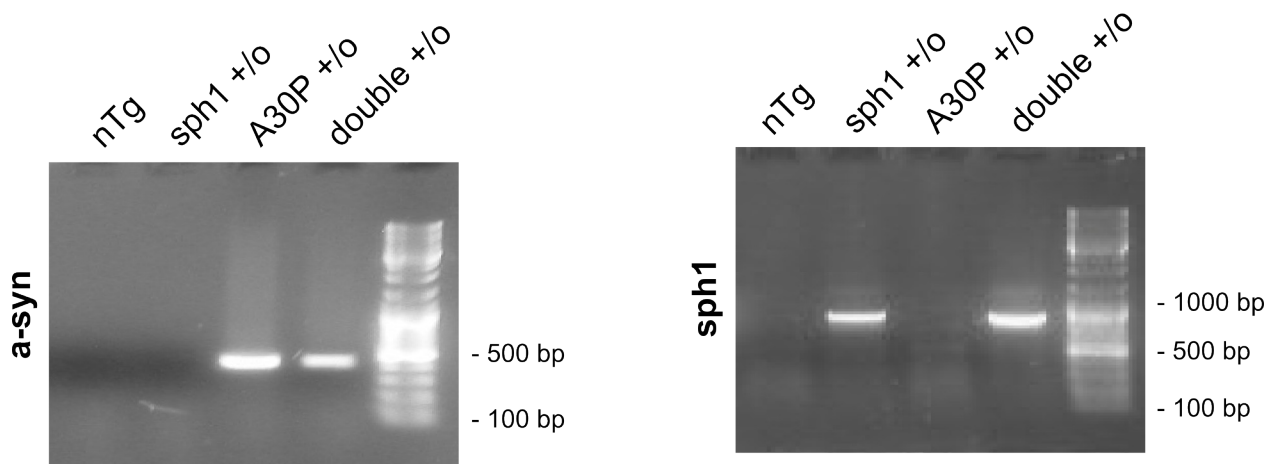
Figure 3-01: Animals genotyping

Animal genotype was determined using PCR from genomic DNA. Specific primer pairs for either a-syn or sph1 transgenes generated amplicons migrating at 400 and 800 base pairs (bp) respectively using electrophoresis of PCR products in 1% agarose gel containing 0.5 µg/ml ethidium bromide.

Zygosity was confirmed via quantitative real-time PCR (Fig. 3-02A) and amplification specificity was investigated using. We did not observe more than one main melting peak per primer pair (Fig. 3-02B), suggesting the presence of a unique amplicon.

A

a-syn

sph1

B

a-syn

b-actin

sph1

Figure 3-02: Transgenes zygosity

*A) Zygosity of the animals was determined using SYBR Green based relative quantitative PCR of 20 µg of genomic DNA; data presented as the mean of relative transgene copy number cal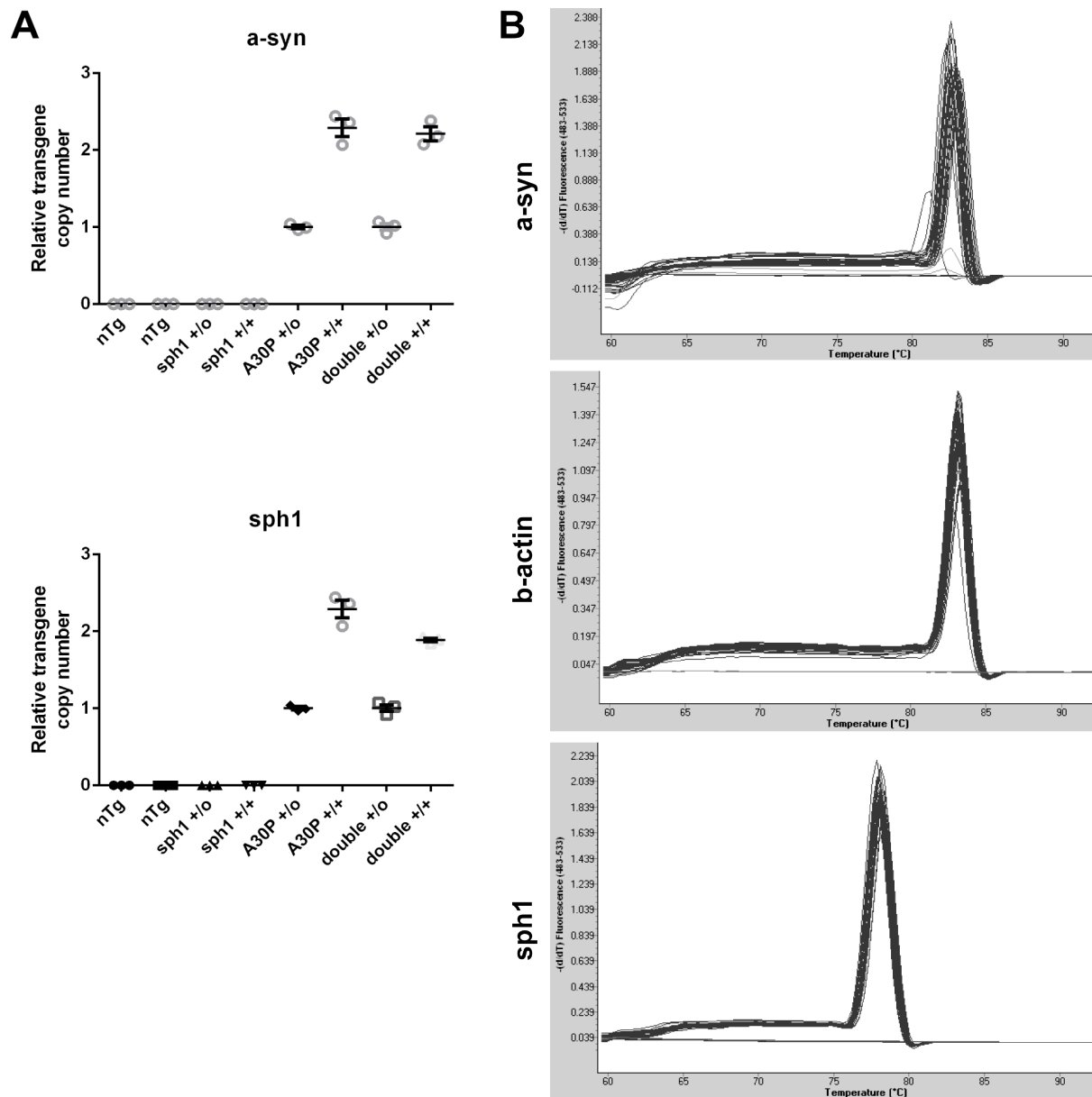culated via the ΔΔCp method ± SEM; number of technical replicates=3. **B)** Specificity of the amplification was analyzed using melting peak method.*

| Results

2)   Neuropathology in mice overexpressing A30P alpha-synuclein

2.1 Alpha-synuclein expression throughout brain of A30P mice

In order to investigate the potential effect(s) of sph1 on synucleinopathy developed in A30P mice, we first confirmed the expression of the transgenic human A30P mutated a-syn protein under the Thy-1 promoter in 12 month-old mice. Immunohistochemical analysis of the transgenic a-syn expression in A30P mouse brain was performed using an antibody specific for the human a-syn and providing no signal in nTg mice (Fig. 3-03A). Expression was found throughout the brain and spinal cord of transgenic mice (Fig. 3-03A). Intracellular distribution of a-syn was investigated at higher magnification and the location of a-syn was found to be in cell soma and neurites (Fig. 3-03B), reflecting a synaptic staining as suggested previously (Kahle et al. 2000).
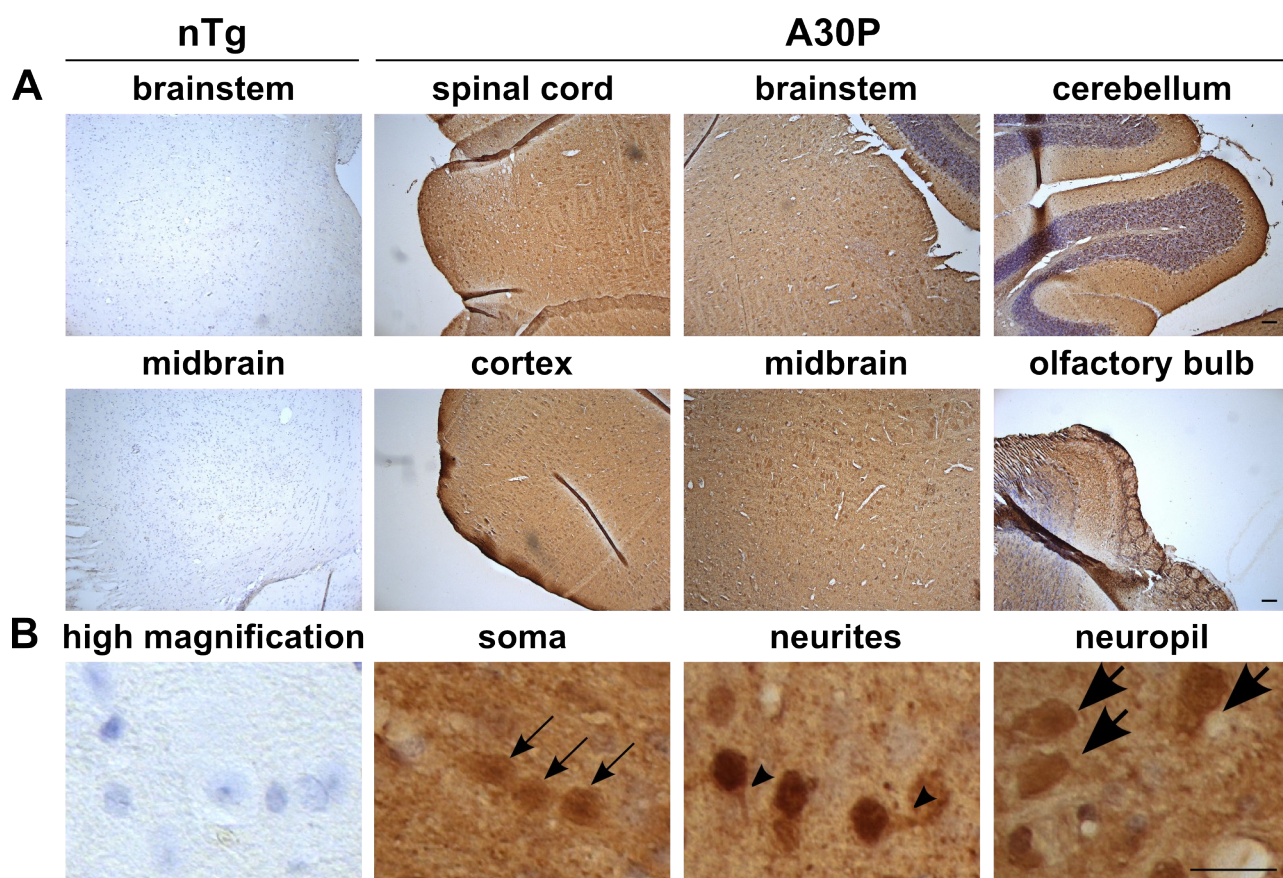
Figure 3-03: Expression of the human A30P alpha-synuclein in different brain regions of A30P mice

A) *Expression of the transgenic human A30P mutated a-syn on 7 µm thick sagittal mouse brain sections embedded in paraffin. Sections were immunostained using a human specific a-syn antibody and counterstained using hematoxylin. The transgene expression was detected throughout the brain of transgenic mice, including the spinal cord, brainstem, cerebellum, cortex, midbrain and olfactory bulb, but no signal was detected in nTg mice. B) Using higher magnification, presence of staining in cell soma (black arrow), neurites (black arrowhead) or generally neuropils (thick black arrow) were observed in the brainstem. Expression pattern was confirmed in at least two different animals; scale bar = 20 µm.*

2.2 Progressive accumulation of proteinase K resistant a-syn in the brainstem of A30P mice

Presence and accumulation of a-syn aggregation was investigated in A30P mice using an assay based on protease digestion resistance. We used proteinase K, a serine protease digesting native proteins, to investigate compactness and insolubility of a-syn, classically used to highlight presence of fibrillar structures (Miake et al. 2002). For this purpose, we digested paraffin sections bound to nitrocellulose membranes with proteinase K. As expected, the signal for a-syn was drastically decreased after digestion (Fig. 3-04A–C). Proteinase K resistant a-syn was detectable in 16 month-old mice (Fig. 3-04B) but almost undetectable in A30P mice at 12 months of age (Fig. 3-04C).

A -Proteinase K 16M A30P

B +Proteinase K 16M A30P

C +Proteinase K 12M A30P

D Proteinase K resistant a-syn
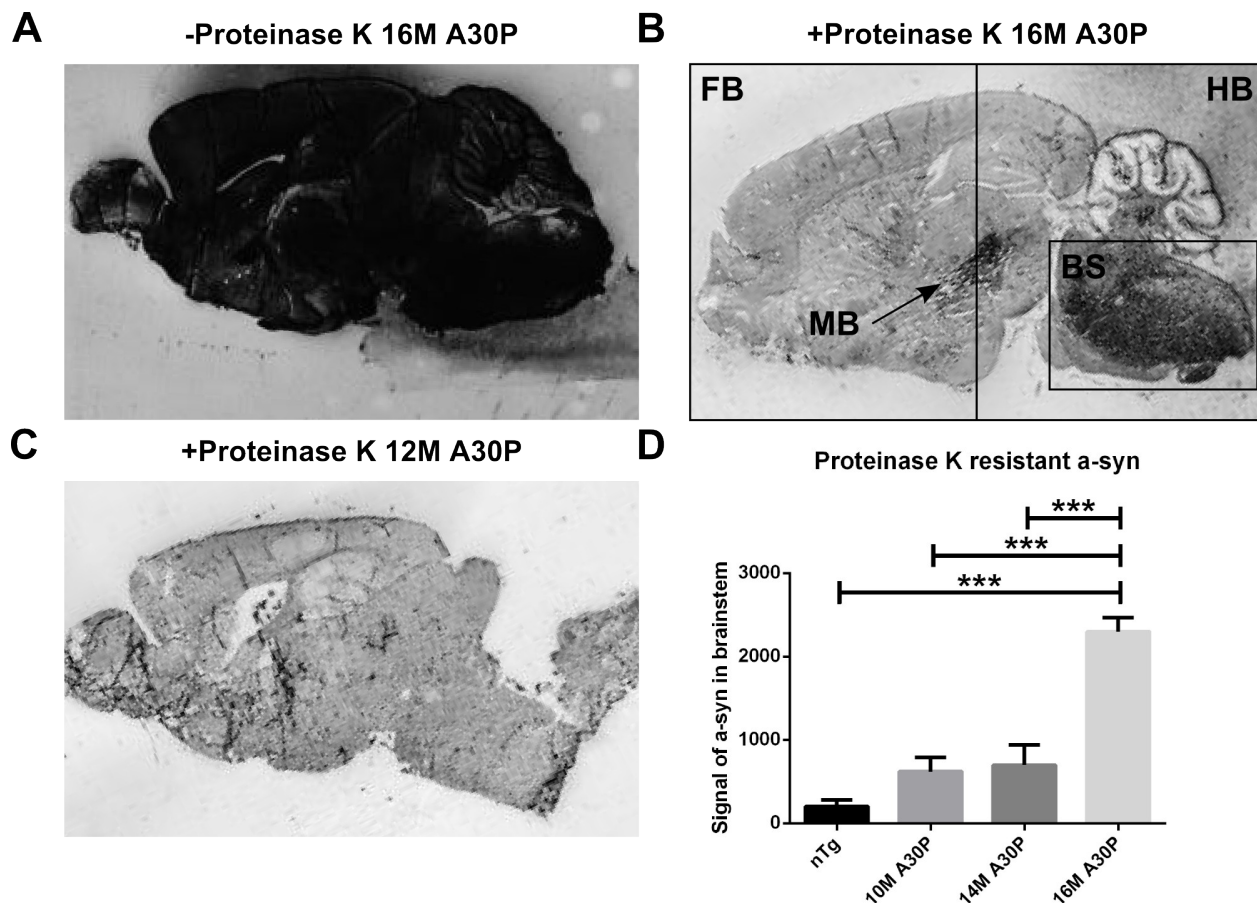
Figure 3-04: Distribution of proteinase K resistant alpha-synuclein in brainstem of 16 month-old A30P mice

IHC detection of transgene using the human a-syn specific antibody 15G7. 7 µm thick paraffin embedded sections were blotted on nitrocellulose membranes and digested using 50 µg/ml of proteinase K for 12 hours. A) Strong staining throughout the brain was observed in non-digested sections of A30P mice. B) Proteinase K resistant a-syn was observed in 16 month-old A30P mice, mainly located in brainstem and in midbrain. C) No resistant a-syn specific staining was observed in 12 month-old A30P mice. D) Densitometric quantifications of a-syn signal in brainstem of A30P mice and nTg control; data presented as the mean ± SEM; n=3; * P<0.05 one-way ANOVA post-hoc LSD. HB: hindbrain; FB: forebrain; MB: midbrain; BS: brainstem.

| Results

Proteinase K resistant a-syn was located mainly in the brainstem of A30P mice. The increase of indigestible a-syn in the brainstem of aging A30P mice (nTg: 204.6 ± 76.46, 10 M A30P: 620.9 ± 169.6, 14 M A30P: 699.2 ± 243.5, 16 M A30P: 2301 ± 169.8, one way ANOVA, p<0.001, Fig. 3-04D) has already been reported previously (Kahle et al. 2000; Neumann et al. 2002; Freichel et al. 2007).

2.3 Accumulation of SDS-insoluble a-syn in A30P mice hindbrain with aging

To confirm the increase of insoluble a-syn levels observed in hindbrain of A30P mice with aging using proteinase K digestion protocol, we extracted proteins based on their solubility in increasing amount of detergents and measured a-syn protein levels using sequential protein extraction.

High concentrations of detergents are of high interest to study protein aggregation as they break non-covalent protein bonds, in contrast to proteinase which cuts proteins into smaller units without cleaving peptide bonds, providing information regarding the stability of different protein filaments. Increase of RIPA insoluble a-syn was previously reported in brains of PD patients (Tofaris et al. 2003), in brain of a patient carrying the a-syn A30P mutation leading to familial form of PD (Seidel et al. 2010), and also in brains of mice overexpressing A30P a-syn (Kahle et al. 2001).

As the protein extraction protocol is based on several centrifugation and suspension steps, pellets that need to be suspended become smaller and more difficult to handle. Therefore, despite the fact that brainstem was the region most strongly stained in proteinase K resistance analysis, we choose to work with the complete hindbrain of 18 month-old mice which also contain the brainstem and which provide two to three time more material that the brainstem region alone.

We studied the RIPA insoluble fraction using western blot and detected immunoblot using the human specific a-syn antibody 15G7 which provided a specific signal at around 17 kDa (nTg: 0.165 ± 0.144, A30P 12 M: 15.03 ± 7.02, A30P 14 M: 16.98 ± 5.14, A30P 16 M: 100 ± 21.99). These results support the hypothesis that insoluble a-syn species are also present in 12 month-old A30P mice (1way ANOVA, p<0.05).

As suggested by the proteinase K digestion results, insoluble a-syn signal increase drastically at 16 months (1way ANOVA, p<0.001, Fig. 3-05A and B). This is also reflected by the presence of smaller and higher molecular weight species of a-syn. When detecting immunoblot using mc42 antibody, specific for human and mouse a-syn, we did not observe RIPA insoluble signal in nTg mice (nTg: 0.57 ± 0.180, A30P 12 M: 10.65 ± 6.92, A30P 14 M: 15.37 ± 6.90, A30P 16 M: 100 ± 21.73), but we confirmed the presence of insoluble a-syn in 12 month-old A30P (1way ANOVA, p<0.05) and an increase of insoluble a-syn in A30P mice with aging (1way ANOVA, p<0.001, Fig. 3-05B and C).
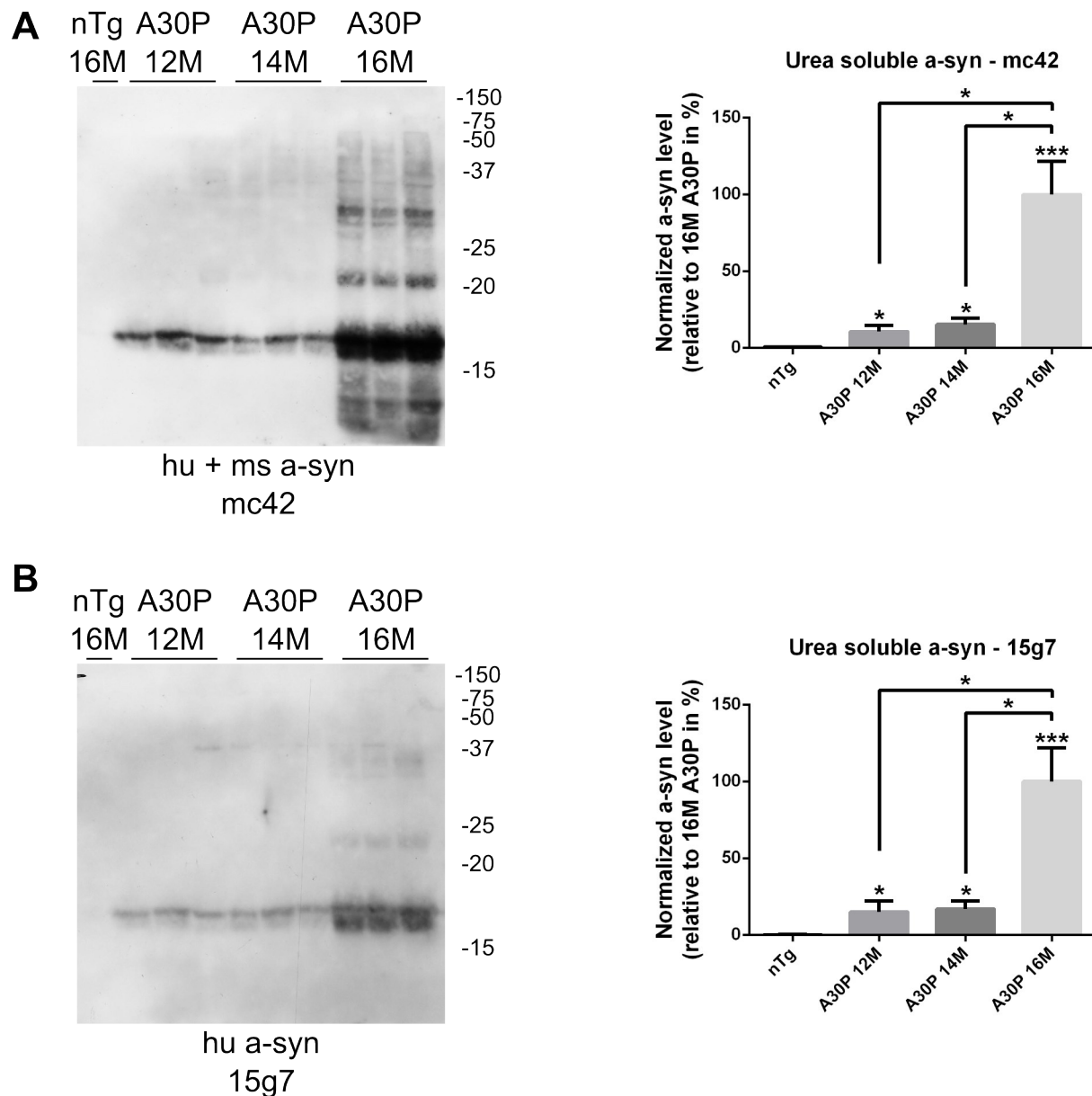
Figure 3-05: Presence of RIPA insoluble alpha-synuclein species in hindbrain of A30P mice

*Insoluble proteins were extracted from mouse hindbrain using a protocol based on detergent solubility. Levels of RIPA insoluble a-syn solubilized in 2 M urea were analyzed using western blot of 30 µg protein. **A)** Using an antibody specific for human and mouse a-syn, we observed a-syn bands at around 15 and 17 kDa in 12 and 14 month-old A30P transgenic mice. In 16 month-old A30P mice, an increasing intensity of the main bands was detected as well as the appearance of other a-syn species. **B)** No major differences could be seen when using an antibody specific for human a-syn. **C and D)** Densitometric quantification of a-syn signal using mc42 and 15G7 antibodies respectively; data presented as the mean ± SEM; n=3; * P<0.05, *** P<0.001 one-way ANOVA post-hoc LSD.*

3)   Reduction of alpha-synuclein aggregation in A30P mice by the coexpression of synphilin-1 in hindbrain of double transgenic mice

As described in the introduction, sph1 was frequently reported to increase a-syn aggregation *in vitro (Engelender et al. 1999; O'Farrell et al. 2001)* but also *in vivo (Krenz et al. 2009; Smith et al. 2010)*.

Recently, Wong et al. demonstrated *in vitro* that sph1 could act as a tag targeting different protein aggregates (including a-syn) to degradation via macroautophagy (Wong et al. 2012). In this section, we analyzed long term effects of sph1 expression on a-syn aggregation by using several methods specific for different forms of a-syn aggregates.

3.1 Synphilin-1 expression in sph1 mice

Similarly to the previous investigation of a-syn, we analyzed brains of sph1 mice to find regions expressing high levels of sph1 and susceptible to impact the pathology induced by a-syn overexpression.

Brains of transgenic mice overexpressing human sph1 under the PrP promoter were embedded in paraffin and immunostained using an antibody specific for the myc-tag, a flag inserted at the N-terminus of transgenic human sph1 (Fig. 3-06A). We observed a homogeneous staining over the whole brain, with the most predominant expression in the cerebellum, the cortex and the brainstem.

By using higher magnification, we also noticed the presence of transgenic sph1 in cell soma and in dendrites, suggesting its presence in the neuropil (Fig. 3-06B). In general, the expression pattern of sph1 in sph1 mice was very similar to expression of a-syn found in the A30P mice.
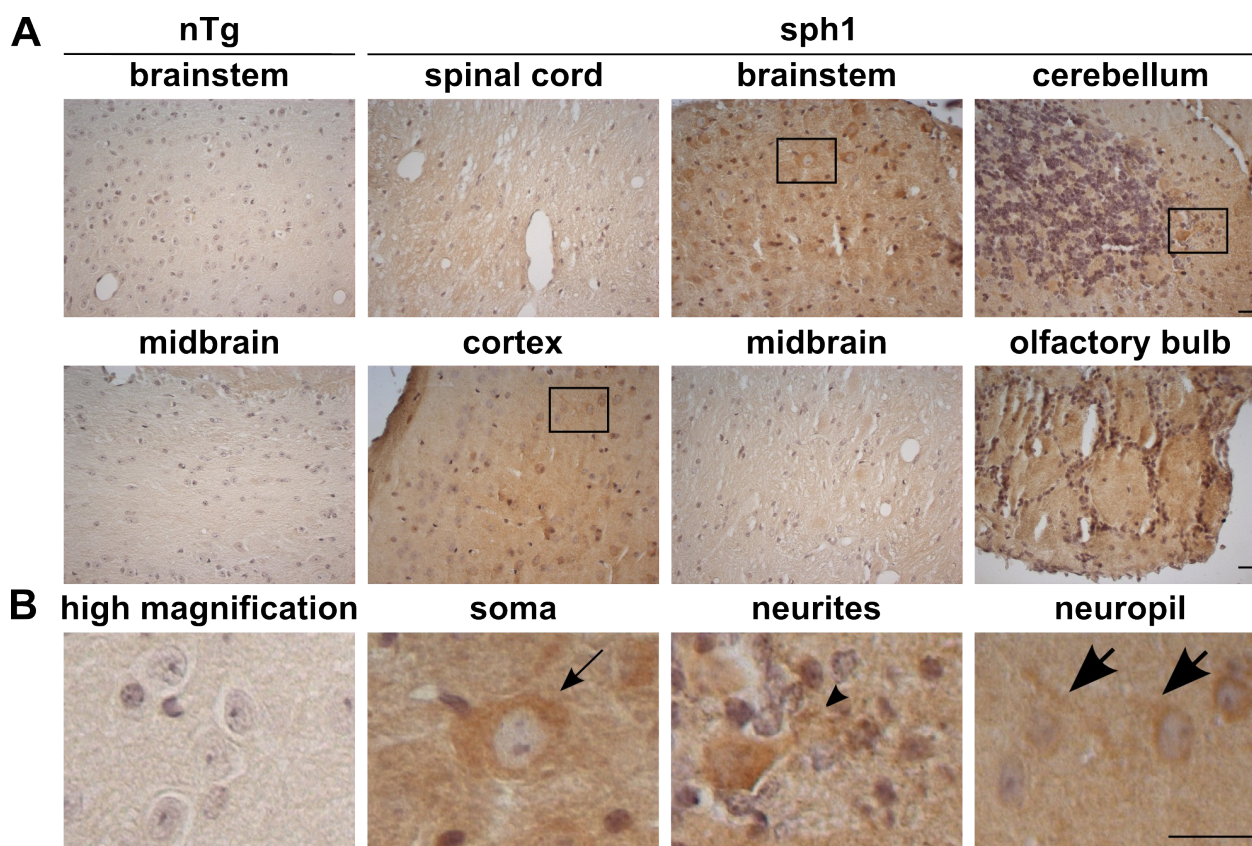
A

nTg	sph1

Figure 3-06: Expression of the transgenic human synphilin-1 in different brain regions of synphilin-1 mice

A) Expression of the transgenic human sph1 was analyzed on 7 µm thick sagittal mouse brain sections embedded in paraffin. Sections were immunostained using an antibody specific for myc-tag conjugated to the sph1 transgenic protein, and counterstained using hematoxylin. The transgene expression was detected throughout the brain of transgenic mice, including the spinal cord, brainstem, cerebellum, cortex, midbrain and olfactory bulb. B) Using higher magnification of selected brain regions (highlighted by black rectangles), presence of staining in cell soma (black arrow), neurites (black arrowhead) or generally neuropils (thick black arrow) were observed. Expression pattern was confirmed at least in two different animals; scale bar = 20 µm.

3.2 Coexpression of alpha-synuclein and synphilin-1 in several brain regions and including brainstem in double transgenic mice

To confirm that brainstem, cerebellum and cortex coexpress a-syn and sph1 in the same subset of neurons, we performed double immunofluorescence staining of human a-syn and of human myc-tagged sph1. In brain of double transgenic mice, we detected neurons containing both sph1 and a-syn transgenic proteins (Fig. 3-07), presenting 1–5 µm round structures in the perinuclear soma both stained with human specific a-syn and myc-tagged sph1 (Fig. 3-07, white arrowheads).
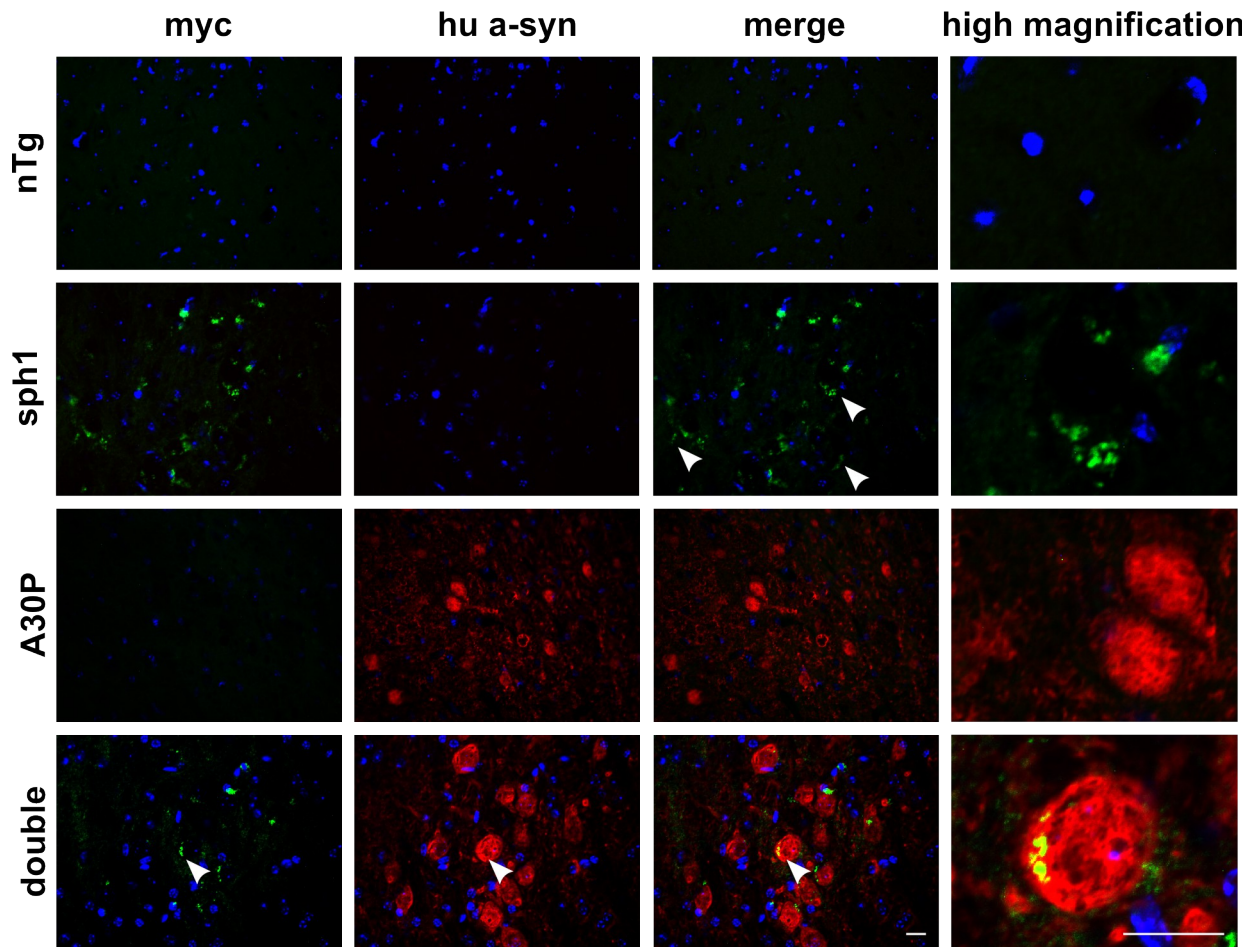
Figure 3-07: Coexpression of alpha-synuclein and synphilin-1 in double transgenic mice

A) Coexpression of the transgenic A30P mutated human a-syn and of the transgenic human sph1 was analyzed on 7 µm thick sagittal mouse brain sections. Sections were immunostained using fluorescent antibodies specific for the human a-syn protein and for myc-tag conjugated to the sph1 transgenic protein. Nuclei were stained with DAPI. Coexpression of both transgenic proteins was confirmed in some cells of double transgenic mice. B) Using higher magnification, presence of perinuclear located 1–5 µm round structures positive for both a-syn and sph1 transgenes was observed (white arrows). Expression pattern was confirmed in 4 different animals; red: a-syn, green: sph1, blue: DAPI; scale-bar=20 µm.

These data confirm the expression of both proteins within some cells, but also suggest a possible interaction of both transgenic proteins in our model. We did not observe any staining in non-transgenic mice using the human a-syn antibody, and only low level of background using myc antibody (Fig. 3-07).

3.3 Decreased levels of soluble alpha-synuclein in brainstem of A30P mice coexpressing synphilin-1

Before investigating any potential effect(s) of sph1 on a-syn aggregation, we first analyzed the effect of sph1 on soluble levels of transgenic a-syn protein. We used western blot analysis of hindbrain lysed in TBS extraction buffer and ultracentrifuged at 120.000 g to extract most soluble proteins of the cytoplasm (Fig. 3-08). Consistent with previous observations, we detected an age-dependent increase of soluble monomeric human (A30P 4 M: 62.72 ± 5.31%; A30P 18 M: 100.00 ± 7.85%) and total a-syn (A30P 4 M: 64.48 ± 9.41%; A30P 18 M: 100.00 ± 12.98%) signals at 17 kDa in brainstem of A30P animals (P<0.05, one way ANOVA, post-hoc LSD). In contrast, we did not observe a significant accumulation of human mutant (double 4 M: 80.69 ± 3.22%; double 18 M: 83.70 ± 8.28%) and total a-syn (double 4 M: 77.16 ± 3.01%; double 18 M: 87.23 ± 12.36%) in age-matched double-transgenic animals (P>0.05, one way ANOVA, post-hoc LSD). Investigation of soluble sph1 in western blot using this extraction method provided signal of poor quality at 120 kDa, allowing the confirmation of animal genotype but making a quantitative analysis of sph1 levels impossible (representative picture in (Fig. 3-08)). These results suggest that another extraction method is necessary to extract sph1 from brain tissue, probably due of a poor solubility of transgenic sph1 in sph1 and in double transgenic mice.
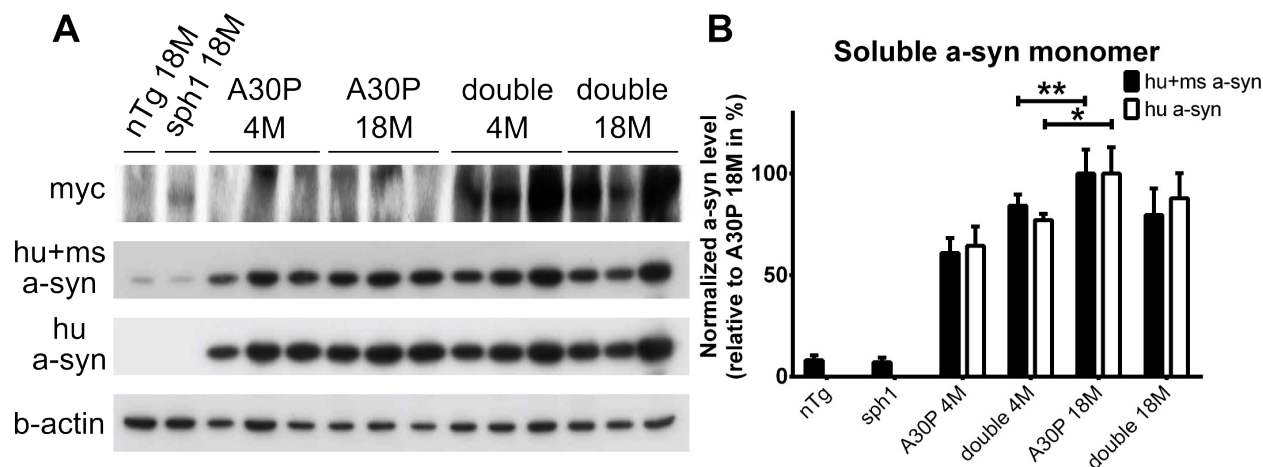
Figure 3-08: Synphilin-1 decreased levels of soluble alpha-synuclein protein in double transgenic mice

*Levels of soluble a-syn were investigated using western blotting. 30 µg of 4 and 18 month-old mouse brain lysed in TBS and ultracentrifuged 30 min at 120 000 g to extract soluble proteins were loaded per lane. A) Immunodetection of a-syn showed increasing levels of soluble a-syn in A30P transgenic animals with aging, but not in double transgenic animals. B) Densitometric quantifications of a-syn signal using mc42 and 15G7 antibodies, respectively, showed a significant difference between 4 and 18 month-old A30P mice; data presented as the mean ± SEM; n=3; * P<0.05 one-way ANOVA post-hoc LSD.*

3.4 Strong reduction of proteinase K resistant alpha-synuclein levels in brainstem of A30P mice coexpressing synphilin-1

To explore levels of a-syn aggregation in mice coexpressing sph1, we performed immunohistological staining of human a-syn using 15G7 antibody on 7 µm thin mouse brain section embedded in paraffin and digested with 50 µg/ml of proteinase K for 30 min. For convenience, proteinase K protocol was established a second time on glass slides as described in (Tanji et al. 2010) (faster protocol, no need to prepare special sections on nitrocellulose). A strong reduction of a-syn staining was observed after digestion in both A30P and double transgenic mice (Fig. 3-09). Antibody specific for the human a-syn did not provide any signal in nTg and sph1 animals. In A30P brain sections digested with the proteinase K we observed the presence of cell soma and neurites completely stained with a-syn antibody (Fig. 3-09). But surprisingly, the frequency of these observations as well as intensity of the staining was lower in double transgenic animals when compared to A30P mice (A30P: 3.917 ± 0.45, double: 0.617 ± 0.331 stained neurons per field, unpaired t test, p<0.01). These data indicate that a-syn aggregation observed in A30P mice can be decreased or slowed down by sph1 coexpression *in vivo*.
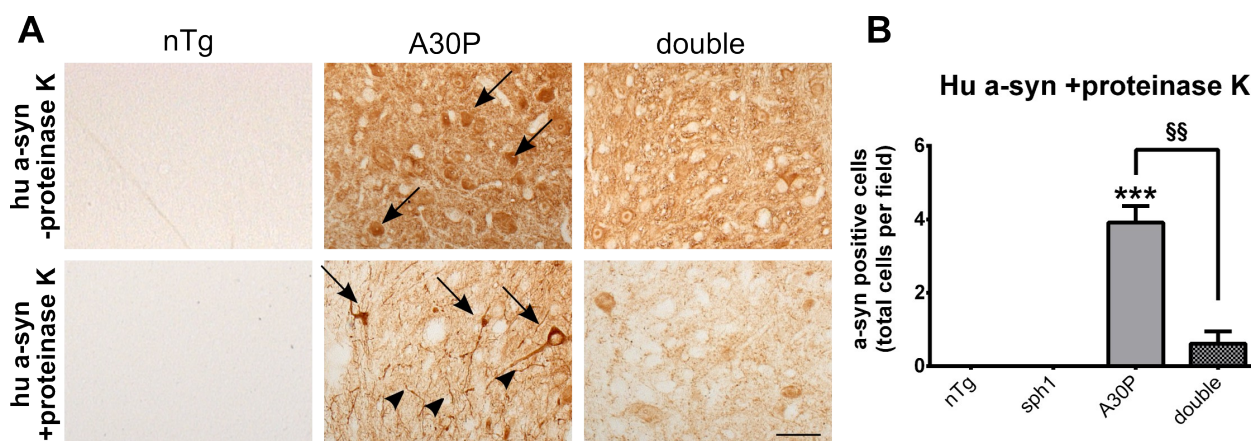
Figure 3-09: Synphilin-1 coexpression decreased proteinase K resistant alpha-synuclein levels in brainstem of A30P mice

*Levels of proteinase K resistant a-syn were investigated by IHC using a specific antibody against the human a-syn 15G7 on 7 µm thick paraffin embedded sections digested 30 min with 50 µg/ml proteinase K. A) Undigested sections of A30P mice displayed a dense a-syn positive staining in larger neurons of the brainstem (black arrows). Interestingly, this dense staining pattern was almost absent in double transgenic mice. In digested sections, a relatively strong a-syn staining was present in cell soma (black arrows) and neurites (black arrowheads) of A30P mice. Less intense and frequent staining was observed in double transgenic mice. B) Quantifications of a-syn positive cells number using 8 fields of 3 sections per animal; data presented as the mean ± SEM; n=3; *** P<0.001 when compared to nTg; §§ P<0.01 when compared to A30P; one-way ANOVA post-hoc LSD.*

3.5 Levels of RIPA insoluble alpha-synuclein are reduced in hindbrain of A30P mice coexpressing synphilin-1

Histological investigation of proteinase K resistant a-syn provided the first insight that the aggregation of a-syn to compact structures might be decreased in A30P animals coexpressing sph1. By using sequential protein extraction based on an increase amount of detergents, we investigated if A30P hemizygous mice also present RIPA insoluble a-syn and if coexpression of sph1 could decrease these a-syn species in double transgenic mice. Therefore, we performed sequential protein extraction of mouse hindbrain and analyzed the RIPA insoluble fraction resolved in 2 M urea using western blot (Fig. 3-10).
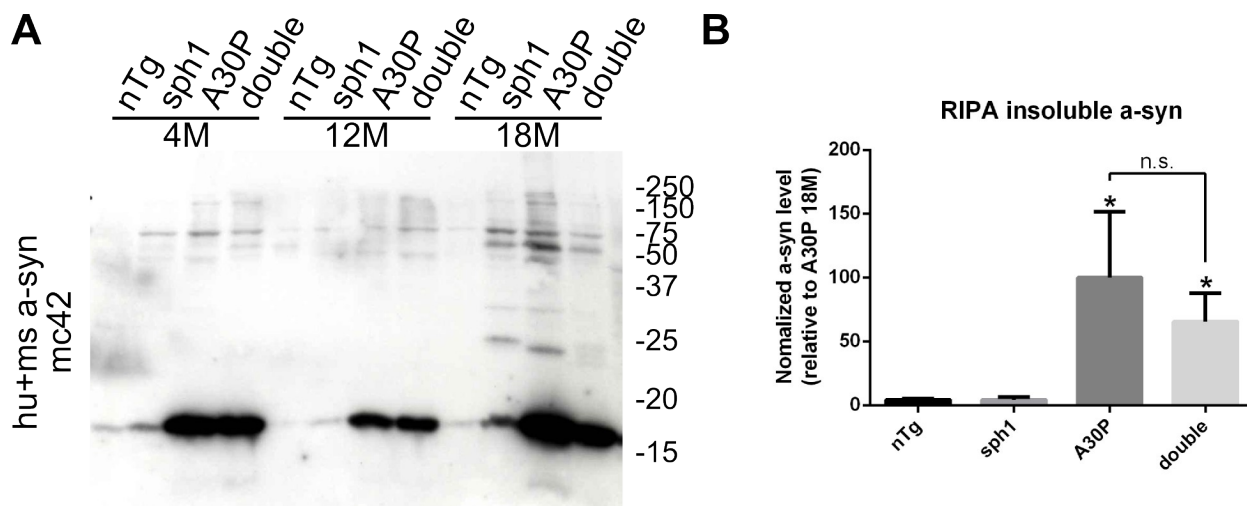

Figure 3-10: Levels of RIPA insoluble a-syn was decreased in A30P mice coexpressing synphilin-1

*Levels of RIPA insoluble a-syn species were investigated in hindbrain of mice. RIPA insoluble proteins solubilized in 2 M urea were analyzed using Western blot. **A)** Immunoblot detections using an antibody specific for the human and mouse a-syn (mc42) showed large increase of insoluble a-syn signals at 17 kDa in A30P and double transgenic when compared to nTg mice. We observed the presence of a RIPA insoluble a-syn fragment at around 12 kDa in A30P and double transgenic mice. We did not observe an accumulation of RIPA insoluble a-syn with aging. **B)** Densitometric quantifications of a-syn signals using mc42 antibody showed significantly higher levels of RIPA insoluble a-syn in A30P and double transgenic mice at 18 months of age when compared to nTg or sph1. No significant difference could be detected between 18 month-old A30P and double transgenic mice; data presented as the mean ± SEM; n=3; * P<0.05 when compared to nTg; one-way ANOVA post-hoc LSD.*

Consistent with previous observations, we detected an increase of insoluble monomeric human and mouse a-syn when using mc42 antibody (nTg: 4.29 ± 0.77%; sph1:4.28 ± 2.17%; A30P: 100.0 ± 51.5%; double: 65.6 ± 22.13%) at 17 kDa in hindbrain of A30P and double transgenic animals when compared to nTg (P<0.05, one way ANOVA, post-hoc LSD; Fig. 3-10A). We observed a decrease of insoluble a-syn in age-matched double-transgenic animals when compared to A30P (Fig. 3-10A). This observation was not statistically significant, which could be the consequence of variability within lines (P>0.05, one way ANOVA, post-hoc LSD).

Moreover, we did not observe an accumulation of RIPA insoluble a-syn monomer or oligomers with age in hemizygous a-syn mice (Fig. 3-10B) suggesting that at 18 months in hemizygous A30P mice, expression level of a-syn is not sufficient to observe an accumulation of RIPA insoluble a-syn. However, we noticed the presence of an a-syn fragment in 18 month-old A30P mice at around 12 kDa which was absent in the other genotypes (Fig. 3-10B). In contrast to the proteinase K digestion, these data suggest that proteinase K resistant a-syn structures have a different nature than a-syn species isolated using the sequential protein extraction.

3.6 Decreasing high molecular weight a-syn aggregates in A30P mice by synphilin-1 coexpression

To identify a-syn species decreased in the proteinase K resistant assay in double transgenic animals, we performed AGERA of proteins isolated from hindbrain in a non-centrifuged RIPA homogenate.

The homogenates were analyzed using 1.5% agarose gel to separate higher molecular structures. We first investigated homozygous mice and found, in a comparable manner to western blot, a strong increase of the monomeric form of a-syn in oldest A30P animals when immunoblots were stained with antibodies specific either for the human or for the mouse and human a-syn (Fig. 3-11A).

When comparing hemizygous A30P with hemizygous double transgenic mice, we observed a smear of a-syn proteins species both in A30P and in double transgenic mice. However, these smears were more comparable in strength and in molecular weight to younger homozygous A30P mice (Fig. 3-11B) suggesting a mild aggregation in hemizygous A30P mice. Interestingly, we did not observe pattern or intensity changes between A30P and double transgenic a-syn smear in AGERA.

A

| nTg 18M | A30P +/+ 10M | A30P +/+ 14M | A30P +/+ 16M | nTg 18M | A30P +/+ 10M | A30P +/+ 14M | A30P +/+ 16M |

hu a-syn   **hu+ms a-syn**

B

| nTg 18M | sph1 +/0 18M | A30P +/0 18M | double +/0 18M | nTg 18M | sph1 +/0 18M | A30P +/0 18M | double +/0 18M |

hu a-syn   **hu+ms a-syn**
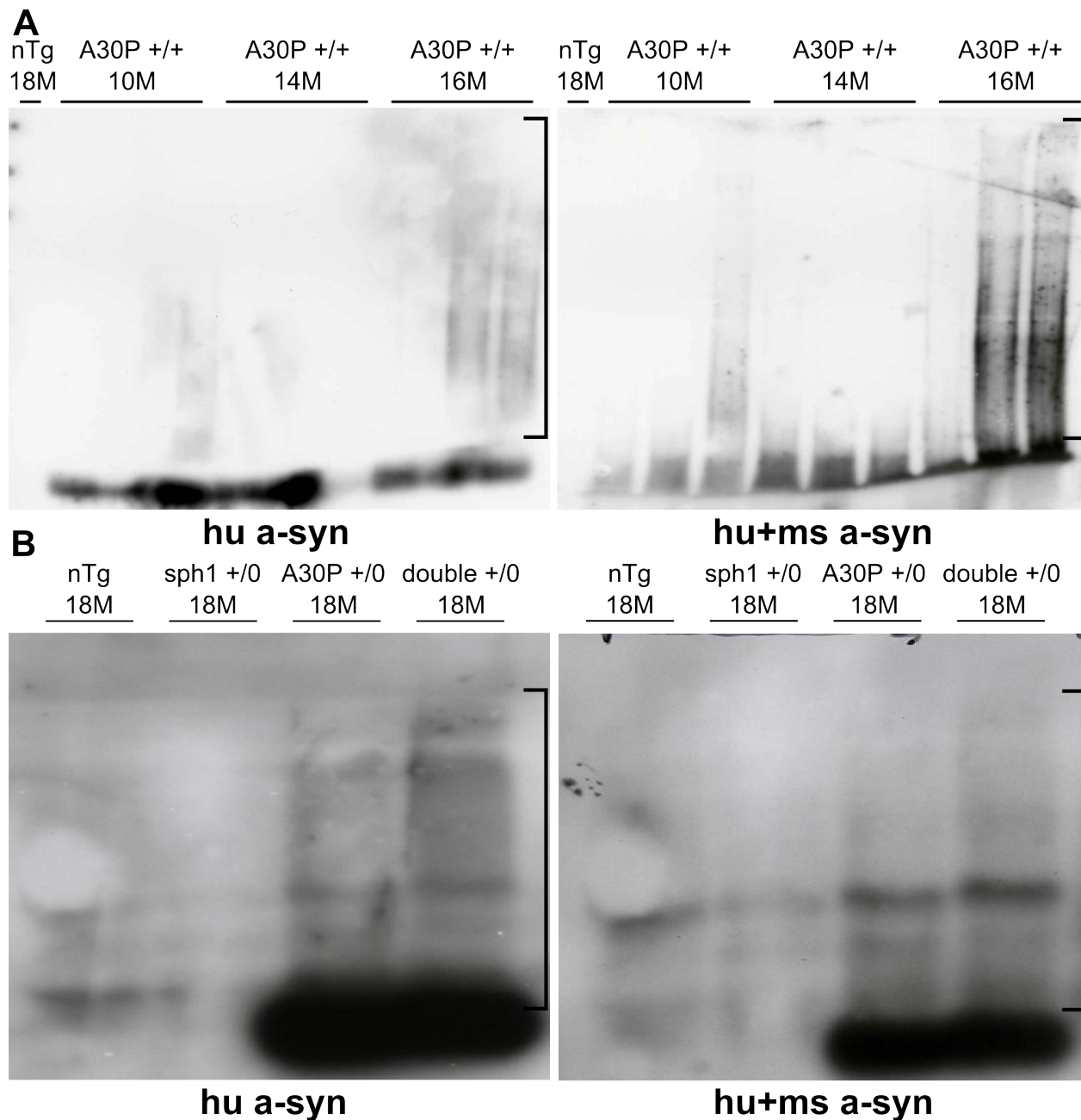
Figure 3-11: Increase in a-syn high molecular weight species in homozygous A30P mice was not detectable in hemizygous mice

*AGERA analysis of RIPA hindbrain homogenates. 50 µg of protein were loaded on an agarose gel and blotted on a PVDF membrane. **A)** A smear of a-syn high molecular weight species could be observed either using a human or using a human and mouse specific antibodies in aging homozygous A30P mice. **B)** No specific high molecular smear of a-syn was observed in both hemizygous A30P and double transgenic animals*

3.7 Homozygous A30P mice present an age-dependent increasing load of alpha-synuclein oligomeric species

In the aggregation process of a-syn, oligomers are considered to represent the first seeds which result in a cascade of protein accumulation [reviewed in (Lashuel et al. 2012)]. We investigated oligomeric forms levels of a-syn using dot blot and antibodies specific for oligomer structures (Fig. 3-12). To establish this method, we investigated the specificity of different oligomer antibodies using as negative control human a-syn protein artificially fibrillized and not presenting the epitope used to raise the antibodies, and as positive control the same a-syn fibrils but sonicated at 40% power for 30 pulses of 0.5 second (Fig. 3-12) and forming seeds with properties close to oligomers.

A

B
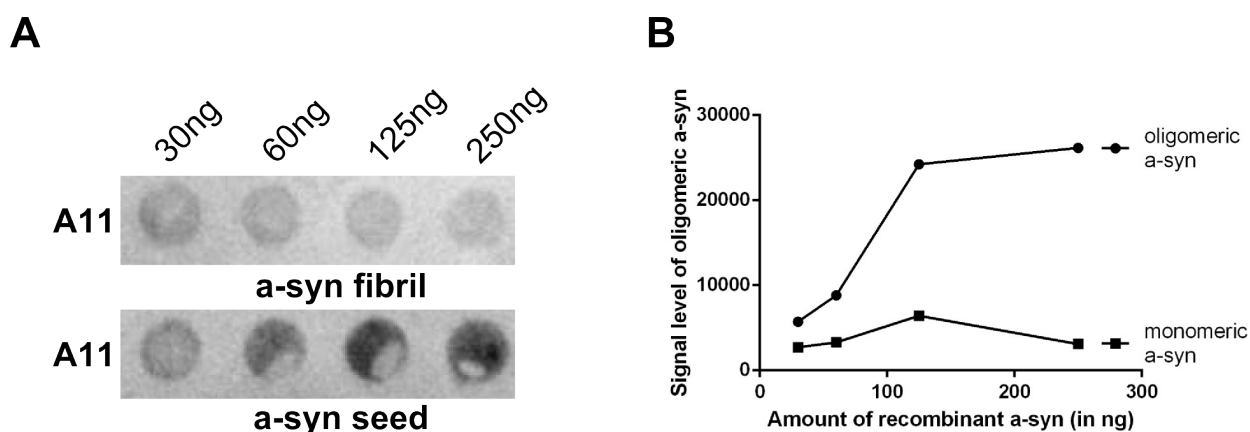
Figure 3-12: Specific detection of alpha-synuclein seeds using dot blot

A) Different dilutions of recombinant a-syn were spotted on a nitrocellulose membrane and detected using the A11 anti-oligomer antibody. No specific signal was observed when using fibrillized a-syn but a specific signal was detected in sonicated a-syn fibrils. B) Densitometric quantifications of oligomeric a-syn using A11 antibody showed a positive correlation between the amounts of material spotted and the signal intensity.

In order to solubilize oligomers without breaking their structures, several lysis buffers and antibodies were tested. We found an age-dependent increase of oligomer in A30P homozygous animals using mouse hindbrain lysed in RIPA buffer without centrifugation and using the Fila1 antibody (Fig. 3-13A–C). A supportive tendency was observed using A11 antibody, but variability within samples did not provide significance. We then also measured oligomer levels in A30P hemizygous mice coexpressing sph1, but did not observed a specific staining (Fig. 3-11D) suggesting that in hemizygous animals the expression level of a-syn is too low to form detectable levels of oligomers. These data are supported by the sequential protein extraction results, where we found a very strong increase of insoluble a-syn species larger that a-syn monomer in A30P homozygous mice (Fig. 3-05A,B) but not in A30P hemizygous mice (Fig. 3-10).
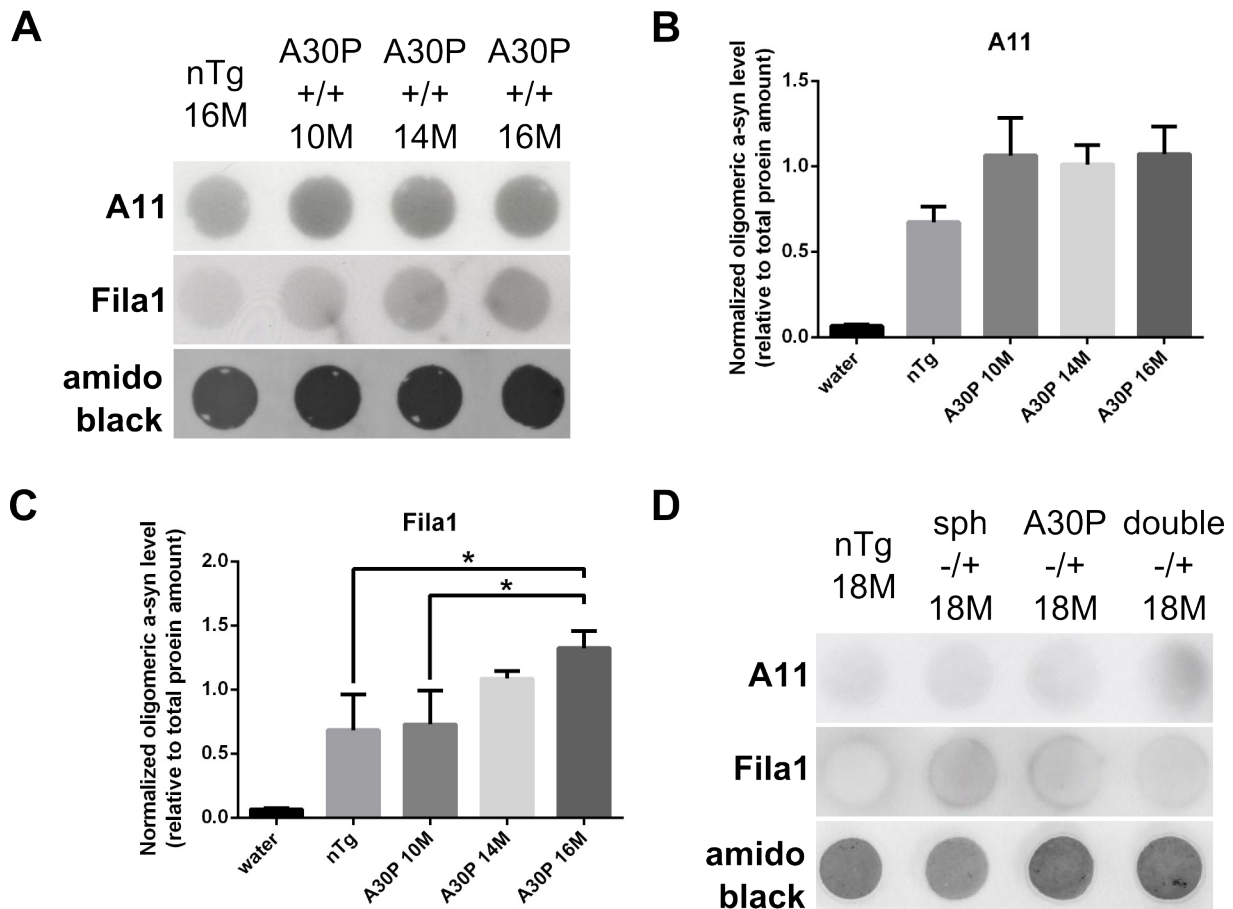
Figure 3-13: Increase of oligomeric species in aging homozygous A30P mice was not detectable in hemizygous mice

A) Dot blot analysis using 10 μg of mouse hindbrain homogenate and detected using A11 and Fila1, both anti-oligomer antibodies. *B)* We observed a non-significant increase of oligomeric signal in A30P mice when compared to nTg mice using A11 antibody. *C)* When using Fila1 antibody, we detected a progressive increase of oligomeric a-syn with mouse aging; data presented as the mean ± SEM; n=3; * P<0.05; one-way ANOVA post-hoc LSD. *D)* No specific oligomeric a-syn was detected with both A11 and with Fila1 antibodies in hindbrain of 18 month-old hemizygous A30P and double transgenic mice.

3.8 Synphilin-1 decreased alpha-synuclein fibril levels in A30P mice

To investigate if the fibrillar structure of a-syn species decreased by sph1 coexpression, we generated a group of 12 month-old animals which was shipped to our collaborator (Prof. Lucas, Madrid, Spain) to perform immunogold electron microscopy. Therefore fractionation of brain lysate was performed to enrichment a-syn fibrils. Fibrils were then immunostained using an antibody specific for human and mouse a-syn and conjugated to gold particles. Weak background staining was found in SNCA KO animals and in nTg mice (SNCA KO: 0.75 ± 0.41, nTg: 2.32 ± 0.70 stained fibrils per field, one-way ANOVA, p>0.05, data not represented) but an important increase was found in A30P mice when compared to nTg mice (nTg: 2.32 ± 0.70, A30P: 8.14 ± 0.55 stained fibrils per field, one-way ANOVA, post hoc Tukey, p<0.001, Fig. 3-14), this increase was totally reversed in A30P mice coexpressing sph1 (A30P: 8.14 ± 0.55, double: 0.80 ± 0.24 stained fibrils per field, one-way ANOVA, post hoc Tukey, p<0.001, Fig. 3-14).
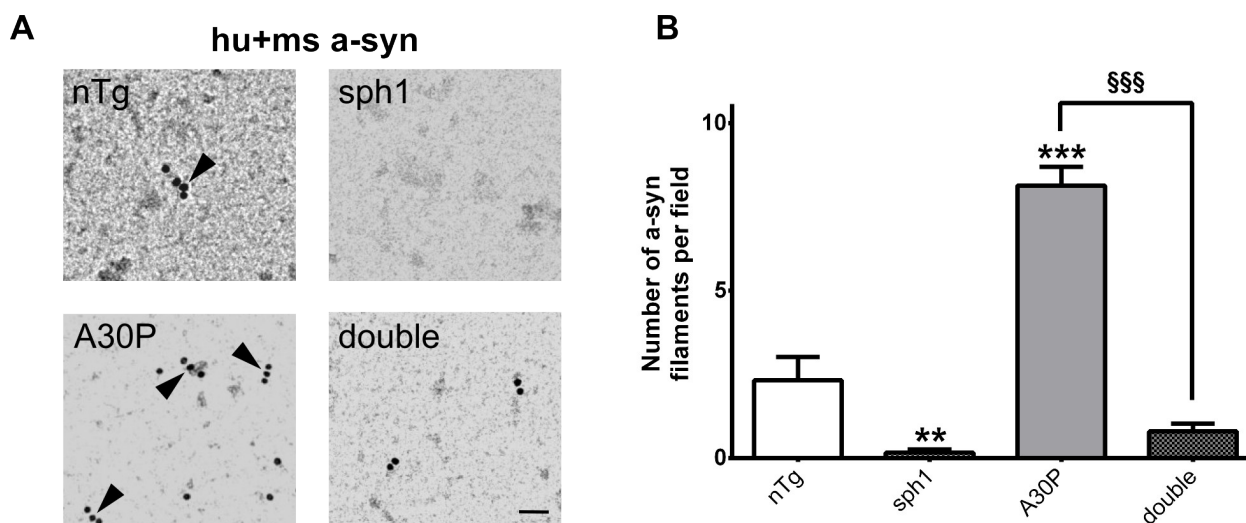
Figure 3-14: Synphilin-1 coexpression decreased a-syn fibrils levels present in A30P mice

Figure provided by Prof. J. Lucas, Madrid, Spain

Immunoelectron microscopy of a-syn filament-enriched fractions obtained from whole brain homogenate of 12 month-old animals. **A)** *Filaments of a-syn were decorated with 10 nm gold particles as indicated by arrowheads.* **B)** *An increased density of a-syn filaments was found in A30P animals when compared to nTg. In contrast, density of a-syn filaments in sph1 and double-transgenic animals was decreased when compared to nTg; data presented as the mean ± SEM; n=3; ** P<0.01, *** P<0.001 when compared to nTg, §§§ P<0.001 when compared to A30P, one-way ANOVA, post-hoc LSD; scale bar: 50 nm.*

3.9 Alpha-synuclein soluble fragments levels present in hindbrain of A30P mice were decreased by synphilin-1 coexpression

In addition to oligomers, truncated a-syn species have also been reported to be prone to aggregation (Crowther et al. 1998; Kim et al. 2002; I. V. J. Murray et al. 2003). In order to investigate whether sph1 expression can change patterns or levels of a-syn fragments, we extracted proteins of 18 month-old mouse hindbrain using TBS extraction buffer ultracentrifuged at 120.000 g to extract the most soluble proteins of the cytoplasm (Fig. 3-15).

Western blot analysis using a-syn antibody specific for the C-terminal part of the human a-syn shows the presence of two a-syn fragments at around 13 and 12 kDa in A30P mice (Fig. 3-15). Interestingly, intensity of a-syn fragment species was higher in A30P mice when compared to double transgenic mice (A30P: 100.0 ± 7.70; double: 30.32 ± 5.04; t test; $p<0.001$). When using an antibody specific for the central NAC domain and detecting both, human and mouse a-syn, two specific fragments were observed in A30P mice and both were reduced when sph1 was coexpressed; fragment f1 at 10 kDa (A30P: 100.0 ± 10.36; double: 8.23 ± 1.53; t test; $p<0.01$) and fragment f2 at 12 kDa (A30P: 100.0 ± 9.94; double: 23.96 ± 3.84; t test; $p<0.01$).

Epitope specificity of the human C-terminus antibody suggests that two N-terminal a-syn truncations of human a-syn were reduced by sph1 coexpression. However, since the mc42 antibody is detecting both, human and mouse a-syn, and because its epitope is targeted against the central part of the protein, we cannot conclude if fragments seen are C- or N-terminal truncation of the human or of the mouse a-syn.
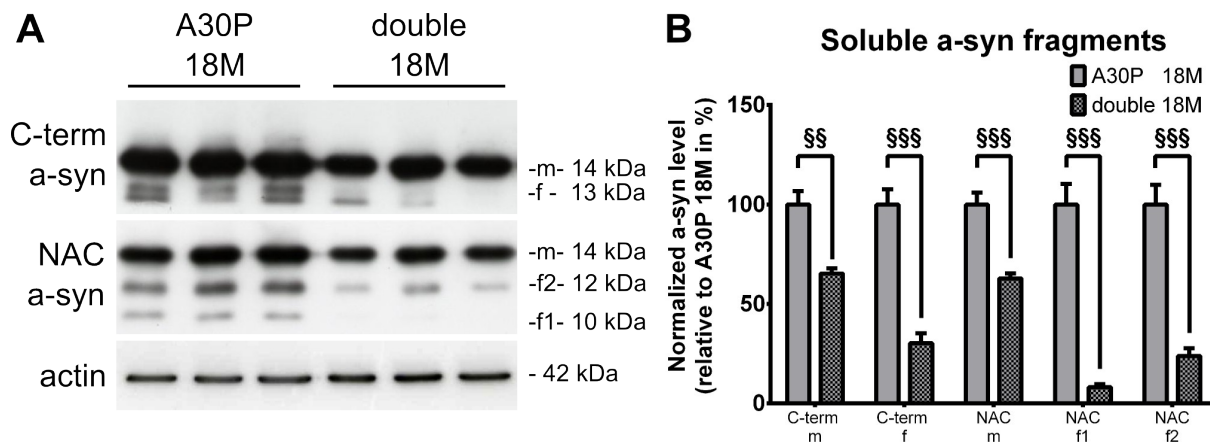
Figure 3-15: Soluble alpha-synuclein fragments in A30P mice were decreased in mice coexpressing synphilin-1

A) Western blot analysis of 10 µg soluble proteins extracted from hindbrain of 18 month-old mice. Detection of a-syn was performed using antibodies specific for the C-terminal or NAC domain. B) We observed with both antibodies a reduction of monomer and a strong reduction of fragments in double transgenic mice when compared to A30P; data presented as the mean ± SEM; n=3; § P<0.05, §§ P<0.01 and §§§ P<0.001 when compared to A30P, one-way ANOVA, post hoc LSD.

4) *Partial restoration of protein degradation impairments observed in A30P mice by synphilin-1 coexpression*

Protein levels are a complex equilibrium between expression, degradation and aggregation. As the a-syn protein levels expressed in young A30P and double transgenic mice was similar, and as aggregation was decreased in double transgenic animals, we suggest that protein degradation levels may be influenced by sph1. We analyzed the influence of sph1 on two majors protein degradation system: the ubiquitin-proteasome system (UPS) and the autophagy-lysosomal pathway (ALP).

4.1 No modulation of ubiquitin-proteasome system activity by alpha-synuclein or by synphilin-1 expression

Activity of the proteasome was first investigated using bioluminescent assays based on labeled nucleotides and measuring the three proteolytic activities of the proteasome which are chymotrypsin-like, trypsin-like, and caspase-like.

For this purpose we used brainstem of 18 month-old mice lysed in TBS buffer supplemented with 5 mM $MgCl_2$ and 5 mM ATP. To establish the time that the mixture of lysate, nucleotide and inhibitor need to get in equilibrium, we first investigated the effect of time on the luminosity measurement (Fig. 3-16A). We observed that in absence of an inhibitor, luminescence signal representing proteasome activity is stable from the first measurement. Furthermore, kinetic analysis of the proteasome inhibitor lactacystin showed a latency of around 50 min to reach its maximal effect.

For this reason, all further measurements were performed 60 min after loading the experiment. We furthermore observed that the maximal effect of lactacystin occurred already at 10µM (Fig. 3-16A–B) and this concentration will be used for all further experiments. We also analyzed the linearity of the response signal by increasing the concentration of protein in the measured lysate (Fig. 3-16C). We found a relative linear response between 0.20 and 0.34 µg/µl of lysate (R=0.92) and used 0.30 µg/µl of proteins in the further experiments. We then measured activity of several proteasome catalytic domains. The normalized and specific signal for proteasomal activity was calculated by subtracting the non-inhibited lysate luminescence signal by the inhibited one and did not found an effect of transgene on chrymotrypsin-like activity (nTg: 2867 ± 172; sph1: 2729 ± 325; A30P: 2603 ± 179; double: 2663 ± 247, one-way ANOVA, p>0.05,Fig. 3-14D).

Despite a limited inhibition or a strong background signal in trypsin-like activity leading to a measurement of only 15% of specific signal, we did not find an effect on the trypsin-like activity (nTg: 397 ± 15; sph1: 398 ± 60; A30P: 453 ± 29; double: 353 ± 89, one-way ANOVA, p>0.05, not shown. For the caspase-like activity, the low inhibition of activity or the strong background leads to the measure of 30% of specific signal and normalized signal suggests a similar activity of this catalytic activity in all mouse lines (nTg: 479 ± 33; sph1: 502 ± 26; A30P: 492 ± 29; double: 484 ± 9, one-way ANOVA, p>0.05, not shown.

We can notice the higher caspase-like activity in A30P mice which did not reach significance and could be the consequence of another protease with a caspase-like activity. Thus, these data suggest that neither a-syn nor sph1 is modulating the proteasome activity.
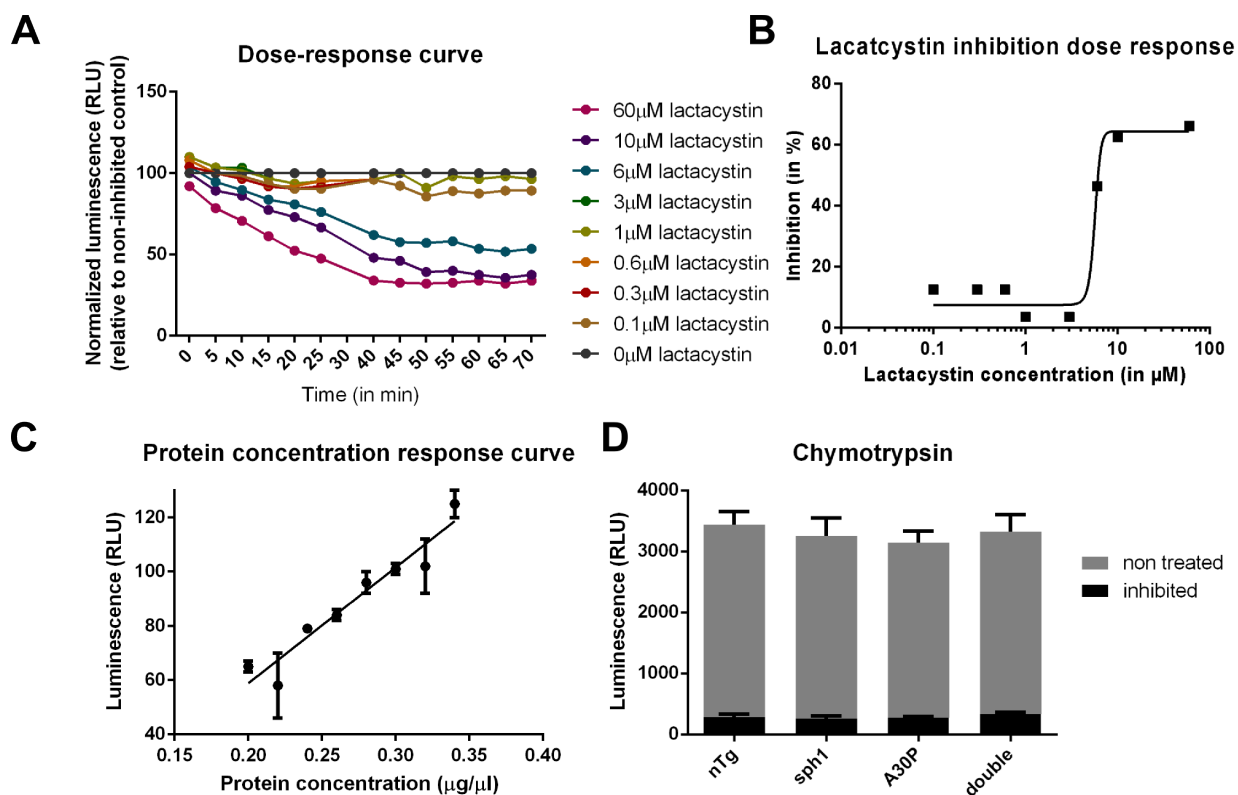
Figure 3-16: Activity of the proteasome was not modulated in A30P and in synphilin-1 mice

*Proteasome activity assay in 18 month-old mouse hindbrain. Tissues were lysed in hypotonic TBS buffer containing 5 mM ATP and 5 mM MgCl2 and analyzed using a luciferase-based Proteasome-Glo assay. **A)** Inhibition of the proteasome was investigated for 70 min using 0,28 µg/µl of proteins and an increasing amount of the proteasome inhibitor lactacystin. In presence of inhibitor, **B)** maximal inhibition was reached after 50 minutes. Inhibitor effect was not measurable for less than 6 µM and a maximal inhibition effect was observed at 10 µM. **C)** Linearity of the response curve was confirmed using an increasing concentration of protein in the measured lysate. Saturation was not observed until 0.34 µg/µl of protein. **D)** Chymotrypsin-like activity of the proteasome was investigated in absence and in presence of 10 µM of lactacystin. Despite relatively effective inhibition of the chymotrypsin-like activity, no differences were observed between mouse lines; data presented as the mean ± SEM; n=4, one-way ANOVA, post hoc LSD.*

4.2 No modulation of ubiquitin-proteasome system subunit levels by alpha-synuclein or synphilin-1 expression

Proteosomal activity measured previously reflects a complex equilibrium between the amount of catalytic complex and abundance of regulatory subunits [reviewed in (Kish-Trier & Hill 2013)]. To assess any potential change of specific proteasomal components we investigated levels of the main catalytic and regulatory subunits of the UPS. Therefore, we analyzed homogenates of mouse hindbrain lysed in RIPA buffer using western blot to quantify proteasome component proteins.

| Results

Functional catalytic 20S core levels were estimated in our samples by using alpha subunits detection, subunits playing a major structural function in the proteasome [reviewed in (Jung & Grune 2012)]. When using an antibody specific for the alpha 5 subunit, we did not find an alteration of the protein levels at around 28 kDa (Fig. 3-17A). This was validated by the utilization of a second antibody detecting an epitope shared by all alpha subunits of the 20S (Fig. 3-17A) providing no general trend which could be distinguished. In cells, the 20S proteasomal core requires assistance of regulatory units to become activated. We first studied the 19S regulatory subunits, which associated with the 20S particle are forming the structurally functional 26S proteasome.

More precisely, we investigated ATPase subunit Rpt2 levels which is required for the 20S gate opening (Köhler et al. 2001), but we did not observe modification of the protein levels at around 55 kDa depending of the animal genotype (Fig. 3-17B). We then analyzed the 11S regulatory complex which facilitates the degradation of small peptides by the 20S (Hill et al. 2002; Whitby et al. 2000). We did not find any potential regulation of 11S beta subunit levels at around 30 kDa (Fig. 3-17C). Despite that we did not investigate all potential regulators of UPS activity (such as levels of proteasomal gate opener protein PA200), our data suggest that UPS levels and activity are not directly related to a-syn or sph1 overexpression.
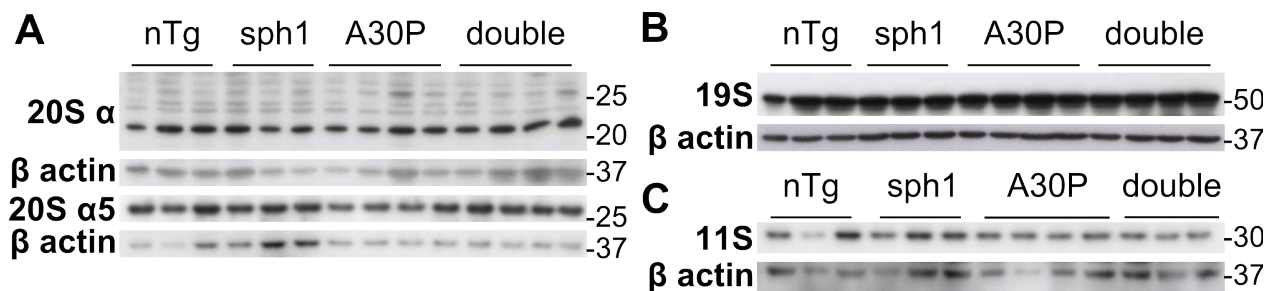
Figure 3-17: Levels of main proteasome subunits were not altered in transgenic animals

*Western blot analysis of soluble proteins extracted from hindbrain of 18 month-old mice. **A)** Analysis of 20S alpha proteasomal subunits shows a multiple band pattern between 20 and 30 kDa representing the different 20S alpha subunit proteins. **B)** Analysis of the 19S proteasomal subunit using an antibody specific for the Rpt2 subunit. **C)** Detection of 11S beta subunit levels at 30 kDa. No obvious changes in proteasomal protein levels were detected in all transgenic mouse lines; n=3 for nTg and sph1 and n=4 for A30P and double.*

4.3 Ubiquitin-proteasome system subunits are mislocalized in A30P mice but are restored in mice coexpressing synphilin-1

To assess possible misslocalization of UPS subunits, we then analyzed their expression and their subcellular distribution in 7 µm thin paraffin embedded mouse brain sections. By using an antibody specific for the 20S alpha 5 subunit, we observed an intense staining in the perinuclear region of the cell soma in all animal lines (Fig. 3-18A). Similarly, when using an antibody specific for the Rpt2 subunit of the 19S, we observed staining in the perinuclear region and a lighter and more diffuse staining in the cell soma (Fig. 3-18B). All transgenic mice also presented this staining pattern except A30P mice which presented a stronger staining in cell soma when compared to the perinuclear region (Fig. 3-18B, black arrow).

We confirmed these results by staining sections with an antibody specific for the beta subunit of the 11S (Fig. 3-18C), showing an abnormal staining in neurites of A30P mice (Fig. 3-18B, black arrowheads) and an abnormal dense staining in the cell soma (Fig. 3-18B, black arrow).

These data suggest a potential recruitment of proteasomal proteins to aggregates developed in A30P mice which is prevented by the coexpression of sph1.
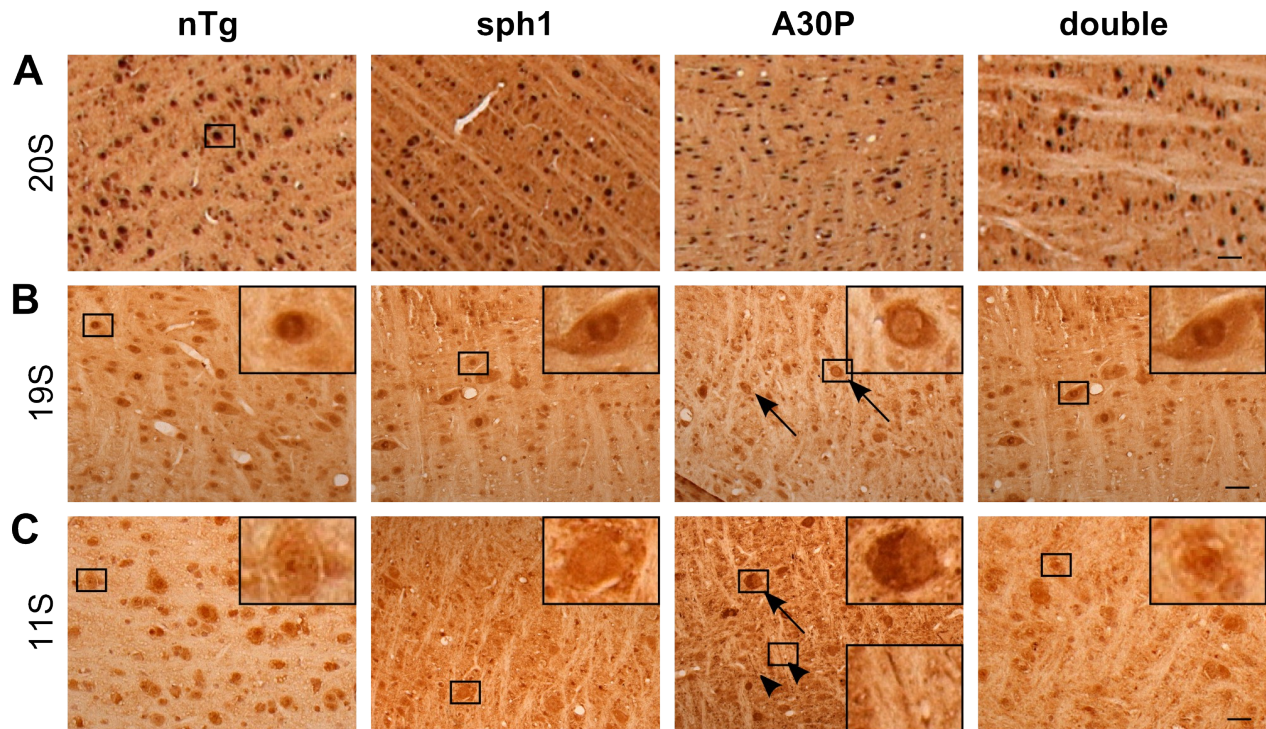
Figure 3-18: Proteasome subunits were abnormally distributed in brain of A30P mice

Subcellular localization of several proteasomal components of the proteasome in brainstem using IHC. A) Analysis of the 20S alpha 5 subunit of the proteasome showed a strong perinuclear staining and a weaker staining in the soma. B) When using an antibody specific for the 19S subunit, a similar pattern with stronger perinuclear staining and weaker staining in the soma could be observed, except for A30P mice in which a stronger staining was also found in the soma (black arrows). C) These data were also endorsed when using an antibody specific for the 11S subunit of the proteasome. Staining was observed in the perinuclear region, except for A30P mice were a stronger staining was detected in the cell cytoplasm (black arrow) and in neurites (black arrowheads); scale bar: 50 μm.

4.4 Partial restoration of autophagy-lysosomal pathway activity markers in A30P mice by synphilin-1 coexpression

In addition to the UPS, we also analyzed the autophagy-lysosomal system to identify any potential effect of sph1. The autophagy pathway is a complex machinery involving more than 20 specific ATG (autophagy-related) proteins to induce the formation of autophagosomes and their degradation into lysosomes. For this reason, we analyzed levels of only some markers of this complex process.

Figure 3-19: Decrease of autophagic flux observed in A30P mice was restored by synphilin-1 coexpression

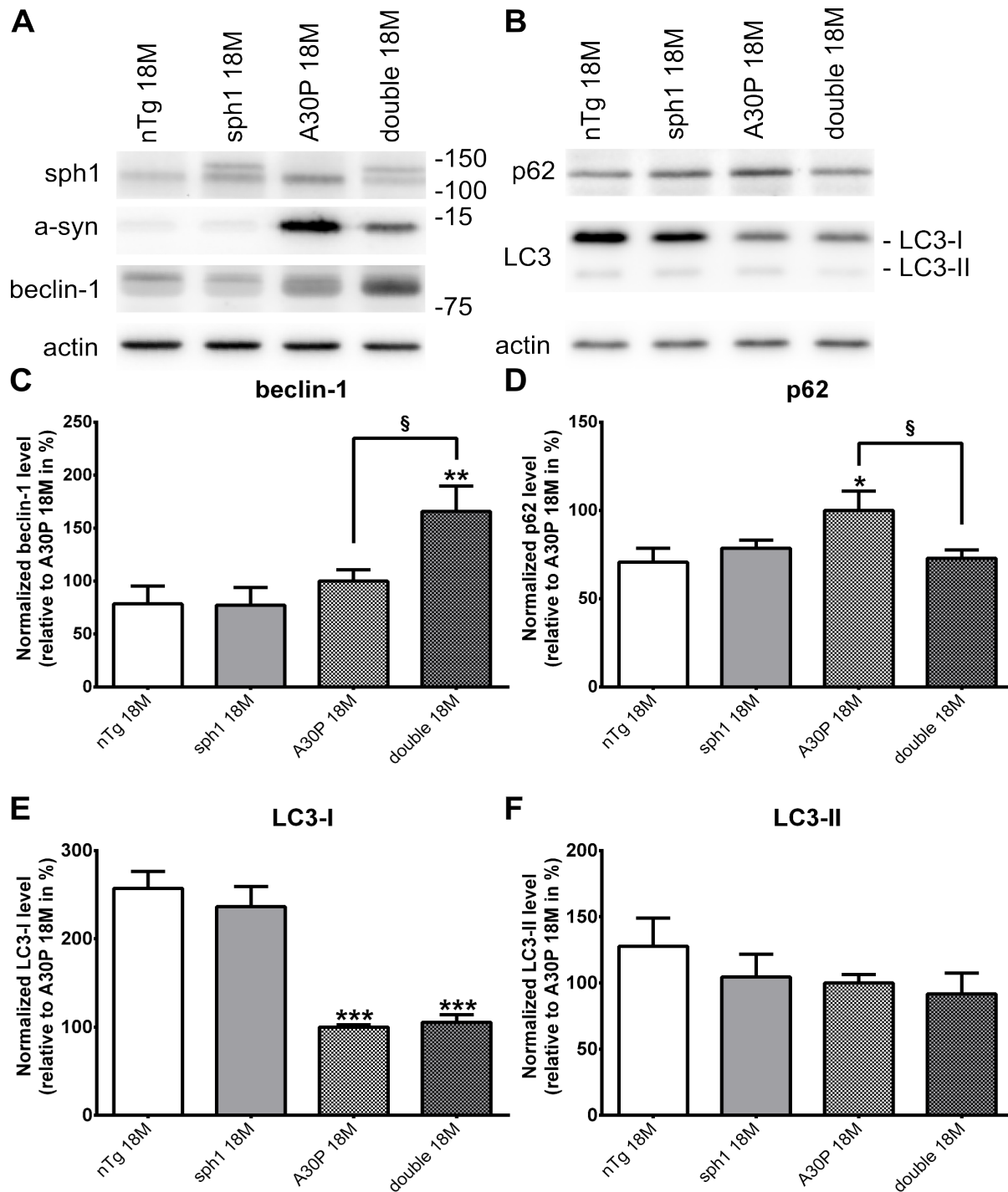*Autophagy marker levels were investigated in proteins extracted from hindbrain of 18 month-old mice using western blotting. **A and B)** Genotypes of animals were confirmed using specific antibody against sph1 and*

*a-syn. Autophagy markers beclin-1, p62 and LC3 were also detected. **C)** Densitometric quantifications showed a non-significant increase of beclin-1 in A30P when compared to nTg mice, but a strong increase in double transgenic mice when compared to nTg, sph1 or A30P mice. **D)** Increased levels of p62 in A30P mice were detected when compared to nTg or double transgenic mice, but no differences were found between nTg and double transgenic mice. **E)** Analysis of the autophagosomal marker LC3 revealed a strong reduction of the LC3-I signal in both A30P and double transgenic mice. **F)** In contrary to the LC3-I results, no significant differences in levels of LC3-II were observed; mean ± SEM; n=3,* p<0.05, ** p<0.01, *** p<0.001 when compared to nTg and § p<0.05 when compared to A30P, one-way ANOVA, post hoc LSD.*

We first investigated beclin-1 levels, a protein which is involved in autophagy by mediating the initial nucleation of the isolation membrane (Bjørkøy et al. 2009) and is playing a role in the initial nucleation of the autophagosome (Kabeya et al. 2000; Tanida et al. 2008). We observed an increase of beclin-1 levels in A30P and double transgenic mice (nTg: 78.5 ± 16.9; sph1: 77.2 ± 16.7; A30P: 100 ± 10.6; double: 165.7 ± 23.9, one-way ANOVA post hoc LSD, p<0.05, Fig. 3-19A) suggesting a higher induction of autophagosome formation in A30P and double transgenic mice. Moreover, we observed increased levels of beclin-1 in double transgenic when compared to A30P mice (one-way ANOVA post hoc LSD, p<0.05) supporting the increased autophagic flux observed in double transgenic mice (Smith et al. 2010).

Then, we used p62, an adapter protein target of the autophagy and accumulating when autophagy is impaired (Wong et al. 2012). We observed an increase of p62 signal in A30P mice that was partially restored in double transgenic mice (nTg: 70.7 ± 7.9; sph1: 78.7 ± 4.5; A30P: 100 ± 11.0; double: 73.0 ± 4.7, one-way ANOVA post hoc LSD, p<0.05, Fig. 3-19B) suggesting an impairment of the autophagic flux in A30P mice.

To confirm and to understand the origin of this autophagic flux decrease, we investigated levels of LC3 in brainstem of 18 month-old mice. LC3-I is a cytosolic protein which conjugates to phosphatidylethanolamine (PE) to form LC3-II. LC3-II is then recruited to autophagosomal membranes, facilitating the fusion of autophagosomes with lysosomes and inducing the degradation of autophagosomes and their components (including LC3-II). Therefore, investigating turn-over of LC3-I and LC3-II provides important information on the formation, accumulation and degradation of autophagosomes (Tanji et al. 2010). We found in A30P and double transgenic animals decreased levels of the cytoplasmic LC-I form (nTg: 257.2 ± 19.1; sph1: 197.3 ± 23.1; A30P: 100 ± 2.8; double: 105.4 ± 8.5, one-way ANOVA post hoc LSD, p<0.001, Fig. 3-19B). Moreover, we also found a slight decrease of the LC3-II form that did not reach significance in A30P and double transgenic (nTg: 127.7 ± 21.3; sph1: 104.4 ± 17.3; A30P: 100 ± 6.4; double: 91.7 ± 15.8, one-way ANOVA post hoc LSD, not significant for A30P and p<0.01 for double transgenic, Fig. 3-19B).

Together, these data suggest that despite a decrease of autophagic flux, a-syn expression is increasing the turn-over of the LC3-I into LC-II without accumulation of LC-II.

4.5 Presence of alpha-synuclein into autophagosomes and lysosomes

To underline the relevance of a-syn degradation by the autophagy in A30P mice, we investigated the presence of a-syn into autophagosomes and lysosomes. Therefore, a group of mice was prepared in our laboratory and brains cross-linked using paraformaldehyde were shipped to the laboratory of Prof. Winkler (Erlangen, Germany).

| Results

A diffuse pattern of the autophagy markers such as LAMP2a and LC3 in the cell soma was observed in young animals (Fig. 3-20) whereas animals overexpressing a-syn exhibited more structured and inclusion-associated distribution throughout the cells (Fig. 3-20). Immunostaining for a-syn in aged A30P and double-transgenic animals revealed both 1) somatic expression in inclusion-like structures, and 2) a presence in swollen neuronal processes. A30P mice revealed already a-syn pathology at 4 months of age in the brainstem despite weak and diffuse signal pattern of both ALP marker Lamp2a and LC3.

Altogether these data are showing the processing of a-syn by lysosomes and therefore the role of the ALP in a-syn degradation in A30P and double transgenic mice.
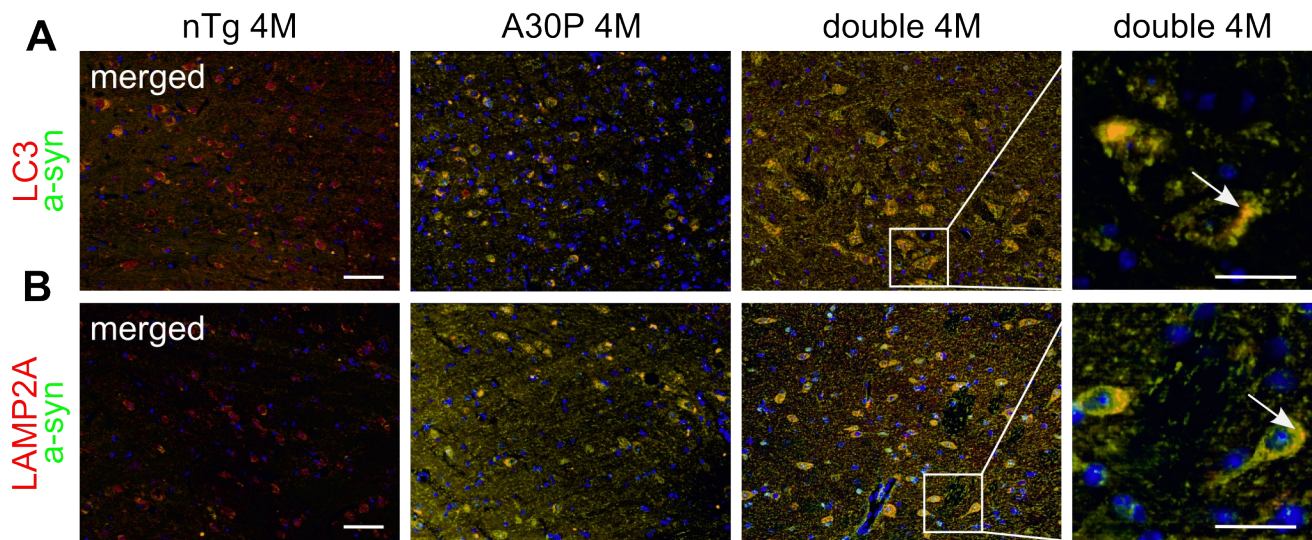
Figure 3-20: Colocalization of alpha-synuclein staining with autophagosomal and lysosomal markers in A30P and double transgenic mice

Figure provided by Prof. J. Winkler, Erlangen, Germany.

*IF analysis of a-syn and either the autophagosomal marker LC3 or the lysosomal marker LAMP2A at the histological level. **A)** Specific fluorescence staining for a-syn and LC3 in 4 month-old animals providing a cytoplasmic LC3 staining with puncta (white arrow). **B)** Similar approach using antibodies specific for a-syn and LAMP2A showed comparable results, LAMP2A and a-syn present a cytoplasmic diffuse staining with presence of double stained puncta (white arrow). Scale bar: 50 µm.*

4.6 Promotion of aggresome-like structures formation by coexpression of synphilin-1 in A30P mice

Sph1 was reported to promote degradation of aggregated proteins via its polyubiquitination and its targeting to the inducible aggrephagy (Liang et al. 1999). Immunofluorescence staining of paraffin sections of mouse brain using antibodies specific for a-syn and sph1 showed a dense staining in the perinuclear region of double transgenic mice (Fig. 3-21A) thereby supporting the potential presence of aggresome-like structures in double transgenic mice. To confirm this finding, we used as aggresome marker gamma-tubulin (Kihara et al. 2001), a protein mainly located in the centrosome (Wong et al. 2012) playing a role in organizing microtubules at the centrosome (Kopito 2000).

Using antibodies specific for gamma-tubulin and either transgenic myc- tagged sph1 (Fig. 3-21B) or human a-syn (Fig. 3-21B) showed a colocalization of both, sph1 and a-syn, with gamma-tubulin in the perinuclear region and supported the presence of aggresome-like structures in double transgenic mice.
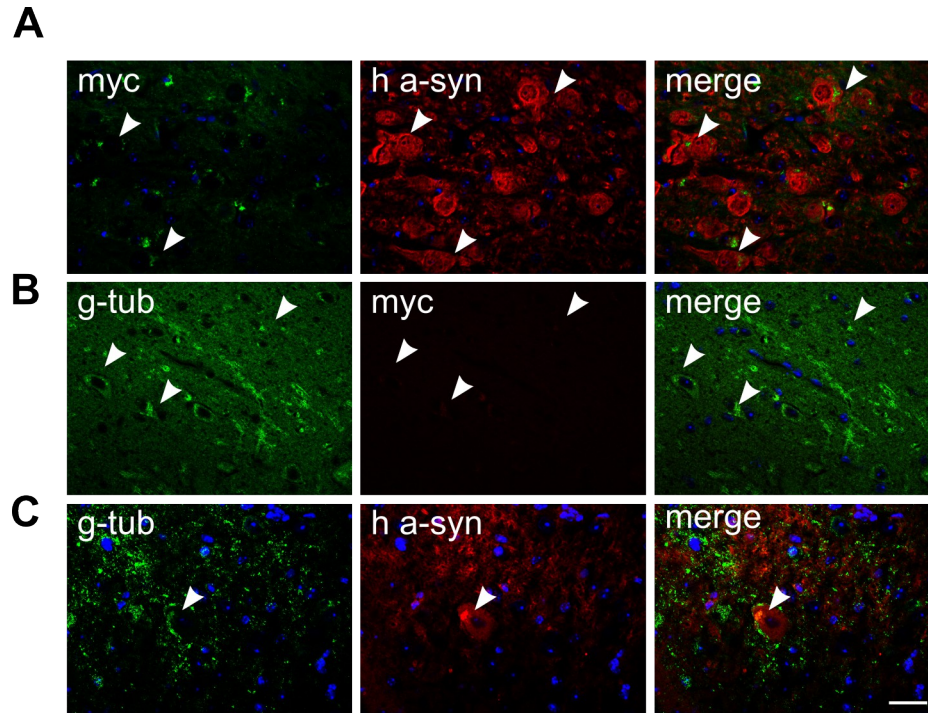
Figure 3-21: Formation of ubiquitinated aggresome-like structures in A30P mice coexpressing synphilin-1

Investigation of aggresome-like structures in brainstem of 18 month-old double transgenic mice. A) Detection of a-syn using a human specific antibody and sph1 using a myc antibody showed the presence of dense perinuclear staining. B and C) Presence of gamma-tubulin in the perinuclear region showed a strong overlap with sph1 and a-syn stainings, implicating the presence of both proteins in aggresome-like structures. Scale bar: 50 µm.

5) *Reduction of histological markers of neuropathology in brainstem of A30P mice coexpressing synphilin-1*

Since the discovery of a-syn, multiple models were proposed to explain pathological mechanisms involved in synucleinopathies. Whereas the relevance of abnormal accumulation of a-syn levels in neurodegeneration is more and more evident (Lashuel et al. 2012), the toxicity of different a-syn species is still actively debated. In this chapter, we aim to correlate the presence of several a-syn species with the neuropathology usually observed in A30P mice and double transgenic mice.

To fulfill this purpose, classical methods used to investigate neuropathology (such as silver and thioflavin S histochemistry staining as well as ubiquitin immunostaining) were applied.

| Results

5.1 Attenuation of silver positive inclusions in brainstem of A30P mice when coexpressing synphilin-1

Silver staining is a method routinely used to investigate protein aggregation in several neurodegenerative diseases (KING 1948). This method has been used for decades by pathologists to confirm the diagnosis of Alzheimer's or Parkinson's disease in *post mortem* patient brains. To generate more reproducible results we used the FD NeuroSilver kit (Fig. 3-22). A yellow-gold color was observed in all mice and is reported to be the typical background observed when staining with this kit (Martin et al. 2006; Smith et al. 2010). Strong staining localized in cells swellings (black arrow) and surrounded by a light diffuse staining halo was observed in A30P mice but less in double transgenic mice (Fig. 3-22).

These data support a potential exacerbated pathology in A30P mice when compared to nTg or to double transgenic. Unfortunately, we also observed unspecific silver retentions in some sections (black arrowhead). These retentions were forming unshaped structures which prevented a precise quantification.
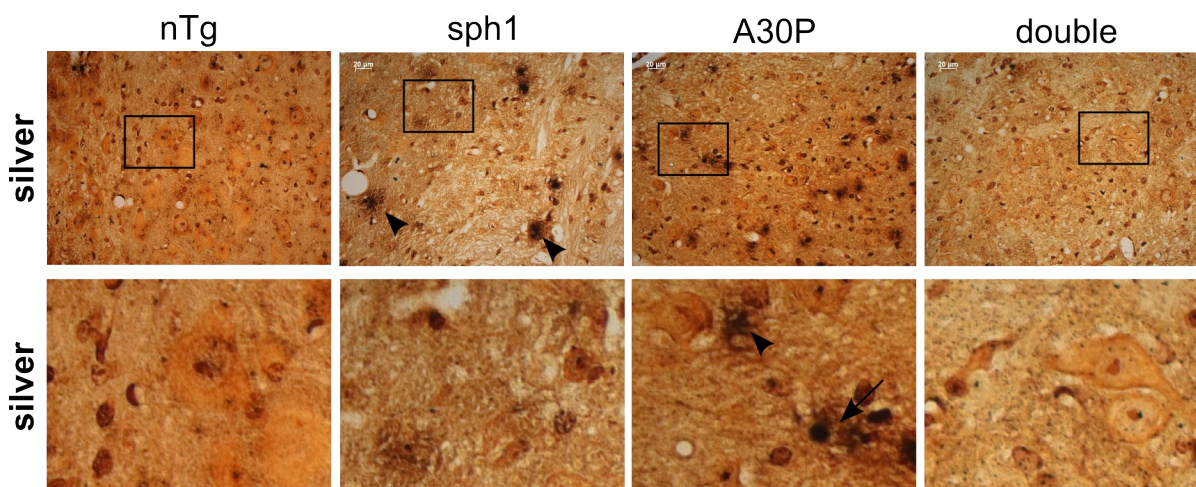
Figure 3-22: Synphilin-1 coexpression decreased silver positive structures in A30P mice

Neurohistological analysis performed in brainstem of 18 month-old mice using the FD NeuroSilver kit. A yellow-gold background was observed in all mice and is typical for this kit. Blurry aspecific retentions of silver were observed in some sections (black arrowheads). No pathology was detected in nTg or in sph1 mice. Cells accumulating silver and surrounded by a light halo (black arrow) were observed in A30P mice.

5.2 Reduced thioflavin S positive inclusions by synphilin-1 coexpression in brainstem A30P mice

Another alternative to silver staining is the thioflavin S staining (Dictenberg et al. 1998). Thioflavin S is an amyloid-binding fluorescent dye which bind to beta-sheets fibrils (O'Toole et al. 2012). Homogenous diffuse light background was observed accompanied by the presence of punctuate background in all mice (punctum < 1 µm). Thioflavin S staining on A30P animals showed a very strong and distinct signal in cell bodies (white arrowhead) and in neurites (white arrow) (nTg: 0.7 ± 0.16; sph1: 0.43 ± 0.04; A30P: 4.7 ± 1.1; double: 0.6 ± 0.3 positive cells per field, one-way ANOVA post hoc LSD, p<0.001, Fig. 3-23).

Surprisingly, we did not find in double transgenic cell bodies or neurites stained with thioflavin S, confirming the tendency observed in silver staining. These data suggest that the accumulation of a-syn seen in double transgenic mice does not result in amyloid structures formation.

Figure 3-23: Synphilin-1 coexpression in A30P mice decreased thioflavin S reactivity in brainstem of A30P mice

*Neuropathology was analyzed using 1% thioflavin S staining in brainstem of 18 month-old mice. **A)** Thioflavin S stainin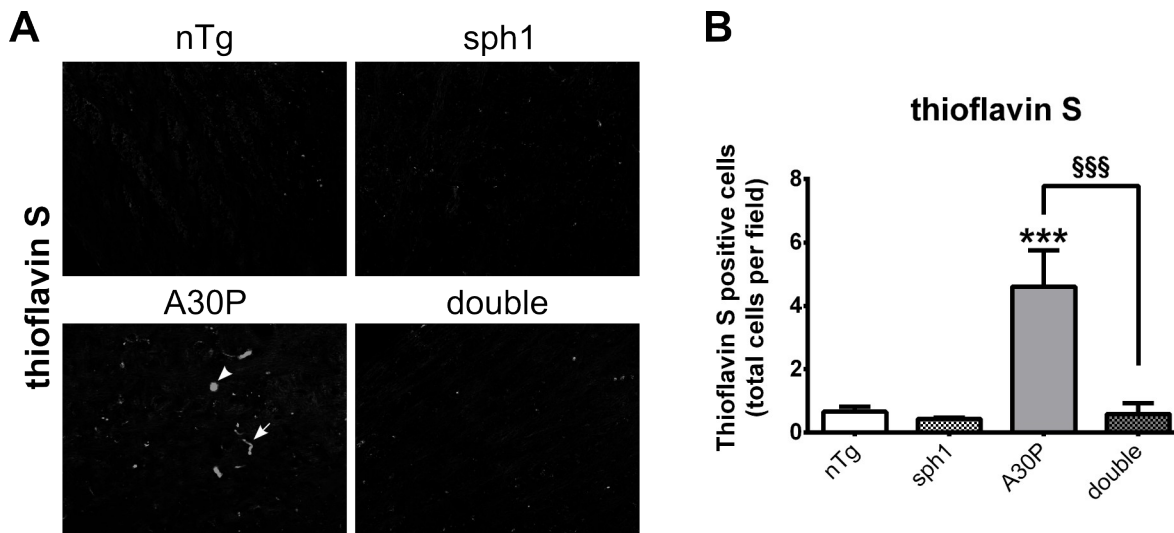g was observed in cell bodies (white arrowhead) and in neurites (white arrow) in A30P mice; scale bar: 50 µm. **B)** Thioflavin S positive cells were counted in 3 different animals, using 4 sections per animal and 8 fields per sections; data presented as the mean ± SEM; *** p<0.001 when compared to nTg and §§§ p<0.001 when compared to A30P, one-way ANOVA, post hoc LSD.*

5.3 Modification of ubiquitin inclusion shapes in A30P mice overexpressing synphilin-1

Ubiquitin immunochemistry is another method used by pathologists to characterize several neurodegenerative diseases [reviewed in (Sun et al. 2002)]. We stained paraffin embedded sections of mouse brain with an ubiquitin antibody and observed, as expected, staining throughout the whole cell in nTg animals. In contrast to A30P mice, double transgenic mice displayed a stronger ubiquitin staining (Fig. 3-24) suggesting an accumulation of ubiquitinated proteins. More interestingly, A30P mice presented a staining pattern composed of several small inclusion dots distributed in the whole cytoplasm, and double transgenic mice presented a main inclusion in the perinuclear region. This staining supports the idea that the decrease of a-syn inclusions observed in double transgenic mice is accompanied by a reorganization of aggregates when compared to A30P mice (Fig. 3-24A). To confirm that the ubiquitin inclusions observed in double transgenic mice are well composed of sph1, we performed immunofluorescent staining using antibodies specific for ubiquitin and sph1. We observed a diffuse ubiquitin staining overlapping the sph1 staining and suggesting a possible colocalization (Fig. 3-24B). These results are consistent with previous studies showing the ubiquitination of sph1 by parkin (Chung et al. 2001), SIAH (Liani et al. 2004; Avraham et al. 2005) or dorfin (Ito et al. 2003).

| Results

A more recent study even suggests a role for sph1 in autophagy-amenable aggresome formation via the K63 polyubiquitination of the ankyrin-like repeat domain 1 (ANK1) (Wong et al. 2012). Therefore, we used an antibody specific for K63 polyubiquitination and observed a diffuse staining of K63 polyubiquitin antibody with presence of more dense structures located in the perinuclear region. These dense structures were also stained by myc antibody, suggesting sph1 polyubiquitination in these perinuclear inclusions (Fig. 3-24C) and highlighting their aggresome-like properties.
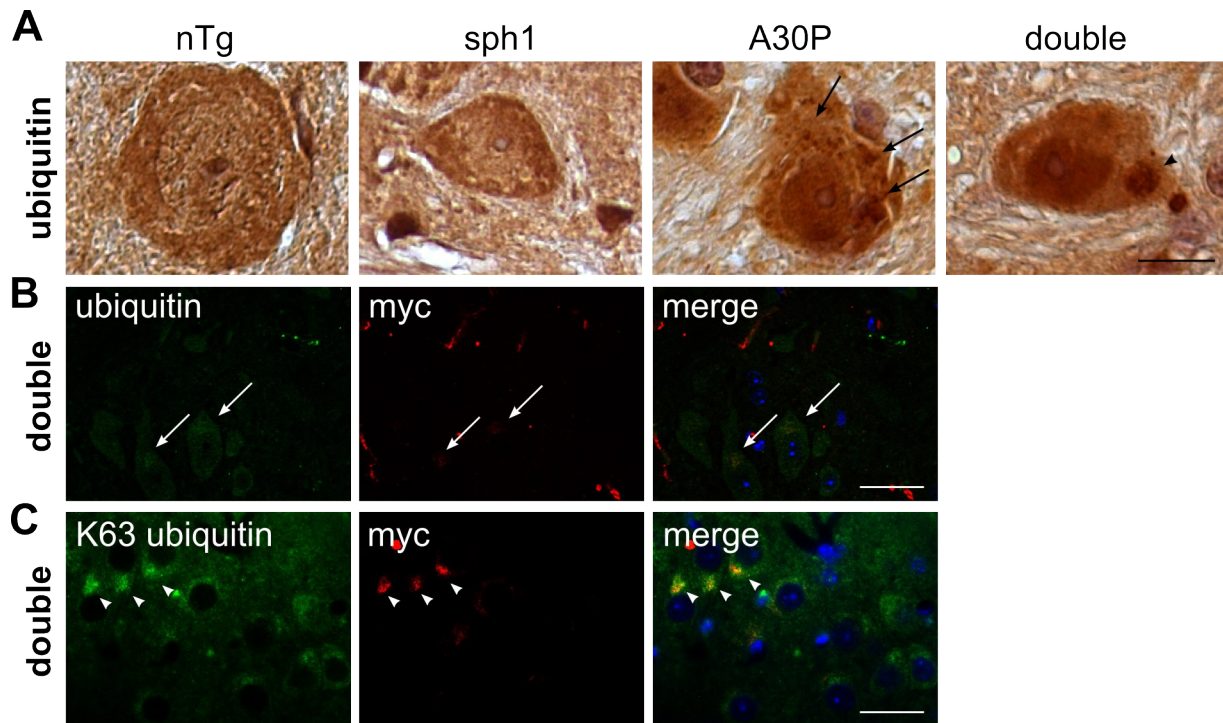
Figure 3-24: Synphilin-1 coexpression in A30P mice modified the structure of ubiquitin positive inclusions

A) *IHC analysis of ubiquitin positive inclusions in brainstem of 18 month-old mice. A ubiquitous staining was observed throughout the brain of all animals. A stronger ubiquitin staining was observed in A30P and double transgenic mice, and was accompanied in A30P mice by numerous small inclusions scattered over the whole cytoplasm (black arrows). In contrary, double transgenic animals showed few large perinuclear inclusions (black arrowhead); scale bar: 10 µm. B) Investigation of sph1 and ubiquitin localization by IF, ubiquitin staining resulted in a general labeling of all cells, inappropriate for colocalization studies; scale bar: 50 µm. C) Stainings using an antibody specific for K63 polyubiquitin chains resulted in a more specific labeling of dense perinuclear structures, corresponding to the sph1 staining pattern; scale bar: 50 µm.*

5.4 Increased levels of high molecular weight ubiquitinated proteins in A30P mice coexpressing synphilin-1

To gain more insight into the accumulation of ubiquitinated proteins observed in histology, we performed western blot analysis of soluble proteins extracted in TBS buffer and of total proteins homogenized in RIPA buffer.
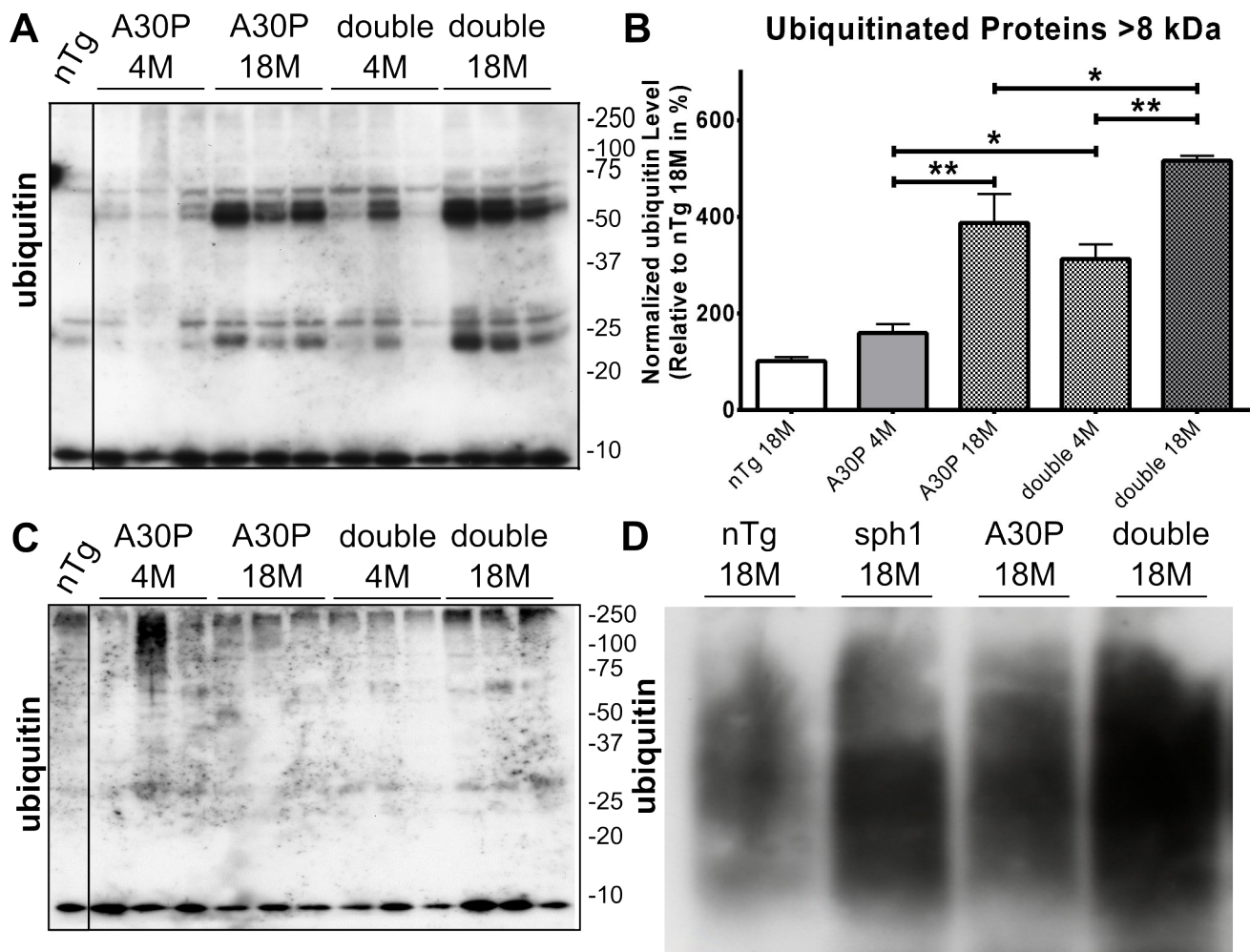
Figure 3-25: Synphilin-1 coexpression increased levels of high molecular weight proteins

A) Soluble levels of ubiquitinated proteins were investigated in hindbrain of both 4 and 18 month-old mice using western blot analysis. Immunoblots were detected with an antibody specific for ubiquitin. Staining provided two bands in nTg at around 25 kDa, as well as presence of two other bands between 50 and 75 kDa in A30P and double transgenic. B) Ubiquitinated proteins between 20 and 75 kDa were quantified by densitometry. A30P and double transgenic mice showed an increased load of ubiquitinated proteins with aging. Ubiquitinated proteins were increased in young and old double transgenic when compared to age-matched A30P mice; data presented as the mean ± SEM; n=3, * p<0.05, ** p<0.01, one-way ANOVA, post hoc LSD. C) Immunoblots detected with a second antibody specific for ubiquitin showed the ubiquitin monomer at around 8 kDa as well as short smear above 250 kDa revealing a strong increase of high molecular weight signals in 18 month-old double transgenic mice; data presented as the mean ± SEM; n=3, * p<0.05, ** p<0.01, one-way ANOVA, post hoc LSD. D) Levels of ubiquitinated high molecular species were investigated in hindbrain of 18 month-old mice using AGERA. Immunoblots were detected with an antibody specific for ubiquitin showing a long smear of ubiquitinated proteins in all mice. Interestingly, ubiquitin smears were stronger in sph1 and double transgenic mice.

| Results

By using western blot, we analyzed levels of ubiquitinated proteins and found an increased amount of ubiquitinated proteins with aging in both, A30P (A30P 4M: 159.5 ± 18.0; A30P 18M: 387.4 ± 59.5, one Way ANOVA, post hoc LSD, $p<0.01$, Fig. 3-25A,B) and double transgenic mice (double 4M: 312.9 ± 29.9; A30P 18M: 516.1 ± 10.22, one Way ANOVA, post hoc LSD, $p<0.01$, Fig. 3-25A,B). However, we also confirmed the accumulation of ubiquitinated proteins in both A30P and double transgenic when compared to nTg (nTg 18M: 100 ± 9.1, one way ANOVA, $p<0.001$, Fig. 3-25A,B). Finally, we detected an increase of ubiquitinated proteins in double transgenic when compared to A30P mice at 4 months (one Way ANOVA, post hoc LSD, $p<0.05$, Fig. 3-25A,B) and at 18 months (one Way ANOVA, post hoc LSD, $p<0.05$, Fig. 3-25A,B).

Similar results were also suggested using another ubiquitin antibody showing a stronger accumulation of high molecular weight ubiquitinated proteins in double transgenic mice that when compared to A30P mice and resulting in a smear stacked in the top of the running gel (Fig. 3-25C).

In order to better characterize these proteins, less soluble structures were investigated by running brain homogenates without centrifugation in agarose gels (Fig. 3-25D). Immunoblots stained with ubiquitin antibody showed a small increase of high molecular weight proteins even stronger in double transgenic animals. We suggest that the formation of aggresome-like structures previously observed may lead to an increase of ubiquitinated proteins in A30P mice coexpressing sph1.

5.5 Reduced levels of activated astrocytes observed in A30P mice coexpressing synphilin-1

Synucleinopathy progression was shown to be accompanied by inflammatory responses and immune abnormalities both in mice overexpressing a-syn (Chu et al. 2000) and in PD patients [reviewed in (Lim et al. 2005)], but mechanisms and roles of this activation remain controversial. Therefore, we used inflammation markers to confirm the decrease levels of neuropathology previously observed in double transgenic mice using aggregation markers.

We first investigated in paraffin embedded mouse brain sections levels of activated astrocytes by using GFAP immunohistological staining. We observed a general increase of activated astrocytes in A30P and in double transgenic mice (nTg: 1.25 ± 0.75; sph1: 1.67 ± 0.88, A30P: 16.33 ± 0.33; double: 10.0 ± 0.58; one Way ANOVA, post hoc LSD, $p<0.01$, Fig. 3-26A) and a decreased levels of activated astrocytes in double transgenic mice when compared to A30P mice (one Way ANOVA, post hoc LSD, $p<0.01$, Fig. 3-26A).

Investigation of activated microglia using Iba1 immunohistological staining shows a general increase of these cells in A30P and double transgenic mice when compared to nTg mice (nTg: 1.56 ± 0.28; sph1: 2.33 ± 1.11, A30P: 7.50 ± 2.53; double: 6.3 ± 1.04; one Way ANOVA, post hoc LSD, $p<0.01$, Fig. 3-26B) but the decrease event number observed in double transgenic when compare to A30P mice did not reach significance (one Way ANOVA, post hoc LSD, $p>0.05$, Fig. 3-26B). These data suggest that coexpression of sph1 in A30P mice is reducing the pathology observed in A30P mice not only at the inclusion level, but also in a more systemic matter.
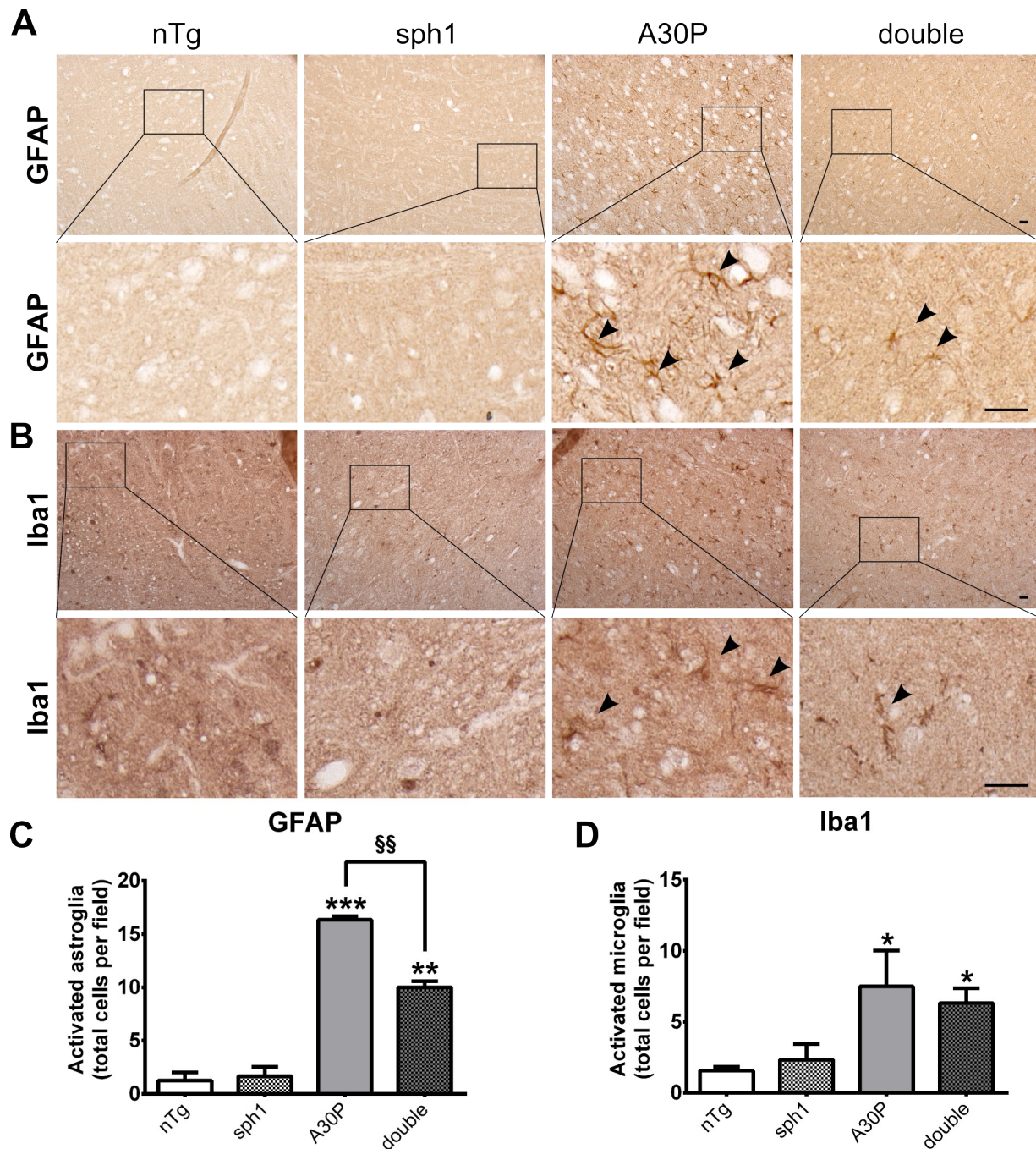
Figure 3-26: Synphilin-1 coexpression reduced levels of inflammation markers in A30P mice

*Inflammation in the brainstem of 18 month-old mice was investigated by counting the number of activated glial cells using IHC. **A)** GFAP staining showed a specific signal of branched cells characteristic for activated astrocytes. **B)** Immunohistological staining of Iba1 show two categories of signal 1) small cells stained in their soma and 2) small cells stained in their soma and branched. Only microglial cells with more than two branches were counted for the quantification. A30P and double transgenic mice presented increased levels of activated*

*microglia when compared to nTg. A decreased intensity of microglial cell activation was found in double transgenic mice when compared to A30P mice but did not reach significance. **C)** Only astrocytes with more than three branches were integrated in the quantification. An increased number of activated astrocytes in A30P was observed when compared to nTg, but the observed inflammation was reduced in double transgenic mice when compared to A30P mice; scale bar: 50 µm; data presented as the mean ± SEM; n=3, *** p<0.001, ** p<0.01, * p<0.05 when compared to nTg and §§ p<0.01 when compared to A30P, one-way ANOVA, post hoc LSD.*

6) Delay of behavioral symptoms observed in A30P mice coexpressing synphilin-1

To investigate the relevance of the decreased neuropathology observed in brainstem, behavioral analysis of A30P mice coexpressing sph1 were performed at a more systemic level. In this section, we explored new and already published phenotypic impairments in A30P mice to study the impact of sph1 on synucleinopathy progression.

Therefore, we first evaluated the general health of the animals. As A30P mice were reported to develop a motor phenotype (Neumann et al. 2002), we then focused on several motor skill tests. Finally, we tested potential sensory and memory abilities already reported to be impaired in A30P mice (Tufekci et al. 2012).

6.1 Normal health status in transgenic mice using SHIRPA

Health status of mice, including potential physical or neurological abnormalities, was monitored using the primary screen of SHIRPA test battery (Neumann et al. 2002; Freichel et al. 2007) in 3 month-old male mice.

Body condition was first assessed by looking at the skin, the coat, the whiskers and the eyes of the animals. Mice did not present any abnormalities such as lesion of the skin, irregular coat or whiskers, presence of biting or excessive lacrimation.

We then investigate sensory functions by looking at toe pinch, palebral closure, pinna and retina reflex and startle response and found normal sensory functions in all mouse lines. Motor functions were assessed by observing the fluidity of gait, posture, muscle tone, and by measuring time mice could stay hold on a reverse grid. We did not observe any abnormal gait fluidity or posture, and we did not measure difference of time hold on the grid (nTg: 30.0 ± 0.00; sph1: 29.82 ± 0.18, A30P: 30.00 ± 0.00; double: 29.73 ± 0.27; one Way ANOVA; post hoc Tukey, p>0.05, Fig. 3-27A).

Anxiety was investigated by evaluating the activity of mice placed into a new cage and by recording both the presence of urine and the number of fecal stools at the end of the test in the novel area. We did not observe obvious difference in activity, in percentage of mice urinating (nTg: 12.5%; sph1: 18.2%, A30P: 7.7% double: 27.3% Fig. 3-27B) and in number of stools (nTg: 4.5 ± 1.2; sph1: 5.4 ± 0.9, A30P: 5.7 ± 0.7 double: 6.0 ± 0.6; one Way ANOVA; post hoc Tukey c, p>0.05, Fig. 3-27C). Surprisingly, weight of all 14 week-old mice was slightly heavier that the physiological range of C57BL/6N mice (C57BL/6: 27 ± 2; nTg: 30.86 ± 1.08; sph1:32.95 ± 0.81, A30P: 33.77 ± 0.53 double: 35.18 ± 0.81; one way ANOVA, post hoc Tukey, * p<0.05, Fig. 3-27D). This effect could reflect an animal housing which has tendency to increase animal body weight. Furthermore, transgenic mice were heavier that nTg mice already at 14 weeks (one Way ANOVA; post hoc Tukey, ** p<0.01, Fig. 3-27D).

A

B

C

D
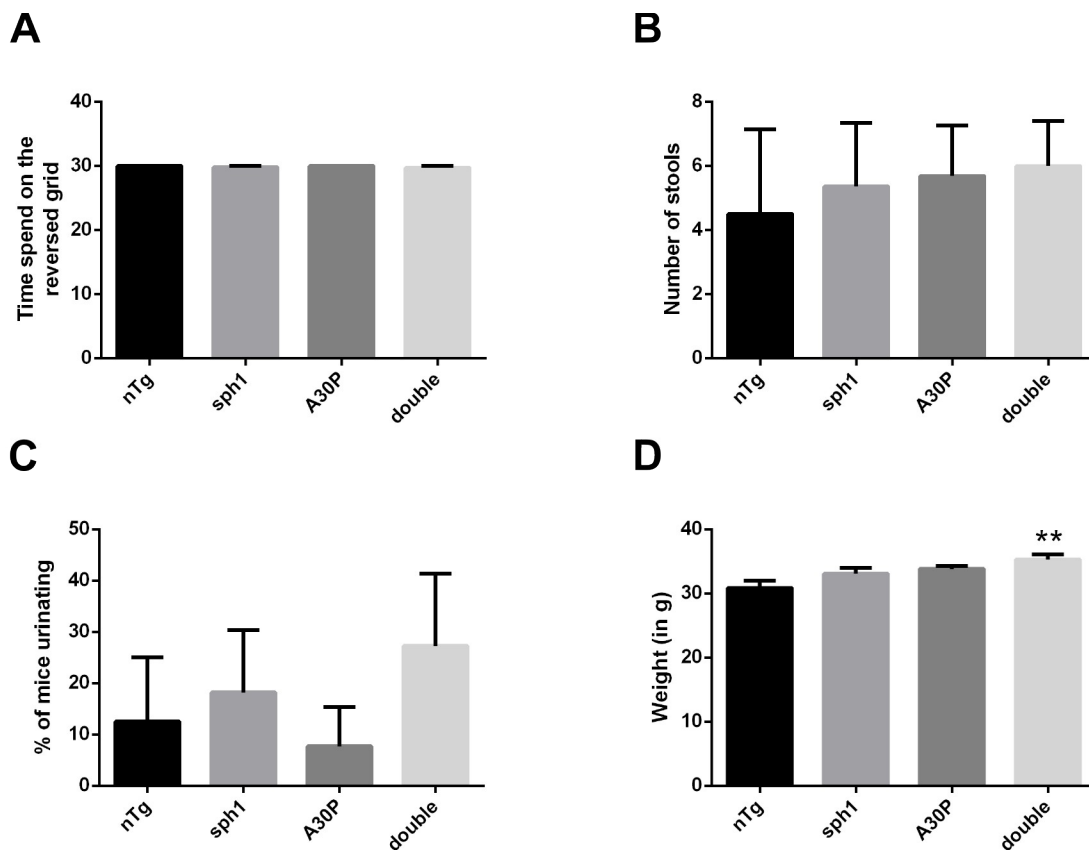
Figure 3-27: Transgenic mice displayed a normal health status

*Health status investigation in 3 month-old mice using SHIRPA. A) Grip strength was analyzed by reversing a mouse placed on a metal grid. No difference between nTg and other transgenic animals was observed. B) Number of fecal stools and C) percentage of animals urinating were investigated when placing mice in a new environment for 10 min. No modifications were observed along the different genotypes. D) Increase of body weight in transgenic mice was measured but only significant in double transgenic animals; data presented as the mean ± SEM; ** p<0.01, n nTg=8, n sph1=11, n A30P=13, n double=11, one-way ANOVA, post hoc Tukey.*

6.2 Mild increase of body weight in A30P mice

To get a better insight into the body weight difference observed during SHIRPA investigation, weight of animals was monitored every 6 weeks for one year (Fig. 3-28). We found a strong correlation between age and weight of mice (two-way ANOVA; post hoc Tukey, p<0.001). By looking at individual time points, no weight difference was observed between lines, except for 46 and 50 weeks old double transgenic and 50 weeks old A30P mice (nTg 44 weeks: 38.55 ± 1.98, sph1 44 weeks: 42.38 ± 2.11, A30P 44 weeks: 43.81 ± 1.19, double 44 weeks: 44.22 ± 0.95, and nTg 50 weeks: 39.29 ± 2.18, sph1 50 weeks: 44.21 ± 2.67, A30P 50 weeks: 46.11 ± 1.39, double 50 weeks: 46.85 ± 1.12; repeated measurement one Way ANOVA; post hoc Tukey; Fig. 3-28). But when analyzing the body weight over one year, we found a significant increase of body weight in all transgenic lines (nTg: 36.93 ± 1.38, sph1: 40.0 ± 1.67, A30P: 40.70 ± 1.96, double: 41.47 ± 1.67; two-way ANOVA; post hoc Tukey; Fig. 3-28).

| Results

Additionally, we also analyzed the body weight of 18 month-old animals, representing the latest time point used for the behavioral analysis. We validated found a general increase of body weight in all transgenic lines, which was significant only in A30P mice (nTg: 38.80 ± 3.27, sph1: 43.18 ± 2.13, A30P: 47.88 ± 1.34, double: 46.40 ± 1.51; one Way ANOVA; post hoc Tukey; Fig. 3-28). These data suggest a slight increase of body weight in all transgenic lines which was more pronounced in A30P mice.
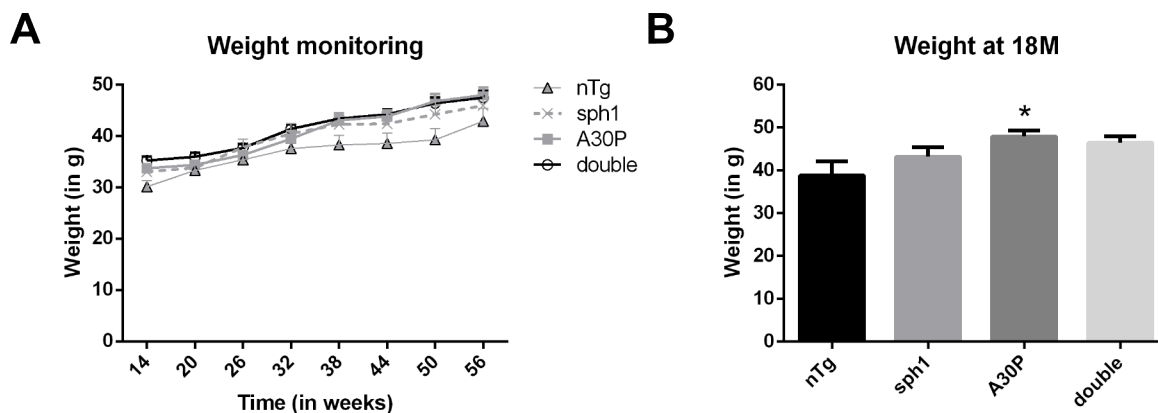
Figure 3-28: Increased body weight in A30P mice

*Body weight was monitored between 12 and 56 weeks with an interval of 6 weeks. **A)** An increase of body weight with aging was observed in all mouse lines. Non-transgenic mice were displaying a lower body weight when compared to transgenic animals; data presented as the mean ± SEM; n nTg=8, n sph1=9, n A30P=9, n double=11, two-way ANOVA, post hoc Tukey. **B)** At 18 months, transgenic mice showed an increased body weight when compared to the nTg; but a significant difference was observed only in A30P mice; data presented as the mean ± SEM; n nTg=8, n sph1=9, n A30P=9, n double=11, two-way ANOVA, post hoc Tukey.*

6.3 Different motor phonotypes observed in A30P and double transgenic mice

Transgenic mice overexpressing a-syn are classical models to study the molecular mechanisms of synucleinopathy and their influence on PD-relevant locomotor function (Fleming et al. 2008; Freichel et al. 2007). Moreover, a progressive motor phenotype was already observed in the human A30P mutated a-syn transgenic mouse used in this study (Rogers et al. 1997). To investigate the potential effect of sph1 on the progressive motor pathology observed in A30 mice, we used a combination of several motor skill tests that have been already reported to detect motor pathology in the A30P mouse and including RotaRod and beam walk. Furthermore, we included automatic gait analysis (using CatWalk) and investigation of home-cage activity (using LabMaster) to detect any potential decrease of activity consequence of pathology.

6.3.1 *Delayed rotarod impairment in A30P mice coexpressing synphilin-1*

Rotarod is a system composed of a rotating beam in which mice are running and the latency to fall from the beam is measured and reflects motor coordination and fatigue (DUNHAM & MIYA 1957). For the first experiment, ability of mice to learn this complex task at 14 weeks was assessed (Masliah et al. 2000; Giasson et al. 2002; Gomez-Isla et al. 2003). Transgenic mice did not present a decrease of motor ability when compare to nTg (nTg: 151.0 ± 3.8, sph1: 179.3 ± 2.7, A30P: 157.5 ± 7.2, double: 142.4 ± 3.9; one Way ANOVA; post hoc Tukey; Fig. 3-29A) nor a difference in motor skill learning (two-way ANOVA; $p > 0.005$; Fig. 3-29A). These data suggest that mice did not present motor skilled impairment at 14 weeks. Evolution of rotarod performances was investigated for 14 months and A30P and double transgenic mice spent less time spend in the rod when compare to nTg mice (nTg: 146.2 ± 4.3, sph1: 163.6 ± 5.6, A30P: 112.0 ± 10.7, double: 130.2 ±10.28; two-way ANOVA; post hoc Tukey; $p < 0.05$; Fig. 3-29B). More precisely, we found a significant difference between A30P mice already at 26 weeks (nTg: 160.3 ± 10.6, sph1: 175.6 ± 29.6, A30P: 131.7 ± 18.7, double: 170.1 ± 22.2; two-way ANOVA; post hoc Tukey; $p < 0.05$; Fig. 3-29B gray arrow) and in double transgenic only at 38 weeks (nTg: 142.5 ± 17.9, sph1: 165.8 ± 31.9, A30P: 84.0 ± 5.6, double: 104.6 ± 18.4; two-way ANOVA; post hoc Tukey; $p < 0.05$; Fig. 3-29B black arrow). These data suggest that pathology observed in A30P can be delayed by sph1 coexpression.

A   **B**
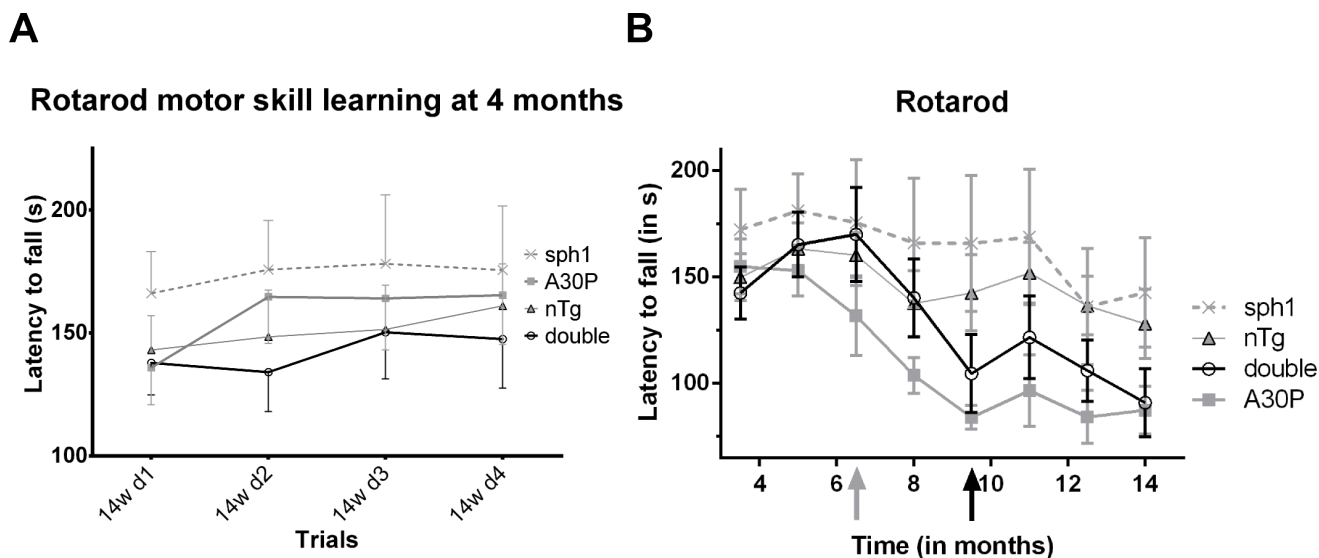
Figure 3-29: Synphilin-1 coexpression delayed rotarod impairment in A30P mice

Rotarod performances were monitored between 12 and 56 weeks with an interval of 6 weeks. Mice were investigated 3 times a day for 5 consecutive days using an acceleration of 4 to 40 RPM in 7 min and the latency to fall was recorded. **A)** *Motor skill learning was analyzed in 12 month-old mice. No differences were observed between nTg and transgenic mice; data presented as the mean of the 3 trials per day ± SEM; n nTg=8, n sph1=11, n A30P=13, n double=11, two-way ANOVA, post hoc Tukey.* **B)** *A decrease of motor performance with aging was observed in A30P and double transgenic mice. First motor symptoms in double transgenic (black arrow) were delayed when compared to A30P mice (gray arrows); data presented as the mean of the 15 trials per time point ± SEM; n nTg=8, n sph1=8, n A30P=9, n double=11, two-way ANOVA, post hoc Tukey.*

6.3.2 Reduced challenging beam walk performances in transgenic mice

In a next step, challenging beam walk (Neumann et al. 2002; Freichel et al. 2007) was performed to investigate coordination disorder in transgenic mice (Shiotsuki et al. 2010).

Challenging beam walk consists of four transparent thermoplastic beams constituting four sections of decreasing width and covered by a wire mesh (Fig. 3-30A and B). Mice were trained to transverse the beam without the wire mesh to their home-cages. On the testing day, mice were placed on the beam with a wire grid. At 12 months, all transgenic mice need more time to traverse the beam (nTg: 9.25 ± 1.05, sph1: 16.89 ± 2.24, A30P: 19.44 ± 5.92, double: 20.18 ± 4.71; two-way ANOVA; post hoc Tukey; $p<0.05$; Fig. 3-30C), supporting that sph1, A30P and double transgenic mice already developed pathology at 12 months.

A

B

C
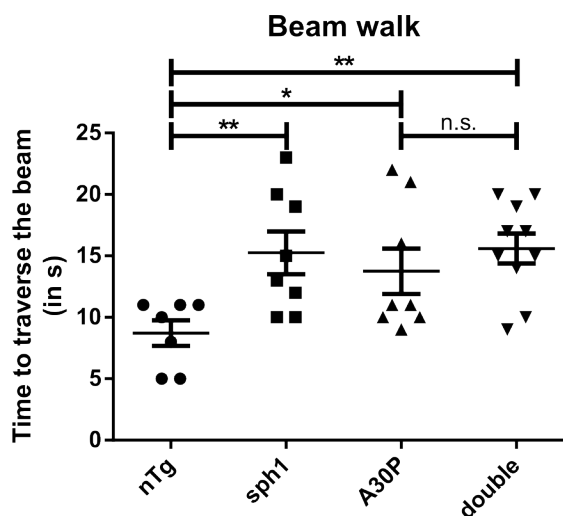
Figure 3-30: Reduced challenging beam walk performances in transgenic mice

*Motor disturbances in transgenic animals by challenging beam walk test. **A)** Mice were trained for two consecutive days to cross a one meter long plastic beam of decreasing width to get back to their home-cage. **B)** The third day, a 1 cm² metal mesh grid was added to the plastic beam and the time to cross it was recorded. **C)** An increase of the time required for crossing the beam was detected in all transgenic mice; data presented as the mean ± SEM; n nTg=8, n sph1=8, n A30P=9, n double=11, one-way ANOVA, post hoc Tukey.*

6.4 Different origin of the motor impairments observed in A30P and sph1 mice

Characterization of motor deficits observed in double transgenic and in sph1 mice was performed using automatic gait analysis. This approach allows the measurement of classical static gait parameters (distance between two consecutive steps or between lateral paws, number of steps to cross the plate...) but also dynamic gait parameters (time needed to cross the plate, step cycle, walking pattern...) which are impossible to measure by more classical methods (such as paw labeling using ink).

Animals were recorded 20 times over 5 days and runs in which animals got a speed variation within the walkway higher that 25% were not investigated. Moreover, runs on which mice clearly stopped or climbed wall of the apparatus were also excluded to reduce the number of run per animal to a maximum of 5. By using this general approach, all transgenic animals presented a reduced walking speed which did not reach significance (nTg: 17.00 ± 0.42, sph1: 15.17 ± 0.83, A30P: 15.54 ± 0.75, double: 15.08 ± 0.55;one Way ANOVA; post hoc Tukey; $p>0.05$; Fig. 3-31A). A30P mice also showed an increase number of steps necessary to cross the walkway (nTg: 19.0 ± 1.5, sph1: 19.0 ± 0.60, A30P: 21.32 ± 1.4, double: 20.0 ± 1.8; one Way ANOVA; post hoc Tukey; $p<0.05$; Fig. 3-31B). These data were confirmed in A30P mice by a decreased stride length, representing distance between two consecutive steps (nTg: 4.42 ± 0.11, sph1: 4.43 ± 0.06, A30P: 3.99 ± 0.08, double: 4.28 ± 0.13; one way ANOVA; post hoc Tukey; $p<0.05$; Fig. 3-31C). These data suggest that A30P mice are using a walking pattern requiring more steps to cross the walk way.

Using the same strategy, analysis of step cycle (represented in Fig. 3-31D) revealed an increase of stand in sph1 and double transgenic mice (nTg: 0.11 ± 0.004, sph1: 0.14 ± 0.009, A30P: 0.12 ± 0.006, double: 0.13 ± 0.003; one way ANOVA; post hoc Tukey; $p<0.05$; Fig. 3-31E). This increase of stand was accompanied by a non-significant increase of swing (nTg: 0.13 ± 0.005, sph1: 0.14 ± 0.008, A30P: 0.12 ± 0.003, double: 0.13 ± 0.004; one way ANOVA; post hoc Tukey; $p<0.05$; Fig. 3-31F) and of step cycle duration (nTg: 0.24 ± 0.006; sph1: 0.28 ± 0.016, A30P: 0.25 ± 0.008, double: 0.27 ± 0.006; one way ANOVA; post hoc Tukey; $p>0.05$; Fig. 3-31G). We suggest that sph1 and double transgenic animals are also showing an abnormal gait pattern, but different from the one observed in A30P mice. This is probably reflecting the longer stand in sph1 and double transgenic mice which increase slightly the step cycle pattern.

When using static gait analysis, no difference was observed in paw overlap (nTg: 0.92 ± 0.09, sph1: 0.81 ± 0.05, A30P: 1.13 ± 0.05, double: 1.06 ± 0.09; one way ANOVA; post hoc Tukey; $p>0.05$; Fig. 3-31G), neither in base of support of lateral, frontal, posterior or epsilateral support (one way ANOVA; post hoc Tukey; $p>0.05$;data not shown). As paw overlap represents mainly the posture of the animal, we suggest that the decrease in stand observed in sph1 and double transgenic mice do not lead to a posture impairment.

| Results

A

Speed

B

Steps

C

Stride length

D

E

Stand

F

Swing

G

Step cycle

H

Print position
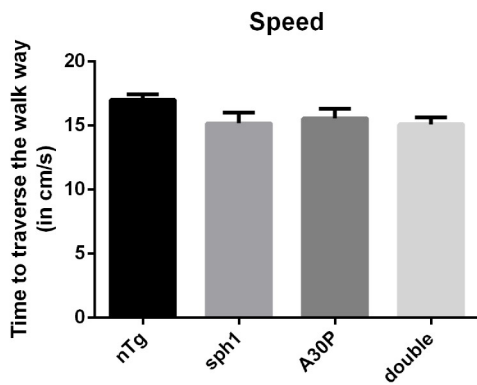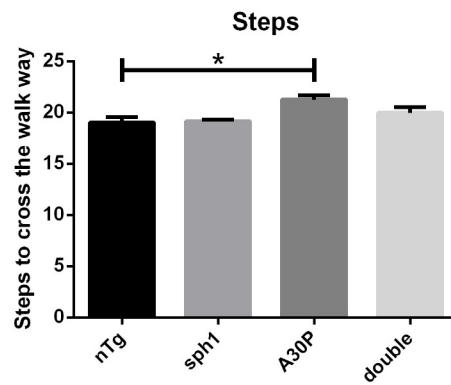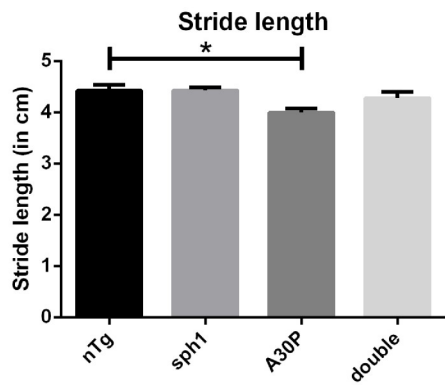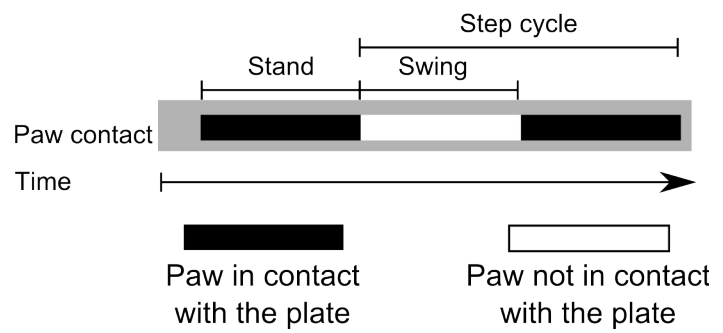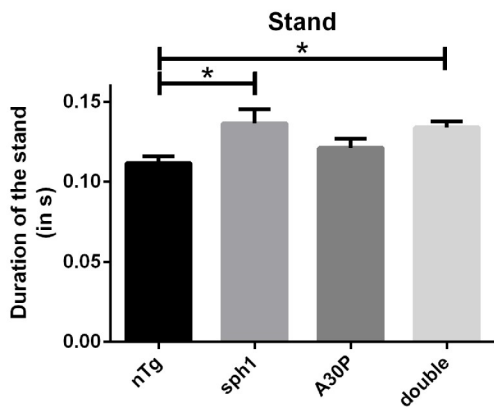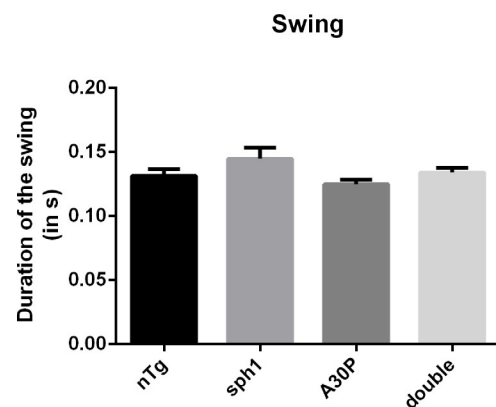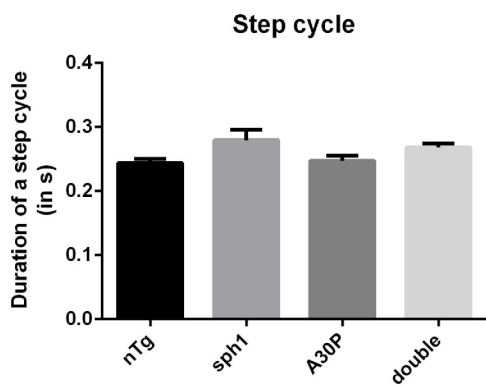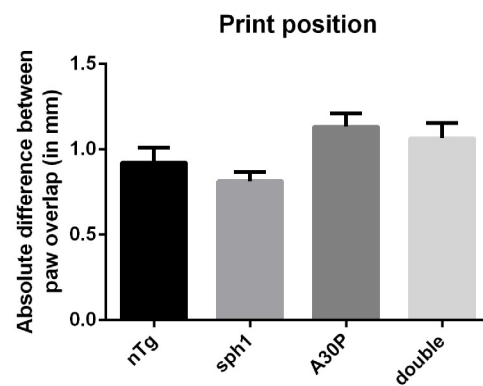
Figure 3-31: Motor deficits present in both A30P and sph1 transgenic mice resulted in gait impairments in CatWalk

*Dynamic and static analysis of automatic gait analysis was performed in 18 month-old mice. **A)** No difference in speed was observed in compliant runs between groups. **B)** An increased number of steps needed to cross the beam was observed in A30P mice, **C)** resulting in a decreased stride length (distance between two consecutive steps). **D)** Step cycle representation. **E)** Increased stand was measured in sph1 and double transgenic mice **F)** which was not accompanied by an increase of swing **G)** or step cycle. **H)** No differences was found in print positions (overlap between hind and front paw prints); data presented as the mean ± SEM; n nTg=8, n sph1=8, n A30P=9, n double=11, one-way ANOVA, post hoc Tukey.*

To understand the origin of the stand decrease in sph1 and double transgenic animals, we also investigated in detail the walking patterns.

Analysis of step patterns, by displaying recorded print, showed an increase number of step for A30P (Fig. 3-32A) and also showed clearly the presence of abnormal paw patterns in sph1 and double transgenic animals resulting to the addition of an extra hind paw step every 3 to 4 step cycles (Fig. 3-32A, white arrowheads).

Deep modifications of the epsilateral walking pattern (usually seen in nTg mice and represented normally as parallel curves by the software) was observed in sph1 and double transgenic (Fig. 3-32B). Analysis of step pattern using a time based axis clearly showed the presence of extra hind paw prints in sph1 and double transgenic mice (Fig. 3-32C, black stars).

To exclude any potential bias, runs with abnormal extra steps were re-visualized using slow motion to exclude potential presence of abnormal behavior (such as stop, sniffing or wall climbing) in the analysis. These data suggest a motor deficit present in both 18 month-old A30P and sph1 mice, leading to the development of different pathologies and resulting in different abnormalities in CatWalk.

| Results

A
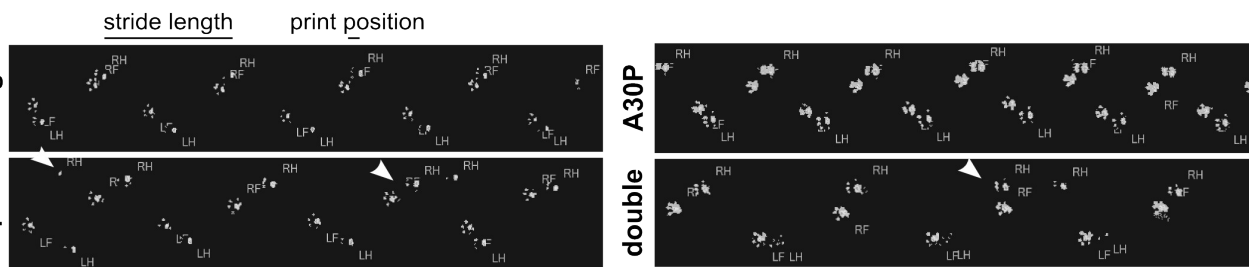
B
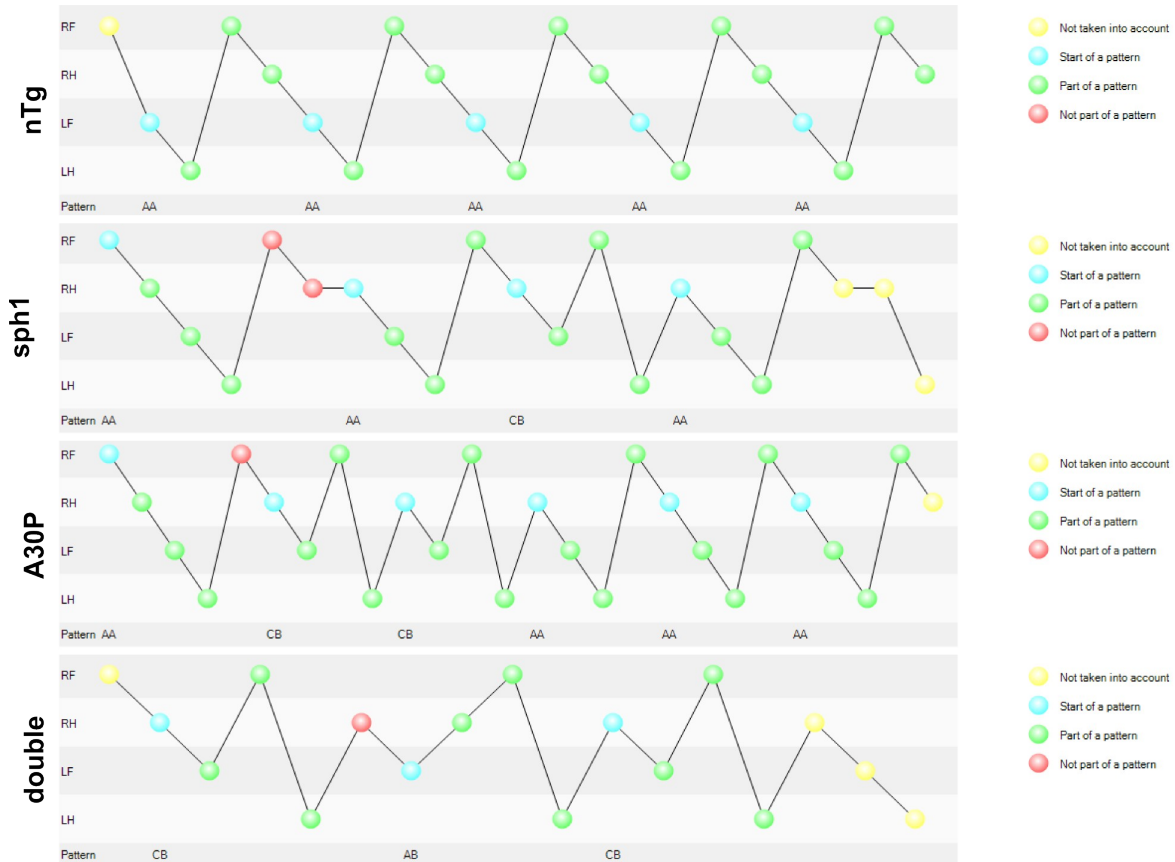
C
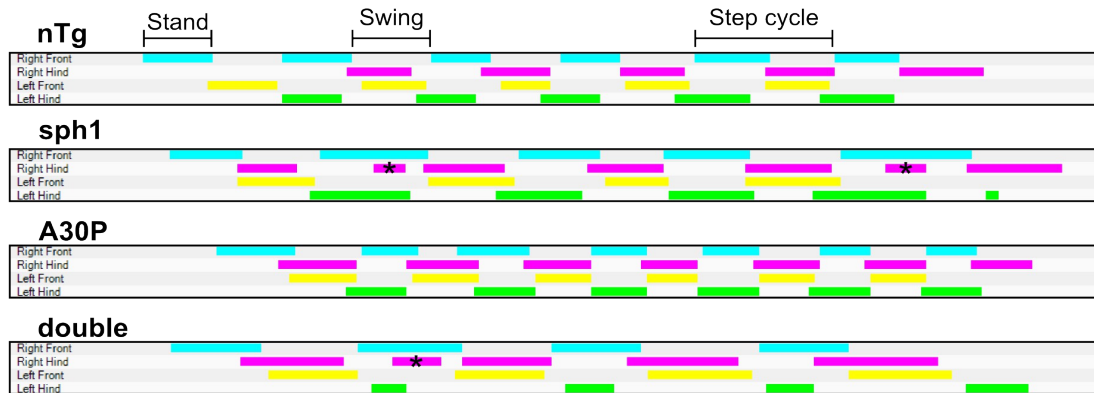
Figure 3-32: Gait impairments in CatWalk suggest a coordination dysfunction in synphilin-1 mice

Walking pattern analysis from the automatic gait analysis performed in 18 month-old mice. **A)** *Spatial representation of prints suggests the presence of abnormal extra hind paw steps in sph1 and double transgenic mice (white arrows). Note that slighter higher body weight in transgenic mice results to an increased paw signal.* **B)** *Walking pattern representation provides a regular curve for nTg animals. Abnormalities in walking pattern were detected in sph1 and double transgenic mice by the analysis software, such as 1) not taken into account or 2) not part of pattern.* **C)** *Time representation of prints are confirming the presence of extra hind paw stands in sph1 and double transgenic mice (black stars).*

6.5 Decreased home-cage activity during exploratory phase in transgenic mice in transgenic A30P mice

In several models of neurodegenerative diseases, motor impairments could be correlated to a reduced home-cage activity (Stanley et al. 2005). Therefore, motor deficit impacts on home-cage activity and locomotion were studied in our transgenic mice using PhenoMaster/LabMaster. Activity was measured by infrared sensors surrounding a cage and recording horizontal (locomotion) and vertical (rearing, cage lid climbing) activity Fig. 3-33A. Water and food intake were additionally monitored.

Activity of mice was measured every minute and data were binned per 30 minutes to normalize the dataset. Usual day/night activity shift was observed (Fig. 3-33B), highlighting the need of performing analysis of the dark and the light phase separately. Moreover, mice placed in a new cages showed an increase activity (Freichel et al. 2007; Nuber et al. 2013) which decreased over the time. Accordingly, an increased activity was observed the first night when compare to the last night (nTg night1: 167.8 ± 11.96, nTg night3: 74.34 ± 3.5, sph1 night1: 124.5 ± 9.24, sph1 night3: 67.4 ± 6.32, A30P night1: 102.2 ± 10.53, A30P night3: 41.31 ± 3.19, double night1: 85.24 ± 8.59, double night3: 57.8 ± 3.72; two-way ANOVA; post hoc Tukey; Fig. 3-33C) indicating that data of different days should be analyzed separately. For this reason, we considered activity of the last night, which better reflects physiological conditions considering that mice were more acclimatized to the system.

All transgenic animals presented a decreased activity during the first night (two-way ANOVA; post hoc Tukey; $p < 0.05$; Fig. 3-33D). Remarkably, A30P mice presented a decreased activity compared to the other mice the last night (two-way ANOVA; post hoc Tukey; Fig. 3-33E). Contrarily to the night phase, motor activity during the light phase was not correlated to the time spend in the system (nTg light1: 23.92 ± 3.44, nTg light3: 30.33 ± 3.392 sph1 light1: 25.57 ± 3.72, sph1 light3: 26.52 ± 4.57, A30P light1: 14.83 ± 2.26, A30P light3: 15.92 ± 3.67, double light1: 16.71 ± 3.06, double light3: 20.76 ± 3.29; two-way ANOVA; post hoc Tukey; $p > 0.05$; Fig. 3-33F). Accordingly, A30P mice also presented a decreased activity during the first and the last light phase (two-way ANOVA; post hoc Tukey; Fig. 3-33G). This effect was also noticeable in double transgenic mice but only when we pooled data of the three light phases (nTg: 27.28 ± 1.94, sph1: 27.15 ± 2.50, A30P: 15.20 ± 1.52, double: 20.00 ± 1.77; one way ANOVA; post hoc Tukey; Fig. 3-33H).

These data imply a loss of home-cage activity over time in all mice, but most strongly in A30P mice.

A

B

DistD 18M over time

C

DistD 18M dark phase (DP)

D

DistD 18M first dark phase

E

DistD 18M last dark phase

F

DistD 18M light phase (LP)

G

DistD 18M last light phase

H

DistD 18M total light phase
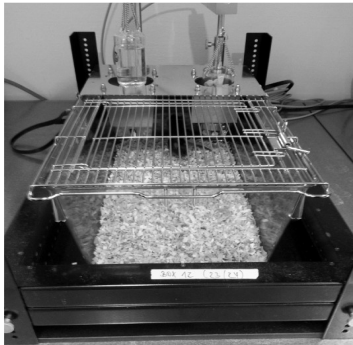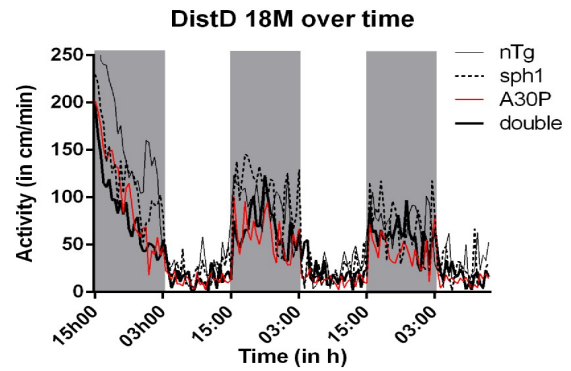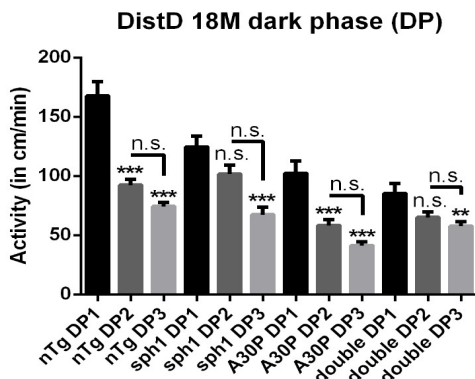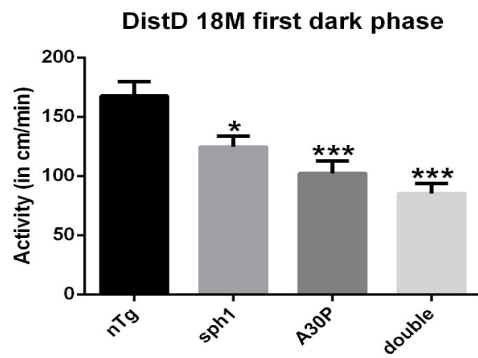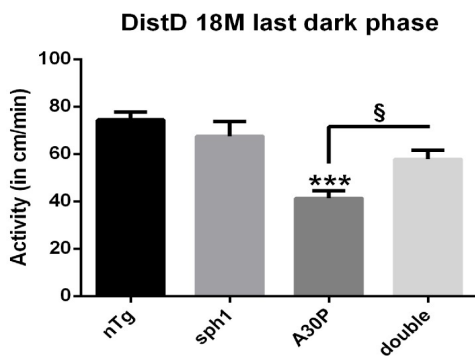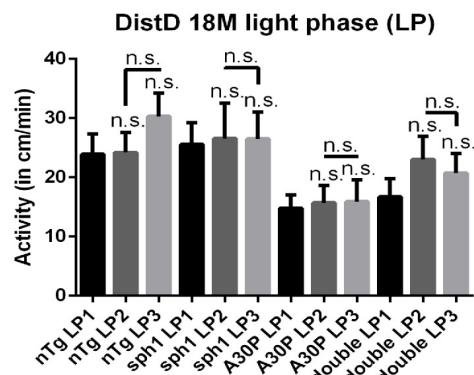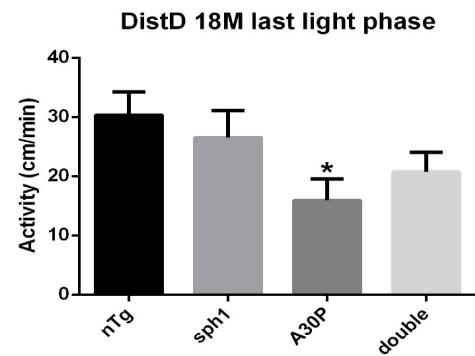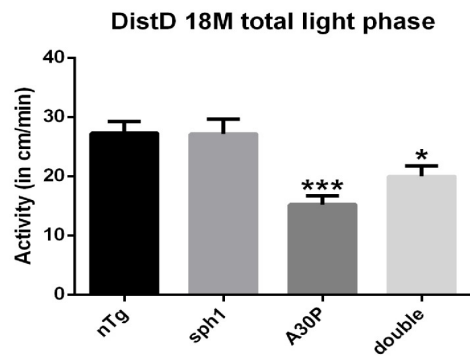
Figure 3-33: Decreased home-cage activity during acclimatization period in all transgenic mice was more exacerbated in A30P mice

A) *Home-cage activity was investigated in 18 month-old animals by using the PhenoMaster/LabMaster* *B)* *Activity was monitored over 70 h and a higher activity was observed during dark phases.* *C)* *Decrease of activity corresponding to acclimatization was observed allover the experiment.* *D)* *The activity of all transgenic mice was reduced during this acclimatization period,* *E)* *but A30P mice stayed hypoactive when compared to nTg at the end of the experiment.* *F)* *Acclimatization was not observed during light phase.* *G)* *A30P mice were showing a lower activity during the last light phase; data presented as the mean ± SEM; *p<0.05, **p<0.01, ***p<0.001, n nTg=8, n sph1=8, n A30P=9, n double=11, two-way ANOVA, post hoc Tukey.* *H)* *Decrease of activity in A30P mice was confirmed when analyzing the complete light period, also showing a slight decrease of activity in double transgenic mice; data presented as the mean ± SEM; *p<0.05, ***p<0.001, n nTg=8, n sph1=8, n A30P=9, n double=11, one-way ANOVA, post hoc Tukey.*

Reduced total distance traveled by A30P mice was also confirmed by the number of vertical beam breaks. The number of breaks was higher during the dark phase (Fig. 3-34A). Vertical beam breaks were more frequent during the first night than during the last night (nTg night1: 28.60 ± 2.15, nTg night3: 13.08 ± 1.14, sph1 night1: 17.25 ± 1.05, sph1 night3: 9.75 ± 1.13, A30P night1: 17.70 ± 1.91, A30P night3: 8.44 ± 1.44, double night1: 15.85 ± 1.54, double night3: 12.29 ± 1.05; two-way ANOVA; post hoc Tukey; Fig. 3-34B). Accordingly, we also observed a decrease of vertical activity in transgenic animals when compared to nTg during the first night (two-way ANOVA; post hoc Tukey; $p<0.05$; Fig. 3-34C), and in the last night, only A30P mice where statistically different from nTg (two-way ANOVA; post hoc Tukey; Fig. 3-34D).

Finally, we measured the amount of food and water consumed by the animals. While no differences in either food intake were observed (nTg: 12.01 ± 0.79, sph1: 12.89 ± 0.74, A30P: 10.81 ± 0.61, double: 11.33 ± 0.72; one way ANOVA; post hoc Tukey; $p>0.05$; Fig. 3-34E), a decrease in water intake was measured (nTg: 16.40 ± 2.31, sph1: 10.99 ± 1.20, A30P: 10.15 ± 0.54, double: 11.75 ± 0.93; one way ANOVA; post hoc Tukey; Fig. 3-34F). These data suggest that despite locomotor deficit, mice can still eat properly, but that the loss of activity may induce a reduction of water intake in transgenic mice.

A Z 18M over time

B Z 18M dark phase (DP)

C Z 18M first dark phase (DP)

D Z 18M last dark phase (DP)

E DistD 18M — DistD 18M 15min

F Z 18M — Z 18M 15min

G Food intake 18M

H Water intake 18M
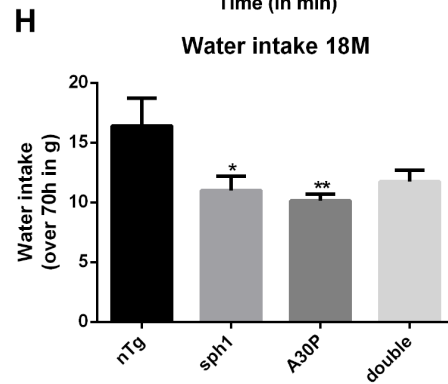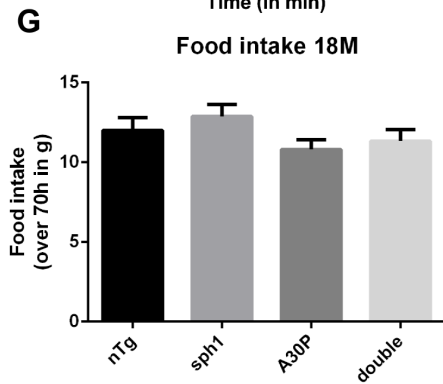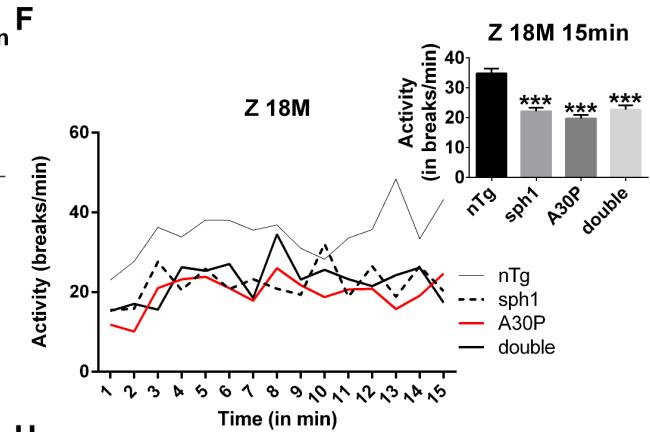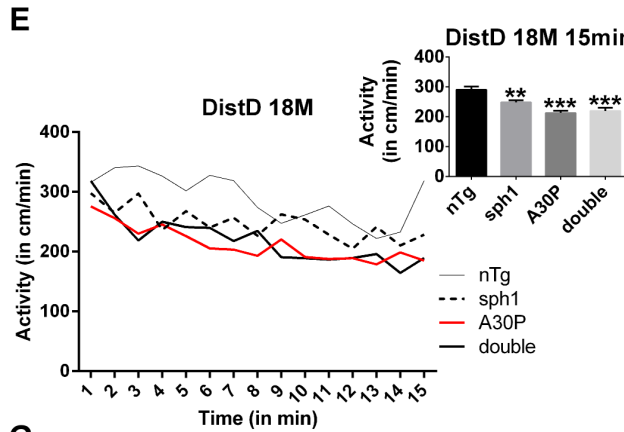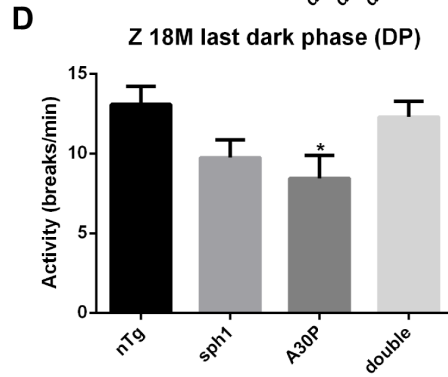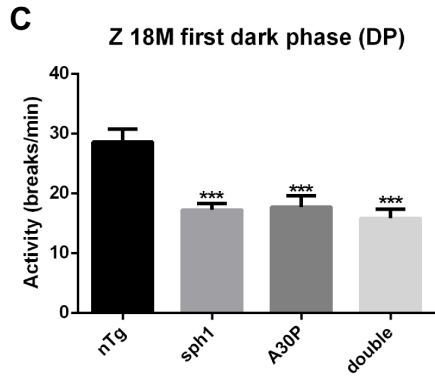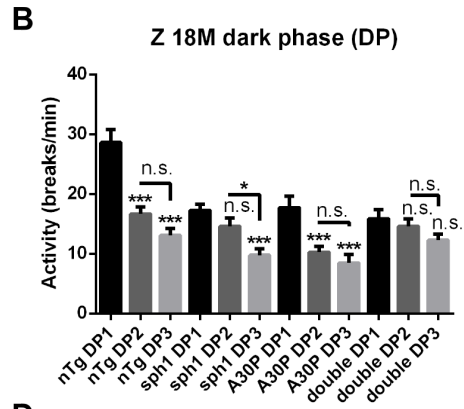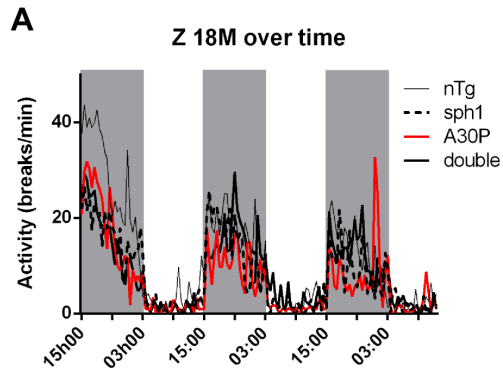
Figure 3-34: Validation of decreased home-cage activity in transgenic mice during acclimatization period using complementary parameters

A) *Vertical activity in home-cage was monitored over 70 h in PhenoMaster/LabMaster. The activity pattern was similar to the ambulation pattern observed previously, including the presence of a dark and light phase effect B) as well as an acclimatization effect over 3 days. C) Vertical activity confirmed the decreased ambulatory activity in all transgenic lines, D) as well as the hypoactivity in A30P mice during the last light phase. E) Decreased activity in transgenic mice during acclimatization could be already observed after 15 min of testing using ambulation F) and vertical activity; data presented as the mean ± SEM; *p<0.05, **p<0.01, ***p<0.001, n nTg=8, n sph1=8, n A30P=9, n double=11, two-way ANOVA, post hoc Tukey. G) No changes in food consumption was observed between lines, H) but a reduction of water intake was measured in sph1 and A30P mice, not significant for double transgenic mice; data presented as the mean ± SEM; *p<0.05, **p<0.01, n nTg=8, n sph1=8, n A30P=9, n double=11, two-way ANOVA, post hoc Tukey.*

6.6 Decreased exploratory activity in transgenic mice lines

To analyze if differences observed in PhenoMaster/LabMaster were related to anxiety or to depression, we analyzed mice in open field (Freichel et al. 2007; Nuber et al. 2013).

We observed a decrease of mice activity during the first 10 min of the test (nTg: 3646 ± 597, sph1: 2462 ± 231, A30P: 23351 ± 170, double: 2336 ± 190; one way ANOVA; post hoc Tukey; Fig. 3-35A) and these data support the decrease of activity seen the first 30 min in the PhenoMaster/LabMaster.

When decomposing the field in several central parts, we observed that mice spent most of the time in the most peripheral part of the field, reflecting the decrease of activity observed when analyzing the whole field (nTg: 3336 ± 577, sph1: 2085 ± 236, A30P: 2056 ± 135, double: 2070 ± 146; one way ANOVA; post hoc Tukey; p<0.05; Fig. 3-35B). Neither differences in the distance in the different central regions (Fig. 3-35B) nor in time spend in the several parts of the open field (Fig. 3-35C), nor the latency to reach the central parts (Fig. 3-35D) were observed.

These data suggest that transgenic mice explored less in the open field but do not present sign of excessive anxiety or depression.
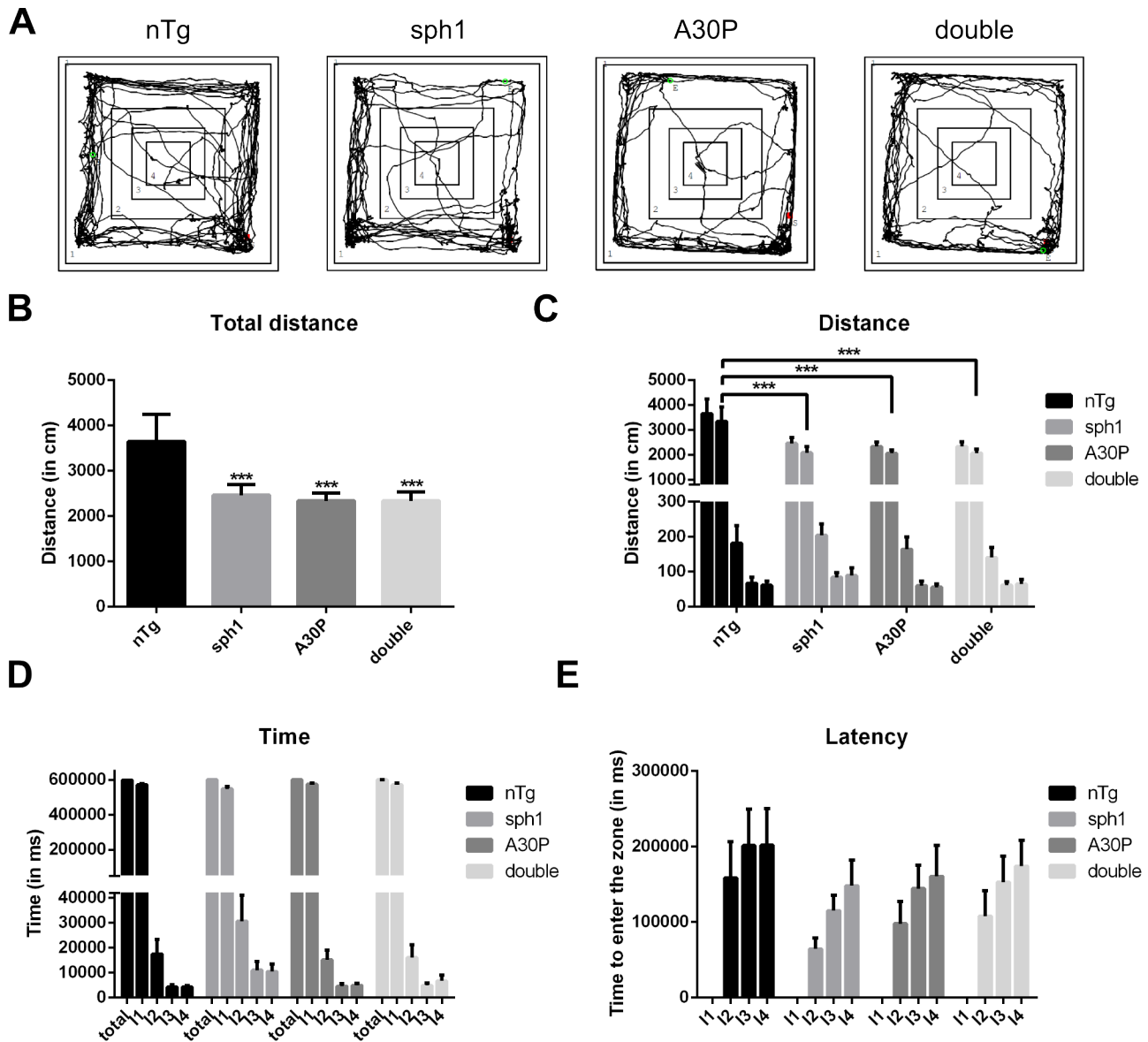
Figure 3-35: Decreased total activity in open field in all transgenic mouse lines

Activity and exploratory behaviors were investigated by exposing mice for 10 min in an open field. To analyze exploratory behavior of mice, open field was virtually divided in four concentric squares of increasing area (I4 to I1). **A)** *Representative exploratory behaviors of animal tracked in open field.* **B)** *Total distance traveled by mice in open field.* **C)** *Distance spent in the different areas of the open field. Distance traveled by transgenic mice was decreased only in the most peripheral part of the open field.* **D)** *Time spent in each part of the open field was similar for every genotype.* **E)** *Latency to reach the center of the open field did not differ between genotypes; data presented as the mean ± SEM; ***p<0.001, n nTg=8, n sph1=8, n A30P=9, n double=11, one-way ANOVA, post hoc Tukey.*

6.7 Reduced olfactory deficit in A30P mice coexpressing synphilin-1

Olfactory deficit has been reported as an early sign of the synucleinopathy both in PD patients and in several mice overexpressing a-syn (Archer 1973; Walsh & Cummins 1976). To assess in our mice potential olfactory impairment, we used a setup consisting of a large cage separated in two compartments of equal size by an opened plastic wall and spread on both side with new bedding material. In a first time, we studied spatial preference and did not observe that mice preferred a specific compartment.

We then added into the cage bedding material of the mouse home-cage in a compartment. Mice were put into the cage compartment containing the new bedding and the latency to leave the compartment as well as the time spent in each compartment was recorded. We did not observe any preference for any of the bedding (nTg familiar: 53.10 ± 3.67, nTg new: 46.90 ± 3.67, sph1 familiar: 55.94 ± 3.09, sph1 new: 44.05 ± 3.09; A30P familiar: 55.97 ± 3.71, A30P new: 44.03 ± 3.71, double familiar: 52.26 ± 2.63, double new: 47.03 ± 2.63; two-way ANOVA; post hoc Tukey; Fig. 3-36A). These data suggest that all mice got a slight smell deficit because of age. However we cannot exclude that the mice got used to be but put in new bedding and do not prefer anymore the older bedding to the fresh one.

Therefore, we repeated the experiment by comparing bedding preference of mice between their own bedding and rat bedding. We observed that mice prefer their own bedding except A30P mice (nTg familiar: 63.55 ± 4.61, nTg rat: 36.45 ± 4.61, sph1 familiar: 75.60 ± 6.06, sph1 rat: 24.41 ± 6.06; A30P familiar: 58.88 ± 4.34, A30P new: 41.12 ± 4.34, double familiar: 65.26 ± 2.30, double new: 34.74 ± 2.30; two-way ANOVA; post hoc Tukey; Fig. 3-36A). These data confirm the observation that over-expression of a-syn lead to an olfactory deficit and that this deficit was restored or delayed by sph1 coexpression.
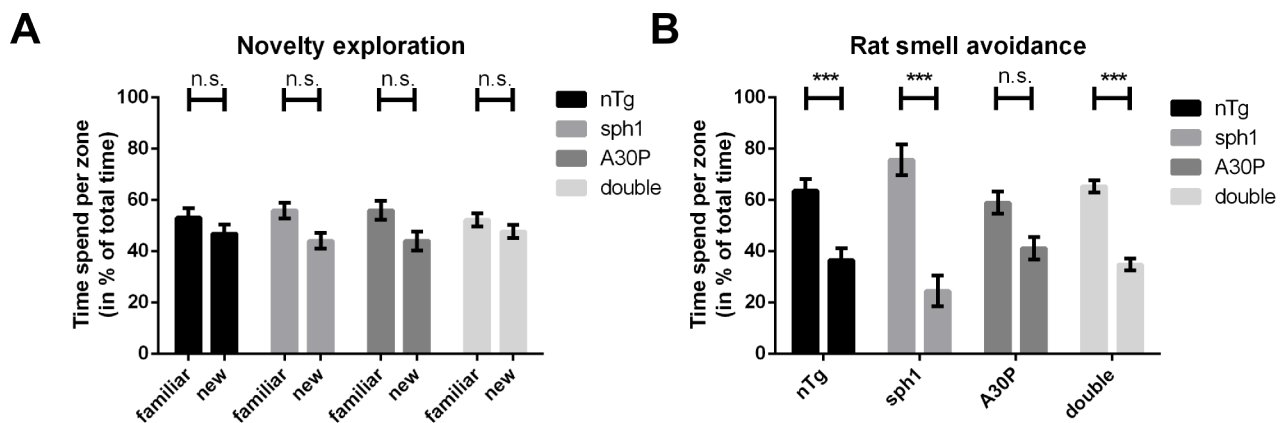
Figure 3-36: Decreased olfaction in A30P mice

*Smell perception was investigated in 18 month-old mice. **A)** Mice were placed in a new cage separated in two equal parts by a plastic wall featuring an opening. One part of the cage contained the familiar bedding and the second one fresh bedding. Time spent in each part of the box was investigated and no preference was found for one of the compartment. **B)** The test was repeated by using rat bedding. Mice spent less time in the rat compartment, except for the A30P line; data presented as the mean ± SEM; ***p<0.001, n nTg=8, n sph1=8, n A30P=9, n double=11, one-way ANOVA, post hoc Tukey.*

6.8 Cognitive function investigation in A30P mice

Finally, we investigated cognitive functions (such as spatial learning and memory) which were reported to be impaired in A30P mice (de Visser et al. 2006). For this purpose, we performed water maze, a test on which mice are trained to memorize the location of an escape platform placed in a tank filled with opaque water.

In a first step, spatial learning was investigated by adding a cue on the platform and exposing the mice four times per day to the water maze during two subsequent days. We observed a general learning effect in all genotypes which was not significant anymore after the third trial (nTg trial1: 168.5 ± 81.4, nTg trial2: 172.2 ± 62.7, nTg trial3: 100.8 ± 12.8, nTg trial4: 86.7 ± 9.1, sph1 trial1: 183.1 ± 35.4, sph1 trial2: 145.1 ± 57.5, sph1 trial3: 94.0 ± 15.2, sph1 trial4: 67.1 ± 3.5, A30P trial1: 270.5 ± 113.5, A30P trial2: 160.8 ± 20.3, A30P trial3: 188.5 ± 40.8, nTg trial4: 89.9 ± 11.3, double trial1: 147.6 ± 22.2, double trial2: 99.3 ± 12.6, double trial3: 128.5 ± 20.0, double trial4: 82.5 ± 6.6;two-way ANOVA; post hoc Tukey; Fig. 3-37A). These data suggest that mice learned the position of the target already after the third trial. Furthermore, we did not observe differences in the distance needed to find the platform either between the fourth and the last trial of the first day or between the fifth and the first trial of the second day (nTg trial5: 93.4 ± 15.7, sph1 trial5: 81.1 ± 18.0, A30P trial5: 81.1 ± 14.4, double trial5: 105.4 ± 16.2; two-way ANOVA; post hoc Tukey; Fig. 3-37A). These data support that mice remembered the position of the cue already at the end of the first day. No difference between the genotypes was observed, suggesting that spatial vision is not impaired by transgene expression.

We then tested the spatial memory by removing the cue. We observed an increased distance needed to find the platform in all genotypes (nTg last cued: 88.1 ± 11.8, nTg first spatial task: 242.8 ± 55.7, sph1 last cued: 81.1 ± 18.0, sph1 first spatial task: 393.3 ± 89.7, A30P last cued: 81.1 ± 14.3, A30P first spatial task: 400.4 ± 124.6, double last cued 105.4 ± 16.2; double first spatial task: 395.2 ± 116.9; two-way ANOVA; post hoc Tukey; Fig. 3-37A and B). Moreover, the genotype of our animal did not have an influence of this observation. Surprisingly, we found only a non-significant improvement of the time needed to find the platform during the spatial task (two-way ANOVA; p>0.075), suggesting that mice did not learn where the platform was located without a clue (Fig. 3-37B). These data were confirmed when we looked for spatial memory by removing the platform and analyzing time spent in quadrant. We did not observe an increase of time spend in quadrant in which platform was previously placed (nTg correct: 29.9 ± 4.5, nTg wrong: 23.4 ± 1.5, sph1 correct: 38.1 ± 7.9, sph1 wrong: 20.3 ± 2.6, A30P correct: 27.6 ± 5.8, A30P wrong: 23.4 ± 1.5, double correct: 35.8 ± 3.8, nTg wrong: 21.4 ± 1.3, two-way ANOVA, p>0.05). These data confirm that mice did not learn the task and the position of the platform, making the interpretation of the genotype effect on this test a complex task.
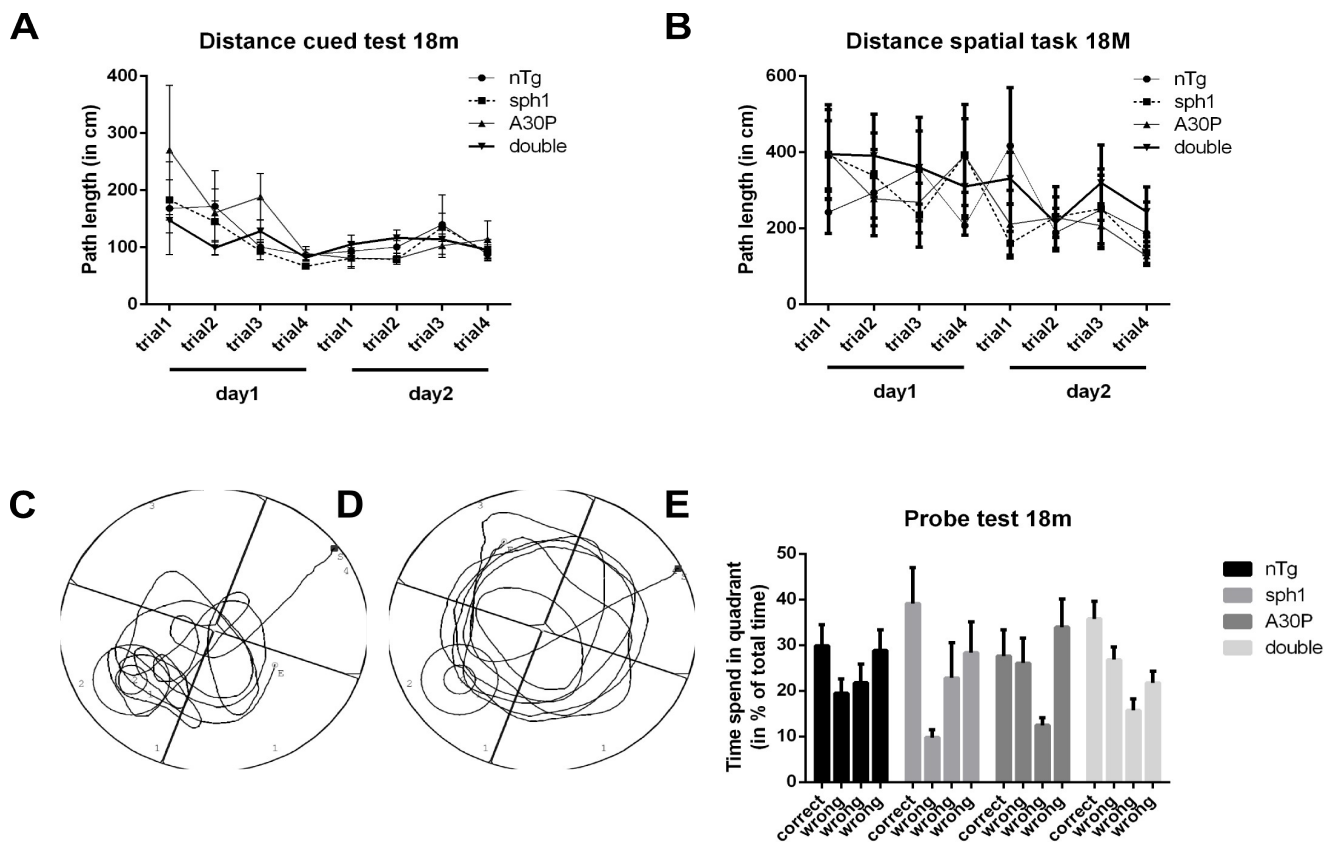
Figure 3-37: Transgenic mice did not develop spatial learning deficits

*Spatial learning and memory were analyzed in 18 month-old mice using the Morris water maze. **A)** Mice were first trained for two days, four times per day, to reach a flag cued platform to escape the water tank. Distance needed to reach the platform was decreasing until the end of the first experimental day. **B)** To test spatial learning, the cue was removed and the distance needed to find the platform was monitored. Time to reach the platform was increased when compared to the cued test. No difference was observed between groups; data presented as the mean ± SEM, n nTg=8, n sph1=8, n A30P=9, n double=11, two-way ANOVA, post hoc Tukey. **C, D)** Representation of animal swimming pattern during the probe test, in which the platform was removed and the time spent in each quadrant of the maze was recorded. **C)** Swimming pattern of an animal which learned where the platform was and **D)** an animal which did not learned it. **E)** No significant preference was observed for the target quadrant in the maze; data presented as the mean ± SEM; n nTg=8, n sph1=8, n A30P=9, n double=11, one-way ANOVA, post hoc Tukey.*

Discussion

Parkinson's disease (PD) is characterized anatomically by the presence of intraneuronal cytoplasmic inclusions, called Lewy bodies (LBs) and Lewy neurites (LNs) (Lewy 1913; Duffy & Tennyson 1965), which are mainly composed of alpha-synuclein (a-syn) (Spillantini et al. 1997). Despite that the localization of LBs in the brains of PD patients was shown to follow a specific distribution in time and space (Braak et al. 2003; Jellinger 2004), the existence of a direct link between LBs and the PD-associated neuropathology is controversial (Kramer & Schulz-Schaeffer 2007; Burke et al. 2008). However, an increasing body of evidence is showing that the presence of insoluble a-syn species in neurites and in presynapses is linked to dendritic spine degeneration and to pathology [(Kramer & Schulz-Schaeffer 2007), reviewed in (Yasuda et al. 2013)]. In this context, studying mechanisms inhibiting a-syn aggregation may lead to novel strategies to target the development of synucleinopathies [reviewed in (Blazer & Neubig 2009)].

Synphilin-1 (sph1) is a well-known interaction partner of a-syn (Engelender et al. 1999), also present in LBs (Wakabayashi et al. 2000), and first reported to promote a-syn aggregation in cell models (O'Farrell et al. 2001), protecting them against a-syn-mediated toxicity (Tanaka et al. 2004) and neurotoxic agents (X Li et al. 2010). Several mouse models overexpressing sph1 were generated using virus-mediated gene transfer or transgenic animals in order to better understand the role of sph1 in synucleinopathy *in vivo* (Jin et al. 2008; Krenz et al. 2009; Nuber et al. 2010; Smith et al. 2010). But the consequences of sph1 overexpression on a-syn aggregation and neuroprotection were not consistent, as described in more detail below.

In this study, we first aimed to investigate the role of sph1 in the development of synucleinopathy *in vivo* and on a more general level, in order to investigate the importance of a-syn aggregation on the development of synucleinopathies. Therefore, we cross-bred a mouse overexpressing the human A30P mutated a-syn under the control of the Thy-1 promoter, which develops a progressive synucleinopathy [reported originally in (Kahle et al. 2000; Kahle et al. 2001)] with a mouse overexpressing human wildtype sph1 under the PrP promoter (Nuber et al. 2010). We investigated in detail the impact of sph1 coexpression on a-syn levels, as well as on a-syn aggregation. To confirm the relevance of protein aggregation in the development of synucleinopathy, we investigated both at the histological and at the behavioral levels the effect of sph1 in mice overexpressing the human A30P mutated a-syn (termed A30P).

Importantly, the breeding strategy applied to generate the experimental group of animals is critical in this project, which consists mainly of a cross study comparison [reviewed in (Yoshiki & Moriwaki 2006)]. However, our approach was simplified by the maintenance of single A30P and sph1 transgenic mice on the same C57BL/6NCrt background. To ensure that these mice did not shift to a specific inbred substrain background (originating for example from numerous inbreeding), we first cross-bred homozygous A30P mice with homozygous sph1 mice to generate a first generation of hemizygous double transgenic mice.

To maintain the experimental group inbred, the first generation of hemizygous mice was crossed in to produce a second generation consisting of a mixed population of non-transgenic animals (nTg; ~6%), transgenic A30P and sph1 mice hemi- and homozygous (respectively ~12% and ~6%), double transgenic hemizygous (~24%) mixed hemi- and homozygous (~24%) and homozygous (~6%) [summarized in table 4-01].

By using this strategy, the direct generation of an experimental group of 30 homozygous animals (a reasonable number of animals for behavioral and neuropathological analyses) would have required the generation of at least 500 mice, which was not achievable within the time-line of this project.

Therefore, we used nTg littermates to cross-breed homozygous mice from the second generation, resulting in a third generation of hemizygous mice with the same background. A strategy including two successive cross-breedings would not have been suitable to get a complete and adequate inbred double transgenic line (statistical model described in (Lynch 1988)). Moreover, as original homozygous lines were regularly back-crossed with commercial C57BL/6NCrt mice every 5-10 generations, substrain divergence can be considered minimal (Taft et al. 2006), and the generation of double transgenic mice may therefore be considered as a cross-in.

Table 4-01: Mendelian distribution of double transgenic hemizygous cross-breeding

genotype	nTg	sph1 +/o	sph1 +/+	A30P +/o	A30P +/+	sph1 +/o A30P +/o	sph1 +/+ A30P +/o	sph1 +/o A30P +/+	sph1 +/+ A30P +/+
probability	~6%	~12%	~6%	~12%	~6%	~24%	~12%	~12%	~6%

1) *Synphilin-1 induced alpha-synuclein levels reduction*

1.1 Levels of soluble alpha-synuclein

Despite that the function of sph1 is still poorly understood, early descriptive studies reported the involvement of sph1 in protein aggregation (Engelender et al. 1999). Therefore, it is surprising that previous *in vivo* studies did not notice any effect of sph1 on levels of endogenous a-syn (Jin et al. 2008; Nuber et al. 2010) or transgenic a-syn (Smith et al. 2010). In our study, we focused mainly on the impact of sph1 on the evolution of soluble a-syn levels. As reported, we observed an accumulation of human A30P mutated levels in single transgenic mice with age (Kahle et al. 2001), but interestingly we did not detect an accumulation of soluble a-syn protein in A30P mice coexpressing sph1.

To better characterize which exact a-syn species are reduced in double transgenic mice, we then tested their solubility using different lysis buffers containing various amount of detergents. When using strong detergents, we observed more pronounced reduction of a-syn levels, confirming that sph1 is reducing abnormal accumulation of soluble a-syn in mice overexpressing A30P a-syn. In contrast to previous studies (Jin et al. 2008; Nuber et al. 2010; Smith et al. 2010), our findings suggest that sph1 decreases endogenous a-syn levels.

| Discussion

As investigation of protein levels using western blot is directly dependent of the protein extraction used to solubilize proteins of interest, and as a-syn is reported to have a very rich structural composition (Ullman et al. 2011), the protein extraction method may have a large effect on the a-syn species solubilized and may lead to contradictory results.

In this context, we tested several protein extraction protocols to measure a-syn protein levels and to limit extraction protocol artifacts related to low solubilization of lipophilic or aggregated proteins. This extensive investigation pointed out a robust reduction of most soluble a-syn forms during aging by sph1 and also demonstrated a pronounced reduction of a-syn species requiring high levels of detergent for solubilization.

Our data stand in contrast with previous observations in mice overexpressing A53T mutated a-syn, reporting that sph1 coexpression do not reduce a-syn levels (Smith et al. 2010). However it is important to note that A30P and A53T a-syn mutations have already been reported to lead to different aggregation properties, illustrated for example by reduced binding to cellular membranes as a consequence of A30P mutation, or by faster aggregation dynamics due to A53T mutation (M. K. Lee et al. 2002; Lim et al. 2011; Martin et al. 2006; Fortin et al. 2004; Yang et al. 2010). We suggest that different a-syn mutations lead to the formation of a different pool of a-syn conformers, which may present different susceptibility to be degraded by sph1. For the first time, we showed that sph1 reduces age-dependent accumulation of soluble a-syn, leading to a protective effect (Zaarur et al. 2008; Smith et al. 2010).

1.2 Levels of insoluble alpha-synuclein

The impact of sph1 on a-syn aggregation was extensively reported *in vitro (Engelender et al. 1999; O'Farrell et al. 2001; Tanaka et al. 2004; Büttner et al. 2010)* but less well studied *in vivo* (Krenz et al. 2009; Smith et al. 2010). In the *in vitro* studies, sph1 was reported to promote a-syn aggregation, but the methods used to investigate aggregates were not consistent. In the first study, the percentage of cells containing cytoplasmic eosinophilic inclusions was investigated (Engelender et al. 1999). Later, fluorescence intensity was used to identify the percentage of cells containing sph1 or a-syn-positive inclusions, in mammalian and yeast cells that overexpressed fluorescent tagged sph1 or a-syn (O'Farrell et al. 2001; Büttner et al. 2010). Finally, other authors counted the percentage of cells presenting perinuclear accumulation of sph1 and ubiquitinated proteins, resembling aggresomes (Tanaka et al. 2004). However, the exact solubility state of a-syn was not investigated in these studies.

The effect of sph1 on a-syn aggregation *in vivo* is still controversial. In the first sph1 transgenic animal generated, the effect of sph1 overexpression on endogenous a-syn levels was not reported (Jin et al. 2008). In a second transgenic mouse, absence of sph1's impact on endogenous a-syn levels was observed using a method based on sequential protein extraction to enrich less soluble proteins (Nuber et al. 2010). In contrast, increased a-syn aggregation was shown in non-transgenic mice using thioflavin S staining when a virus-mediated approach was used to overexpress sph1 (Krenz et al. 2009). Finally, double transgenic mice overexpressing sph1 and human A53T mutated a-syn did not provide a clear readout, showing increased proteinase K resistant a-syn levels in tissue lysate, but not at the histological level, and a decreased number of silver positive inclusions (Smith et al. 2010).

To better characterize the effect of sph1 on a-syn solubility, we enriched less soluble proteins from brain homogenate using a sequential protein extraction based on detergents (Culvenor et al. 1999; Tofaris et al. 2003) and another method based on the separation of high molecular weight proteins using AGERA (Weiss et al. 2008). In both methods, we did not observe a drastic effect of sph1 on a-syn solubility. When investigating the presence of highly folded aggregates at the histological level using proteinase K digestion (Schulz-Schaeffer et al. 2000; Neumann et al. 2002; Tanji et al. 2010), we found a strong decrease of insoluble a-syn in both cell bodies and their processes of double transgenic animals. These data were confirmed by extracting less soluble a-syn species, then labeling them with gold-conjugated anti-a-syn antibody and finally analyzing these structures by electron microscopy (Díaz-Hernández et al. 2004; Tomás-Zapico et al. 2012). By using this method, we suggest that the precise a-syn species decreased in double transgenic mice present a filamentous nature. At the histological level, we observed a decrease of inclusion quantity when performing staining of paraffin embedded sections with an anti-a-syn antibody. However, this method is less suitable for quantification and does not reflect the low protein solubility.

Reduction of a-syn aggregation by sph1 overexpression was investigated mainly in the hindbrain of hemizygous A30P mice and more precisely in the brainstem. It is important to point out that we did not observe obvious a-syn aggregation in other brain structures of these mice. Thus, we were unable to confirm sph1's effect on a-syn aggregation in other brain regions. However, it is unlikely that sph1's effects are specific to only particular cells of the brainstem due to its rich diversity of neuron types (Smith & DeMyer 2003), but we cannot exclude that the amount of a-syn may regulate the efficiency of sph1-mediated degradation, and that an increased amount of a-syn would result in the inhibition of this pathway. This hypothesis could be tested in homozygous animals which are overexpressing a-syn at higher level than the hemizygous mice. It is also interesting to mention that despite the similar spatial expression patterns of sph1 and a-syn, we detected only few specific cell subpopulations coexpressing high amounts of both transgenes in double transgenic mice. This result is surprising because both promoters were reported to drive protein expression mainly in neurons (Baybutt & Manson 1997; Vidal et al. 1990). Therefore it would be interesting to identify these cells and molecular mechanisms driving this effect.

For the first time, we showed *in vivo* that sph1 does not increase a-syn aggregation, but even decreases the levels of some specific a-syn species and especially a-syn fibrils. The reduction of a-syn aggregation by sph1 was already suggested previously in cells (Wong et al. 2012) but was never reported *in vivo*.

Levels of oligomeric alpha-synuclein

Toxicity of a-syn is reported to be driven by the formation of oligomers, possibly representing intermediate structures between soluble and fibrillar forms of a-syn [reviewed in (Lashuel et al. 2012)]. Therefore, investigation of a-syn oligomers is necessary in order to understand the potential protective effect of sph1 on a-syn-related toxicity. By using dot blot and FRET, we detected a-syn oligomers in homozygous A30P mice but not in hemizygous mice, supporting that a-syn levels play a critical role in the formation of oligomers. It is discussable whether a-syn oligomer levels were too low to be detected in hemizygous animals or whether oligomers are not formed or degraded or transformed in other species with a higher kinetic.

| Discussion

Thus, it is unclear if sph1 in our study plays a role in the formation of a-syn oligomers. It is interesting to note that the authors of a recent study (Wagner et al. 2013) also described the presence of oligomers in the same A30P mice. For further analysis, we suggest another protocol described in a recent study (Fagerqvist et al. 2013), in which the authors were using a reducible amino-reactive crosslinker (DSP) to protect protein-protein interactions. However, despite the use of this method, authors noticed a large variation in oligomer levels among transgenic animals, stressing the complexity of oligomer analysis.

1.3 Levels of soluble synphilin-1

To assess if the mechanism leading to the reduction of a-syn levels also involves the degradation of sph1, we used western blot to measure sph1 levels. Reduction of sph1 in brain lysates of mice coexpressing A30P a-syn was observed when using a stringent protein extraction buffer. However, data generated using human A53T mutated a-syn overexpression did not suggest any influence of a-syn expression on sph1 levels (Smith et al. 2010). However, this hypothesis was not further explored in this study, which was probably a consequence of the complexity of sph1 immunostaining, due to the existence of multiple sph1 isoforms (I. J. Murray et al. 2003; Humbert et al. 2007) and from the few antibodies available.

We noticed in our study that the absence of detergents in the lysis buffer (TBS fraction of the sequential protein extraction) resulted in a poor electrophoresis separation, thereby making protein quantification difficult. We were able to overcome this problem by using detergents (0.5% SDS and 1% NP-40) suggesting a low solubility of sph1 as observed previously (Nuber et al. 2010). In this context, the lower levels of sph1 observed in double transgenic mice may either result from decreased levels of soluble sph1 or result from an increased aggregation. Similarly to the reduction of soluble a-syn levels, we cannot conclude if the difference observed between our study and the study using A53T a-syn animals (Smith et al. 2010) results from the different a-syn mutations or from the different experimental conditions. Therefore, it is unclear if reduced sph1 levels in double transgenic mice are a consequence of a-syn-induced degradation of soluble sph1 or a-syn-mediated coaggregation. Protein solubility gradient-based assays are an alternative that may help to define more precisely if lower levels of sph1 result from a decreased levels of protein or from its reduced solubility, which can be confirmed using sph1 tracking during protein degradation induction.

2)   *Synphilin-1 coexpression induced an increase of soluble ubiquitinated proteins as well as autophagy activity in A30P mice*

2.1 Synphilin-1 did not modulate alpha-synuclein expression

In the previous paragraph we reported that sph1 decreased the age-dependent accumulation of a-syn in mice overexpressing the human A30P mutated a-syn. To understand the origin of this a-syn reduction, it is important to consider that intracellular protein levels undergo a continuous synthesis/degradation cycle to keep a pool of functional proteins and to avoid accumulation of damaged proteins [schematized in Fig. 4-01. and reviewed in (Goldberg 2003)]. Therefore, it is possible that the reduction of a-syn in double transgenic mice results from a higher synthesis, from a lower degradation of a-syn, or from both.

To investigate the a-syn synthesis, we determined a-syn levels in young animals using western blot and did not observe differences in levels of the monomeric a-syn form between A30P and double transgenic animals. Moreover, preliminary transcriptional analysis using Affymetrix did not reveal dysregulation of endogenous *snca*, *thy-1* or *prp* mRNA levels. These results also suggest that sph1 is not modulating the expression of endogenous nor transgenic a-syn. However, microarrays are a method originally conceptualized to screen whole organisms' transcriptomes and screening technologies may present variability resulting from normalization issues. In the specific case of genechip technologies, noise or low affinity originating from a non-optimal primer design, as well as low abundance of RNA of interest (Ji & Davis 2006), may induce false negative data (Choe et al. 2005). Confirmation of these results at the single mRNA level could have been performed by qPCR. However, the comparison of western blots from young animals and Affymetrix from old animals suggests that levels of a-syn are probably not deregulated at the transcriptional level but may rather originate from a dysregulation of protein degradation.

2.2 Synphilin-1 promoted autophagosomal degradation

We started protein degradation investigation with the autophagy-lysosome pathway (ALP), a pathway which was reported to play a major role in the degradation of excess levels of a-syn [reviewed in (Ebrahimi-Fakhari et al. 2012)]. For this purpose, we analyzed levels of autophagy markers using western blot and observed in A30P mice an accumulation of p62, which is a cargo receptor for ubiquitinated proteins targeted for degradation by the ALP and which itself is a substrate for autophagy (Komatsu et al. 2007; Pankiv et al. 2007; Bjørkøy et al. 2009). We suggest that p62 accumulation in A30P mice indicates a potential impairment of autophagosomal degradation which is not present anymore in double transgenic mice. Accordingly, changes in p62 levels between A30P and double transgenic mice were confirmed by an increase of beclin-1 levels in double transgenic mice. Indeed, elevated levels of beclin-1 are inducing autophagy [suggested by drastic autophagy attenuation in beclin-1 heterozygous knockout mice (Qu et al. 2003) and by the rescue of autophagy impairments in several animal models overexpressing beclin-1 (Spencer et al. 2009; Fields et al. 2013)]. Consistently, an increase of beclin-1 was also reported in other double transgenic mice overexpressing A53T a-syn and sph1 (Smith et al. 2010).

Two different hypotheses can emerge from these observations: either sph1 can interfere with the inhibition of the ALP in A30P mice or sph1 promotes protein degradation via autophagy during abnormal protein accumulation. An increasing body of evidence is supporting an elevated level of autophagy in models overexpressing sph1 (Zaarur et al. 2008; Wong et al. 2008; Wong et al. 2012). In these multiple cell models overexpressing various proteins prone to aggregate, sph1 coexpression was reported to mediate a specific aggregate degradation but the numerous steps involved in autophagic flux are making this molecular pathway highly dynamic and complex to study [reviewed in (Xilouri et al. 2013; Lamark & Johansen 2012; Lynch-Day et al. 2012)]. This analysis is simplified by stopping cell machinery during tissue lysis and quantification of autophagy-markers using western blot is well established and accepted [reviewed in (Klionsky et al. 2012)]. To better understand autophagy activation by sph1, specific enzymatic kinetics and a detailed pathway analysis should be performed. Unfortunately these studies cannot be performed ideally in adult brain tissue lysate.

| Discussion

Despite these limitations, the decrease of autophagic flux observed in A30P single transgenic mice as well as the recovery of autophagy in double transgenic mice, were supported by several studies showing that a-syn inhibits autophagy [(Klucken et al. 2012), reviewed in (Winslow & Rubinsztein 2011)] and that sph1 promotes autophagy [(Wong et al. 2008; Smith et al. 2010; Wong et al. 2012)].

In addition to the modulation of p62 and beclin-1 levels observed in A30P and double transgenic mice, the observation of similar numbers of autophagosomes and reduced LC3-I levels (without changes in LC3-II levels) suggest that a-syn and sph1 do most likely not play a role in the formation of autophagosomes. Therefore, it remains unclear whether a-syn and/or sph1 modulate autophagic flux.
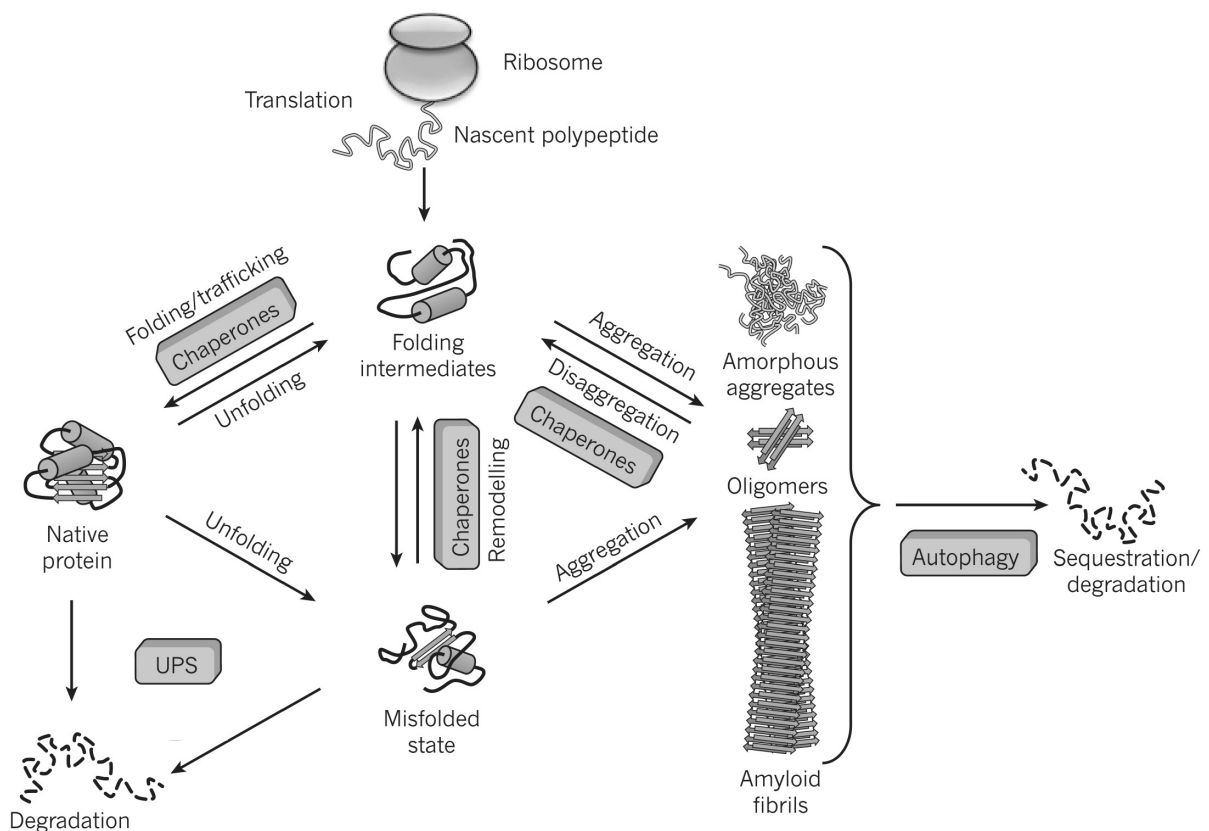
Figure 4-01: Proteostasis network

Picture copied from (Hartl et al. 2011)

The protein quality control network integrates chaperone pathways to facilitate the folding of newly synthesized proteins into their native conformations. Chaperones also prevent and remodel misfolded proteins. Absence of either refolding or degradation by UPS may lead to protein aggregation. Some molecular chaperones slow or prevent protein misfolding and aggregation, but in case of overwhelmed chaperone network capacity, non-native proteins may form large and amorphous aggregates. Degradation of these aggregates by chaperone extraction or by autophagy could be considered as the ultimate mechanisms to rescue cells from wide aggregation spread.

2.3 Synphilin-1 promoted the formation and the redistribution of high molecular weight polyubiquitinated structures

The role of sph1 in aggregate formation was found directly after sph1 discovery (Engelender et al. 1999). But ten years later, a function of sph1 in aggregate removal by autophagy via aggresome formation and K63 polyubiquitination was suggested (Wong et al. 2008; Wong et al. 2012). To test if ubiquitin signaling played a role in the reduced a-syn aggregation and/or in the increased autophagy observed in A30P mice coexpressing sph1, we first used western blot to quantify the total levels of ubiquitinated proteins. In double transgenic mice, we observed a general increase of soluble ubiquitinated proteins which was confirmed when using several protein extraction buffers and different types of electrophoresis. Despite that sph1 was reported to induce the formation of aggresomes in a ubiquitin-dependent pathway (Wong et al. 2012), effects of sph1 overexpression on levels of ubiquitinated proteins were not reported previously.

As ubiquitination is an abundant and versatile post-translational protein modification which may originate from multiple mechanisms [reviewed in (Kulathu & Komander 2012)], we investigated patterns of ubiquitin staining at the histological level. We detected in A30P mice the presence of multiple small somatic ubiquitinated structures which were contrasting with the presence of large and dense ubiquitin-positive structures at the perinuclear region of double transgenic mice. Additionally, ubiquitin-positive structures found in double transgenic mice were also sharing main aggresome properties such as perinuclear location, presence of microtubules and colocalization with K63 polyubiquitinated proteins.

These different ubiquitin-positive structures, which were present in both A30P and double transgenic mice, indicate different inclusion-like properties. Effects of sph1 on aggregate removal were suggested in several cell models (Zaarur et al. 2008; Wong et al. 2008; Wong et al. 2012) which additionally showed that sph1 properties are not only specific to a-syn but also to other aggregation-prone proteins. We propose that coexpression of sph1 may induce transport of a-syn (and other proteins) to the perinuclear region where these complexes could be sequestered into aggresomes susceptible to autophagic degradation (Fig. 4-02).

We also investigated the UPS in our mice since an increasing body of evidence suggests its critical role in a-syn turn-over [reviewed in (Ebrahimi-Fakhari et al. 2012)]. When analyzing proteasomal activity in brain lysates using specific catalytic substrates, we did not observe genotype-related differences in proteasome activity between mice overexpressing the human A30P mutated a-syn and mice overexpressing the human sph1 protein. These results were already suggested in a previous study using mice overexpressing a-syn (Martìn-Clemente et al. 2004), but face multiple *in vitro* studies in which fibrillar and oligomeric forms of a-syn (but not the monomer) were shown to inhibit the overall proteasomal degradation based on a recombinant UPS system (Lindersson et al. 2004). However, it is also interesting to note that our data fit the previous report of (Alvarez-Castelao & Castaño 2011) in which the authors did not observe an effect of sph1 on UPS activity but a decreased degradation of a-syn by the UPS. This may reflect a potential of sph1 to shift a-syn degradation from the UPS to the ALP.

| Discussion
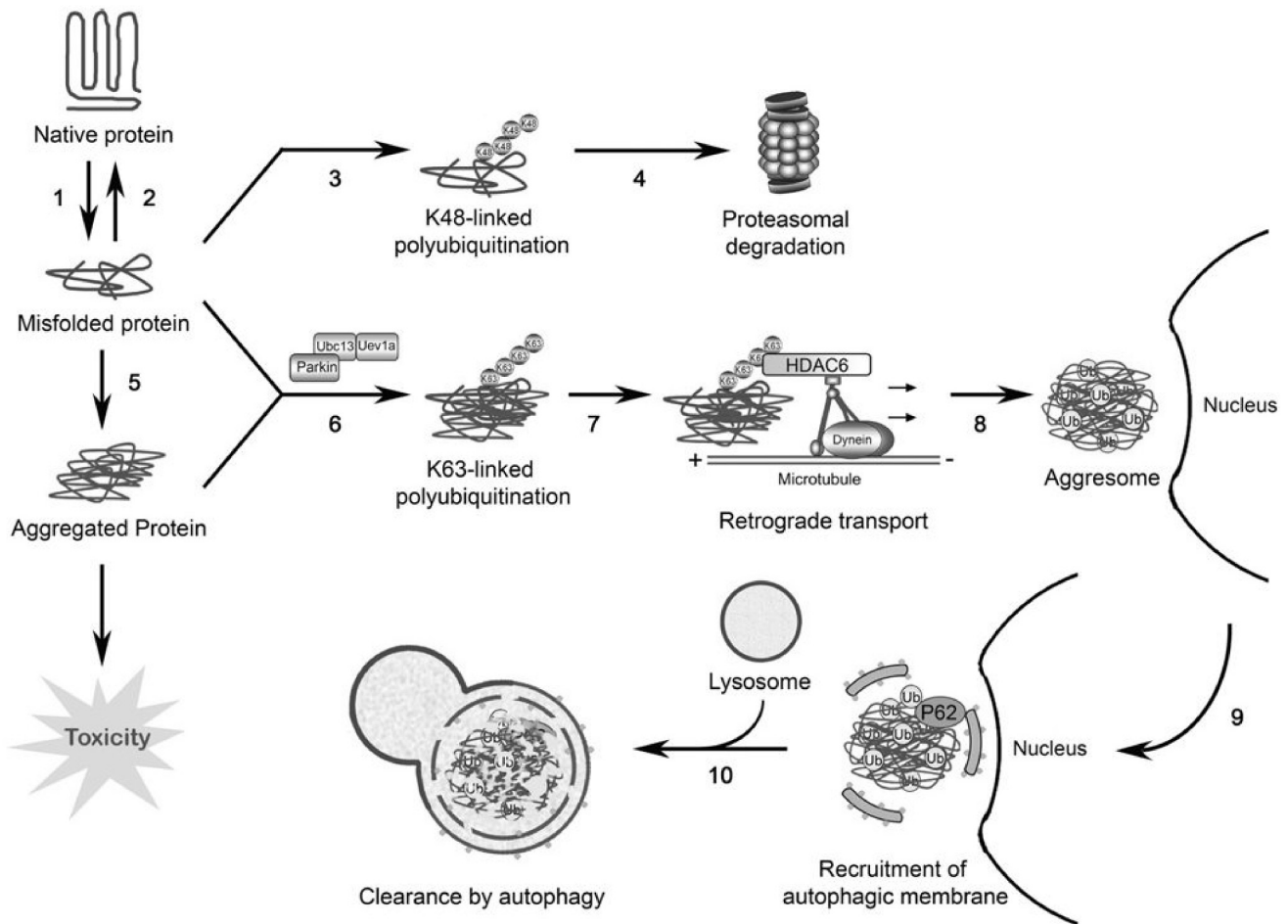
Figure 4-02: Aggresome autophagy pathway

Picture modified from (Chin et al. 2010)

Proteins misfolded (1) may be either refolded by chaperones (2) or tagged with Lys48-linked polyubiquitin chains (3) to be degraded by the proteasome (4). Failure of chaperone and proteasome systems result in an accumulation of misfolded proteins leading to the formation of oligomerized and aggregated species (5) which were reported to cause cytotoxicity. Misfolded proteins can also be tagged with Lys63-linked polyubiquitin by several E3 ligases (such as parkin cooperating with E2 enzyme Ubc13/ Uev1a) (6), we suggest that sph1 acts on a-syn toxicity at this level. Lys63-linked polyubiquitin chains promote binding of misfolded proteins to HDAC6 (7) and thereby to the dynein motor complex for retrograde transport towards the MTOC to form aggresomes (8). Lys63-linked polyubiquitination promotes the binding of p62 and facilitates its recruitment to autophagosomal membranes (9). Subsequent fusion of autophagosomes with lysosomes allows the degradation of misfolded and aggregated proteins by lysosomal hydrolases (10).

However, direct comparison between our *ex vivo* assay and other *in vitro* studies is not relevant because absolute levels of a-syn fibrils and cell diversity in tissue lysate cannot be reproduced in cell culture or recombinant models. Furthermore, the concentration of a-syn used in *in vitro* assays *(Snyder et al. 2005)* was 5000 times higher than in brain lysate from the current mouse model (Kahle et al. 2001), making the physiological relevance of this observation questionable (a-syn was reported to inhibit the proteasome at 5 µM *in vitro* but concentration of a-syn is less that 1 nM in mouse brain). Despite that reduced proteasome

activity was repeatedly reported in PD patients (McNaught & Jenner 2001; McNaught, Belizaire, et al. 2002; McNaught et al. 2003), the relevance of a-syn in this process is controversial (Tofaris et al. 2003) as this effect was only observed in the substantia nigra but not in other brain regions featuring LBs and LNs. Still, we cannot exclude that subtle effects on proteasomal activity by transgenic protein expression could be evened out due to the conditions of our experiments (such as ATP addition or stress induced by tissue lysis to the proteasomal machinery). But these conditions seem acceptable when compared to the original report in which samples collected several days *post mortem* were processed similarly.

It is also important to note that the proteasomal activity is directly dependent on the subunit composition of the 26S proteasome (such as 11S or 19S cap). To investigate this issue, we measured protein levels of different UPS subunits and did not observe that a-syn or sph1 influenced the levels of catalytic or regulatory subunits. But interestingly, analysis of proteasome at the histological level showed an abnormal distribution of the regulatory subunits of the proteasome in A30P mice. More precisely, proteasomal subunits are classically reported to be located in the perinuclear region or in the nucleus. But in A30P mice, this pattern was replaced by a more somatic staining, suggesting the recruitment of proteasome subunits into inclusions. This hypothesis is supported by previous studies showing the recruitment of proteasomal subunits in a-syn positive inclusions (Ii et al. 1997; Snyder et al. 2003; Zhou et al. 2004). This observation, in addition to the increase of a-syn fragments observed in A30P when compared to double transgenic mice, suggest that these fragments might be a product of the UPS that may promote the formation of major a-syn fibrils (C.-W. Liu et al. 2005).

Following this logic, we suggest that the recruitment of UPS regulatory subunits in these inclusions does not inhibit the UPS function, but induces a vicious cycle of increased higher a-syn truncation, leading to increased aggregation.

3) Synphilin-1 reduced pathology in mice overexpressing the human A30P mutated alpha-synuclein

3.1 Reduced beta sheet structures in mice coexpressing synphilin-1

When sph1 was discovered during screening for a-syn interacting partners (Engelender et al. 1999), its abnormal presence in the brain of PD patients within LBs (Wakabayashi et al. 2000) led to the hypothesis that sph1 may have a pathological function in synucleinopathy. This hypothesis was opposed rapidly when it was observed that 1) parkin-ubiquitination of sph1 is disrupted by familial-linked *PARK2* mutations (Chung et al. 2001) and that 2) the sph1 mutation R621C was found to be associated with PD development (Marx et al. 2003).

Numerous cell culture models consistently showed that overexpression of sph1 promoted the formation of inclusions and these inclusions were characterized later in more detail as perinuclear ubiquitinated aggresomes (Tanaka et al. 2004). The impact of aggresomes on cells survival is contradictory. It was reported that aggresomes either increase cell toxicity (G. Lee et al. 2002; Eyal et al. 2006; Alvarez-Castelao & Castaño 2011), do not modulate cell toxicity (O'Farrell et al. 2001) or are even protective against a-syn induced toxicity (Tanaka et al. 2004; Wong et al. 2008; X Li et al. 2010; Wong et al. 2012). Similarly, sph1 overexpression

| Discussion

in mouse models provided inconsistent results. These animals were shown to develop either no pathology (Smith et al. 2010), a mild pathology (Jin et al. 2008; Nuber et al. 2010) or a strong pathology in a study based on intracranial injection of viral vectors (Krenz et al. 2009).

In this context, we investigated the impact of sph1 on the neuropathology developed in the hindbrain of A30P transgenic mice. We focused particularly on the brainstem of these animals as this brain region was reported to demonstrate the highest pathology when using PK resistant a-syn staining (Schulz-Schaeffer et al. 2000; Neumann et al. 2002; Tanji et al. 2010). In a first approach, we investigated neuropathology using silver staining (Braak & Braak 1999; Uchihara 2007) and thioflavin S (Sun et al. 2002) in parallel because both dyes were reported to lead to the same staining pattern (Vallet et al. 1992; Cullen et al. 1996; Sun et al. 2002). These stainings, reflecting both degenerating axons (Gallyas et al. 1980) and the presence of beta sheet-structures (Biancalana & Koide 2010), were showing characteristic synucleinopathy-related processes and cellular inclusions in the brainstem of A30P mice. Interestingly, these patterns were drastically reduced in double transgenic mice, supporting results reported in A53T mutated a-syn transgenic mice (Smith et al. 2010). We would like to mention that another study showed contrary observations when using a viral vector to induce sph1 expression (Krenz et al. 2009). However, injection-related complications (killing almost 10% of dopaminergic cells in the SN) and high viral titer (resulting in a very strong expression of sph1 which cannot be reached using a transgenic animal model) may explain the differences observed in this study. It is also important to notice that animals used in this study were relatively young (6 months) and did not present neuropathology (as demonstrated with thioflavin S staining). We suggest that the protective effect of sph1 in A30P mice presented in our study could also be replicated in mice injected with viral vectors inducing sph1 expression. However, the age of the mice and the viral charge injected would have to be optimized. Finally, the viral vector approach induces a strong expression of the transgene in a short time, therefore we cannot exclude that this strong and very located expression may result in an exacerbated pathology when compared to transgenic animal models.

Gallyas silver staining and thioflavin S are usually reported to identify inclusions, but as levels of aggregates are debated to be a reliable pathology marker [reviewed in (Bendor et al. 2013)] we cannot conclude using these stainings that sph1 had a neuroprotective function in A30P mice. This was illustrated in a recent study showing that G51D mutated a-syn leads to cell toxicity without promoting a-syn aggregation (Lesage et al. 2013). However, it is known that a direct increase of a-syn degradation results in an improved phenotype in mice overexpressing a-syn (Spencer et al. 2009). Despite that we cannot conclude from these stainings that sph1 coexpression in A30P mice was reducing their neuropathology, these experiments support the decrease of aggregate load in double transgenic animals.

To endorse the neuroprotective effect of sph1, other neurodegeneration markers should be investigated. Ideally, the impact of reduced a-syn aggregates on nigrostriatal degeneration (and particularly loss of SN dopaminergic cells) should be investigated [reviewed in (Blandini & Armentero 2012)]. Unfortunately, mice overexpressing the human A30P mutated a-syn cannot be used for this purpose as they do not present nigrostriatal cell loss.

3.2 Reduced neuroinflammation in mice coexpressing synphilin-1

It is intriguing that despite the similar origin of synucleinopathy in familial forms of PD, which are consequence of *SNCA* duplication or triplication, and transgenic mice with a 2- to 5-fold overexpression of human a-syn, transgenic mice do not present a loss of nigral cells (Kuo et al. 2010). It would be a tentative interpretation to suggest that the nigrostriatal system of rodents may cope with higher levels of a-syn than the human brain, especially because transgenic mice overexpressing a-syn are also known to reproduce neuroinflammation, oxidative and proteolytic stress [reviewed in (Blesa et al. 2012; Bezard et al. 2013)], neuropathology at the histological level [oxidative stress reviewed in (Bosco et al. 2006; Nakabeppu et al. 2007), proteolytic stress (Ebrahimi-Fakhari et al. 2012; Cook et al. 2012; Xilouri et al. 2013) and inflammation (Perry 2012)].

In this context, we also used inflammation markers (such as microglial and astroglial activation), to confirm that the aggregation found in A30P mice is accompanied by neuroinflammation at the histological level. Accordingly, we observed neuroinflammation marks in A30P mice which were strongly reduced in double transgenic mice. However, the origin of the inflammation observed in the brain of A30P transgenic mice is unknown and the relevance of this inflammation as a causative or a protective mechanism is discussable [reviewed in (Tufekci et al. 2012)]. Despite that neuroinflammation levels are usually poorly reported when investigating potential effects of transgenes (Fan et al. 2006; Spencer et al. 2009) or drugs (Wagner et al. 2013; Hebron et al. 2013), few other studies also showed that a decreased synucleinopathy goes along with a decreased inflammation [reviewed in (Hirsch & Hunot 2009; Koppula et al. 2012)]. However, most of these studies were based on toxin induced animal models, which are themselves inducing the production of ROS and inflammation. For example, this could be illustrated by the injection of rotenone in mice treated with the non-steroidal anti-inflammatory sodium salicylate (Thakur & Nehru 2013) or MPTP intoxicated mice treated with the anti-inflammatory CNI-1493 (Noelker et al. 2013).

Finally, we also would like to point out that the observed neuroinflammation may result from multiple pathways which may lead to abnormal glial activity. But most studied origins of neuroinflammation in synucleinopathy are mitochondrial dysfunction [reviewed in detail in (Hernández-Aguilera et al. 2013; López-Armada et al. 2013)] and exocytosis of a-syn [reviewed in (Marques & Outeiro 2012)].

Our results are supported by a previous study showing that sph1 is reducing a-syn-related neuroinflammation (Smith et al. 2010). Therefore, it is interesting to note that the effect of sph1 is stronger on astroglial cells than on microglial cells. Accordingly, astrocytic a-syn deposition was shown to initiate the recruitment of phagocytes and microglias that attack and kill neurons (Halliday & Stevens 2011). As levels of microglial activity were suggested to be correlated with neuronal dysfunction [reviewed in (Hirsch & Hunot 2009)], low levels of activated microglia may reflect a neuroprotective effect occurring in double transgenic mice. To validate this hypothesis, inhibiting or activating microgliosis in A30P mice presenting would be an interesting strategy to study a-syn aggregation and toxicity.

All together, we suggest that the reduced a-syn accumulation and neuroinflammation observed in double transgenic mice speaks for a neuroprotective effect of sph1 coexpression.

4) *Synphilin-1 reduced motor phenotype in mice overexpressing the human A30P mutated alpha-synuclein*

4.1 Coexpression of synphilin-1 delayed motor phenotype onset observed in mice overexpressing alpha-synuclein

In the last chapter, we presented the impact of sph1 coexpression on soluble and insoluble a-syn levels, as well as on the neuropathology observed in transgenic mice overexpressing human A30P mutated a-syn.

To confirm the relevance of the neuroprotection suggested by histological observations, we investigated a potential modification of the pathophysiology observed in A30P mice [reported previously in (Freichel et al. 2007)]. We first focused on the progressive locomotor impairment developed by A30P mice using an accelerating rotarod. We found that the first signs of motor abnormalities were observed in A30P mice at 26 weeks and were delayed to 38 weeks in double transgenic mice, suggesting that coexpression of sph1 may delay synucleinopathy.

Rotarod, and especially protocols using accelerating speed, are sensitive and reproducible methods to detect motor impairment in transgenic animals [reviewed in (Karl et al. 2003)]. But interestingly, in the first characterization of A30P mice (Freichel et al. 2007), a motor deficit on the rotarod was found only in 51 week-old animals using rotarod, whereas it appeared at 38 weeks of age in our study. It is important to note that the protocols used to investigate the motor phenotype were different in the two studies (protocols described in table 4-02). Because motivation and motor learning may play an important role for rotarod performance, we adapted the original protocol of (Freichel et al. 2007) following recommendations from (Karl et al. 2003). In short, a training period was added and a larger number of trials were given, leading to a longer testing period.

Table 4-02: Differences in rotarod protocol between Freichel et al. 2007 and Casadei et al. 2013

Study	Freichel et al. 2007	Casadei et al. 2013
Number of animals used	6 males + 6 females	12 males
First locomotor investigation	8 month-old	4 month-old
Test frequency	Every week	Every 6 weeks
Training	No	Yes (1 day with 4 trials)
Testing day per investigation	1	4
Trial per testing day	3	4
Rotarod speed	0-32 rpm in 4 minutes	4-40 rpm in 7 minutes

In top of the impact of motivation and motor learning on rotarod performance, we also would like to highlight that cardiopulmonary endurance, anxiety or body weight may influence rotarod outcome. Therefore, we confirmed that motor skill learning and body weight were not different between A30P and double transgenic mice, but we could not directly investigate cardiopulmonary performance of our animals.

When using a challenging beam walk approach, an alternative test of motor performance, we detected deficits in both A30P and double transgenic mice. However, it is important to mention that this test was performed in 12 month-old animals, and differences in rotarod performance between A30P and double transgenic mice were no longer present at this age. A surprising finding was that sph1 mice, which exhibited a motor phenotype at 12 months of age in the challenging beam walk, did not present deficits in rotarod at any age.

To better understand these discrepancies, we performed automated gait analysis and observed in A30P mice multiple gait abnormalities such as shorter steps and higher cadence, which are possibly reflecting rigidity. We also observed in sph1 and in double transgenic mice a conceptually different phenotype than A30P animals consisting of an increased stand and abnormal walking pattern, which may reflect a coordination impairment or a muscular weakness.

It is unlikely that the gait abnormalities found in sph1 and double transgenic animals, using challenging beam walk test or Catwalk, affected rotarod performance. Thus, it is unclear if the late-onset phenotype found on the rotarod in double transgenic mice truly reflects a synucleinopathy or a sph1-mediated pathology.

4.2 Mice overexpressing synphilin-1 or alpha-synuclein did not display abnormal anxiety behavior

The investigation of motor ability in rodents is a sophisticated task: abnormal motor performance may arise from a combination of complex traits (such as psychiatric abnormalities or learning deficits), which may partially imitate the consequences of balancing or coordination impairment resulting from neurodegeneration [reviewed in (Bailey et al. 2006; Crawley 2008)].

Thus, to exclude possible artifacts in our study, a complete phenotyping was performed. In a first approach, we tested anxiety in our transgenic animals using an open field test and detected a decreased locomotor activity in all transgenic lines without observing an abnormal number of visits or time spent to explore the center of the field. This suggests that the motor deficits observed in transgenic mice in the aforementioned tests might have resulted in a reduced exploratory activity which was not stress-related. This could have been confirmed using multiple component analysis of motor deficits and anxiety index.

Literature reviewing open field tests in mice overexpressing a-syn identifies hyperactivity in young transgenic animals as a common readout which contrasts extremely with a progressive motor phenotype observed at older ages. Interpretation of open field behavior becomes therefore complex, as each model is characterized by a specific age of motor phenotype onset, as well as a specific character of early hyperactivity, and a specific pathology progression. Because of their strong influence on mice's behavior, all these parameters can possibly lead to contradictory results. Accordingly, contradictory results were found for mice overexpressing a-syn. For example, no anxiety impairment was reported for transgenic mouse models overexpressing human Y39C mutated a-syn or murine a-syn under the Thy-1 promoter (Zhou et al. 2008; Rieker et al. 2011), but increased anxiety was described for mice overexpressing human or human A53T mutated a-syn (Lam et al. 2011; Rothman et al. 2013).

| Discussion

In this context, the presence of motor impairments in transgenic animals may also limit the total distance traveled by animals, thus resulting in a reduction of time spent in the center of the apparatus and imitating a possible anxiety-like behavior in old transgenic animals. Despite this potential source of artifacts, we did not observe a reduced time spent in the center of the open field, confirming that the reduced activity is not a consequence of increased anxiety leading to a lower activity, but is more a direct consequence of a motor impairment. Therefore open field data suggest that deficits observed in several tests of motor function (i.e. rotarod, challenging beam walk and gait analysis) did not result from anxiety-like behavior.

Obviously, the confirmation of these results using anxiety tests less dependent on motor skills would have been a better choice. Many solutions using stimulus extinction and shock sensitivity would have been possible [such as the Vogel conflict test (Vogel et al. 1971)]. Nowadays, less stressful protocols based on animal behavior within automated cages and stimulus extinction based on air-puff were shown to be more robust and less stressful for mice (Marsicano et al. 2002).

4.3 Coexpression of synphilin-1 improved home-cage activity reduction observed in mice overexpressing alpha-synuclein

We then investigated the relevance of improved motor ability observed in A30P mice overexpressing sph1 by tracking different activity patterns such as acclimatization or global activity in a home-cage-like environment. Under these conditions, we observed in 18 month-old A30P mice a reduced activity during both acclimatization and the dark phase on the third day of observation (period in which mice were most acclimatized to the system in our experiment). Despite similarly reduced activity observed during the acclimatization phase, sph1 and double transgenic mice did not show reduced activity after acclimatization. These data might suggest that the motor deficit observed earlier led to a reduced acute activity of all transgenic mice. Moreover, the milder pathology in sph1 mice, as well as the delayed motor deficit in double transgenic mice, did not reduce the baseline home-cage activity suggesting a protective effect of sph1 on motor functions.

These conclusions are supported by several studies performed in our institute, in which mice that presented motor phenotypes in rotarod and/or in beam walk tests also presented a reduced of home-cage activity (Portal et al. 2013; Hübener et al. 2012). It is interesting to note that in the original description of the A30P mouse pathology (Freichel et al. 2007), an increased home-cage activity was measured in A30P mice when investigating 8 or 12 month-old mice for 2 hours. As described previously for the anxiety test, these data cannot be directly compared to our experiment in which older mice (18 month-old) were examined. It is possible that hyperactivity in 8 or 12 month-old mice were masked by motor pathology.

When interpreting these results, it is also important to consider that automated behavioral testing systems are conceptualized and reported to be similar to home-cages (Tecott & Nestler 2004; de Visser et al. 2006). However, considerable differences between these systems and typical home-cage environments have been noted, and suggested to induce stress in animals (Clemens et al. 2013).

In this context, we suggest that the decreased activity observed during the acclimatization period is a consequence of an advanced motor phenotype and does not result from a difference response to stress. To gain insight in the origin of the decreased activity observed in light phases, it would have been interesting to investigate circadian rhythm, and more specifically sleep/wake cycle. As sleep disturbances are frequent nonmotor symptoms occurring in PD patients [reviewed in (Lyons & Pahwa 2011)], the potential impact of a-syn on rest/sleep time periods could have been investigate by measuring inactivity cycles or by performing electroencephalography.

4.4 Coexpression of synphilin-1 improved olfactory deficits observed in mice overexpressing alpha-synuclein

Among non-motor symptoms, impaired olfaction is frequently observed in patients with PD (Ward et al. 1983; Doty et al. 1989; Berendse et al. 2001; Parrao et al. 2012). Accordingly, olfactory deficits were also reported in mice overexpressing the human a-syn under the Thy-1 promoter (Fleming et al. 2008). We found in 18 month-old A30P mice a smell deficit illustrated by an abnormal lack of rat smell avoidance which was not observed in double transgenic mice. The presence of olfactory deficits in mice overexpressing the human A30P mutated a-syn under the Thy-1 promoter is also confirmed by a recent article, in which the authors describe an abnormal integration of adult born neurons in the olfactory bulb of transgenic mice (Neuner et al. 2014).

It is important to note that abnormal anxiety or exploratory behavior may have a major impact on this protocol. However, this hypothesis could be refuted as we did not observe an anxiety-related phenotype of the transgenic lines in novel environment as suggested by the open field test.

This experiment again is suggesting a general reduction of neuropathology in A30P mice coexpressing sph1, even in regions with less remarkable aggregation such as olfactory bulb. However, it would be important to confirm these results in other brain region less prone to degeneration with aging.

4.5 Influence of synphilin-1 and alpha-synuclein on spatial memory

With this objective, we also checked for possible cognitive deficits in A30P mice, reported originally in (Freichel et al. 2007) using a Morris water maze to investigate spatial learning. After training the mice for two consecutive days, we observed that they did not learn properly the position of the platform. This was reflected by a low slope during the spatial learning (which consists of putting animals at a pseudo-random position into the water tank and letting them find the platform) and suggesting that mice were not able to reach the platform in a distance as small as during the training using cued platform. Furthermore, mice did not remember the position of the platform in the water maze, resulting in a random strategy to find the escape.

In this context, it would be incorrect to compare spatial learning between transgenic and wildtype animals. We suggest that this behavior may result from a too short training, and/or insufficient spatial cues in the room. Therefore, it would have helped to validate the absence of spatial preferences in the room and increase the learning period.

Perspective

1)   Confirmation of phenotype using synphilin-1 knock-out mice to confirm its function

To confirm the potential of molecular mechanisms induced by human synphilin-1 overexpression in transgenic mice overexpressing human A30P mutated a-syn protein, it is mandatory to show that the transgene introduced to modulate synucleinopathy was fully functional. This statement could be difficult, or even impossible, when studying proteins with unknown role or function.

In this particular case, confirmation of the transgene activity/function could be avoided by analyzing the effect of removing the gene from an animal (knock-out).

2)   Investigation of aggresome function and mechanisms in order to reduce synucleinopathy

To identify mechanisms leading to aggresome formation and degradation, we suggest to use a cell model. Using proteasome inhibitor to induce protein aggregation and formation of aggresomes, it would be possible to study proteins reported to play a potential role in aggresome formation such as hdac6 or gamma-tubulin. But also drugs which may increase protein transport or inhibit K63 degradation to promote aggresome formation and degradation of a-syn, could be studied.

Conclusion

Altogether, this study shows that coexpression of sph1 in a mouse model overexpressing a-syn reduced the accumulation of soluble forms of a-syn, promoted the formation of aggresome-like structures without reducing detergent-insoluble a-syn. This resulted in a reduced neuropathology and behavioral improvements in mice overexpressing a-syn. Therefore, we suggest that the recruitment of a-syn into aggresome-like structures may lead to its degradation by inducing autophagy, slowing synucleinopathy development in the mouse. Moreover, our data clearly demonstrate that aggregates observed in our double transgenic model do not share insolubility and content in a-filament, suggesting that sph1 does not increase the load of a-syn aggregates, but changes a-syn inclusion structures. All in all, we suggest that mechanisms induced by the overexpression of sph1 *in vivo* represent specific and valuable strategies to treat synucleinopathy without disturbing normal cell function.

Abbreviation

6-OHDA: 6-hydroxydopamine

aa: amino acid

a-syn: alpha-synuclein

ADP: adenosine diphosphate

AGERA: agarose gel electrophoresis for resolving aggregates

ALP: autophagy-lysosome pathway

ANK: ankyrin

atg: autophagy-related gene

ATP: adenosine triphosphate

BAC: bacterial artificial chromosome

CK: casein kinases 1 and 2

CMA: chaperone-mediated autophagy

Cp: crossing point

DAPI: 4',6-diamidino-2-phenylindole

DAT: dopamine active transporter (also termed SLC6A3)

Dpi: dot per inch

DNA: deoxyribonucleic acid

EDTA: ethylenediaminetetraacetic acid

ER: Endoplasmic reticulum

GABA: gamma-aminobutyric acid

GTP: guanosine triphosphate

HDAC6: histone deacetylase 6

HSP: heat shock protein

Hu: human

IHC: immunohistochemistry

IPD: idiopathic Parkinson's disease

IP: intraperitonial

KO: knock-out

LB: Lewy body

LN: Lewy neurit

LAMP-2A: lysosome-associated membrane protein type 2A

LRRK2: leucine-rich repeat kinase 2

MMP: matrix metalloproteinases

MPP+: 1-methyl-4-phenylpyridinium

MPTP: 1-methyl-4-phenyl-1,2,3,6-tetrahydropyridine

Ms: mouse

MTOC: microtubule organizing center

NAC: non-amyloid β component

NACP: non-amyloid β component precursor

PAGE: polyacrylamide gel electrophoresis

PBS: phosphate-buffered saline

PCR: polymerase chain reation

PD: Parkinson's disease

PDGFβ: platelet-derived growth factor β

PFA: paraformaldehyde

PINK1: PTEN-induced putative kinase 1

PK: proteinase K

PrP: prion protein

PTEN: phosphatase and tensin

PVDF: polyvinylidene fluoride

RIPA: radioimmunoprecipitation assay buffer

ROS: reactive oxygen species

RPM: revolutions per minute

RNA: ribonucleic acid

SDS: sodium dodecyl sulfate

SEM: standard error on the mean

SNCA: synuclein alpha gene

SNCAIP: synuclein alpha interactor partner gene

SNP: single-nucleotide polymorphism

| Abbreviation

SNpc: substantia nigra pars compacta

Sph1: synphilin-1

Tg: transgenic

TH: tyrosine hydroxylase

UPS: ubiquitin-proteasome system

Bibliography

Abeliovich, A. et al., 2000. Mice lacking alpha-synuclein display functional deficits in the nigrostriatal dopamine system. *Neuron*, 25(1), pp.239–52.

Ahmed, N., 2005. Advanced glycation endproducts--role in pathology of diabetic complications. *Diabetes research and clinical practice*, 67(1), pp.3–21.

Ahn, B.-H. et al., 2002. alpha-Synuclein interacts with phospholipase D isozymes and inhibits pervanadate-induced phospholipase D activation in human embryonic kidney-293 cells. *The Journal of biological chemistry*, 277(14), pp.12334–42.

Alegre-Abarrategui, J. et al., 2008. LRRK2 is a component of granular alpha-synuclein pathology in the brainstem of Parkinson's disease. *Neuropathology and applied neurobiology*, 34(3), pp.272–83.

Alegre-Abarrategui, J. et al., 2009. LRRK2 regulates autophagic activity and localizes to specific membrane microdomains in a novel human genomic reporter cellular model. *Human molecular genetics*, 18(21), pp.4022–34.

Ali, M.H. & Imperiali, B., 2005. Protein oligomerization: how and why. *Bioorganic & medicinal chemistry*, 13(17), pp.5013–20.

Alim, M.A. et al., 2002. Tubulin seeds alpha-synuclein fibril formation. *The Journal of biological chemistry*, 277(3), pp.2112–7.

Alvarez-Castelao, B. & Castaño, J.G., 2011. Synphilin-1 inhibits alpha-synuclein degradation by the proteasome. *Cellular and molecular life sciences : CMLS*, 68(15), pp.2643–54.

Alvarez-Erviti, L. et al., 2010. Chaperone-mediated autophagy markers in Parkinson disease brains. *Archives of neurology*, 67(12), pp.1464–72.

Anderson, J.P. et al., 2006. Phosphorylation of Ser-129 is the dominant pathological modification of alpha-synuclein in familial and sporadic Lewy body disease. *The Journal of biological chemistry*, 281(40), pp.29739–52.

Anderson, P.C. & Daggett, V., 2008. Molecular basis for the structural instability of human DJ-1 induced by the L166P mutation associated with Parkinson's disease. *Biochemistry*, 47(36), pp.9380–93.

Andres-Mateos, E. et al., 2009. Unexpected lack of hypersensitivity in LRRK2 knock-out mice to MPTP (1-methyl-4-phenyl-1,2,3,6-tetrahydropyridine). *The Journal of neuroscience : the official journal of the Society for Neuroscience*, 29(50), pp.15846–50.

Andreux, P. a et al., 2013. Pharmacological approaches to restore mitochondrial function. *Nature reviews. Drug discovery*, 12(6), pp.465–83.

Anfinsen, C.B., 1973. Principles that govern the folding of protein chains. *Science (New York, N.Y.)*, 181(4096), pp.223–30.

| Bibliography

Anglade, P. et al., 1997. Apoptosis and autophagy in nigral neurons of patients with Parkinson's disease. *Histology and histopathology*, 12(1), pp.25–31.

Apetri, M.M. et al., 2006. Secondary structure of alpha-synuclein oligomers: characterization by raman and atomic force microscopy. *Journal of molecular biology*, 355(1), pp.63–71.

Appel-Cresswell, S. et al., 2013. Alpha-synuclein p.H50Q, a novel pathogenic mutation for Parkinson's disease. *Movement disorders : official journal of the Movement Disorder Society*, 28(6), pp.811–3.

Ara, J. et al., 1998. Inactivation of tyrosine hydroxylase by nitration following exposure to peroxynitrite and 1-methyl-4-phenyl-1,2,3,6-tetrahydropyridine (MPTP). *Proceedings of the National Academy of Sciences of the United States of America*, 95(13), pp.7659–63.

Archer, J., 1973. Tests for emotionality in rats and mice: a review. *Animal behaviour*, 21(2), pp.205–35.

Avraham, E. et al., 2005. Glycogen synthase kinase 3beta modulates synphilin-1 ubiquitylation and cellular inclusion formation by SIAH: implications for proteasomal function and Lewy body formation. *The Journal of biological chemistry*, 280(52), pp.42877–86.

Azeredo da Silveira, S. et al., 2009. Phosphorylation does not prompt, nor prevent, the formation of alpha-synuclein toxic species in a rat model of Parkinson's disease. *Human molecular genetics*, 18(5), pp.872–87.

Badiola, N. et al., 2011. Tau enhances α-synuclein aggregation and toxicity in cellular models of synucleinopathy. *PloS one*, 6(10), p.e26609.

Bailey, K.R., Rustay, N.R. & Crawley, J.N., 2006. Behavioral phenotyping of transgenic and knockout mice: practical concerns and potential pitfalls. *ILAR journal / National Research Council, Institute of Laboratory Animal Resources*, 47(2), pp.124–31.

Balch, W.E. et al., 2008. Adapting proteostasis for disease intervention. *Science (New York, N.Y.)*, 319(5865), pp.916–9.

Barbour, R. et al., 2008. Red blood cells are the major source of alpha-synuclein in blood. *Neuro-degenerative diseases*, 5(2), pp.55–9.

Baybutt, H. & Manson, J., 1997. Characterisation of two promoters for prion protein (PrP) gene expression in neuronal cells. *Gene*, 184(1), pp.125–31.

Bedford, L. et al., 2008. Depletion of 26S proteasomes in mouse brain neurons causes neurodegeneration and Lewy-like inclusions resembling human pale bodies. *The Journal of neuroscience : the official journal of the Society for Neuroscience*, 28(33), pp.8189–98.

Bender, A. et al., 2013. TOM40 mediates mitochondrial dysfunction induced by α-synuclein accumulation in Parkinson's disease. *PloS one*, 8(4), p.e62277.

Bendor, J.T., Logan, T.P. & Edwards, R.H., 2013. The Function of α-Synuclein. *Neuron*, 79(6), pp.1044–1066.

Bennett, M.C. et al., 1999. Degradation of alpha-synuclein by proteasome. *The Journal of*

biological chemistry, 274(48), pp.33855–8.

Bereczki, D., 2010. The description of all four cardinal signs of Parkinson's disease in a Hungarian medical text published in 1690. *Parkinsonism & related disorders*, 16(4), pp.290–3.

Berendse, H.W. et al., 2001. Subclinical dopaminergic dysfunction in asymptomatic Parkinson's disease patients' relatives with a decreased sense of smell. *Annals of neurology*, 50(1), pp.34–41.

Bergman, H. & Deuschl, G., 2002. Pathophysiology of Parkinson's disease: from clinical neurology to basic neuroscience and back. *Movement disorders : official journal of the Movement Disorder Society*, 17 Suppl 3, pp.S28–40.

Bernadó, P. et al., 2005. Defining long-range order and local disorder in native alpha-synuclein using residual dipolar couplings. *Journal of the American Chemical Society*, 127(51), pp.17968–9.

Bertoncini, C.W. et al., 2005. Familial mutants of alpha-synuclein with increased neurotoxicity have a destabilized conformation. *The Journal of biological chemistry*, 280(35), pp.30649–52.

Betarbet, R. et al., 2000. Chronic systemic pesticide exposure reproduces features of Parkinson's disease. *Nature neuroscience*, 3(12), pp.1301–6.

Beyer, K., 2006. Alpha-synuclein structure, posttranslational modification and alternative splicing as aggregation enhancers. *Acta neuropathologica*, 112(3), pp.237–51.

Bezard, E. et al., 2013. Animal models of Parkinson's disease: limits and relevance to neuroprotection studies. *Movement disorders : official journal of the Movement Disorder Society*, 28(1), pp.61–70.

Bezard, E. & Przedborski, S., 2011. A tale on animal models of Parkinson's disease. *Movement disorders : official journal of the Movement Disorder Society*, 26(6), pp.993–1002.

Biancalana, M. & Koide, S., 2010. Molecular mechanism of Thioflavin-T binding to amyloid fibrils. *Biochimica et biophysica acta*, 1804(7), pp.1405–12.

Lo Bianco, C. et al., 2004. Lentiviral vector delivery of parkin prevents dopaminergic degeneration in an alpha-synuclein rat model of Parkinson's disease. *Proceedings of the National Academy of Sciences of the United States of America*, 101(50), pp.17510–5.

Biere, A.L. et al., 2000. Parkinson's disease-associated alpha-synuclein is more fibrillogenic than beta- and gamma-synuclein and cannot cross-seed its homologs. *The Journal of biological chemistry*, 275(44), pp.34574–9.

Biskup, S. et al., 2006. Localization of LRRK2 to membranous and vesicular structures in mammalian brain. *Annals of neurology*, 60(5), pp.557–69.

Biskup, S. & West, A.B., 2009. Zeroing in on LRRK2-linked pathogenic mechanisms in Parkinson's disease. *Biochimica et biophysica acta*, 1792(7), pp.625–33.

| Bibliography

Bjørkøy, G. et al., 2009. Monitoring autophagic degradation of p62/SQSTM1. *Methods in enzymology*, 452, pp.181–97.

Blandini, F. & Armentero, M.-T., 2012. Animal models of Parkinson's disease. *The FEBS journal*, 279(7), pp.1156–66.

Blazer, L.L. & Neubig, R.R., 2009. Small molecule protein-protein interaction inhibitors as CNS therapeutic agents: current progress and future hurdles. *Neuropsychopharmacology: official publication of the American College of Neuropsychopharmacology*, 34(1), pp.126–41.

Blesa, J. et al., 2012. Classic and new animal models of Parkinson's disease. *Journal of biomedicine & biotechnology*, 2012, p.845618.

Bodles, A.M. et al., 2001. Identification of the region of non-Abeta component (NAC) of Alzheimer's disease amyloid responsible for its aggregation and toxicity. *Journal of neurochemistry*, 78(2), pp.384–95.

Bonifati, V. et al., 2005. Early-onset parkinsonism associated with PINK1 mutations: frequency, genotypes, and phenotypes. *Neurology*, 65(1), pp.87–95.

Bonini, N.M. & Giasson, B.I., 2005. Snaring the function of alpha-synuclein. *Cell*, 123(3), pp.359–61.

Bosco, D.A. et al., 2006. Elevated levels of oxidized cholesterol metabolites in Lewy body disease brains accelerate alpha-synuclein fibrilization. *Nature chemical biology*, 2(5), pp.249–53.

Bové, J. et al., 2006. Proteasome inhibition and Parkinson's disease modeling. *Annals of neurology*, 60(2), pp.260–4.

Braak, E. & Braak, H., 1999. Silver staining method for demonstrating Lewy bodies in Parkinson's disease and argyrophilic oligodendrocytes in multiple system atrophy. *Journal of neuroscience methods*, 87(1), pp.111–5.

Braak, H. et al., 1999. Extensive axonal Lewy neurites in Parkinson's disease: a novel pathological feature revealed by alpha-synuclein immunocytochemistry. *Neuroscience letters*, 265(1), pp.67–9.

Braak, H. et al., 2004. Stages in the development of Parkinson's disease-related pathology. *Cell and tissue research*, 318(1), pp.121–34.

Braak, H. et al., 2003. Staging of brain pathology related to sporadic Parkinson's disease. *Neurobiology of Aging*, 24(2), pp.197–211.

Braithwaite, S.P., Stock, J.B. & Mouradian, M.M., 2012. α-Synuclein phosphorylation as a therapeutic target in Parkinson's disease. *Reviews in the neurosciences*, 23(2), pp.191–8.

Brand, M.D., 2000. Uncoupling to survive? The role of mitochondrial inefficiency in ageing. *Experimental gerontology*, 35(6-7), pp.811–20.

Bucciantini, M. et al., 2002. Inherent toxicity of aggregates implies a common mechanism for

protein misfolding diseases. *Nature*, 416(6880), pp.507–11.

Buchman, V.L. et al., 1998. Persyn, a member of the synuclein family, has a distinct pattern of expression in the developing nervous system. *The Journal of neuroscience : the official journal of the Society for Neuroscience*, 18(22), pp.9335–41.

Burke, R.E., Dauer, W.T. & Vonsattel, J.P.G., 2008. A critical evaluation of the Braak staging scheme for Parkinson's disease. *Annals of neurology*, 64(5), pp.485–91.

Burnett, B.G. & Pittman, R.N., 2005. The polyglutamine neurodegenerative protein ataxin 3 regulates aggresome formation. *Proceedings of the National Academy of Sciences of the United States of America*, 102(12), pp.4330–5.

Burré, J. et al., 2010. Alpha-synuclein promotes SNARE-complex assembly in vivo and in vitro. *Science (New York, N.Y.)*, 329(5999), pp.1663–7.

Burré, J., Sharma, M. & Südhof, T.C., 2012. Systematic mutagenesis of α-synuclein reveals distinct sequence requirements for physiological and pathological activities. *The Journal of neuroscience : the official journal of the Society for Neuroscience*, 32(43), pp.15227–42.

Büttner, S. et al., 2010. Synphilin-1 enhances α-synuclein aggregation in yeast and contributes to cellular stress and cell death in a Sir2-dependent manner. *PloS one*, 5(10), p.e13700.

Cabin, D.E. et al., 2002. Synaptic vesicle depletion correlates with attenuated synaptic responses to prolonged repetitive stimulation in mice lacking alpha-synuclein. *The Journal of neuroscience : the official journal of the Society for Neuroscience*, 22(20), pp.8797–807.

Cadet, J.L. & Brannock, C., 1998. Free radicals and the pathobiology of brain dopamine systems. *Neurochemistry international*, 32(2), pp.117–31.

Campbell, B.C. et al., 2001. The solubility of alpha-synuclein in multiple system atrophy differs from that of dementia with Lewy bodies and Parkinson's disease. *Journal of neurochemistry*, 76(1), pp.87–96.

Campion, D. et al., 1995. The NACP/synuclein gene: chromosomal assignment and screening for alterations in Alzheimer disease. *Genomics*, 26(2), pp.254–7.

Canet-Avilés, R.M. et al., 2004. The Parkinson's disease protein DJ-1 is neuroprotective due to cysteine-sulfinic acid-driven mitochondrial localization. *Proceedings of the National Academy of Sciences of the United States of America*, 101(24), pp.9103–8.

Cannon, J.R. et al., 2009. A highly reproducible rotenone model of Parkinson's disease. *Neurobiology of disease*, 34(2), pp.279–90.

Carlson, G.A. et al., 1997. Genetic modification of the phenotypes produced by amyloid precursor protein overexpression in transgenic mice. *Human molecular genetics*, 6(11), pp.1951–9.

Castagnet, P.I. et al., 2005. Fatty acid incorporation is decreased in astrocytes cultured from

alpha-synuclein gene-ablated mice. *Journal of neurochemistry*, 94(3), pp.839–49.

Castellani, R. et al., 1996. Glycoxidation and oxidative stress in Parkinson disease and diffuse Lewy body disease. *Brain research*, 737(1-2), pp.195–200.

Castellani, R.J. et al., 2000. Sequestration of iron by Lewy bodies in Parkinson's disease. *Acta neuropathologica*, 100(2), pp.111–4.

Chance, B., Sies, H. & Boveris, A., 1979. Hydroperoxide metabolism in mammalian organs. *Physiological reviews*, 59(3), pp.527–605.

Chandra, S. et al., 2005. Alpha-synuclein cooperates with CSPalpha in preventing neurodegeneration. *Cell*, 123(3), pp.383–96.

Chandra, S. et al., 2004. Double-knockout mice for alpha- and beta-synucleins: effect on synaptic functions. *Proceedings of the National Academy of Sciences of the United States of America*, 101(41), pp.14966–71.

Charcot, J.M., 1877. Lecture V: On Paralysis Agitans. In *Lect. Dis. Nerv. Syst. Deliv. La Salpêtrière Transl. by Georg. Seigerson*. The New Sydenham Society, pp. 129–156.

Chaudhuri, K.R., Healy, D.G. & Schapira, A.H. V, 2006. Non-motor symptoms of Parkinson's disease: diagnosis and management. *Lancet neurology*, 5(3), pp.235–45.

Chaudhuri, K.R. & Odin, P., 2010. The challenge of non-motor symptoms in Parkinson's disease. *Progress in brain research*, 184, pp.325–41.

Chen, H. & Chan, D.C., 2009. Mitochondrial dynamics--fusion, fission, movement, and mitophagy--in neurodegenerative diseases. *Human molecular genetics*, 18(R2), pp.R169–76.

Chen, L. et al., 2009. Tyrosine and serine phosphorylation of alpha-synuclein have opposing effects on neurotoxicity and soluble oligomer formation. *The Journal of clinical investigation*, 119(11), pp.3257–65.

Chen, L. & Feany, M.B., 2005. Alpha-synuclein phosphorylation controls neurotoxicity and inclusion formation in a Drosophila model of Parkinson disease. *Nature neuroscience*, 8(5), pp.657–63.

Chen, X. et al., 1995. The human NACP/alpha-synuclein gene: chromosome assignment to 4q21.3-q22 and TaqI RFLP analysis. *Genomics*, 26(2), pp.425–7.

Cheng, F., Vivacqua, G. & Yu, S., 2011. The role of α-synuclein in neurotransmission and synaptic plasticity. *Journal of chemical neuroanatomy*, 42(4), pp.242–8.

Cheng, H.-C., Ulane, C.M. & Burke, R.E., 2010. Clinical progression in Parkinson disease and the neurobiology of axons. *Annals of neurology*, 67(6), pp.715–25.

Cherra, S.J. & Chu, C.T., 2008. Autophagy in neuroprotection and neurodegeneration: A question of balance. *Future neurology*, 3(3), pp.309–323.

Chesselet, M.-F. et al., 2012. A progressive mouse model of Parkinson's disease: the Thy1-aSyn ("Line 61") mice. *Neurotherapeutics : the journal of the American Society for*

Experimental NeuroTherapeutics, 9(2), pp.297–314.

Chiba-Falek, O. et al., 2005. Regulation of alpha-synuclein expression by poly (ADP ribose) polymerase-1 (PARP-1) binding to the NACP-Rep1 polymorphic site upstream of the SNCA gene. *American journal of human genetics*, 76(3), pp.478–92.

Chin, L.-S., Olzmann, J.A. & Li, L., 2010. Parkin-mediated ubiquitin signalling in aggresome formation and autophagy. *Biochemical Society transactions*, 38(Pt 1), pp.144–9.

Choe, S.E. et al., 2005. Preferred analysis methods for Affymetrix GeneChips revealed by a wholly defined control dataset. *Genome biology*, 6(2), p.R16.

Chothia, C. & Janin, J., 1975. Principles of protein-protein recognition. *Nature*, 256(5520), pp.705–8.

Chu, C.T. et al., 2000. Ubiquitin immunochemistry as a diagnostic aid for community pathologists evaluating patients who have dementia. *Modern pathology : an official journal of the United States and Canadian Academy of Pathology, Inc*, 13(4), pp.420–6.

Chu, Y. et al., 2009. Alterations in lysosomal and proteasomal markers in Parkinson's disease: relationship to alpha-synuclein inclusions. *Neurobiology of disease*, 35(3), pp.385–98.

Chua, C.E.L. & Tang, B.L., 2011. Rabs, SNAREs and α-synuclein--membrane trafficking defects in synucleinopathies. *Brain research reviews*, 67(1-2), pp.268–81.

Chung, K.K. et al., 2001. Parkin ubiquitinates the alpha-synuclein-interacting protein, synphilin-1: implications for Lewy-body formation in Parkinson disease. *Nature medicine*, 7(10), pp.1144–50.

Ciechanover, A., 2005. Intracellular protein degradation: from a vague idea thru the lysosome and the ubiquitin-proteasome system and onto human diseases and drug targeting. *Cell death and differentiation*, 12(9), pp.1178–90.

Ciechanover, A. & Schwartz, A.L., 1998. The ubiquitin-proteasome pathway: the complexity and myriad functions of proteins death. *Proceedings of the National Academy of Sciences of the United States of America*, 95(6), pp.2727–30.

Clayton, D.F. & George, J.M., 1998. The synucleins: a family of proteins involved in synaptic function, plasticity, neurodegeneration and disease. *Trends in neurosciences*, 21(6), pp.249–54.

Clemens, L.E. et al., 2013. A behavioral comparison of the common laboratory rat strains Lister Hooded, Lewis, Fischer 344 and Wistar in an automated homecage system. *Genes, brain, and behavior*, pp.1–17.

Clough, R.L. & Stefanis, L., 2007. A novel pathway for transcriptional regulation of alpha-synuclein. *FASEB journal : official publication of the Federation of American Societies for Experimental Biology*, 21(2), pp.596–607.

Von Coelln, R. et al., 2006. Inclusion body formation and neurodegeneration are parkin independent in a mouse model of alpha-synucleinopathy. *The Journal of neuroscience : the official journal of the Society for Neuroscience*, 26(14), pp.3685–96.

| Bibliography

Coleman, D.L. & Hummel, K.P., 1973. The influence of genetic background on the expression of the obese (Ob) gene in the mouse. *Diabetologia*, 9(4), pp.287–93.

Colla, E. et al., 2012. Accumulation of Toxic -Synuclein Oligomer within Endoplasmic Reticulum Occurs in -Synucleinopathy In Vivo. *Journal of Neuroscience*, 32(10), pp.3301–3305.

Collins, L.M. et al., 2012. Contributions of central and systemic inflammation to the pathophysiology of Parkinson's disease. *Neuropharmacology*, 62(7), pp.2154–68.

Comellas, G. et al., 2012. Structural intermediates during α-synuclein fibrillogenesis on phospholipid vesicles. *Journal of the American Chemical Society*, 134(11), pp.5090–9.

Conway, K.A. et al., 2000. Accelerated oligomerization by Parkinson's disease linked alpha-synuclein mutants. *Annals of the New York Academy of Sciences*, 920, pp.42–5.

Conway, K.A. et al., 2001. Kinetic stabilization of the alpha-synuclein protofibril by a dopamine-alpha-synuclein adduct. *Science (New York, N.Y.)*, 294(5545), pp.1346–9.

Conway, K.A., Harper, J.D. & Lansbury, P.T., 1998. Accelerated in vitro fibril formation by a mutant alpha-synuclein linked to early-onset Parkinson disease. *Nature medicine*, 4(11), pp.1318–20.

Cook, C., Stetler, C. & Petrucelli, L., 2012. Disruption of protein quality control in Parkinson's disease. *Cold Spring Harbor perspectives in medicine*, 2(5), p.a009423.

Cookson, M.R., 2010. The role of leucine-rich repeat kinase 2 (LRRK2) in Parkinson's disease. *Nature reviews. Neuroscience*, 11(12), pp.791–7.

Cooper, A.A. et al., 2006. Alpha-synuclein blocks ER-Golgi traffic and Rab1 rescues neuron loss in Parkinson's models. *Science (New York, N.Y.)*, 313(5785), pp.324–8.

Cooper-Knock, J. et al., 2012. Gene expression profiling in human neurodegenerative disease. *Nature reviews. Neurology*, 8(9), pp.518–30.

Corrochano, S. et al., 2012. α-Synuclein levels modulate Huntington's disease in mice. *Human molecular genetics*, 21(3), pp.485–94.

Corti, O. & Brice, A., 2013. Mitochondrial quality control turns out to be the principal suspect in parkin and PINK1-related autosomal recessive Parkinson's disease. *Current opinion in neurobiology*, 23(1), pp.100–8.

Corti, O., Lesage, S. & Brice, A., 2011. What genetics tells us about the causes and mechanisms of Parkinson's disease. *Physiological reviews*, 91(4), pp.1161–218.

Crawley, J.N., 2008. Behavioral phenotyping strategies for mutant mice. *Neuron*, 57(6), pp.809–18.

Cremades, N. et al., 2012. Direct observation of the interconversion of normal and toxic forms of α-synuclein. *Cell*, 149(5), pp.1048–59.

Crews, L. et al., 2010. Selective molecular alterations in the autophagy pathway in patients with Lewy body disease and in models of alpha-synucleinopathy. *PloS one*, 5(2),

p.e9313.

Crowther, R.A. et al., 1998. Synthetic filaments assembled from C-terminally truncated alpha-synuclein. *FEBS letters*, 436(3), pp.309–12.

Cuervo, A.M. et al., 1995. Activation of a selective pathway of lysosomal proteolysis in rat liver by prolonged starvation. *The American journal of physiology*, 269(5 Pt 1), pp.C1200–8.

Cuervo, A.M. et al., 2004. Impaired degradation of mutant alpha-synuclein by chaperone-mediated autophagy. *Science (New York, N.Y.)*, 305(5688), pp.1292–5.

Cuervo, A.M. & Dice, J.F., 2000. Age-related decline in chaperone-mediated autophagy. *The Journal of biological chemistry*, 275(40), pp.31505–13.

Cui, M. et al., 2009. The organic cation transporter-3 is a pivotal modulator of neurodegeneration in the nigrostriatal dopaminergic pathway. *Proceedings of the National Academy of Sciences of the United States of America*, 106(19), pp.8043–8.

Cullen, K.M. et al., 1996. Improved selectivity and sensitivity in the visualization of neurofibrillary tangles, plaques and neuropil threads. *Neurodegeneration : a journal for neurodegenerative disorders, neuroprotection, and neuroregeneration*, 5(2), pp.177–87.

Culvenor, J.G. et al., 1999. Non-Abeta component of Alzheimer's disease amyloid (NAC) revisited. NAC and alpha-synuclein are not associated with Abeta amyloid. *The American journal of pathology*, 155(4), pp.1173–81.

D'Costa, D.F. et al., 1995. The levodopa test in Parkinson's disease. *Age and ageing*, 24(3), pp.210–2.

Daher, J.P.L. et al., 2009. Conditional transgenic mice expressing C-terminally truncated human alpha-synuclein (alphaSyn119) exhibit reduced striatal dopamine without loss of nigrostriatal pathway dopaminergic neurons. *Molecular neurodegeneration*, 4, p.34.

Daher, J.P.L. et al., 2012. Neurodegenerative phenotypes in an A53T α-synuclein transgenic mouse model are independent of LRRK2. *Human molecular genetics*, 21(11), pp.2420–31.

Dalfó, E., Gómez-Isla, T., et al., 2004. Abnormal alpha-synuclein interactions with Rab proteins in alpha-synuclein A30P transgenic mice. *Journal of neuropathology and experimental neurology*, 63(4), pp.302–13.

Dalfó, E., Barrachina, M., et al., 2004. Abnormal alpha-synuclein interactions with rab3a and rabphilin in diffuse Lewy body disease. *Neurobiology of disease*, 16(1), pp.92–7.

Dalfó, E. et al., 2005. Evidence of oxidative stress in the neocortex in incidental Lewy body disease. *Journal of neuropathology and experimental neurology*, 64(9), pp.816–30.

Damier, P. et al., 1999. The substantia nigra of the human brain. II. Patterns of loss of dopamine-containing neurons in Parkinson's disease. *Brain : a journal of neurology*, 122 (Pt 8, pp.1437–48.

Daniels, M.P., 2012. The role of agrin in synaptic development, plasticity and signaling in the central nervous system. *Neurochemistry international*, 61(6), pp.848–53.

| Bibliography

Danzer, K.M. et al., 2007. Different species of alpha-synuclein oligomers induce calcium influx and seeding. *The Journal of neuroscience : the official journal of the Society for Neuroscience*, 27(34), pp.9220–32.

Dauer, W. et al., 2002. Resistance of alpha -synuclein null mice to the parkinsonian neurotoxin MPTP. *Proceedings of the National Academy of Sciences of the United States of America*, 99(22), pp.14524–9.

Dauer, W. & Przedborski, S., 2003. Parkinson's disease: mechanisms and models. *Neuron*, 39(6), pp.889–909.

Davidson, W.S. et al., 1998. Stabilization of alpha-synuclein secondary structure upon binding to synthetic membranes. *The Journal of biological chemistry*, 273(16), pp.9443–9.

Davis, G.C. et al., 1979. Chronic Parkinsonism secondary to intravenous injection of meperidine analogues. *Psychiatry research*, 1(3), pp.249–54.

Day, B.J. et al., 1999. A mechanism of paraquat toxicity involving nitric oxide synthase. *Proceedings of the National Academy of Sciences of the United States of America*, 96(22), pp.12760–5.

Deas, E., Plun-Favreau, H. & Wood, N.W., 2009. PINK1 function in health and disease. *EMBO molecular medicine*, 1(3), pp.152–65.

Dehay, B. et al., 2010. Pathogenic lysosomal depletion in Parkinson's disease. *The Journal of neuroscience : the official journal of the Society for Neuroscience*, 30(37), pp.12535–44.

Deretic, V., 2010. Autophagy in infection. *Current opinion in cell biology*, 22(2), pp.252–62.

Dev, K., 2003. Part II: α-synuclein and its molecular pathophysiological role in neurodegenerative disease. *Neuropharmacology*, 45(1), pp.14–44.

Devi, L. et al., 2008. Mitochondrial import and accumulation of alpha-synuclein impair complex I in human dopaminergic neuronal cultures and Parkinson disease brain. *The Journal of biological chemistry*, 283(14), pp.9089–100.

Dexter, D.T. et al., 1989. Increased nigral iron content and alterations in other metal ions occurring in brain in Parkinson's disease. *Journal of neurochemistry*, 52(6), pp.1830–6.

Díaz-Hernández, M. et al., 2004. Biochemical, ultrastructural, and reversibility studies on huntingtin filaments isolated from mouse and human brain. *The Journal of neuroscience : the official journal of the Society for Neuroscience*, 24(42), pp.9361–71.

Dickson, D.W. et al., 2010. Evidence in favor of Braak staging of Parkinson's disease. *Movement disorders : official journal of the Movement Disorder Society*, 25 Suppl 1, pp.S78–82.

Dictenberg, J.B. et al., 1998. Pericentrin and gamma-tubulin form a protein complex and are organized into a novel lattice at the centrosome. *The Journal of cell biology*, 141(1), pp.163–74.

Ding, T.T. et al., 2002. Annular alpha-synuclein protofibrils are produced when spherical protofibrils are incubated in solution or bound to brain-derived membranes. *Biochemistry*,

41(32), pp.10209–17.

Dobson, C.M., 2003. Protein folding and misfolding. *Nature*, 426(6968), pp.884–90.

Døskeland, A.P. & Flatmark, T., 2002. Ubiquitination of soluble and membrane-bound tyrosine hydroxylase and degradation of the soluble form. *European journal of biochemistry / FEBS*, 269(5), pp.1561–9.

Doty, R.L. et al., 1989. The olfactory and cognitive deficits of Parkinson's disease: evidence for independence. *Annals of neurology*, 25(2), pp.166–71.

Driver, J.A. et al., 2009. Incidence and remaining lifetime risk of Parkinson disease in advanced age. *Neurology*, 72(5), pp.432–8.

Driver, J.A. et al., 2008. Parkinson disease and risk of mortality: a prospective comorbidity-matched cohort study. *Neurology*, 70(16 Pt 2), pp.1423–30.

Drolet, R.E. et al., 2006. Substrate-mediated enhancement of phosphorylated tyrosine hydroxylase in nigrostriatal dopamine neurons: evidence for a role of alpha-synuclein. *Journal of neurochemistry*, 96(4), pp.950–9.

Dubouloz, F. et al., 2005. The TOR and EGO protein complexes orchestrate microautophagy in yeast. *Molecular cell*, 19(1), pp.15–26.

Duda, J.E. et al., 2000. Widespread nitration of pathological inclusions in neurodegenerative synucleinopathies. *The American journal of pathology*, 157(5), pp.1439–45.

Duffy, P.E. & Tennyson, V.M., 1965. Phase and electron microscopic observations of Lewy bodies and melanin granules in the substantia nigra and locus caeruleus in Parkinson's disease. *Journal of Neuropathology & Experimental Neurology*, 24(3), pp.398–414.

Dufty, B.M. et al., 2007. Calpain-cleavage of alpha-synuclein: connecting proteolytic processing to disease-linked aggregation. *The American journal of pathology*, 170(5), pp.1725–38.

DUNHAM, N.W. & MIYA, T.S., 1957. A note on a simple apparatus for detecting neurological deficit in rats and mice. *Journal of the American Pharmaceutical Association. American Pharmaceutical Association*, 46(3), pp.208–9.

Dyllick-Brenzinger, M. et al., 2010. Reciprocal effects of alpha-synuclein overexpression and proteasome inhibition in neuronal cells and tissue. *Neurotoxicity research*, 17(3), pp.215–27.

Dzamko, N. & Halliday, G.M., 2012. An emerging role for LRRK2 in the immune system. *Biochemical Society transactions*, 40(5), pp.1134–9.

Ebrahimi-Fakhari, D. et al., 2011. Distinct roles in vivo for the ubiquitin-proteasome system and the autophagy-lysosomal pathway in the degradation of α-synuclein. *The Journal of neuroscience : the official journal of the Society for Neuroscience*, 31(41), pp.14508–20.

Ebrahimi-Fakhari, D., Wahlster, L. & McLean, P.J., 2012. Protein degradation pathways in Parkinson's disease: curse or blessing. *Acta neuropathologica*, 124(2), pp.153–72.

| Bibliography

Eisbach, S.E. & Outeiro, T.F., 2013. alpha-Synuclein and intracellular trafficking: impact on the spreading of Parkinson's disease pathology. *Journal of molecular medicine (Berlin, Germany)*.

El-Agnaf, O.M. et al., 1998. Effects of the mutations Ala30 to Pro and Ala53 to Thr on the physical and morphological properties of alpha-synuclein protein implicated in Parkinson's disease. *FEBS letters*, 440(1-2), pp.67–70.

el-Agnaf, O.M.A. & Irvine, G.B., 2002. Aggregation and neurotoxicity of alpha-synuclein and related peptides. *Biochemical Society transactions*, 30(4), pp.559–65.

Eliezer, D. et al., 2001. Conformational properties of alpha-synuclein in its free and lipid-associated states. *Journal of molecular biology*, 307(4), pp.1061–73.

Ellis, C.E. et al., 2001. alpha-synuclein is phosphorylated by members of the Src family of protein-tyrosine kinases. *The Journal of biological chemistry*, 276(6), pp.3879–84.

Engelender, S. et al., 1999. Synphilin-1 associates with alpha-synuclein and promotes the formation of cytosolic inclusions. *Nature genetics*, 22(1), pp.110–4.

Eyal, A. et al., 2006. Synphilin-1A: an aggregation-prone isoform of synphilin-1 that causes neuronal death and is present in aggregates from alpha-synucleinopathy patients. *Proceedings of the National Academy of Sciences of the United States of America*, 103(15), pp.5917–22.

Fagerqvist, T. et al., 2013. Monoclonal antibodies selective for α-synuclein oligomers/protofibrils recognize brain pathology in Lewy body disorders and α-synuclein transgenic mice with the disease-causing A30P mutation. *Journal of neurochemistry*, 126(1), pp.131–44.

Fan, Y. et al., 2006. Beta-synuclein modulates alpha-synuclein neurotoxicity by reducing alpha-synuclein protein expression. *Human molecular genetics*, 15(20), pp.3002–11.

Faull, R.L. & Laverty, R., 1969. Changes in dopamine levels in the corpus striatum following lesions in the substantia nigra. *Experimental neurology*, 23(3), pp.332–40.

Fauvet, B. et al., 2012. α-Synuclein in central nervous system and from erythrocytes, mammalian cells, and Escherichia coli exists predominantly as disordered monomer. *The Journal of biological chemistry*, 287(19), pp.15345–64.

Feil, R. et al., 1997. Regulation of Cre recombinase activity by mutated estrogen receptor ligand-binding domains. *Biochemical and biophysical research communications*, 237(3), pp.752–7.

Fernagut, P.O. et al., 2007. Behavioral and histopathological consequences of paraquat intoxication in mice: effects of alpha-synuclein over-expression. *Synapse (New York, N.Y.)*, 61(12), pp.991–1001.

Ferrante, R.J. et al., 1997. Systemic administration of rotenone produces selective damage in the striatum and globus pallidus, but not in the substantia nigra. *Brain research*, 753(1), pp.157–62.

Fields, J. et al., 2013. Age-dependent molecular alterations in the autophagy pathway in HIVE patients and in a gp120 tg mouse model: reversal with beclin-1 gene transfer. *Journal of neurovirology*, 19(1), pp.89–101.

Fink, A.L., 2006. The aggregation and fibrillation of alpha-synuclein. *Accounts of chemical research*, 39(9), pp.628–34.

Fischer, F., Hamann, A. & Osiewacz, H.D., 2012. Mitochondrial quality control: an integrated network of pathways. *Trends in biochemical sciences*, 37(7), pp.284–92.

Fleming, S.M. et al., 2006. Behavioral effects of dopaminergic agonists in transgenic mice overexpressing human wildtype alpha-synuclein. *Neuroscience*, 142(4), pp.1245–53.

Fleming, S.M. et al., 2008. Olfactory deficits in mice overexpressing human wildtype alpha-synuclein. *The European journal of neuroscience*, 28(2), pp.247–56.

Floor, E. & Wetzel, M.G., 1998. Increased protein oxidation in human substantia nigra pars compacta in comparison with basal ganglia and prefrontal cortex measured with an improved dinitrophenylhydrazine assay. *Journal of neurochemistry*, 70(1), pp.268–75.

Fornai, F. et al., 2005. Parkinson-like syndrome induced by continuous MPTP infusion: convergent roles of the ubiquitin-proteasome system and alpha-synuclein. *Proceedings of the National Academy of Sciences of the United States of America*, 102(9), pp.3413–8.

Forno, L.S., 1996. Neuropathology of Parkinson's disease. *Journal of neuropathology and experimental neurology*, 55(3), pp.259–72.

Forno, L.S. et al., 1993. Similarities and differences between MPTP-induced parkinsonsim and Parkinson's disease. Neuropathologic considerations. *Advances in neurology*, 60, pp.600–8.

Forsaa, E.B. et al., 2010. What predicts mortality in Parkinson disease?: a prospective population-based long-term study. *Neurology*, 75(14), pp.1270–6.

Fortin, D.L. et al., 2004. Lipid rafts mediate the synaptic localization of alpha-synuclein. *The Journal of neuroscience : the official journal of the Society for Neuroscience*, 24(30), pp.6715–23.

Fortin, D.L. et al., 2005. Neural activity controls the synaptic accumulation of alpha-synuclein. *The Journal of neuroscience : the official journal of the Society for Neuroscience*, 25(47), pp.10913–21.

Fortun, J. et al., 2003. Emerging role for autophagy in the removal of aggresomes in Schwann cells. *The Journal of neuroscience : the official journal of the Society for Neuroscience*, 23(33), pp.10672–80.

Fournier, M. et al., 2009. Parkin deficiency delays motor decline and disease manifestation in a mouse model of synucleinopathy. *PloS one*, 4(8), p.e6629.

Fredriksson, A. & Archer, T., 1994. MPTP-induced behavioural and biochemical deficits: a parametric analysis. *Journal of neural transmission. Parkinson's disease and dementia section*, 7(2), pp.123–32.

| Bibliography

Freichel, C. et al., 2007. Age-dependent cognitive decline and amygdala pathology in alpha-synuclein transgenic mice. *Neurobiology of aging*, 28(9), pp.1421–35.

Fujiwara, H. et al., 2002. alpha-Synuclein is phosphorylated in synucleinopathy lesions. *Nature cell biology*, 4(2), pp.160–4.

Furukawa, K. et al., 2006. Plasma membrane ion permeability induced by mutant alpha-synuclein contributes to the degeneration of neural cells. *Journal of neurochemistry*, 97(4), pp.1071–7.

Gai, W.P., Blessing, W.W. & Blumbergs, P.C., 1995. Ubiquitin-positive degenerating neurites in the brainstem in Parkinson's disease. *Brain : a journal of neurology*, 118 (Pt 6, pp.1447–59.

Gallyas, F., Zaborszky, L. & Wolff, J.R., 1980. Experimental studies of mechanisms involved in methods demonstrating axonal and terminal degeneration. *Stain technology*, 55(5), pp.281–90.

Garcia-Mata, R., Gao, Y.-S. & Sztul, E., 2002. Hassles with taking out the garbage: aggravating aggresomes. *Traffic (Copenhagen, Denmark)*, 3(6), pp.388–96.

Gardet, A. et al., 2010. LRRK2 is involved in the IFN-gamma response and host response to pathogens. *Journal of immunology (Baltimore, Md. : 1950)*, 185(9), pp.5577–85.

Gassmann, M. et al., 2009. Quantifying Western blots: pitfalls of densitometry. *Electrophoresis*, 30(11), pp.1845–55.

Gautier, C.A., Kitada, T. & Shen, J., 2008. Loss of PINK1 causes mitochondrial functional defects and increased sensitivity to oxidative stress. *Proceedings of the National Academy of Sciences of the United States of America*, 105(32), pp.11364–9.

George, J.M. et al., 1995. Characterization of a novel protein regulated during the critical period for song learning in the zebra finch. *Neuron*, 15(2), pp.361–72.

Gertz, H.J., Siegers, A. & Kuchinke, J., 1994. Stability of cell size and nucleolar size in Lewy body containing neurons of substantia nigra in Parkinson's disease. *Brain research*, 637(1-2), pp.339–41.

Giasson, B.I. et al., 2001. A hydrophobic stretch of 12 amino acid residues in the middle of alpha-synuclein is essential for filament assembly. *The Journal of biological chemistry*, 276(4), pp.2380–6.

Giasson, B.I. et al., 2006. Biochemical and pathological characterization of Lrrk2. *Annals of neurology*, 59(2), pp.315–22.

Giasson, B.I. et al., 2003. Initiation and synergistic fibrillization of tau and alpha-synuclein. *Science (New York, N.Y.)*, 300(5619), pp.636–40.

Giasson, B.I., 1999. Mutant and Wild Type Human alpha -Synucleins Assemble into Elongated Filaments with Distinct Morphologies in Vitro. *Journal of Biological Chemistry*, 274(12), pp.7619–7622.

Giasson, B.I. et al., 2002. Neuronal alpha-synucleinopathy with severe movement disorder in

mice expressing A53T human alpha-synuclein. *Neuron*, 34(4), pp.521–33.

Giasson, B.I. et al., 2000. Oxidative damage linked to neurodegeneration by selective alpha-synuclein nitration in synucleinopathy lesions. *Science (New York, N.Y.)*, 290(5493), pp.985–9.

Gispert, S. et al., 2009. Parkinson phenotype in aged PINK1-deficient mice is accompanied by progressive mitochondrial dysfunction in absence of neurodegeneration. *PloS one*, 4(6), p.e5777.

Gitler, A.D. et al., 2008. The Parkinson's disease protein alpha-synuclein disrupts cellular Rab homeostasis. *Proceedings of the National Academy of Sciences of the United States of America*, 105(1), pp.145–50.

Glickman, M.H. & Ciechanover, A., 2002. The ubiquitin-proteasome proteolytic pathway: destruction for the sake of construction. *Physiological reviews*, 82(2), pp.373–428.

Goedert, M., 2001. Alpha-synuclein and neurodegenerative diseases. *Nature reviews. Neuroscience*, 2(7), pp.492–501.

Goers, J. et al., 2003. Nuclear localization of alpha-synuclein and its interaction with histones. *Biochemistry*, 42(28), pp.8465–71.

Goetz, C.G., 2011. The history of Parkinson's disease: early clinical descriptions and neurological therapies. *Cold Spring Harbor perspectives in medicine*, 1(1), p.a008862.

Goldberg, A.L., 2003. Protein degradation and protection against misfolded or damaged proteins. *Nature*, 426(6968), pp.895–9.

Goldberg, M.S. et al., 2005. Nigrostriatal dopaminergic deficits and hypokinesia caused by inactivation of the familial Parkinsonism-linked gene DJ-1. *Neuron*, 45(4), pp.489–96.

Goldberg, M.S. et al., 2003. Parkin-deficient mice exhibit nigrostriatal deficits but not loss of dopaminergic neurons. *The Journal of biological chemistry*, 278(44), pp.43628–35.

Goldman, J.E. et al., 1983. Lewy bodies of Parkinson's disease contain neurofilament antigens. *Science (New York, N.Y.)*, 221(4615), pp.1082–4.

Goloubinoff, P. & De Los Rios, P., 2007. The mechanism of Hsp70 chaperones: (entropic) pulling the models together. *Trends in biochemical sciences*, 32(8), pp.372–80.

Golovko, M.Y. et al., 2005. Alpha-synuclein gene deletion decreases brain palmitate uptake and alters the palmitate metabolism in the absence of alpha-synuclein palmitate binding. *Biochemistry*, 44(23), pp.8251–9.

Gomez-Isla, T. et al., 2003. Motor dysfunction and gliosis with preserved dopaminergic markers in human alpha-synuclein A30P transgenic mice. *Neurobiology of aging*, 24(2), pp.245–58.

Gómez-Tortosa, E. et al., 2002. Patterns of protein nitration in dementia with Lewy bodies and striatonigral degeneration. *Acta neuropathologica*, 103(5), pp.495–500.

Gonçalves, S. & Outeiro, T.F., 2013. Assessing the subcellular dynamics of alpha-synuclein

using photoactivation microscopy. *Molecular neurobiology*, 47(3), pp.1081–92.

Good, P.F. et al., 1998. Protein nitration in Parkinson's disease. *Journal of neuropathology and experimental neurology*, 57(4), pp.338–42.

Goodsell, D.S. & Olson, A.J., 2000. Structural symmetry and protein function. *Annual review of biophysics and biomolecular structure*, 29, pp.105–53.

Gorbatyuk, O.S. et al., 2008. The phosphorylation state of Ser-129 in human alpha-synuclein determines neurodegeneration in a rat model of Parkinson disease. *Proceedings of the National Academy of Sciences of the United States of America*, 105(2), pp.763–8.

Gossen, M. & Bujard, H., 1992. Tight control of gene expression in mammalian cells by tetracycline-responsive promoters. *Proceedings of the National Academy of Sciences of the United States of America*, 89(12), pp.5547–51.

Graham, D.G. et al., 1978. Autoxidation versus covalent binding of quinones as the mechanism of toxicity of dopamine, 6-hydroxydopamine, and related compounds toward C1300 neuroblastoma cells in vitro. *Molecular pharmacology*, 14(4), pp.644–53.

Gray, D.A., Tsirigotis, M. & Woulfe, J., 2003. Ubiquitin, proteasomes, and the aging brain. *Science of aging knowledge environment : SAGE KE*, 2003(34), p.RE6.

Groenewegen, H.J., 2003. The basal ganglia and motor control. *Neural plasticity*, 10(1-2), pp.107–20.

Guerrero, E. et al., 2013. Recent advances in α-synuclein functions, advanced glycation, and toxicity: implications for Parkinson's disease. *Molecular neurobiology*, 47(2), pp.525–36.

Guo, J.L. et al., 2013. Distinct α-synuclein strains differentially promote tau inclusions in neurons. *Cell*, 154(1), pp.103–17.

Halliday, G.M. & Stevens, C.H., 2011. Glia: initiators and progressors of pathology in Parkinson's disease. *Movement disorders : official journal of the Movement Disorder Society*, 26(1), pp.6–17.

Hansen, C. et al., 2013. A novel α-synuclein-GFP mouse model displays progressive motor impairment, olfactory dysfunction and accumulation of α-synuclein-GFP. *Neurobiology of disease*, 56, pp.145–55.

Hara, T. et al., 2006. Suppression of basal autophagy in neural cells causes neurodegenerative disease in mice. *Nature*, 441(7095), pp.885–9.

Hardy, J. et al., 2006. Genetics of Parkinson's disease and parkinsonism. *Annals of neurology*, 60(4), pp.389–98.

Hartl, F.U., Bracher, A. & Hayer-Hartl, M., 2011. Molecular chaperones in protein folding and proteostasis. *Nature*, 475(7356), pp.324–32.

Hartmann, A., 2004. Postmortem studies in Parkinson's disease. *Dialogues in clinical neuroscience*, 6(3), pp.281–93.

Hasegawa, M. et al., 2002. Phosphorylated alpha-synuclein is ubiquitinated in alpha-

synucleinopathy lesions. *The Journal of biological chemistry*, 277(50), pp.49071–6.

Hashimoto, M. et al., 1998. Human recombinant NACP/alpha-synuclein is aggregated and fibrillated in vitro: relevance for Lewy body disease. *Brain research*, 799(2), pp.301–6.

Hashimoto, M. et al., 1999. Oxidative stress induces amyloid-like aggregate formation of NACP/alpha-synuclein in vitro. *Neuroreport*, 10(4), pp.717–21.

Hauser, D.N. & Hastings, T.G., 2013. Mitochondrial dysfunction and oxidative stress in Parkinson's disease and monogenic parkinsonism. *Neurobiology of disease*, 51, pp.35–42.

Hayashi, S. et al., 2000. An autopsy case of autosomal-recessive juvenile parkinsonism with a homozygous exon 4 deletion in the parkin gene. *Movement disorders : official journal of the Movement Disorder Society*, 15(5), pp.884–8.

Haywood, A.F.M. & Staveley, B.E., 2004. Parkin counteracts symptoms in a Drosophila model of Parkinson's disease. *BMC neuroscience*, 5, p.14.

Hebron, M.L., Lonskaya, I. & Moussa, C.E.-H., 2013. Nilotinib reverses loss of dopamine neurons and improves motor behavior via autophagic degradation of α-synuclein in Parkinson's disease models. *Human molecular genetics*, 22(16), pp.3315–28.

Heikkila, R.E. et al., 1985. Dopaminergic toxicity of rotenone and the 1-methyl-4-phenylpyridinium ion after their stereotaxic administration to rats: implication for the mechanism of 1-methyl-4-phenyl-1,2,3,6-tetrahydropyridine toxicity. *Neuroscience letters*, 62(3), pp.389–94.

Heikkila, R.E., Hess, A. & Duvoisin, R.C., 1984. Dopaminergic neurotoxicity of 1-methyl-4-phenyl-1,2,5,6-tetrahydropyridine in mice. *Science (New York, N.Y.)*, 224(4656), pp.1451–3.

Heir, R. et al., 2006. The UBL domain of PLIC-1 regulates aggresome formation. *EMBO reports*, 7(12), pp.1252–8.

Hermeking, H. & Benzinger, A., 2006. 14-3-3 proteins in cell cycle regulation. *Seminars in cancer biology*, 16(3), pp.183–92.

Hernández-Aguilera, A. et al., 2013. Mitochondrial Dysfunction: A Basic Mechanism in Inflammation-Related Non-Communicable Diseases and Therapeutic Opportunities. *Mediators of Inflammation*, 2013, pp.1–13.

Hertzman, C. et al., 1990. Parkinson's disease: a case-control study of occupational and environmental risk factors. *American journal of industrial medicine*, 17(3), pp.349–55.

Higashi, S. et al., 2011. Localization of MAP1-LC3 in vulnerable neurons and Lewy bodies in brains of patients with dementia with Lewy bodies. *Journal of neuropathology and experimental neurology*, 70(4), pp.264–80.

Hill, C.P., Masters, E.I. & Whitby, F.G., 2002. The 11S regulators of 20S proteasome activity. *Current topics in microbiology and immunology*, 268, pp.73–89.

Hinkle, K.M. et al., 2012. LRRK2 knockout mice have an intact dopaminergic system but

display alterations in exploratory and motor co-ordination behaviors. *Molecular neurodegeneration*, 7, p.25.

Hirsch, E.C. & Hunot, S., 2009. Neuroinflammation in Parkinson's disease: a target for neuroprotection? *Lancet neurology*, 8(4), pp.382–97.

Hirtz, D. et al., 2007. How common are the "common" neurologic disorders? *Neurology*, 68(5), pp.326–37.

Hlavacek, W.S. et al., 2003. The complexity of complexes in signal transduction. *Biotechnology and bioengineering*, 84(7), pp.783–94.

Hodara, R. et al., 2004. Functional consequences of alpha-synuclein tyrosine nitration: diminished binding to lipid vesicles and increased fibril formation. *The Journal of biological chemistry*, 279(46), pp.47746–53.

Hodge, G.K. & Butcher, L.L., 1980. Pars compacta of the substantia nigra modulates motor activity but is not involved importantly in regulating food and water intake. *Naunyn-Schmiedeberg's archives of pharmacology*, 313(1), pp.51–67.

Holdorff, B., 2002. Friedrich Heinrich Lewy (1885-1950) and his work. *Journal of the history of the neurosciences*, 11(1), pp.19–28.

Hossain, S.M., Wong, B.K.Y. & Simpson, E.M., 2004. The dark phase improves genetic discrimination for some high throughput mouse behavioral phenotyping. *Genes, brain, and behavior*, 3(3), pp.167–77.

Houlden, H. & Singleton, A.B., 2012. The genetics and neuropathology of Parkinson's disease. *Acta neuropathologica*, 124(3), pp.325–38.

Hsu, L.J. et al., 2000. alpha-synuclein promotes mitochondrial deficit and oxidative stress. *The American journal of pathology*, 157(2), pp.401–10.

Hübener, J. et al., 2012. Automated Behavioral Phenotyping Reveals Presymptomatic Alterations in a SCA3 Genetrap Mouse Model. *Journal of genetics and genomics = Yi chuan xue bao*, 39(6), pp.287–99.

Hughes, A.J. et al., 1992. Accuracy of clinical diagnosis of idiopathic Parkinson's disease: a clinico-pathological study of 100 cases. *Journal of Neurology, Neurosurgery & Psychiatry*, 55(3), pp.181–184.

Humbert, J. et al., 2007. Parkin and synphilin-1 isoform expression changes in Lewy body diseases. *Neurobiology of disease*, 26(3), pp.681–7.

Ibáñez, P. et al., 2004. Causal relation between alpha-synuclein gene duplication and familial Parkinson's disease. *Lancet*, 364(9440), pp.1169–71.

Ii, K. et al., 1997. Immunocytochemical co-localization of the proteasome in ubiquitinated structures in neurodegenerative diseases and the elderly. *Journal of neuropathology and experimental neurology*, 56(2), pp.125–31.

Inglis, K.J. et al., 2009. Polo-like kinase 2 (PLK2) phosphorylates alpha-synuclein at serine 129 in central nervous system. *The Journal of biological chemistry*, 284(5), pp.2598–602.

Irizarry, M.C. et al., 1996. Characterization of the precursor protein of the non-A beta component of senile plaques (NACP) in the human central nervous system. *Journal of neuropathology and experimental neurology*, 55(8), pp.889–95.

Itier, J.-M. et al., 2003. Parkin gene inactivation alters behaviour and dopamine neurotransmission in the mouse. *Human molecular genetics*, 12(18), pp.2277–91.

Ito, T. et al., 2003. Dorfin localizes to Lewy bodies and ubiquitylates synphilin-1. *The Journal of biological chemistry*, 278(31), pp.29106–14.

Iwai, A. et al., 1995. The precursor protein of non-Aβ component of Alzheimer's disease amyloid is a presynaptic protein of the central nervous system. *Neuron*, 14(2), pp.467–475.

Iwata, A. et al., 2005. HDAC6 and microtubules are required for autophagic degradation of aggregated huntingtin. *The Journal of biological chemistry*, 280(48), pp.40282–92.

Jakes, R., Spillantini, M.G. & Goedert, M., 1994. Identification of two distinct synucleins from human brain. *FEBS letters*, 345(1), pp.27–32.

Jankovic, J., 2008. Parkinson's disease: clinical features and diagnosis. *Journal of neurology, neurosurgery, and psychiatry*, 79(4), pp.368–76.

Jellinger, K.A., 2003. Alpha-synuclein pathology in Parkinson's and Alzheimer's disease brain: incidence and topographic distribution--a pilot study. *Acta neuropathologica*, 106(3), pp.191–201.

Jellinger, K.A., 2004. Lewy body-related alpha-synucleinopathy in the aged human brain. *Journal of neural transmission (Vienna, Austria : 1996)*, 111(10-11), pp.1219–35.

Jellinger, K.A., 1991. Pathology of Parkinson's disease. Changes other than the nigrostriatal pathway. *Molecular and chemical neuropathology / sponsored by the International Society for Neurochemistry and the World Federation of Neurology and research groups on neurochemistry and cerebrospinal fluid*, 14(3), pp.153–97.

Jenco, J.M. et al., 1998. Regulation of phospholipase D2: selective inhibition of mammalian phospholipase D isoenzymes by alpha- and beta-synucleins. *Biochemistry*, 37(14), pp.4901–9.

Jeon, B.S., Jackson-Lewis, V. & Burke, R.E., 1995. 6-Hydroxydopamine lesion of the rat substantia nigra: time course and morphology of cell death. *Neurodegeneration : a journal for neurodegenerative disorders, neuroprotection, and neuroregeneration*, 4(2), pp.131–7.

Ji, H. et al., 1997. Identification of a breast cancer-specific gene, BCSG1, by direct differential cDNA sequencing. *Cancer research*, 57(4), pp.759–64.

Ji, H. & Davis, R.W., 2006. Data quality in genomics and microarrays. *Nature biotechnology*, 24(9), pp.1112–3.

Jin, H.-G. et al., 2008. Synphilin-1 transgenic mice exhibit mild motor impairments. *Neuroscience letters*, 445(1), pp.12–7.

| Bibliography

Johansen, T. & Lamark, T., 2011. Selective autophagy mediated by autophagic adapter proteins. *Autophagy*, 7(3), pp.279–96.

Johnston, J.A., Illing, M.E. & Kopito, R.R., 2002. Cytoplasmic dynein/dynactin mediates the assembly of aggresomes. *Cell motility and the cytoskeleton*, 53(1), pp.26–38.

Johnston, J.A., Ward, C.L. & Kopito, R.R., 1998. Aggresomes: a cellular response to misfolded proteins. *The Journal of cell biology*, 143(7), pp.1883–98.

Jones, S. & Thornton, J.M., 1996. Principles of protein-protein interactions. *Proceedings of the National Academy of Sciences of the United States of America*, 93(1), pp.13–20.

Jung, T. & Grune, T., 2012. *Structure of the proteasome.* 1st ed., Elsevier Inc.

Junn, E. et al., 2005. Interaction of DJ-1 with Daxx inhibits apoptosis signal-regulating kinase 1 activity and cell death. *Proceedings of the National Academy of Sciences of the United States of America*, 102(27), pp.9691–6.

Kabeya, Y. et al., 2000. LC3, a mammalian homologue of yeast Apg8p, is localized in autophagosome membranes after processing. *The EMBO journal*, 19(21), pp.5720–8.

Kahle, P.J. et al., 2001. Selective insolubility of alpha-synuclein in human Lewy body diseases is recapitulated in a transgenic mouse model. *The American journal of pathology*, 159(6), pp.2215–25.

Kahle, P.J. et al., 2000. Subcellular localization of wild-type and Parkinson's disease-associated mutant alpha -synuclein in human and transgenic mouse brain. *The Journal of neuroscience : the official journal of the Society for Neuroscience*, 20(17), pp.6365–73.

Kalia, S.K., Kalia, L. V & McLean, P.J., 2010. Molecular chaperones as rational drug targets for Parkinson's disease therapeutics. *CNS & neurological disorders drug targets*, 9(6), pp.741–53.

Kamel, F. et al., 2007. Pesticide exposure and self-reported Parkinson's disease in the agricultural health study. *American journal of epidemiology*, 165(4), pp.364–74.

Kamp, F. et al., 2010. Inhibition of mitochondrial fusion by α-synuclein is rescued by PINK1, Parkin and DJ-1. *The EMBO journal*, 29(20), pp.3571–89.

Kanazawa, T. et al., 2008. Three-layered structure shared between Lewy bodies and lewy neurites-three-dimensional reconstruction of triple-labeled sections. *Brain pathology (Zurich, Switzerland)*, 18(3), pp.415–22.

Karl, T., Pabst, R. & von Hörsten, S., 2003. Behavioral phenotyping of mice in pharmacological and toxicological research. *Experimental and toxicologic pathology : official journal of the Gesellschaft für Toxikologische Pathologie*, 55(1), pp.69–83.

Karube, H. et al., 2008. N-terminal region of alpha-synuclein is essential for the fatty acid-induced oligomerization of the molecules. *FEBS letters*, 582(25-26), pp.3693–700.

Kasai, T. et al., 2008. Cleavage of normal and pathological forms of alpha-synuclein by neurosin in vitro. *Neuroscience letters*, 436(1), pp.52–6.

Kaushik, S. & Cuervo, A.M., 2012. Chaperone-mediated autophagy: a unique way to enter the lysosome world. *Trends in cell biology*, 22(8), pp.407–17.

Kawaguchi, Y. et al., 2003. The deacetylase HDAC6 regulates aggresome formation and cell viability in response to misfolded protein stress. *Cell*, 115(6), pp.727–38.

Kawamata, H. et al., 2001. Interaction of alpha-synuclein and synphilin-1: effect of Parkinson's disease-associated mutations. *Journal of neurochemistry*, 77(3), pp.929–34.

Kessler, J.C., Rochet, J.-C. & Lansbury, P.T., 2003. The N-terminal repeat domain of alpha-synuclein inhibits beta-sheet and amyloid fibril formation. *Biochemistry*, 42(3), pp.672–8.

Kiely, A.P. et al., 2013. α-Synucleinopathy associated with G51D SNCA mutation: a link between Parkinson's disease and multiple system atrophy? *Acta neuropathologica*, 125(5), pp.753–69.

Kihara, A. et al., 2001. Beclin-phosphatidylinositol 3-kinase complex functions at the trans-Golgi network. *EMBO reports*, 2(4), pp.330–5.

Kilpatrick, K. et al., 2013. Chemical Induction of Hsp70 Reduces α-Synuclein Aggregation in Neuroglioma Cells. *ACS chemical biology*.

Kim, H.J. et al., 2006. Calpain-resistant fragment(s) of alpha-synuclein regulates the synuclein-cleaving activity of 20S proteasome. *Archives of biochemistry and biophysics*, 455(1), pp.40–7.

Kim, R.H. et al., 2005. Hypersensitivity of DJ-1-deficient mice to 1-methyl-4-phenyl-1,2,3,6-tetrahydropyrindine (MPTP) and oxidative stress. *Proceedings of the National Academy of Sciences of the United States of America*, 102(14), pp.5215–20.

Kim, T.D., Paik, S.R. & Yang, C.-H., 2002. Structural and functional implications of C-terminal regions of alpha-synuclein. *Biochemistry*, 41(46), pp.13782–90.

KING, L.S., 1948. Atypical amyloid disease, with observations on a new silver stain for amyloid. *The American journal of pathology*, 24(5), pp.1095–1115.

Kirik, D. et al., 2003. Nigrostriatal alpha-synucleinopathy induced by viral vector-mediated overexpression of human alpha-synuclein: a new primate model of Parkinson's disease. *Proceedings of the National Academy of Sciences of the United States of America*, 100(5), pp.2884–9.

Kirik, D. et al., 2002. Parkinson-like neurodegeneration induced by targeted overexpression of alpha-synuclein in the nigrostriatal system. *The Journal of neuroscience : the official journal of the Society for Neuroscience*, 22(7), pp.2780–91.

Kirkin, V. et al., 2009. A role for NBR1 in autophagosomal degradation of ubiquitinated substrates. *Molecular cell*, 33(4), pp.505–16.

Kish-Trier, E. & Hill, C.P., 2013. Structural biology of the proteasome. *Annual review of biophysics*, 42, pp.29–49.

Kitada, T. et al., 2007. Impaired dopamine release and synaptic plasticity in the striatum of PINK1-deficient mice. *Proceedings of the National Academy of Sciences of the United*

| Bibliography

States of America, 104(27), pp.11441–6.

Klein, C. & Westenberger, A., 2012. Genetics of Parkinson's disease. *Cold Spring Harbor perspectives in medicine*, 2(1), p.a008888.

Klionsky, D.J. et al., 2012. Guidelines for the use and interpretation of assays for monitoring autophagy. *Autophagy*, 8(4), pp.445–544.

Klivenyi, P. et al., 2006. Mice lacking alpha-synuclein are resistant to mitochondrial toxins. *Neurobiology of disease*, 21(3), pp.541–8.

Klotz, I.M., Langerman, N.R. & Darnall, D.W., 1970. Quaternary structure of proteins. *Annual review of biochemistry*, 39, pp.25–62.

Klucken, J. et al., 2012. Alpha-synuclein aggregation involves a bafilomycin A 1-sensitive autophagy pathway. *Autophagy*, 8(5), pp.754–766.

Ko, H.S. et al., 2006. Identification of far upstream element-binding protein-1 as an authentic Parkin substrate. *The Journal of biological chemistry*, 281(24), pp.16193–6.

Köhler, A. et al., 2001. The axial channel of the proteasome core particle is gated by the Rpt2 ATPase and controls both substrate entry and product release. *Molecular cell*, 7(6), pp.1143–52.

Komatsu, M. et al., 2007. Homeostatic levels of p62 control cytoplasmic inclusion body formation in autophagy-deficient mice. *Cell*, 131(6), pp.1149–63.

Komatsu, M. et al., 2006. Loss of autophagy in the central nervous system causes neurodegeneration in mice. *Nature*, 441(7095), pp.880–4.

Kontopoulos, E., Parvin, J.D. & Feany, M.B., 2006. Alpha-synuclein acts in the nucleus to inhibit histone acetylation and promote neurotoxicity. *Human molecular genetics*, 15(20), pp.3012–23.

Kopito, R.R., 2000. Aggresomes, inclusion bodies and protein aggregation. *Trends in cell biology*, 10(12), pp.524–30.

Koppula, S. et al., 2012. Reactive oxygen species and inhibitors of inflammatory enzymes, NADPH oxidase, and iNOS in experimental models of Parkinson's disease. *Mediators of inflammation*, 2012, p.823902.

Kordower, J.H. et al., 2006. Failure of proteasome inhibitor administration to provide a model of Parkinson's disease in rats and monkeys. *Annals of neurology*, 60(2), pp.264–8.

Kramer, M.L. & Schulz-Schaeffer, W.J., 2007. Presynaptic alpha-synuclein aggregates, not Lewy bodies, cause neurodegeneration in dementia with Lewy bodies. *The Journal of neuroscience : the official journal of the Society for Neuroscience*, 27(6), pp.1405–10.

Kravtsova-Ivantsiv, Y. & Ciechanover, A., 2012. Non-canonical ubiquitin-based signals for proteasomal degradation. *Journal of cell science*, 125(Pt 3), pp.539–48.

Krenz, A. et al., 2009. Aggregate formation and toxicity by wild-type and R621C synphilin-1 in the nigrostriatal system of mice using adenoviral vectors. *Journal of neurochemistry*,

108(1), pp.139–46.

Krüger, R. et al., 1998. Ala30Pro mutation in the gene encoding alpha-synuclein in Parkinson's disease. *Nature genetics*, 18(2), pp.106–8.

Kulathu, Y. & Komander, D., 2012. Atypical ubiquitylation - the unexplored world of polyubiquitin beyond Lys48 and Lys63 linkages. *Nature reviews. Molecular cell biology*, 13(8), pp.508–23.

Kuo, Y.-M. et al., 2010. Extensive enteric nervous system abnormalities in mice transgenic for artificial chromosomes containing Parkinson disease-associated alpha-synuclein gene mutations precede central nervous system changes. *Human molecular genetics*, 19(9), pp.1633–50.

Kuzuhara, S. et al., 1988. Lewy bodies are ubiquitinated. A light and electron microscopic immunocytochemical study. *Acta neuropathologica*, 75(4), pp.345–53.

Lam, H.A. et al., 2011. Elevated tonic extracellular dopamine concentration and altered dopamine modulation of synaptic activity precede dopamine loss in the striatum of mice overexpressing human α-synuclein. *Journal of neuroscience research*, 89(7), pp.1091–102.

Lamark, T. & Johansen, T., 2012. Aggrephagy: selective disposal of protein aggregates by macroautophagy. *International journal of cell biology*, 2012, p.736905.

Lane-Petter, W., 1968. Cannibalism in rats and mice. *Proceedings of the Royal Society of Medicine*, 61(12), pp.1295–6.

Langston, J.W. et al., 1983. Chronic Parkinsonism in humans due to a product of meperidine-analog synthesis. *Science (New York, N.Y.)*, 219(4587), pp.979–80.

Larsen, C.N., Krantz, B.A. & Wilkinson, K.D., 1998. Substrate specificity of deubiquitinating enzymes: ubiquitin C-terminal hydrolases. *Biochemistry*, 37(10), pp.3358–68.

Larsen, K.E. et al., 2006. Alpha-synuclein overexpression in PC12 and chromaffin cells impairs catecholamine release by interfering with a late step in exocytosis. *The Journal of neuroscience : the official journal of the Society for Neuroscience*, 26(46), pp.11915–22.

Lashuel, H. a. et al., 2012. The many faces of α-synuclein: from structure and toxicity to therapeutic target. *Nature Reviews Neuroscience*, 14(1), pp.38–48.

Lashuel, H.A. et al., 2002. Alpha-synuclein, especially the Parkinson's disease-associated mutants, forms pore-like annular and tubular protofibrils. *Journal of molecular biology*, 322(5), pp.1089–102.

De Lau, L.M.L. & Breteler, M.M.B., 2006. Epidemiology of Parkinson's disease. *Lancet neurology*, 5(6), pp.525–35.

De Laureto, P.P. et al., 2006. Conformational properties of the SDS-bound state of alpha-synuclein probed by limited proteolysis: unexpected rigidity of the acidic C-terminal tail. *Biochemistry*, 45(38), pp.11523–31.

Lauwers, E. et al., 2003. Neuropathology and neurodegeneration in rodent brain induced by

lentiviral vector-mediated overexpression of alpha-synuclein. *Brain pathology (Zurich, Switzerland)*, 13(3), pp.364–72.

Lavedan, C. et al., 1998. Identification, localization and characterization of the human gamma-synuclein gene. *Human genetics*, 103(1), pp.106–12.

Lavedan, C., 1998. The synuclein family. *Genome research*, 8(9), pp.871–80.

Lee, B.D. et al., 2010. Inhibitors of leucine-rich repeat kinase-2 protect against models of Parkinson's disease. *Nature medicine*, 16(9), pp.998–1000.

Lee, B.R. et al., 2013. Role of Ser129 phosphorylation of α-synuclein in melanoma cells. *Journal of cell science*, 126(Pt 2), pp.696–704.

Lee, F.K.M. et al., 2009. The role of ubiquitin linkages on alpha-synuclein induced-toxicity in a Drosophila model of Parkinson's disease. *Journal of neurochemistry*, 110(1), pp.208–19.

Lee, G. et al., 2004. Casein kinase II-mediated phosphorylation regulates alpha-synuclein/synphilin-1 interaction and inclusion body formation. *The Journal of biological chemistry*, 279(8), pp.6834–9.

Lee, G. et al., 2002. Synphilin-1 degradation by the ubiquitin-proteasome pathway and effects on cell survival. *Journal of neurochemistry*, 83(2), pp.346–52.

Lee, H.-J. et al., 2004. Clearance of alpha-synuclein oligomeric intermediates via the lysosomal degradation pathway. *The Journal of neuroscience : the official journal of the Society for Neuroscience*, 24(8), pp.1888–96.

Lee, H.-J., Choi, C. & Lee, S.-J., 2002. Membrane-bound alpha-synuclein has a high aggregation propensity and the ability to seed the aggregation of the cytosolic form. *The Journal of biological chemistry*, 277(1), pp.671–8.

Lee, H.-J. & Lee, S.-J., 2002. Characterization of cytoplasmic alpha-synuclein aggregates. Fibril formation is tightly linked to the inclusion-forming process in cells. *The Journal of biological chemistry*, 277(50), pp.48976–83.

Lee, J.T. et al., 2008. Ubiquitination of alpha-synuclein by Siah-1 promotes alpha-synuclein aggregation and apoptotic cell death. *Human molecular genetics*, 17(6), pp.906–17.

Lee, K.-W. et al., 2011. Enhanced phosphatase activity attenuates α-synucleinopathy in a mouse model. *The Journal of neuroscience : the official journal of the Society for Neuroscience*, 31(19), pp.6963–71.

Lee, M.K. et al., 2002. Human alpha-synuclein-harboring familial Parkinson's disease-linked Ala-53 --> Thr mutation causes neurodegenerative disease with alpha-synuclein aggregation in transgenic mice. *Proceedings of the National Academy of Sciences of the United States of America*, 99(13), pp.8968–73.

Leisman, G. & Melillo, R., 2013. The basal ganglia: motor and cognitive relationships in a clinical neurobehavioral context. *Reviews in the neurosciences*, 24(1), pp.9–25.

Lennox, G. et al., 1989. Diffuse Lewy body disease: correlative neuropathology using anti-ubiquitin immunocytochemistry. *Journal of neurology, neurosurgery, and psychiatry*,

52(11), pp.1236–47.

Lesage, S. et al., 2013. G51D α-synuclein mutation causes a novel parkinsonian-pyramidal syndrome. *Annals of neurology.*

Lev, N. et al., 2013. Knocking out DJ-1 attenuates astrocytes neuroprotection against 6-hydroxydopamine toxicity. *Journal of molecular neuroscience : MN*, 50(3), pp.542–50.

Levin, J. et al., 2009. Increased alpha-synuclein aggregation following limited cleavage by certain matrix metalloproteinases. *Experimental neurology*, 215(1), pp.201–8.

Lewy, F.H., 1921. Die Veränderungen des fibrillären und kanalikulären Apparates der Ganglienzelle im Senium. *Verhandlungen der Deutschen Pathologischen Gesellschaft*, 18, pp.311–312.

Lewy, F.H., 1913. Zur pathologischen Anatomie der Paralysis Agitans. *Deutsche Zeitschrift fur Nervenheilkunde*, 50, pp.50–55.

Li, W. et al., 2005. Aggregation promoting C-terminal truncation of alpha-synuclein is a normal cellular process and is enhanced by the familial Parkinson's disease-linked mutations. *Proceedings of the National Academy of Sciences of the United States of America*, 102(6), pp.2162–7.

Li, W., Li, J. & Bao, J., 2012. Microautophagy: lesser-known self-eating. *Cellular and molecular life sciences : CMLS*, 69(7), pp.1125–36.

Li, W.-W. et al., 2007. Localization of alpha-synuclein to mitochondria within midbrain of mice. *Neuroreport*, 18(15), pp.1543–6.

Li, X. et al., 2010. Enhanced striatal dopamine transmission and motor performance with LRRK2 overexpression in mice is eliminated by familial Parkinson's disease mutation G2019S. *The Journal of neuroscience : the official journal of the Society for Neuroscience*, 30(5), pp.1788–97.

Li, X. et al., 2010. Synphilin-1 exhibits trophic and protective effects against Rotenone toxicity. *Neuroscience*, 165(2), pp.455–62.

Li, Y. et al., 2005. Clinicogenetic study of PINK1 mutations in autosomal recessive early-onset parkinsonism. *Neurology*, 64(11), pp.1955–7.

Li, Y. et al., 2009. Mutant LRRK2(R1441G) BAC transgenic mice recapitulate cardinal features of Parkinson's disease. *Nature neuroscience*, 12(7), pp.826–8.

Liang, X.H. et al., 1999. Induction of autophagy and inhibition of tumorigenesis by beclin 1. *Nature*, 402(6762), pp.672–6.

Liani, E. et al., 2004. Ubiquitylation of synphilin-1 and alpha-synuclein by SIAH and its presence in cellular inclusions and Lewy bodies imply a role in Parkinson's disease. *Proceedings of the National Academy of Sciences of the United States of America*, 101(15), pp.5500–5.

Licker, V. et al., 2009. Proteomics in human Parkinson's disease research. *Journal of proteomics*, 73(1), pp.10–29.

| Bibliography

Lim, K.L. et al., 2005. Parkin mediates nonclassical, proteasomal-independent ubiquitination of synphilin-1: implications for Lewy body formation. *The Journal of neuroscience : the official journal of the Society for Neuroscience*, 25(8), pp.2002–9.

Lim, Y. et al., 2011. α-Syn suppression reverses synaptic and memory defects in a mouse model of dementia with Lewy bodies. *The Journal of neuroscience : the official journal of the Society for Neuroscience*, 31(27), pp.10076–87.

Lin, X. et al., 2009. Leucine-rich repeat kinase 2 regulates the progression of neuropathology induced by Parkinson's-disease-related mutant alpha-synuclein. *Neuron*, 64(6), pp.807–27.

Lin, X.-J. et al., 2006. Secondary structural formation of alpha-synuclein amyloids as revealed by g-factor of solid-state circular dichroism. *Biopolymers*, 83(3), pp.226–32.

Lindersson, E. et al., 2004. Proteasomal inhibition by alpha-synuclein filaments and oligomers. *The Journal of biological chemistry*, 279(13), pp.12924–34.

Liou, H.H. et al., 1997. Environmental risk factors and Parkinson's disease: a case-control study in Taiwan. *Neurology*, 48(6), pp.1583–8.

Liu, C.-W. et al., 2005. A precipitating role for truncated alpha-synuclein and the proteasome in alpha-synuclein aggregation: implications for pathogenesis of Parkinson disease. *The Journal of biological chemistry*, 280(24), pp.22670–8.

Liu, C.-W. et al., 2003. Endoproteolytic activity of the proteasome. *Science (New York, N.Y.)*, 299(5605), pp.408–11.

Liu, I.-H. et al., 2005. Agrin binds alpha-synuclein and modulates alpha-synuclein fibrillation. *Glycobiology*, 15(12), pp.1320–31.

Liu, Y. et al., 2002. The UCH-L1 gene encodes two opposing enzymatic activities that affect alpha-synuclein degradation and Parkinson's disease susceptibility. *Cell*, 111(2), pp.209–18.

Lohmann, E. et al., 2003. How much phenotypic variation can be attributed to parkin genotype? *Annals of neurology*, 54(2), pp.176–85.

López-Armada, M.J. et al., 2013. Mitochondrial dysfunction and the inflammatory response. *Mitochondrion*, 13(2), pp.106–18.

Lotharius, J. & Brundin, P., 2002a. Impaired dopamine storage resulting from alpha-synuclein mutations may contribute to the pathogenesis of Parkinson's disease. *Human molecular genetics*, 11(20), pp.2395–407.

Lotharius, J. & Brundin, P., 2002b. Pathogenesis of Parkinson's disease: dopamine, vesicles and alpha-synuclein. *Nature reviews. Neuroscience*, 3(12), pp.932–42.

Löw, K. & Aebischer, P., 2012. Use of viral vectors to create animal models for Parkinson's disease. *Neurobiology of disease*, 48(2), pp.189–201.

Ltic, S. et al., 2004. Alpha-synuclein is expressed in different tissues during human fetal development. *Journal of molecular neuroscience : MN*, 22(3), pp.199–204.

Lu, X. et al., 2009. Bacterial artificial chromosome transgenic mice expressing a truncated mutant parkin exhibit age-dependent hypokinetic motor deficits, dopaminergic neuron degeneration, and accumulation of proteinase K-resistant alpha-synuclein. *The Journal of neuroscience : the official journal of the Society for Neuroscience*, 29(7), pp.1962–76.

Lücking, C.B. et al., 2000. Association between early-onset Parkinson's disease and mutations in the parkin gene. *The New England journal of medicine*, 342(21), pp.1560–7.

Luk, K.C. et al., 2009. Exogenous alpha-synuclein fibrils seed the formation of Lewy body-like intracellular inclusions in cultured cells. *Proceedings of the National Academy of Sciences of the United States of America*, 106(47), pp.20051–6.

Lundblad, M. et al., 2012. Impaired neurotransmission caused by overexpression of α-synuclein in nigral dopamine neurons. *Proceedings of the National Academy of Sciences of the United States of America*, 109(9), pp.3213–9.

Luthman, J. et al., 1989. Selective lesion of central dopamine or noradrenaline neuron systems in the neonatal rat: motor behavior and monoamine alterations at adult stage. *Behavioural brain research*, 33(3), pp.267–77.

Lynch, M., 1988. Design and analysis of experiments on random drift and inbreeding depression. *Genetics*, 120(3), pp.791–807.

Lynch-Day, M. a et al., 2012. The role of autophagy in Parkinson's disease. *Cold Spring Harbor perspectives in medicine*, 2(4), p.a009357.

Lyons, K.E. & Pahwa, R., 2011. The impact and management of nonmotor symptoms of Parkinson's disease. *The American journal of managed care*, 17 Suppl 1(october), pp.S308–14.

Maiuri, M.C. et al., 2007. Self-eating and self-killing: crosstalk between autophagy and apoptosis. *Nature reviews. Molecular cell biology*, 8(9), pp.741–52.

Majeski, A.E. & Dice, J.F., 2004. Mechanisms of chaperone-mediated autophagy. *The international journal of biochemistry & cell biology*, 36(12), pp.2435–44.

Mak, S.K. et al., 2010. Lysosomal degradation of alpha-synuclein in vivo. *The Journal of biological chemistry*, 285(18), pp.13621–9.

Malgieri, G. & Eliezer, D., 2008. Structural effects of Parkinson's disease linked DJ-1 mutations. *Protein science : a publication of the Protein Society*, 17(5), pp.855–68.

Malkus, K.A., Tsika, E. & Ischiropoulos, H., 2009. Oxidative modifications, mitochondrial dysfunction, and impaired protein degradation in Parkinson's disease: how neurons are lost in the Bermuda triangle. *Molecular neurodegeneration*, 4, p.24.

Manning-Bog, A.B. et al., 2002. The herbicide paraquat causes up-regulation and aggregation of alpha-synuclein in mice: paraquat and alpha-synuclein. *The Journal of biological chemistry*, 277(3), pp.1641–4.

Manzoni, C. & Lewis, P. a, 2013. Dysfunction of the autophagy/lysosomal degradation pathway is a shared feature of the genetic synucleinopathies. *FASEB journal : official*

publication of the Federation of American Societies for Experimental Biology, 27(9), pp.3424–9.

Maroteaux, L., Campanelli, J.T. & Scheller, R.H., 1988. Synuclein: a neuron-specific protein localized to the nucleus and presynaptic nerve terminal. *The Journal of neuroscience : the official journal of the Society for Neuroscience*, 8(8), pp.2804–15.

Maroteaux, L. & Scheller, R.H., 1991. The rat brain synucleins; family of proteins transiently associated with neuronal membrane. *Brain research. Molecular brain research*, 11(3-4), pp.335–43.

Marques, O. & Outeiro, T.F., 2012. Alpha-synuclein: from secretion to dysfunction and death. *Cell death & disease*, 3(7), p.e350.

Marsicano, G. et al., 2002. The endogenous cannabinoid system controls extinction of aversive memories. *Nature*, 418(6897), pp.530–4.

Martin, L.J. et al., 2006. Parkinson's disease alpha-synuclein transgenic mice develop neuronal mitochondrial degeneration and cell death. *The Journal of neuroscience : the official journal of the Society for Neuroscience*, 26(1), pp.41–50.

Martinat, C. et al., 2004. Sensitivity to oxidative stress in DJ-1-deficient dopamine neurons: an ES- derived cell model of primary Parkinsonism. *PLoS biology*, 2(11), p.e327.

Martìn-Clemente, B. et al., 2004. alpha-Synuclein expression levels do not significantly affect proteasome function and expression in mice and stably transfected PC12 cell lines. *The Journal of biological chemistry*, 279(51), pp.52984–90.

Martinez-Vicente, M. et al., 2008. Dopamine-modified alpha-synuclein blocks chaperone-mediated autophagy. *The Journal of clinical investigation*, 118(2), pp.777–88.

Marx, F.P. et al., 2003. Identification and functional characterization of a novel R621C mutation in the synphilin-1 gene in Parkinson's disease. *Human molecular genetics*, 12(11), pp.1223–31.

Marx, F.P. et al., 2007. The proteasomal subunit S6 ATPase is a novel synphilin-1 interacting protein--implications for Parkinson's disease. *FASEB journal : official publication of the Federation of American Societies for Experimental Biology*, 21(8), pp.1759–67.

Maskri, L. et al., 2004. Influence of different promoters on the expression pattern of mutated human alpha-synuclein in transgenic mice. *Neuro-degenerative diseases*, 1(6), pp.255–65.

Masliah, E. et al., 2000. Dopaminergic loss and inclusion body formation in alpha-synuclein mice: implications for neurodegenerative disorders. *Science (New York, N.Y.)*, 287(5456), pp.1265–9.

Massey, A.C. et al., 2006. Consequences of the selective blockage of chaperone-mediated autophagy. *Proceedings of the National Academy of Sciences of the United States of America*, 103(15), pp.5805–10.

Massey, A.C., Kaushik, S. & Cuervo, A.M., Lysosomal chat maintains the balance. *Autophagy*,

2(4), pp.325–7.

Matsuoka, Y. et al., 2001. Lack of nigral pathology in transgenic mice expressing human alpha-synuclein driven by the tyrosine hydroxylase promoter. *Neurobiology of disease*, 8(3), pp.535–9.

Mbefo, M.K. et al., 2010. Phosphorylation of synucleins by members of the Polo-like kinase family. *The Journal of biological chemistry*, 285(4), pp.2807–22.

McCormack, A.L. et al., 2002. Environmental risk factors and Parkinson's disease: selective degeneration of nigral dopaminergic neurons caused by the herbicide paraquat. *Neurobiology of disease*, 10(2), pp.119–27.

McCormack, A.L. & Di Monte, D.A., 2003. Effects of L-dopa and other amino acids against paraquat-induced nigrostriatal degeneration. *Journal of neurochemistry*, 85(1), pp.82–6.

McGeer, P.L. & McGeer, E.G., 2004. Inflammation and the degenerative diseases of aging. *Annals of the New York Academy of Sciences*, 1035, pp.104–16.

McIlwain, K.L. et al., 2001. The use of behavioral test batteries: effects of training history. *Physiology & behavior*, 73(5), pp.705–17.

McLean, P.J. & Hyman, B.T., 2002. An alternatively spliced form of rodent alpha-synuclein forms intracellular inclusions in vitro: role of the carboxy-terminus in alpha-synuclein aggregation. *Neuroscience letters*, 323(3), pp.219–23.

McLean, P.J., Ribich, S. & Hyman, B.T., 2000. Subcellular localization of alpha-synuclein in primary neuronal cultures: effect of missense mutations. *Journal of neural transmission. Supplementum*, (58), pp.53–63.

McNaught, K.S. et al., 2001. Failure of the ubiquitin-proteasome system in Parkinson's disease. *Nature reviews. Neuroscience*, 2(8), pp.589–94.

McNaught, K.S.. & Jenner, P., 2001. Proteasomal function is impaired in substantia nigra in Parkinson's disease. *Neuroscience letters*, 297(3), pp.191–4.

McNaught, K.S.P., Shashidharan, P., et al., 2002. Aggresome-related biogenesis of Lewy bodies. *The European journal of neuroscience*, 16(11), pp.2136–48.

McNaught, K.S.P. et al., 2003. Altered proteasomal function in sporadic Parkinson's disease. *Experimental neurology*, 179(1), pp.38–46.

McNaught, K.S.P., Mytilineou, C., et al., 2002. Impairment of the ubiquitin-proteasome system causes dopaminergic cell death and inclusion body formation in ventral mesencephalic cultures. *Journal of neurochemistry*, 81(2), pp.301–6.

McNaught, K.S.P., Belizaire, R., et al., 2002. Selective loss of 20S proteasome alpha-subunits in the substantia nigra pars compacta in Parkinson's disease. *Neuroscience letters*, 326(3), pp.155–8.

McNaught, K.S.P. et al., 2004. Systemic exposure to proteasome inhibitors causes a progressive model of Parkinson's disease. *Annals of neurology*, 56(1), pp.149–62.

| Bibliography

Meredith, G.E., Sonsalla, P.K. & Chesselet, M.-F., 2008. Animal models of Parkinson's disease progression. *Acta neuropathologica*, 115(4), pp.385–98.

Meriin, A.B., Wang, Y. & Sherman, M.Y., 2010. Isolation of aggresomes and other large aggregates. *Current protocols in cell biology / editorial board, Juan S. Bonifacino ... [et al.]*, Chapter 3, p.Unit 3.38.1–9.

Miake, H. et al., 2002. Biochemical characterization of the core structure of alpha-synuclein filaments. *The Journal of biological chemistry*, 277(21), pp.19213–9.

Michell, A.W. et al., 2007. The effect of truncated human alpha-synuclein (1-120) on dopaminergic cells in a transgenic mouse model of Parkinson's disease. *Cell transplantation*, 16(5), pp.461–74.

Mijaljica, D., Prescott, M. & Devenish, R.J., 2011. Microautophagy in mammalian cells: revisiting a 40-year-old conundrum. *Autophagy*, 7(7), pp.673–82.

Milber, J.M. et al., 2012. Lewy pathology is not the first sign of degeneration in vulnerable neurons in Parkinson disease. *Neurology,* 79(24), pp.2307–14.

Miller, D.W. et al., 2004. Alpha-synuclein in blood and brain from familial Parkinson disease with SNCA locus triplication. *Neurology*, 62(10), pp.1835–8.

Mishizen-Eberz, A.J. et al., 2003. Distinct cleavage patterns of normal and pathologic forms of alpha-synuclein by calpain I in vitro. *Journal of neurochemistry*, 86(4), pp.836–47.

Mizuno, Y., Sone, N. & Saitoh, T., 1987. Effects of 1-methyl-4-phenyl-1,2,3,6-tetrahydropyridine and 1-methyl-4-phenylpyridinium ion on activities of the enzymes in the electron transport system in mouse brain. *Journal of neurochemistry*, 48(6), pp.1787–93.

Mizushima, N. et al., 2008. Autophagy fights disease through cellular self-digestion. *Nature*, 451(7182), pp.1069–75.

Moehle, M.S. et al., 2012. LRRK2 inhibition attenuates microglial inflammatory responses. *The Journal of neuroscience : the official journal of the Society for Neuroscience*, 32(5), pp.1602–11.

Moravec, R.A. et al., 2009. Cell-based bioluminescent assays for all three proteasome activities in a homogeneous format. *Analytical biochemistry*, 387(2), pp.294–302.

Moremen, K.W., Tiemeyer, M. & Nairn, A. V, 2012. Vertebrate protein glycosylation: diversity, synthesis and function. *Nature reviews. Molecular cell biology*, 13(7), pp.448–62.

Mori, F. et al., 2002. Immunohistochemical comparison of alpha- and beta-synuclein in adult rat central nervous system. *Brain research*, 941(1-2), pp.118–26.

Muangpaisan, W. et al., 2011. A systematic review of the worldwide prevalence and incidence of Parkinson's disease. *Journal of the Medical Association of Thailand = Chotmaihet thangphaet*, 94(6), pp.749–55.

Mullin, S. & Schapira, A., 2013. A-synuclein and mitochondrial dysfunction in Parkinson's disease. *Molecular neurobiology*, 47(2), pp.587–97.

Murphy, D.D. et al., 2000. Synucleins are developmentally expressed, and alpha-synuclein regulates the size of the presynaptic vesicular pool in primary hippocampal neurons. *The Journal of neuroscience : the official journal of the Society for Neuroscience*, 20(9), pp.3214–20.

Murray, I.J. et al., 2003. Synphilin in normal human brains and in synucleinopathies: studies with new antibodies. *Acta neuropathologica*, 105(2), pp.177–84.

Murray, I.V.J. et al., 2003. Role of alpha-synuclein carboxy-terminus on fibril formation in vitro. *Biochemistry*, 42(28), pp.8530–40.

Myhre, R. et al., 2008. Genetic association study of synphilin-1 in idiopathic Parkinson's disease. *BMC medical genetics*, 9, p.19.

Nagano, Y. et al., 2003. Siah-1 facilitates ubiquitination and degradation of synphilin-1. *The Journal of biological chemistry*, 278(51), pp.51504–14.

Nakabeppu, Y. et al., 2007. Oxidative damage in nucleic acids and Parkinson's disease. *Journal of neuroscience research*, 85(5), pp.919–34.

Nakajo, S. et al., 1993. A new brain-specific 14-kDa protein is a phosphoprotein. Its complete amino acid sequence and evidence for phosphorylation. *European journal of biochemistry / FEBS*, 217(3), pp.1057–63.

Nakajo, S. et al., 1990. Purification and characterization of a novel brain-specific 14-kDa protein. *Journal of neurochemistry*, 55(6), pp.2031–8.

Nakamura, T. et al., 2001. Activated Fyn phosphorylates alpha-synuclein at tyrosine residue 125. *Biochemical and biophysical research communications*, 280(4), pp.1085–92.

Nakamura, T. et al., 2002. Activation of Pyk2/RAFTK induces tyrosine phosphorylation of alpha-synuclein via Src-family kinases. *FEBS letters*, 521(1-3), pp.190–4.

Negro, A. et al., 2002. Multiple phosphorylation of alpha-synuclein by protein tyrosine kinase Syk prevents eosin-induced aggregation. *FASEB journal : official publication of the Federation of American Societies for Experimental Biology*, 16(2), pp.210–2.

Nemani, V.M. et al., 2010. Increased expression of alpha-synuclein reduces neurotransmitter release by inhibiting synaptic vesicle reclustering after endocytosis. *Neuron*, 65(1), pp.66–79.

Neumann, M. et al., 2002. Misfolded proteinase K-resistant hyperphosphorylated alpha-synuclein in aged transgenic mice with locomotor deterioration and in human alpha-synucleinopathies. *The Journal of clinical investigation*, 110(10), pp.1429–39.

Neuner, J. et al., 2014. A30P α-Synuclein interferes with the stable integration of adult-born neurons into the olfactory network. *Scientific reports*, 4(i), p.3931.

Nicklas, W.J., Vyas, I. & Heikkila, R.E., 1985. Inhibition of NADH-linked oxidation in brain mitochondria by 1-methyl-4-phenyl-pyridine, a metabolite of the neurotoxin, 1-methyl-4-phenyl-1,2,5,6-tetrahydropyridine. *Life sciences*, 36(26), pp.2503–8.

Noelker, C. et al., 2013. CNI-1493 attenuates neuroinflammation and dopaminergic

neurodegeneration in the acute MPTP mouse model of Parkinson's disease. *Neuro-degenerative diseases*, 12(2), pp.103–10.

Nonaka, T., Iwatsubo, T. & Hasegawa, M., 2005. Ubiquitination of alpha-synuclein. *Biochemistry*, 44(1), pp.361–8.

Nooren, I.M.A. & Thornton, J.M., 2003. Structural characterisation and functional significance of transient protein-protein interactions. *Journal of molecular biology*, 325(5), pp.991–1018.

Norris, E.H. et al., 2005. Reversible inhibition of alpha-synuclein fibrillization by dopaminochrome-mediated conformational alterations. *The Journal of biological chemistry*, 280(22), pp.21212–9.

Noyce, A.J. et al., 2012. Meta-analysis of early nonmotor features and risk factors for Parkinson disease. *Annals of neurology*, 72(6), pp.893–901.

Nuber, S. et al., 2013. A progressive dopaminergic phenotype associated with neurotoxic conversion of α-synuclein in BAC-transgenic rats. *Brain : a journal of neurology*, 136(Pt 2), pp.412–32.

Nuber, S. et al., 2008. Neurodegeneration and motor dysfunction in a conditional model of Parkinson's disease. *The Journal of neuroscience : the official journal of the Society for Neuroscience*, 28(10), pp.2471–84.

Nuber, S. et al., 2010. Transgenic overexpression of the alpha-synuclein interacting protein synphilin-1 leads to behavioral and neuropathological alterations in mice. *Neurogenetics*, 11(1), pp.107–20.

Nuytemans, K. et al., 2010. Genetic etiology of Parkinson disease associated with mutations in the SNCA, PARK2, PINK1, PARK7, and LRRK2 genes: a mutation update. *Human mutation*, 31(7), pp.763–80.

O'Farrell, C. et al., 2001. Transfected synphilin-1 forms cytoplasmic inclusions in HEK293 cells. *Brain research. Molecular brain research*, 97(1), pp.94–102.

O'Toole, E. et al., 2012. The role of γ-tubulin in centrosomal microtubule organization. *PloS one*, 7(1), p.e29795.

Ogawa, K. et al., 2000. Localization of a novel type trypsin-like serine protease, neurosin, in brain tissues of Alzheimer's disease and Parkinson's disease. *Psychiatry and clinical neurosciences*, 54(4), pp.419–26.

Ogawa, N. et al., 1985. A simple quantitative bradykinesia test in MPTP-treated mice. *Research communications in chemical pathology and pharmacology*, 50(3), pp.435–41.

Okochi, M. et al., 2000. Constitutive phosphorylation of the Parkinson's disease associated alpha-synuclein. *The Journal of biological chemistry*, 275(1), pp.390–7.

Olanow, C.W. et al., 2004. Lewy-body formation is an aggresome-related process: a hypothesis. *Lancet neurology*, 3(8), pp.496–503.

Ono, Y. & Sorimachi, H., 2012. Calpains: an elaborate proteolytic system. *Biochimica et*

biophysica acta, 1824(1), pp.224–36.

Orenstein, S.J. et al., 2013. Interplay of LRRK2 with chaperone-mediated autophagy. *Nature neuroscience*, 16(4), pp.394–406.

Orlowski, D. & Bjarkam, C.R., 2012. A simple reproducible and time saving method of semi-automatic dendrite spine density estimation compared to manual spine counting. *Journal of neuroscience methods*, 208(2), pp.128–33.

Oueslati, A. et al., 2012. Mimicking phosphorylation at serine 87 inhibits the aggregation of human α-synuclein and protects against its toxicity in a rat model of Parkinson's disease. *The Journal of neuroscience : the official journal of the Society for Neuroscience*, 32(5), pp.1536–44.

Oueslati, A., Fournier, M. & Lashuel, H. a, 2010. *Role of post-translational modifications in modulating the structure, function and toxicity of alpha-synuclein: implications for Parkinson's disease pathogenesis and therapies.*, Elsevier B.V.

Outeiro, T.F. et al., 2006. Small heat shock proteins protect against alpha-synuclein-induced toxicity and aggregation. *Biochemical and biophysical research communications*, 351(3), pp.631–8.

Padmaraju, V. et al., 2011. Role of advanced glycation on aggregation and DNA binding properties of α-synuclein. *Journal of Alzheimer's disease : JAD*, 24 Suppl 2, pp.211–21.

Pakkenberg, B. et al., 1991. The absolute number of nerve cells in substantia nigra in normal subjects and in patients with Parkinson's disease estimated with an unbiased stereological method. *Journal of neurology, neurosurgery, and psychiatry*, 54(1), pp.30–3.

Paleologou, K.E. et al., 2009. Detection of elevated levels of soluble alpha-synuclein oligomers in post-mortem brain extracts from patients with dementia with Lewy bodies. *Brain : a journal of neurology*, 132(Pt 4), pp.1093–101.

Paleologou, K.E. et al., 2010. Phosphorylation at S87 is enhanced in synucleinopathies, inhibits alpha-synuclein oligomerization, and influences synuclein-membrane interactions. *The Journal of neuroscience : the official journal of the Society for Neuroscience*, 30(9), pp.3184–98.

Paleologou, K.E. et al., 2008. Phosphorylation at Ser-129 but not the phosphomimics S129E/D inhibits the fibrillation of alpha-synuclein. *The Journal of biological chemistry*, 283(24), pp.16895–905.

Palikaras, K. & Tavernarakis, N., 2012. Mitophagy in neurodegeneration and aging. *Frontiers in genetics*, 3, p.297.

Pandey, U.B. et al., 2007. HDAC6 rescues neurodegeneration and provides an essential link between autophagy and the UPS. *Nature*, 447(7146), pp.859–63.

Pankiv, S. et al., 2007. p62/SQSTM1 binds directly to Atg8/LC3 to facilitate degradation of ubiquitinated protein aggregates by autophagy. *The Journal of biological chemistry*, 282(33), pp.24131–45.

| Bibliography

Pankratz, N. et al., 2006. Mutations in DJ-1 are rare in familial Parkinson disease. *Neuroscience letters*, 408(3), pp.209–13.

Papay, R. et al., 2002. Mice expressing the alpha(1B)-adrenergic receptor induces a synucleinopathy with excessive tyrosine nitration but decreased phosphorylation. *Journal of neurochemistry*, 83(3), pp.623–34.

Parihar, M.S. et al., 2009. Alpha-synuclein overexpression and aggregation exacerbates impairment of mitochondrial functions by augmenting oxidative stress in human neuroblastoma cells. *The international journal of biochemistry & cell biology*, 41(10), pp.2015–24.

Parihar, M.S. et al., 2008. Mitochondrial association of alpha-synuclein causes oxidative stress. *Cellular and molecular life sciences : CMLS*, 65(7-8), pp.1272–84.

Park, H.H., 2013. Structural basis of membrane trafficking by rab family small g protein. *International journal of molecular sciences*, 14(5), pp.8912–23.

Parkinson, J., 1817. An essay on the shaking palsy. *London: Sherwood, Neely, and Jones*.

Parrao, T. et al., 2012. Olfactory deficits and cognitive dysfunction in Parkinson's disease. *Neuro-degenerative diseases*, 10(1-4), pp.179–82.

Paterna, J.-C. et al., 2007. DJ-1 and Parkin modulate dopamine-dependent behavior and inhibit MPTP-induced nigral dopamine neuron loss in mice. *Molecular therapy : the journal of the American Society of Gene Therapy*, 15(4), pp.698–704.

Patt, S. et al., 1991. Pathological changes in dendrites of substantia nigra neurons in Parkinson's disease: a Golgi study. *Histology and histopathology*, 6(3), pp.373–80.

Paxinou, E. et al., 2001. Induction of alpha-synuclein aggregation by intracellular nitrative insult. *The Journal of neuroscience : the official journal of the Society for Neuroscience*, 21(20), pp.8053–61.

Payton, J.E. et al., 2004. Structural determinants of PLD2 inhibition by alpha-synuclein. *Journal of molecular biology*, 337(4), pp.1001–9.

Pearce, J.M., 1989. Aspects of the history of Parkinson's disease. *Journal of neurology, neurosurgery, and psychiatry*, Suppl(20), pp.6–10.

Peng, X. et al., 2005. Alpha-synuclein activation of protein phosphatase 2A reduces tyrosine hydroxylase phosphorylation in dopaminergic cells. *Journal of cell science*, 118(Pt 15), pp.3523–30.

Perez, F.A., Curtis, W.R. & Palmiter, R.D., 2005. Parkin-deficient mice are not more sensitive to 6-hydroxydopamine or methamphetamine neurotoxicity. *BMC neuroscience*, 6, p.71.

Perez, R.G. et al., 2002. A role for alpha-synuclein in the regulation of dopamine biosynthesis. *The Journal of neuroscience : the official journal of the Society for Neuroscience*, 22(8), pp.3090–9.

Perrin, R.J. et al., 2001. Exposure to long chain polyunsaturated fatty acids triggers rapid multimerization of synucleins. *The Journal of biological chemistry*, 276(45), pp.41958–62.

Perry, V.H., 2012. Innate inflammation in Parkinson's disease. *Cold Spring Harbor perspectives in medicine*, 2(9), p.a009373.

Petrucelli, L. et al., 2002. Parkin protects against the toxicity associated with mutant alpha-synuclein: proteasome dysfunction selectively affects catecholaminergic neurons. *Neuron*, 36(6), pp.1007–19.

Phillips, N.J., Reay, J. & Martyn, C.N., 1999. Validity of mortality data for Parkinson's disease. *Journal of epidemiology and community health*, 53(9), pp.587–8.

Piccini, P. & Brooks, D.J., 2006. New developments of brain imaging for Parkinson's disease and related disorders. *Movement disorders : official journal of the Movement Disorder Society*, 21(12), pp.2035–41.

Picconi, B., Piccoli, G. & Calabresi, P., 2012. Synaptic dysfunction in Parkinson's disease. *Advances in experimental medicine and biology*, 970, pp.553–72.

Pickart, C.M. & Fushman, D., 2004. Polyubiquitin chains: polymeric protein signals. *Current opinion in chemical biology*, 8(6), pp.610–6.

Pihlstrøm, L. & Toft, M., 2011. Genetic variability in SNCA and Parkinson's disease. *Neurogenetics*, 12(4), pp.283–93.

Polymeropoulos, M.H. et al., 1997. Mutation in the alpha-synuclein gene identified in families with Parkinson's disease. *Science (New York, N.Y.)*, 276(5321), pp.2045–7.

Portal, E., Riess, O. & Nguyen, H.P., 2013. Automated home cage assessment shows behavioral changes in a transgenic mouse model of spinocerebellar ataxia type 17. *Behavioural brain research*, 250, pp.157–65.

Pountney, D.L., Voelcker, N.H. & Gai, W.P., 2005. Annular alpha-synuclein oligomers are potentially toxic agents in alpha-synucleinopathy. Hypothesis. *Neurotoxicity research*, 7(1-2), pp.59–67.

Pramstaller, P.P. et al., 2005. Lewy body Parkinson's disease in a large pedigree with 77 Parkin mutation carriers. *Annals of neurology*, 58(3), pp.411–22.

Prasad, K. et al., 2011. Automation of immunohistochemical evaluation in breast cancer using image analysis. *World journal of clinical oncology*, 2(4), pp.187–94.

Pronin, A.N. et al., 2000. Synucleins are a novel class of substrates for G protein-coupled receptor kinases. *The Journal of biological chemistry*, 275(34), pp.26515–22.

Proukakis, C. et al., 2013. A novel α-synuclein missense mutation in parkinson disease. *Neurology*, 80(11), pp.1062–4.

Van der Putten, H. et al., 2000. Neuropathology in mice expressing human alpha-synuclein. *The Journal of neuroscience : the official journal of the Society for Neuroscience*, 20(16), pp.6021–9.

Qiao, L. et al., 2008. Lysosomal enzyme cathepsin D protects against alpha-synuclein aggregation and toxicity. *Molecular brain*, 1, p.17.

| Bibliography

Qing, H. et al., 2009. Lrrk2 phosphorylates alpha synuclein at serine 129: Parkinson disease implications. *Biochemical and biophysical research communications*, 387(1), pp.149–52.

Qu, X. et al., 2003. Promotion of tumorigenesis by heterozygous disruption of the beclin 1 autophagy gene. *The Journal of clinical investigation*, 112(12), pp.1809–20.

R Development Core Team, R., 2008. *Computational Many-Particle Physics* H. Fehske, R. Schneider, & A. Weiße, eds., Berlin, Heidelberg: Springer Berlin Heidelberg.

Ramirez, A. et al., 2006. Hereditary parkinsonism with dementia is caused by mutations in ATP13A2, encoding a lysosomal type 5 P-type ATPase. *Nature genetics*, 38(10), pp.1184–91.

Ramonet, D. et al., 2011. Dopaminergic neuronal loss, reduced neurite complexity and autophagic abnormalities in transgenic mice expressing G2019S mutant LRRK2. *PloS one*, 6(4), p.e18568.

Rathke-Hartlieb, S. et al., 2001. Sensitivity to MPTP is not increased in Parkinson's disease-associated mutant alpha-synuclein transgenic mice. *Journal of neurochemistry*, 77(4), pp.1181–4.

Reichmann, H., 2010. Clinical criteria for the diagnosis of Parkinson's disease. *Neuro-degenerative diseases*, 7(5), pp.284–90.

Ribeiro, C.S. et al., 2002. Synphilin-1 is developmentally localized to synaptic terminals, and its association with synaptic vesicles is modulated by alpha-synuclein. *The Journal of biological chemistry*, 277(26), pp.23927–33.

Richardson, J.R. et al., 2005. Paraquat neurotoxicity is distinct from that of MPTP and rotenone. *Toxicological sciences : an official journal of the Society of Toxicology*, 88(1), pp.193–201.

Richfield, E.K. et al., 2002. Behavioral and neurochemical effects of wild-type and mutated human alpha-synuclein in transgenic mice. *Experimental neurology*, 175(1), pp.35–48.

Rideout, H.J., Lang-Rollin, I. & Stefanis, L., 2004. Involvement of macroautophagy in the dissolution of neuronal inclusions. *The international journal of biochemistry & cell biology*, 36(12), pp.2551–62.

Rideout, H.J. & Stefanis, L., 2002. Proteasomal inhibition-induced inclusion formation and death in cortical neurons require transcription and ubiquitination. *Molecular and cellular neurosciences*, 21(2), pp.223–38.

Rieker, C. et al., 2011. Neuropathology in mice expressing mouse alpha-synuclein. K. M. Iijima, ed. *PLoS ONE*, 6(9), p.e24834.

Riley, B.E. et al., 2013. Structure and function of Parkin E3 ubiquitin ligase reveals aspects of RING and HECT ligases. *Nature communications*, 4, p.1982.

Ritchie, C.M. & Thomas, P.J., 2012. Alpha-synuclein truncation and disease. *Health*, 04(11), pp.1167–1177.

Rockenstein, E. et al., 2002. Differential neuropathological alterations in transgenic mice

expressing alpha-synuclein from the platelet-derived growth factor and Thy-1 promoters. *Journal of neuroscience research*, 68(5), pp.568–78.

Rockenstein, E. et al., 2005. Lysosomal pathology associated with alpha-synuclein accumulation in transgenic models using an eGFP fusion protein. *Journal of neuroscience research*, 80(2), pp.247–59.

Rogaeva, E. et al., 2004. Analysis of the PINK1 gene in a large cohort of cases with Parkinson disease. *Archives of neurology*, 61(12), pp.1898–904.

Rogers, D.C. et al., 1997. Behavioral and functional analysis of mouse phenotype: SHIRPA, a proposed protocol for comprehensive phenotype assessment. *Mammalian genome : official journal of the International Mammalian Genome Society*, 8(10), pp.711–3.

Ross, C.A. & Poirier, M.A., 2004. Protein aggregation and neurodegenerative disease. *Nature medicine*, 10 Suppl, pp.S10–7.

Rothman, S.M. et al., 2013. Neuronal expression of familial Parkinson's disease A53T α-synuclein causes early motor impairment, reduced anxiety and potential sleep disturbances in mice. *Journal of Parkinson's disease*, 3(2), pp.215–29.

Rott, R. et al., 2008. Monoubiquitylation of alpha-synuclein by seven in absentia homolog (SIAH) promotes its aggregation in dopaminergic cells. *The Journal of biological chemistry*, 283(6), pp.3316–28.

Rott, R. et al., 2011. α-Synuclein fate is determined by USP9X-regulated monoubiquitination. *Proceedings of the National Academy of Sciences of the United States of America*, 108(46), pp.18666–71.

Rousseaux, M.W.C. et al., 2012. Progressive dopaminergic cell loss with unilateral-to-bilateral progression in a genetic model of Parkinson disease. *Proceedings of the National Academy of Sciences of the United States of America*, 109(39), pp.15918–23.

Roy, S. & Wolman, L., 1969. Ultrastructural observations in Parkinsonism. *The Journal of pathology*, 99(1), pp.39–44.

Rozas, G. et al., 1998. The overall rod performance test in the MPTP-treated-mouse model of Parkinsonism. *Journal of neuroscience methods*, 83(2), pp.165–75.

Safran, M. et al., 2003. Human Gene-Centric Databases at the Weizmann Institute of Science: GeneCards, UDB, CroW 21 and HORDE. *Nucleic acids research*, 31(1), pp.142–6.

Saigoh, K. et al., 1999. Intragenic deletion in the gene encoding ubiquitin carboxy-terminal hydrolase in gad mice. *Nature genetics*, 23(1), pp.47–51.

Saito, Y. et al., 2003. Accumulation of phosphorylated alpha-synuclein in aging human brain. *Journal of neuropathology and experimental neurology*, 62(6), pp.644–54.

Sakamoto, M. et al., 2009. Contribution of endogenous G-protein-coupled receptor kinases to Ser129 phosphorylation of alpha-synuclein in HEK293 cells. *Biochemical and biophysical research communications*, 384(3), pp.378–82.

| Bibliography

Sampaio-Marques, B. et al., 2012. SNCA (α-synuclein)-induced toxicity in yeast cells is dependent on sirtuin 2 (Sir2)-mediated mitophagy. *Autophagy*, 8(10), pp.1494–509.

Sampathu, D.M. et al., 2003. Ubiquitination of alpha-synuclein is not required for formation of pathological inclusions in alpha-synucleinopathies. *The American journal of pathology*, 163(1), pp.91–100.

Saner, A. & Thoenen, H., 1971. Model experiments on the molecular mechanism of action of 6-hydroxydopamine. *Molecular pharmacology*, 7(2), pp.147–54.

Santens, P. et al., 2003. The pathophysiology of motor symptoms in Parkinson's disease. *Acta neurologica Belgica*, 103(3), pp.129–34.

Sato, H., Kato, T. & Arawaka, S., 2013. The role of Ser129 phosphorylation of α-synuclein in neurodegeneration of Parkinson's disease: a review of in vivo models. *Reviews in the neurosciences*, 24(2), pp.115–23.

Sauer, B., 1987. Functional expression of the cre-lox site-specific recombination system in the yeast Saccharomyces cerevisiae. *Molecular and cellular biology*, 7(6), pp.2087–96.

Schell, H. et al., 2009. Nuclear and neuritic distribution of serine-129 phosphorylated alpha-synuclein in transgenic mice. *Neuroscience*, 160(4), pp.796–804.

Schneider, A. & Simons, M., 2013. Exosomes: vesicular carriers for intercellular communication in neurodegenerative disorders. *Cell and tissue research*, 352(1), pp.33–47.

Scholz, S.W. et al., 2012. Genomics and bioinformatics of Parkinson's disease. *Cold Spring Harbor perspectives in medicine*, 2(7), p.a009449.

Schulz-Schaeffer, W.J. et al., 2000. The paraffin-embedded tissue blot detects PrP(Sc) early in the incubation time in prion diseases. *The American journal of pathology*, 156(1), pp.51–6.

Schulz-Schaeffer, W.J., 2010. The synaptic pathology of alpha-synuclein aggregation in dementia with Lewy bodies, Parkinson's disease and Parkinson's disease dementia. *Acta neuropathologica*, 120(2), pp.131–43.

Scott, D.A. et al., 2010. A pathologic cascade leading to synaptic dysfunction in alpha-synuclein-induced neurodegeneration. *The Journal of neuroscience : the official journal of the Society for Neuroscience*, 30(24), pp.8083–95.

Segrest, J.P. et al., 1992. The amphipathic helix in the exchangeable apolipoproteins: a review of secondary structure and function. *Journal of lipid research*, 33(2), pp.141–66.

Seidel, K. et al., 2010. First appraisal of brain pathology owing to A30P mutant alpha-synuclein. *Annals of neurology*, 67(5), pp.684–9.

Serpell, L.C. et al., 2000. Fiber diffraction of synthetic alpha-synuclein filaments shows amyloid-like cross-beta conformation. *Proceedings of the National Academy of Sciences of the United States of America*, 97(9), pp.4897–902.

Setsuie, R. et al., 2007. Dopaminergic neuronal loss in transgenic mice expressing the

Parkinson's disease-associated UCH-L1 I93M mutant. *Neurochemistry international*, 50(1), pp.119–29.

Sevlever, D., Jiang, P. & Yen, S.-H.C., 2008. Cathepsin D is the main lysosomal enzyme involved in the degradation of alpha-synuclein and generation of its carboxy-terminally truncated species. *Biochemistry*, 47(36), pp.9678–87.

Shaikh, S. & Nicholson, L.F.B., 2008. Advanced glycation end products induce in vitro cross-linking of alpha-synuclein and accelerate the process of intracellular inclusion body formation. *Journal of neuroscience research*, 86(9), pp.2071–82.

Sharon, R. et al., 2001. alpha-Synuclein occurs in lipid-rich high molecular weight complexes, binds fatty acids, and shows homology to the fatty acid-binding proteins. *Proceedings of the National Academy of Sciences of the United States of America*, 98(16), pp.9110–5.

Sharon, R. et al., 2003. The formation of highly soluble oligomers of alpha-synuclein is regulated by fatty acids and enhanced in Parkinson's disease. *Neuron*, 37(4), pp.583–95.

Shibasaki, Y. et al., 1995. High-resolution mapping of SNCA encoding alpha-synuclein, the non-A beta component of Alzheimer's disease amyloid precursor, to human chromosome 4q21.3-->q22 by fluorescence in situ hybridization. *Cytogenetics and cell genetics*, 71(1), pp.54–5.

Shibayama-Imazu, T. et al., 1993. Cell and tissue distribution and developmental change of neuron specific 14 kDa protein (phosphoneuroprotein 14). *Brain research*, 622(1-2), pp.17–25.

Shimizu, K. et al., 2001. Carrier-mediated processes in blood--brain barrier penetration and neural uptake of paraquat. *Brain research*, 906(1-2), pp.135–42.

Shimshek, D.R. et al., 2012. Excess α-synuclein worsens disease in mice lacking ubiquitin carboxy-terminal hydrolase L1. *Scientific reports*, 2, p.262.

Shimura, H. et al., 2001. Ubiquitination of a new form of alpha-synuclein by parkin from human brain: implications for Parkinson's disease. *Science (New York, N.Y.)*, 293(5528), pp.263–9.

Shin, J.-H. et al., 2011. PARIS (ZNF746) repression of PGC-1α contributes to neurodegeneration in Parkinson's disease. *Cell*, 144(5), pp.689–702.

Shiotsuki, H. et al., 2010. A rotarod test for evaluation of motor skill learning. *Journal of neuroscience methods*, 189(2), pp.180–5.

Shortle, D., 1996. The denatured state (the other half of the folding equation) and its role in protein stability. *FASEB journal : official publication of the Federation of American Societies for Experimental Biology*, 10(1), pp.27–34.

Shults, C.W., 2006. Lewy bodies. *Proceedings of the National Academy of Sciences of the United States of America*, 103(6), pp.1661–8.

Sidhu, A., Wersinger, C. & Vernier, P., 2004. alpha-Synuclein regulation of the dopaminergic transporter: a possible role in the pathogenesis of Parkinson's disease. *FEBS letters*,

| Bibliography

565(1-3), pp.1–5.

Singleton, A.B. et al., 2003. alpha-Synuclein locus triplication causes Parkinson's disease. *Science (New York, N.Y.)*, 302(5646), p.841.

Smith, L.H. & DeMyer, W.E., 2003. Anatomy of the brainstem. *Seminars in pediatric neurology*, 10(4), pp.235–40.

Smith, W.W. et al., 2005. Alpha-synuclein phosphorylation enhances eosinophilic cytoplasmic inclusion formation in SH-SY5Y cells. *The Journal of neuroscience : the official journal of the Society for Neuroscience*, 25(23), pp.5544–52.

Smith, W.W. et al., 2010. Synphilin-1 attenuates neuronal degeneration in the A53T alpha-synuclein transgenic mouse model. *Human molecular genetics*, 19(11), pp.2087–98.

Snyder, H. et al., 2003. Aggregated and monomeric alpha-synuclein bind to the S6' proteasomal protein and inhibit proteasomal function. *The Journal of biological chemistry*, 278(14), pp.11753–9.

Snyder, H. et al., 2005. beta-Synuclein reduces proteasomal inhibition by alpha-synuclein but not gamma-synuclein. *The Journal of biological chemistry*, 280(9), pp.7562–9.

Snyder, S.H. & D'Amato, R.J., Predicting Parkinson's disease. *Nature*, 317(6034), pp.198–9.

Song, D.D. et al., 2004. Enhanced substantia nigra mitochondrial pathology in human alpha-synuclein transgenic mice after treatment with MPTP. *Experimental neurology*, 186(2), pp.158–72.

Soto, C., 2003. Unfolding the role of protein misfolding in neurodegenerative diseases. *Nature reviews. Neuroscience*, 4(1), pp.49–60.

Souza, J.M., Giasson, B.I., Lee, V.M., et al., 2000. Chaperone-like activity of synucleins. *FEBS letters*, 474(1), pp.116–9.

Souza, J.M., Giasson, B.I., Chen, Q., et al., 2000. Dityrosine cross-linking promotes formation of stable alpha -synuclein polymers. Implication of nitrative and oxidative stress in the pathogenesis of neurodegenerative synucleinopathies. *The Journal of biological chemistry*, 275(24), pp.18344–9.

Spencer, B. et al., 2009. Beclin 1 gene transfer activates autophagy and ameliorates the neurodegenerative pathology in alpha-synuclein models of Parkinson's and Lewy body diseases. *The Journal of neuroscience : the official journal of the Society for Neuroscience*, 29(43), pp.13578–88.

Spillantini, M.G. et al., 1998. alpha-Synuclein in filamentous inclusions of Lewy bodies from Parkinson's disease and dementia with lewy bodies. *Proceedings of the National Academy of Sciences of the United States of America*, 95(11), pp.6469–73.

Spillantini, M.G. et al., 1997. Alpha-synuclein in Lewy bodies. *Nature*, 388(6645), pp.839–40.

St Martin, J.L. et al., 2007. Dopaminergic neuron loss and up-regulation of chaperone protein mRNA induced by targeted over-expression of alpha-synuclein in mouse substantia nigra. *Journal of neurochemistry*, 100(6), pp.1449–57.

Stanley, J.L. et al., 2005. The mouse beam walking assay offers improved sensitivity over the mouse rotarod in determining motor coordination deficits induced by benzodiazepines. *Journal of psychopharmacology (Oxford, England)*, 19(3), pp.221–7.

Stefanis, L. et al., 2001. Expression of A53T mutant but not wild-type alpha-synuclein in PC12 cells induces alterations of the ubiquitin-dependent degradation system, loss of dopamine release, and autophagic cell death. *The Journal of neuroscience : the official journal of the Society for Neuroscience*, 21(24), pp.9549–60.

Stefanis, L., 2012. α-Synuclein in Parkinson's Disease. *Cold Spring Harbor perspectives in medicine*, 2(2), p.a009399.

Stern, G., 1989. Did parkinsonism occur before 1817? *Journal of neurology, neurosurgery, and psychiatry*, Suppl(20), pp.11–2.

Südhof, T.C. & Rizo, J., 2011. Synaptic vesicle exocytosis. *Cold Spring Harbor perspectives in biology*, 3(12).

Sun, A., Nguyen, X. V. & Bing, G., 2002. Comparative Analysis of an Improved Thioflavin-S Stain, Gallyas Silver Stain, and Immunohistochemistry for Neurofibrillary Tangle Demonstration on the Same Sections. *Journal of Histochemistry & Cytochemistry*, 50(4), pp.463–472.

Sung, J.Y. et al., 2005. Proteolytic cleavage of extracellular secreted {alpha}-synuclein via matrix metalloproteinases. *The Journal of biological chemistry*, 280(26), pp.25216–24.

Surguchov, A., 2008. Molecular and cellular biology of synucleins. *International review of cell and molecular biology*, 270(08), pp.225–317.

Surguchov, A. et al., 1999. Synoretin--A new protein belonging to the synuclein family. *Molecular and cellular neurosciences*, 13(2), pp.95–103.

Szargel, R. et al., 2009. Synphilin-1A inhibits seven in absentia homolog (SIAH) and modulates alpha-synuclein monoubiquitylation and inclusion formation. *The Journal of biological chemistry*, 284(17), pp.11706–16.

Taft, R.A., Davisson, M. & Wiles, M. V, 2006. Know thy mouse. *Trends in genetics : TIG*, 22(12), pp.649–53.

Takahashi, T. et al., 2006. Interactions of Synphilin-1 with phospholipids and lipid membranes. *FEBS letters*, 580(18), pp.4479–84.

Takahashi, T. et al., 2002. Tyrosine 125 of alpha-synuclein plays a critical role for dimerization following nitrative stress. *Brain research*, 938(1-2), pp.73–80.

Takalo, M. et al., 2013. Protein aggregation and degradation mechanisms in neurodegenerative diseases. *American journal of neurodegenerative disease*, 2(1), pp.1–14.

Takeuchi, M. & Yamagishi, S., 2009. Involvement of toxic AGEs (TAGE) in the pathogenesis of diabetic vascular complications and Alzheimer's disease. *Journal of Alzheimer's disease : JAD*, 16(4), pp.845–58.

| Bibliography

Tanaka, M. et al., 2004. Aggresomes formed by alpha-synuclein and synphilin-1 are cytoprotective. *The Journal of biological chemistry*, 279(6), pp.4625–31.

Tanaka, Y. et al., 2001. Inducible expression of mutant alpha-synuclein decreases proteasome activity and increases sensitivity to mitochondria-dependent apoptosis. *Human molecular genetics*, 10(9), pp.919–26.

Tanida, I., Ueno, T. & Kominami, E., 2008. LC3 and Autophagy. *Methods in molecular biology (Clifton, N.J.)*, 445, pp.77–88.

Tanji, K. et al., 2011. Alteration of autophagosomal proteins (LC3, GABARAP and GATE-16) in Lewy body disease. *Neurobiology of disease*, 43(3), pp.690–7.

Tanji, K. et al., 2003. Glycogen synthase kinase-3beta phosphorylates synphilin-1 in vitro. *Neuropathology : official journal of the Japanese Society of Neuropathology*, 23(3), pp.199–202.

Tanji, K. et al., 2010. Proteinase K-resistant alpha-synuclein is deposited in presynapses in human Lewy body disease and A53T alpha-synuclein transgenic mice. *Acta neuropathologica*, 120(2), pp.145–54.

Taylor, C.R. & Levenson, R.M., 2006. Quantification of immunohistochemistry--issues concerning methods, utility and semiquantitative assessment II. *Histopathology*, 49(4), pp.411–24.

Tecott, L.H. & Nestler, E.J., 2004. Neurobehavioral assessment in the information age. *Nature neuroscience*, 7(5), pp.462–6.

Thakur, P. & Nehru, B., 2013. Anti-inflammatory properties rather than anti-oxidant capability is the major mechanism of neuroprotection by sodium salicylate in a chronic rotenone model of Parkinson's disease. *Neuroscience*, 231, pp.420–31.

Thayanidhi, N. et al., 2010. Alpha-synuclein delays endoplasmic reticulum (ER)-to-Golgi transport in mammalian cells by antagonizing ER/Golgi SNAREs. *Molecular biology of the cell*, 21(11), pp.1850–63.

Thiruchelvam, M. et al., 2003. Age-related irreversible progressive nigrostriatal dopaminergic neurotoxicity in the paraquat and maneb model of the Parkinson's disease phenotype. *The European journal of neuroscience*, 18(3), pp.589–600.

Thiruchelvam, M. et al., 2000. The nigrostriatal dopaminergic system as a preferential target of repeated exposures to combined paraquat and maneb: implications for Parkinson's disease. *The Journal of neuroscience : the official journal of the Society for Neuroscience*, 20(24), pp.9207–14.

Thoenen, H. & Tranzer, J.P., 1968. Chemical sympathectomy by selective destruction of adrenergic nerve endings with 6-Hydroxydopamine. *Naunyn-Schmiedebergs Archiv für experimentelle Pathologie und Pharmakologie*, 261(3), pp.271–88.

Thomas, B. et al., 2007. MPTP and DSP-4 susceptibility of substantia nigra and locus coeruleus catecholaminergic neurons in mice is independent of parkin activity. *Neurobiology of disease*, 26(2), pp.312–22.

Thomas, B. & Beal, M.F., 2007. Parkinson's disease. *Human molecular genetics*, 16 Spec No, pp.R183–94.

Tieu, K., 2011. A guide to neurotoxic animal models of Parkinson's disease. *Cold Spring Harbor perspectives in medicine*, 1(1), p.a009316.

Todde, V., Veenhuis, M. & van der Klei, I.J., 2009. Autophagy: principles and significance in health and disease. *Biochimica et biophysica acta*, 1792(1), pp.3–13.

Tofaris, G.K. et al., 2011. Ubiquitin ligase Nedd4 promotes alpha-synuclein degradation by the endosomal-lysosomal pathway. *Proceedings of the National Academy of Sciences of the United States of America*, 108(41), pp.17004–9.

Tofaris, G.K. et al., 2003. Ubiquitination of alpha-synuclein in Lewy bodies is a pathological event not associated with impairment of proteasome function. *The Journal of biological chemistry*, 278(45), pp.44405–11.

Tofaris, G.K., Layfield, R. & Spillantini, M.G., 2001. alpha-synuclein metabolism and aggregation is linked to ubiquitin-independent degradation by the proteasome. *FEBS letters*, 509(1), pp.22–6.

Tomás-Zapico, C. et al., 2012. α-Synuclein accumulates in huntingtin inclusions but forms independent filaments and its deficiency attenuates early phenotype in a mouse model of Huntington's disease. *Human molecular genetics*, 21(3), pp.495–510.

Tompkins, M.M. et al., 2003. Alpha-synuclein expression localizes to the Golgi apparatus in bovine adrenal medullary chromaffin cells. *Brain research*, 984(1-2), pp.233–6.

Tompkins, M.M. & Hill, W.D., 1997. Contribution of somal Lewy bodies to neuronal death. *Brain research*, 775(1-2), pp.24–9.

Tong, Y. et al., 2010. Loss of leucine-rich repeat kinase 2 causes impairment of protein degradation pathways, accumulation of alpha-synuclein, and apoptotic cell death in aged mice. *Proceedings of the National Academy of Sciences of the United States of America*, 107(21), pp.9879–84.

Tranzer, J.P. & Thoenen, H., 1973. Selective destruction of adrenergic nerve terminals by chemical analogues of 6-hydroxydopamine. *Experientia*, 29(3), pp.314–5.

Trifunovic, A. & Larsson, N.-G., 2008. Mitochondrial dysfunction as a cause of ageing. *Journal of internal medicine*, 263(2), pp.167–78.

Trinh, J. & Farrer, M., 2013. Advances in the genetics of Parkinson disease. *Nature reviews. Neurology*, 9(8), pp.445–454.

Trojanowski, J.Q. & Lee, V.M., 1998. Aggregation of neurofilament and alpha-synuclein proteins in Lewy bodies: implications for the pathogenesis of Parkinson disease and Lewy body dementia. *Archives of neurology*, 55(2), pp.151–2.

Tsai, Y.-C. et al., 2012. The Guanine nucleotide exchange factor kalirin-7 is a novel synphilin-1 interacting protein and modifies synphilin-1 aggregate transport and formation. *PloS one*, 7(12), p.e51999.

| Bibliography

Tufekci, K.U. et al., 2012. Inflammation in Parkinson's disease. *Advances in protein chemistry and structural biology*, 88(null), pp.69–132.

Tyedmers, J., Mogk, A. & Bukau, B., 2010. Cellular strategies for controlling protein aggregation. *Nature reviews. Molecular cell biology*, 11(11), pp.777–88.

Uchihara, T., 2007. Silver diagnosis in neuropathology: principles, practice and revised interpretation. *Acta neuropathologica*, 113(5), pp.483–99.

Uéda, K. et al., 1993. Molecular cloning of cDNA encoding an unrecognized component of amyloid in Alzheimer disease. *Proceedings of the National Academy of Sciences of the United States of America*, 90(23), pp.11282–6.

Uéda, K., Saitoh, T. & Mori, H., 1994. Tissue-dependent alternative splicing of mRNA for NACP, the precursor of non-A beta component of Alzheimer's disease amyloid. *Biochemical and biophysical research communications*, 205(2), pp.1366–72.

Ullman, O., Fisher, C.K. & Stultz, C.M., 2011. Explaining the structural plasticity of α-synuclein. *Journal of the American Chemical Society*, 133(48), pp.19536–46.

Unni, V.K. et al., 2010. In vivo imaging of alpha-synuclein in mouse cortex demonstrates stable expression and differential subcellular compartment mobility. *PloS one*, 5(5), p.e10589.

Uversky, V.N., Li, J., et al., 2002. Biophysical properties of the synucleins and their propensities to fibrillate: inhibition of alpha-synuclein assembly by beta- and gamma-synucleins. *The Journal of biological chemistry*, 277(14), pp.11970–8.

Uversky, V.N., Yamin, G., et al., 2002. Methionine oxidation inhibits fibrillation of human alpha-synuclein in vitro. *FEBS letters*, 517(1-3), pp.239–44.

Uversky, V.N., Li, J. & Fink, A.L., 2001. Metal-triggered structural transformations, aggregation, and fibrillation of human alpha-synuclein. A possible molecular NK between Parkinson's disease and heavy metal exposure. *The Journal of biological chemistry*, 276(47), pp.44284–96.

Valente, E.M. et al., 2004. Hereditary early-onset Parkinson's disease caused by mutations in PINK1. *Science (New York, N.Y.)*, 304(5674), pp.1158–60.

Vallet, P.G. et al., 1992. A comparative study of histological and immunohistochemical methods for neurofibrillary tangles and senile plaques in Alzheimer's disease. *Acta neuropathologica*, 83(2), pp.170–8.

Varkey, J. et al., 2013. α-Synuclein oligomers with broken helical conformation form lipoprotein nanoparticles. *The Journal of biological chemistry*, 288(24), pp.17620–30.

Vicente Miranda, H. & Outeiro, T.F., 2010. The sour side of neurodegenerative disorders: the effects of protein glycation. *The Journal of pathology*, 221(1), pp.13–25.

Vidal, M. et al., 1990. Tissue-specific control elements of the Thy-1 gene. *The EMBO journal*, 9(3), pp.833–40.

De Visser, L. et al., 2006. Novel approach to the behavioural characterization of inbred mice:

automated home cage observations. *Genes, brain, and behavior*, 5(6), pp.458–66.

Vogel, J.R., Beer, B. & Clody, D.E., 1971. A simple and reliable conflict procedure for testing anti-anxiety agents. *Psychopharmacologia*, 21(1), pp.1–7.

Vogiatzi, T. et al., 2008. Wild type alpha-synuclein is degraded by chaperone-mediated autophagy and macroautophagy in neuronal cells. *The Journal of biological chemistry*, 283(35), pp.23542–56.

Volles, M.J. & Lansbury, P.T., 2002. Vesicle permeabilization by protofibrillar alpha-synuclein is sensitive to Parkinson's disease-linked mutations and occurs by a pore-like mechanism. *Biochemistry*, 41(14), pp.4595–602.

De Vries, R.L. a & Przedborski, S., 2013. Mitophagy and Parkinson's disease: be eaten to stay healthy. *Molecular and cellular neurosciences*, 55, pp.37–43.

Wagner, J. et al., 2013. Anle138b: a novel oligomer modulator for disease-modifying therapy of neurodegenerative diseases such as prion and Parkinson's disease. *Acta neuropathologica*, 125(6), pp.795–813.

Wakabayashi, K. et al., 1997. NACP, a presynaptic protein, immunoreactivity in Lewy bodies in Parkinson's disease. *Neuroscience letters*, 239(1), pp.45–8.

Wakabayashi, K. et al., 2000. Synphilin-1 is present in Lewy bodies in Parkinson's disease. *Annals of neurology*, 47(4), pp.521–3.

Wakabayashi, K. et al., 2007. The Lewy body in Parkinson's disease: molecules implicated in the formation and degradation of alpha-synuclein aggregates. *Neuropathology : official journal of the Japanese Society of Neuropathology*, 27(5), pp.494–506.

Wakamatsu, M. et al., 2007. Accumulation of phosphorylated alpha-synuclein in dopaminergic neurons of transgenic mice that express human alpha-synuclein. *Journal of neuroscience research*, 85(8), pp.1819–25.

Wakamatsu, M. et al., 2008. Selective loss of nigral dopamine neurons induced by overexpression of truncated human alpha-synuclein in mice. *Neurobiology of aging*, 29(4), pp.574–85.

Walker, R.A., 2006. Quantification of immunohistochemistry--issues concerning methods, utility and semiquantitative assessment I. *Histopathology*, 49(4), pp.406–10.

Walsh, R.N. & Cummins, R.A., 1976. The Open-Field Test: a critical review. *Psychological bulletin*, 83(3), pp.482–504.

Wang, Y., Luo, W. & Reiser, G., 2008. Trypsin and trypsin-like proteases in the brain: proteolysis and cellular functions. *Cellular and molecular life sciences : CMLS*, 65(2), pp.237–52.

Ward, C.D., Hess, W.A. & Calne, D.B., 1983. Olfactory impairment in Parkinson's disease. *Neurology*, 33(7), pp.943–6.

Watanabe, Y. et al., 2012. p62/SQSTM1-dependent autophagy of Lewy body-like α-synuclein inclusions. *PloS one*, 7(12), p.e52868.

| Bibliography

Waterston, R.H. et al., 2002. Initial sequencing and comparative analysis of the mouse genome. *Nature*, 420(6915), pp.520–62.

Waxman, E.A. & Giasson, B.I., 2011. Characterization of kinases involved in the phosphorylation of aggregated α-synuclein. *Journal of neuroscience research*, 89(2), pp.231–47.

Waxman, E.A. & Giasson, B.I., 2008. Specificity and regulation of casein kinase-mediated phosphorylation of alpha-synuclein. *Journal of neuropathology and experimental neurology*, 67(5), pp.402–16.

Webb, J.L. et al., 2003. Alpha-Synuclein is degraded by both autophagy and the proteasome. *The Journal of biological chemistry*, 278(27), pp.25009–13.

Weinreb, P.H. et al., 1996. NACP, a protein implicated in Alzheimer's disease and learning, is natively unfolded. *Biochemistry*, 35(43), pp.13709–15.

Weiss, A. et al., 2008. Sensitive biochemical aggregate detection reveals aggregation onset before symptom development in cellular and murine models of Huntington's disease. *Journal of neurochemistry*, 104(3), pp.846–58.

Weitzman, P.D. & Kinghorn, H.A., 1978. Occurrence of "large" or "small" forms of succinate thiokinase in diverse organisms. *FEBS letters*, 88(2), pp.255–8.

Welsh, M., 2004. Parkinson's disease and quality of life: issues and challenges beyond motor symptoms. *Neurologic clinics*, 22(3 Suppl), pp.S141–8.

Whitby, F.G. et al., 2000. Structural basis for the activation of 20S proteasomes by 11S regulators. *Nature*, 408(6808), pp.115–20.

WHITTEN, M.K., 1957. Effect of exteroceptive factors on the oestrous cycle of mice. *Nature*, 180(4599), p.1436.

Whone, A.L. et al., 2003. Plasticity of the nigropallidal pathway in Parkinson's disease. *Annals of neurology*, 53(2), pp.206–13.

Winklhofer, K.F. & Haass, C., 2010. Mitochondrial dysfunction in Parkinson's disease. *Biochimica et biophysica acta*, 1802(1), pp.29–44.

Winner, B. et al., 2004. Human wild-type alpha-synuclein impairs neurogenesis. *Journal of neuropathology and experimental neurology*, 63(11), pp.1155–66.

Winner, B. et al., 2008. Mutant alpha-synuclein exacerbates age-related decrease of neurogenesis. *Neurobiology of aging*, 29(6), pp.913–25.

Winslow, A.R. et al., 2010. α-Synuclein impairs macroautophagy: implications for Parkinson's disease. *The Journal of cell biology*, 190(6), pp.1023–37.

Winslow, A.R. & Rubinsztein, D.C., 2011. The Parkinson disease protein α-synuclein inhibits autophagy. *Autophagy*, 7(4), pp.429–31.

Wirdefeldt, K. et al., 2011. Epidemiology and etiology of Parkinson's disease: a review of the evidence. *European journal of epidemiology*, 26 Suppl 1, pp.S1–58.

Witt, S.N., 2010. Hsp70 molecular chaperones and Parkinson's disease. *Biopolymers*, 93(3), pp.218–28.

Wolff, S., Weissman, J.S. & Dillin, A., 2014. Differential scales of protein quality control. *Cell*, 157(1), pp.52–64.

Wong, E. et al., 2012. Molecular determinants of selective clearance of protein inclusions by autophagy. *Nature communications*, 3, p.1240.

Wong, E.S.P. et al., 2008. Autophagy-mediated clearance of aggresomes is not a universal phenomenon. *Human molecular genetics*, 17(16), pp.2570–82.

Woods, W.S. et al., 2007. Conformation-specific binding of alpha-synuclein to novel protein partners detected by phage display and NMR spectroscopy. *The Journal of biological chemistry*, 282(47), pp.34555–67.

Wu, K.-P. et al., 2009. Structural reorganization of alpha-synuclein at low pH observed by NMR and REMD simulations. *Journal of molecular biology*, 391(4), pp.784–96.

Xie, Y.-Y. et al., 2010. Interaction with synphilin-1 promotes inclusion formation of alpha-synuclein: mechanistic insights and pathological implication. *FASEB journal : official publication of the Federation of American Societies for Experimental Biology*, 24(1), pp.196–205.

Xilouri, M., Brekk, O.R. & Stefanis, L., 2013. Alpha-synuclein and protein degradation systems: a reciprocal relationship. *Molecular neurobiology*, 47(2), pp.537–51.

Xu, J. et al., 2002. Dopamine-dependent neurotoxicity of alpha-synuclein: a mechanism for selective neurodegeneration in Parkinson disease. *Nature medicine*, 8(6), pp.600–6.

Yamin, G., Uversky, V.N. & Fink, A.L., 2003. Nitration inhibits fibrillation of human alpha-synuclein in vitro by formation of soluble oligomers. *FEBS letters*, 542(1-3), pp.147–52.

Yang, M.-L. et al., 2010. Dynamic transport and localization of alpha-synuclein in primary hippocampal neurons. *Molecular neurodegeneration*, 5(1), p.9.

Yang, Y. et al., 2003. Parkin suppresses dopaminergic neuron-selective neurotoxicity induced by Pael-R in Drosophila. *Neuron*, 37(6), pp.911–24.

Yasuda, T. et al., 2013. Neurodegenerative changes initiated by presynaptic dysfunction. *Translational neurodegeneration*, 2(1), p.16.

Yavich, L. et al., 2004. Role of alpha-synuclein in presynaptic dopamine recruitment. *The Journal of neuroscience : the official journal of the Society for Neuroscience*, 24(49), pp.11165–70.

Yen, J.C., Chang, F.J. & Chang, S., 1995. A new criterion for automatic multilevel thresholding. *IEEE transactions on image processing : a publication of the IEEE Signal Processing Society*, 4(3), pp.370–8.

Yong, V.W., 2005. Metalloproteinases: mediators of pathology and regeneration in the CNS. *Nature reviews. Neuroscience*, 6(12), pp.931–44.

| Bibliography

Yoshiki, A. & Moriwaki, K., 2006. Mouse phenome research: implications of genetic background. *ILAR journal / National Research Council, Institute of Laboratory Animal Resources*, 47(2), pp.94–102.

Yoshimoto, M. et al., 1995. NACP, the precursor protein of the non-amyloid beta/A4 protein (A beta) component of Alzheimer disease amyloid, binds A beta and stimulates A beta aggregation. *Proceedings of the National Academy of Sciences of the United States of America*, 92(20), pp.9141–5.

Youle, R.J. & Narendra, D.P., 2011. Mechanisms of mitophagy. *Nature reviews. Molecular cell biology*, 12(1), pp.9–14.

Zaarur, N. et al., 2008. Triggering aggresome formation. Dissecting aggresome-targeting and aggregation signals in synphilin 1. *The Journal of biological chemistry*, 283(41), pp.27575–84.

Zarranz, J.J. et al., 2004. The new mutation, E46K, of alpha-synuclein causes Parkinson and Lewy body dementia. *Annals of neurology*, 55(2), pp.164–73.

Zheng, G.-Q., 2009. Therapeutic history of Parkinson's disease in Chinese medical treatises. *Journal of alternative and complementary medicine (New York, N.Y.)*, 15(11), pp.1223–30.

Zhou, W., Milder, J.B. & Freed, C.R., 2008. Transgenic mice overexpressing tyrosine-to-cysteine mutant human alpha-synuclein: a progressive neurodegenerative model of diffuse Lewy body disease. *The Journal of biological chemistry*, 283(15), pp.9863–70.

Zhou, Y. et al., 2004. Analysis of alpha-synuclein-associated proteins by quantitative proteomics. *The Journal of biological chemistry*, 279(37), pp.39155–64.

Zhu, J.-H. et al., 2003. Localization of phosphorylated ERK/MAP kinases to mitochondria and autophagosomes in Lewy body diseases. *Brain pathology (Zurich, Switzerland)*, 13(4), pp.473–81.

Zhu, M., Li, W. & Lu, C., 2012. Role of alpha-synuclein protein levels in mitochondrial morphology and cell survival in cell lines. *PloS one*, 7(4), p.e36377.

Appendix A: Activity analysis

Animal activity was assessed using the PhenoMaster/LabMaster, a system consisting of infrared light-beam frames surrounding an animal cage. In the system, X represents the cage length, Y the width and Z the height. Infrared beams are monitored by a control unit which converts the electronic signal to a numeric output file recording beam breaks every 10 ms.

1)   Generation of PhenoMaster/LabMaster output files

Metadata (including individual animal number, box, weight, line, gender and age) were entered before the start of the experiment. An example of the input generated by the system is represented in table 5-01. An example of extracted database is given in table 5-02.

Table 5-01: Information file input example

Nicolas_sph1-asyn-dtg_1;Exp021;Genotype;sex;
Box;Animal No.;Weight [g];Text1;Text2;Text3;
1;290;33,9;male;nTg;18m
2;291;34,0;male;nTg;18m
3;294;36,2;male;nTg;18m
4;284;38,7;male;nTg 18m
5;297;35,0;male;nTg;18m
Date; Time; Animal No.; Box; XT+YT; XT; XA; XF; YT; YA; YF; Z; CenT; CenA; CenF; PerT;
PerA; PerF; DistK; DistD; Speed; Drink; Feed;
;;;;[Cnts];[Cnts];[Cnts];[Cnts];[Cnts];[Cnts];[Cnts];[Cnts];[Cnts];[Cnts];[Cnts];[Cnts];
[Cnts];[Cnts];[cm];[cm];[cm/s];[ml];[g];
28-02-14;13:58;290;1;109;62;44;18;47;35;12;4;26;19;7;83;60;23;155;155;3;0.01;0.01;
28-02-14;13:59;290;1;130;70;43;27;60;40;20;5;59;38;21;71;45;26;333;178;3;0.02;0.01;
28-02-14;14:00;290;1;179;100;68;32;79;53;26;3;45;27;18;134;94;40;559;226;4;0.02;0.01;

To perform personalized analysis, some basic parameters are collected in temporary variables (including time binning, experiment length and acclimatization time).

```
# define binning (for graphic plotting), experiment length and acclimatization time
merged.time            <- 30           # define time use for the data binning
length.experiment      <- 70           # define experiment length in hours
begin.time             <- 30           # acclimatization time for the analysis

# define time when the dark phase start (in this example dark phase start at 15 h)
# time should be expressed in minutes (in this example 15 hours x 60 minutes = 900)
begin.dark             <- 900
```

| Appendix A: Activity analysis

```
# definition of variables (in this example two files generated by the system called
# analysis01 and analysis02
phenofiles  <- c(analysis01, analysis02)  # list of files to analyze
info        <- NULL                       # variable recording metadata
info.tmp    <- NULL                       # create a new temporary variable
file        <- NULL                       # create a new temporary variable
cage.exper  <- NULL                       # variable recording cages per experiment

# read each output file metadatas and save them into the variable "info"
for (file in phenofiles) {                # loop over all file to analyze

# metadata incorporated at the beginning of the output file contain less field than
# the database. To record the number of animals per experiment, we used the line
# number when the large database start minus two unnecessary lines (containing the
# file title and the header of the table)
number.cage      <- count.fields(file, sep=";")          # count fields per row

# find the last row with less fields that the maximal and remove the 2 lines
animal.per.run   <- max(which(number.cage<max(number.cage))-2

# read the experiment output file skipping the two first rows which do not contain
# relevant information
info.tmp    <- read.csv2(file, blank.lines.skip=TRUE, header=TRUE,
                    nrows=animal.per.run, skip=2, dec=",", sep=";")

# add to the variable info the new rows
info             <- rbind(info, info.tmp, deparse.level=1)
cage.exper.tmp   <- c(which(phenofiles==file), animal.per.run)
cage.exper       <- rbind(cage.exper, cage.exper.tmp)
}

# change column names
colnames(info) <- c("Box", "Animal.No.", "Weight", "Gender", "Genotype", "Age")

# create a backup file called "genotype.txt" that user can open at the end of the
# calculation to plot data or do more statistic in another software
write.table(info, file="genotype.txt", append=FALSE, quote=FALSE,
                sep=";", dec=".", row.namesFALSE)
```

Table 5-02: Information file output example

Box	Animal No.	Weight	Gender	Genotype	Age
1	290	33.9	male	nTg	18m
2	291	34.0	male	nTg	18m
3	292	36.2	male	nTg	18m
4	293	38.7	male	nTg	18m
5	294	35.0	male	nTg	18m

The PhenoMaster/LabMaster software creates a database for each experiment performed. These databases contain X, Y or Z beams break, distance traveled, speed and amount of food or water consumed. The parameters are saved by default every minute. Furthermore, the system separates fine movements (animal breaking twice the same beam) from ambulation (animal breaking two different beams) and movements in the center (breaks in the most central beam of the X and Y axis) from movements in the periphery of the cage.

An example of a simplified output file (one animal, 5 minutes and for the ambulation movement) is represented in table 5-03.

Table 5-03: PhenoMaster/LabMaster output file example

Date	Time	Animal No.	Box	XA	YA	Z	CenA	PerA	DistD	Speed	Drink	Feed
28-02-2014	13:45	290	1	44	35	4	19	60	155	3	0.01	0.01
28-02-2014	13:46	290	1	43	40	5	38	45	178	3	0.02	0.01
28-02-2014	13:47	290	1	68	53	3	27	94	226	4	0.02	0.01
28-02-2014	13:48	290	1	102	59	4	72	89	276	5	0.02	0.01
28-02-2014	13:49	290	1	51	42	6	23	70	178	3	0.03	0.01

LabMaster/PhenoMaster software converts a list of beam breaks to a number representing the sum of breaks (or the distance) per minute. But the output files generated neither allow an easy comparison between genotypes, nor for selecting specific time periods (such as acclimatization time or last active phase), and they also do not contain genotype of animals.

```
# correction of files by deleting unit raws
m.table.tmp <- NULL                                 # create a temporary variable

for (file in phenofiles) {                          # for each file to analyze
     m.table.2   <- NULL                            # create a new temporary variable

# extract the header of the database which contain animal metadata
     m.table <- read.csv2(file, skip=(cage.exper[which(phenofiles==file), 2]+5))

# rename column
     colnames(m.table) <- colnames(read.csv2(file, skip=
                                  (cage.exper[which(phenofiles==file), 2]+3))

# save mouse age (represents different experiments/time points)
     age <- head(read.csv2(file, skip=2, sep=";"), n=cage.exper[n, 2])

# create the column "Age"
     for (tmp in unique(m.table$Animal.No.)){        # search age of each mouse
          age.t <- age[age$Animal.No.==tmp, "Text3"]        # read animal age
          col.l <- length(m.table[m.table$Animal.No.==tmp, ])   # number of row
          m.table[m.table$Animal.No.==tmp, "Age"]<- rep(age.tmp, rep=length.col)
          }
```

| Appendix A: Activity analysis

```r
# create a backup file for each output
write.table(m.table.2, file=paste("LabMaster", which(phenofiles==file), ".csv",
sep=""), append=FALSE, quote=FALSE, sep=";", dec=".", row.names=FALSE)
          }
```

Modified output files are extracted and merged into a single large database and results are binned to allow the user to plot the evolution through the time easily.

```r
# define files to analyze
phenofiles <- list.files(path=getwd(), pattern=".csv", all.files=TRUE,
                         full.names=FALSE, recursive=FALSE, ignore.case=FALSE)


# import tables and read data
res        <- NULL                       # large merged database
res.tmp    <- NULL                       # temporary variable
res.g      <- NULL                       # merged and binned database
res.g.tmp  <- NULL                       # temporary variable
file       <- NULL                       # output files modified
for (file in phenofiles) {

# read modified outputs and pick most interesting columns
      res.tmp <- data.frame(read.csv2(file, header=TRUE, dec="."))
      res.tmp <- res.tmp[, c("Age", "Date", "Time", "Animal.No.", "Box", "XT",
                        "XA", "XF", "YT", "YA", "YF", "DistD", "Z", "CenT",
                        "CenA", "CenF", "PerT", "PerA", "PerF", "Drink",
                        "Feed")]

# change date by a list of number (allow to compare experimental days)
      date             <- unique(res.tmp$Date)
      res.tmp$Date     <- match(res.tmp$Date, date)

# aggregate values by mean, if text increment it
      res.g.tmp   <- aggregate(res.tmp,
                        by=list((0:(nrow(res.tmp)-1))%/% merged.time),
                        function(x) ifelse(is.numeric(x), mean(x), x[1]))

# correct time which cannot be binned
      res.g.tmp$Time <- res.tmp[head((c(1:nrow(res.tmp))* merged.time),
                        n=nrow(res.g.tmp)), "Time"]

# correct date by displaying an integrate number (no fractionated date)
      res.g.tmp$Date <- as.integer(res.g.tmp$Date)

# bind tables together
      res   <- rbind(res, res.tmp, deparse.level=0)
      res.g <- rbind(res.g, res.g.tmp, deparse.level=0)
      }

# modify line of animal (which cannot be aggregated)
merg*i.e.*line                 <- merge(res.g, info, all.x=TRUE, sort=FALSE)
res.g$Line                     <- merg*i.e.*line$Genotype
```

```
# create backup files
write.table(res, file=paste("res-before-exclusion.txt", sep=""), append=FALSE,
                          quote=FALSE, sep=";", dec=".", row.names=FALSE)
write.table(res.g, file=paste("resg-before-exclusion.txt", sep=""), append=FALSE,
                          quote=FALSE, sep=";", dec=".", row.names=FALSE)
```

2) Calculation of new parameters and separation of day phases

The activity of an animal was analyzed using the sum of X and Y activity, providing less variability than the analysis of X and Y activity separately. Similarly, activity in the center of the cage was analyzed using the ratio of the activity in the center and the total activity. The following code will be applied to the database providing results per minute only, but can also be applied to the binned database. An output example is provided in table 5-04.

To facilitate the analysis, the complete database is divided in several phases (such as first dark phase, first light phase, first day...) and exported in separated files (example in table 5-04).

```
# variables analyzed
variable.to.analyze <- c("Age", "Date", "Time", "Animal.No.", "Line", "XA.YA",
                         "DistD", "Z", "AnxA", "CenA", "Drink", "Feed")

# calculation of new variables
res$XA.YA   <- res$XA       +     res$YA       # sum of the X and Y axis
res$ActT    <- res$CenT     +     res$PerT
res$AnxT    <- res$CenT     /     res$ActT     # ratio center by total activity
res$XF.YF   <- res$XF       +     res$YF       # sum of the X and Y axis
res$ActA    <- res$CenA     +     res$PerA
res$AnxA    <- res$CenA     /     res$ActA     # ratio center by total activity
res$XT.YT   <- res$XT       +     res$YT       # sum of the X and Y axis

# keep only interesting rows (decrease database size and algorithm speed)
res.tmp <- NULL

for (n in variable.to.analyze){
     res.tmp <- cbind(res.tmp, as.numeric(res[, colnames(res)==n]))
     }
```

Table 5-04: Database output example

Age	Date	Time	Animal. No	Line	XA.YA	DistD	Z	AnxA	CenA	Drink	Feed
06m	1	825	290	nTg	79	155	4	0.24	19	0.01	0.01
06m	1	826	290	nTg	83	178	5	0.46	38	0.02	0.01
06m	1	827	290	nTg	121	226	3	0.22	27	0.02	0.01
06m	1	828	290	nTg	161	276	4	0.45	72	0.02	0.01
06m	1	829	290	nTg	93	178	6	0.25	23	0.03	0.01

| Appendix A: Activity analysis

```r
# store date, time, animals and line in an extra variable to run selection loops
date  <-    sort(res[duplicated(res$Date)==F, ]$Date)
time  <-    sort(res[duplicated(res$Time)==F, ]$Time)
line  <-    sort(res[duplicated(res$Line)==F, ]$Line)

# creation of a table containing only the adaptation time
res.b       <- NULL                          # temporary variable
animal.tmp  <- NULL                          # temporary variable

# loop over ages and animal numbers
for (age.tmp in unique(res$Age)){
    res.tmp <- res[res$Age==age.tmp, ]
for (animal.tmp in unique(res.tmp$Animal.No.)){
    res.b.tmp   <- res.tmp[res.tmp$Animal.No.==animal.tmp, ]

# select only the number of rows according to the acclimatization time
    res.b.tmp   <- res.b.tmp[1:begin.time, ]
    res.b       <- rbind(res.b, res.b.tmp, deparse.level=0)
    }}

# save light phases data over the experiment, for complete or binned dataset
light <- NULL                                  # temporary variable

for (age.tmp in unique(res$Age)){
    res.tmp     <- res[res$Age==age.tmp, ]

# Select light phase: light phase > begin.dark+12h and light phase < begin.dark
    light.tmp   <- res.tmp[(strptime(res.tmp$Time, format="%R") >
                            (strptime(begin.dark, format="%R")-(12*3600)-60)) &
                            (strptime(res.tmp$Time, format="%R")) <
                            (strptime(begin.dark, format="%R"))), ]
    light       <- rbind(light, light.tmp)
    }

# Select dark phases: light phase < begin.dark+12h or light phase > begin.dark
dark  <- NULL                                  # temporary variable

for (age.tmp in unique(res$Age)){
    res.tmp     <- res[res$Age==age.tmp, ]
    dark.tmp    <- res.tmp[(strptime(res.tmp$Time, format="%R") <
                            (strptime(begin.dark, format="%R")-(12*3600)) |
                            (strptime(res.tmp$Time, format="%R") >
                            (strptime(begin.dark, format="%R")-60))), ]
    dark        <- rbind(dark, dark.tmp)
}

# saving tables
write.table(    res, file="allexperiment_table.txt", append=FALSE, quote=FALSE,
                sep=";", dec=".", row.names=FALSE)


write.table(    res.b, file="begginexperiment_table.txt", append=FALSE,
                quote=FALSE, sep=";", dec=".", row.names=FALSE)
```

Table 5-05: Result table example

Animal. No	variable	value	Line	Age
290	XA.YA	138.1	nTg	18m
290	DistD	239.8	nTg	18m
290	Z	8.2	nTg	18m
290	AnxA	0.374	nTg	18m
290	CenA	54.2	nTg	18m
290	Drink	0.05	nTg	18m
290	Feed	0.01	nTg	18m

3) Statistical analysis and generation of graphics

A function was created to plot data, to perform one-way ANOVA and to show possible outliers within the same figure, allowing a fast investigation of the main activity readout.

```
MyBarplot        <- function(mean) {                        # start a function
    y1           <- mean$value                              # select a variable
    x1           <- mean$group                              # select a group
    z1           <- mean$animal                             # select an animal
    mean1        <- tapply(y1, x1, mean, na.rm=TRUE)        # calculate the mean

# function to define the standard error on the mean
    sem          <- tapply(y1, x1, function(x) sd(x, na.rm=TRUE)/sqrt(length(x)))

# highlight outliers based on 95% confidence interval using
# first (or last) interquartile + (or -) 1.5*interquartile range (McGill 1978)
    out          <- boxplot.stats(y1)$out             # outliers calculation
    gen.out      <- mean[names(out), "group"]         # allow to insertion in graph

# draw barplot with standard error of the mean, and add one way ANOVA in the title
# and one-way ANOVA with post hoc Tukey correction in top of each column
    barx  <- barplot(mean1, ylim=c(0, max(y1, na.rm=TRUE)*1.2), main=variable,
                     sub=paste("p=", format(anova(lm(y1~x1))[1, 5], digit=2)))
    segments(barx, mean1-sem, barx, mean1+sem)
    segments(barx-0.1, mean1+sem, barx+0.1, mean1+sem)
    segments(barx-0.1, mean1-sem, barx+0.1, mean1-sem)
    pval <- TukeyHSD(aov(y1~x1))$x1[, 4]

    text(y=0.92*max(y1, na.rm=TRUE)*1.2, x=c(0.1:((length(pval))))/1.3,
         labels=paste("p=", format(pval, digits=2)), cex=0.7, pos=4)

    text(y=0.98*max(y1, na.rm=TRUE)*1.2, x=c(0.1:((length(pval))))/1.3,
         labels=(format(names(pval))), cex=0.7, pos=4)

if (length(out)>0) text(y=out, x=gen.out, labels=paste("x", names(out)))
}
```

| Appendix A: Activity analysis

To investigate if animal genotype has an influence on a variable for a specific time period, the mean per genotype over the complete time period was displayed using a barplot.

```
# define a list containing the tables to analyze
stat.tables <-    "allexperiment_table.txt"

# open a new pdf file
graphics.off()
pdf("04_boxplot-one-variable2.pdf", onefile=TRUE)

# open tables
for (file.tmp in stat.tables) {
      res.animal <- read.csv2(file.tmp, header=TRUE, dec= ".")
# for each variable run the graphic
          for (variable.tmp in unique(res.animal$variable)){
      for (age.tmp in unique(res$Age)){
          table.tmp         <- res.animal[res.animal$Age==age.tmp, ]
          table.tmp         <- table.tmp[table.tmp$variable==variable.tmp, ]

# remove NA (Not Applicable)which appear when dividing by 0
          mean              <- na.exclude(table.tmp)
          colnames(mean)    <- c("animal", "variable", "value", "group", "age")
          variable          <- variable.tmp
          myBarplot(mean)
}}}

# close the pdf
dev.off()
graphics.off()
```


Feed_18m_testing-over-all.txt
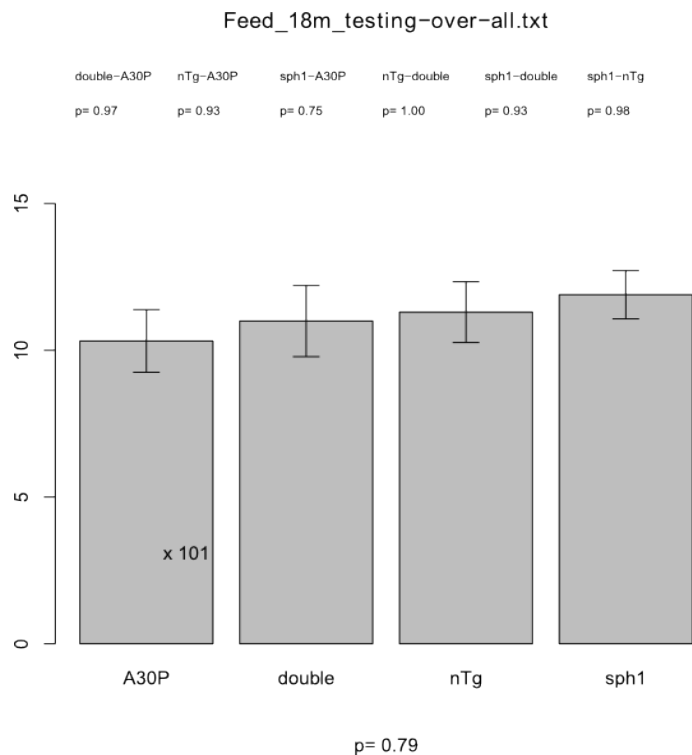
Figure 5-01: Plot example

The barplot shows the mean and the standard error of each group. A cross indicates potential outliers and is followed by the respective animal name. The barplot title contains the name of the parameter investigated, the time point when the experiment was performed and the time phase considered. Subtitle contains results of one-way ANOVA for the complete dataset to facilitate data exploration. Below the title, the results of one-way ANOVA using post hoc Tukey comparison for all animal groups are indicated.

Appendix B: Image analysis

Immunohistochemistry staining, classically evaluated qualitatively, needs to be quantified to determine the relevance of potential changes observed (Taylor & Levenson 2006). The extraction of information via image analysis represents a critical step in the quantification and interpretation of stainings (Walker 2006). This is illustrated by the estimation of positive cells analyzed by manual counting, which on top of being time consuming and laborious, is also biased by inter-observer variations (Prasad et al. 2011; Orlowski & Bjarkam 2012). In this context, image analysis using an algorithm, presents not only a method with higher reproducibility giving a faster readout, but also provides the opportunity to quantify areas or intensities of stainings. The following macros were designed using ImageJ, an open source software based on Java, allowing image processing (noise reduction, signal transformation), signal detection (refine detection, selection of a particular signal) and the use of multiple analysis tools (measure area, particle analysis).

1) Image capture

The first macro aims at making the counting of activated astrocytes easier, faster and more reproducible (staining protocol described in the Materials and Methods section 1.13 and 1.14). Pictures to analyze were taken using a 3× 12-bit channel color Zeiss Axio-cam MRc camera mounted on an AxioPlan 2 microscope with a picture size of 1388×1040 pixels and captured using AxioVision. A 20× objective was used to provide a good definition of single astrocytes, resulting in an image of approximately 688×515 µm.

The second macro aims to fully automatize counting of cells positive for proteinase K resistant alpha-synuclein staining (staining protocol described in Materials and Methods section 1.16). A 4× objective was used to provide a large investigation field and resulting in an image representing approximately 3500×2630 µm.

2) Astrocytes counting

To help performing manual counting, ImageJ was used to highlight staining patterns (procedure illustrated in Fig. 5-02). First, original uncompressed TIFF files were exported using AxioVision and opened in ImageJ (Fig. 5-02A). Then, a color threshold using complex restrictive threshold (based on multilevel thresholding scheme via class entropy (Yen et al. 1995) was applied. Threshold output is shown in Fig. 5-02B and final output of the macro is shown in Fig. 5-02C. Finally, cell counter function of ImageJ was used to estimate the number of cells containing more than three stained branches.

```
// need to open pictures to analyze in ImageJ prior running the macro
// opening two copies with a specified name (trial1.TIF and trial2.TIF)
run("Duplicate...", "title=trial1.TIF");
run("Duplicate...", "title=trial2.TIF");
```

| Appendix B: Image analysis

```
// trial2.TIF converted in 16-bit then a threshold is applied to delimit staining
run("16-bit");
setAutoThreshold("Yen");
run("Convert to Mask");

// trial1.TIF and trial2.TIF added to facilitate counting
imageCalculator("AND create", "trial1.TIF","trial2.TIF");
selectWindow("Result of trial1.TIF");
```


A   **B**   **C**
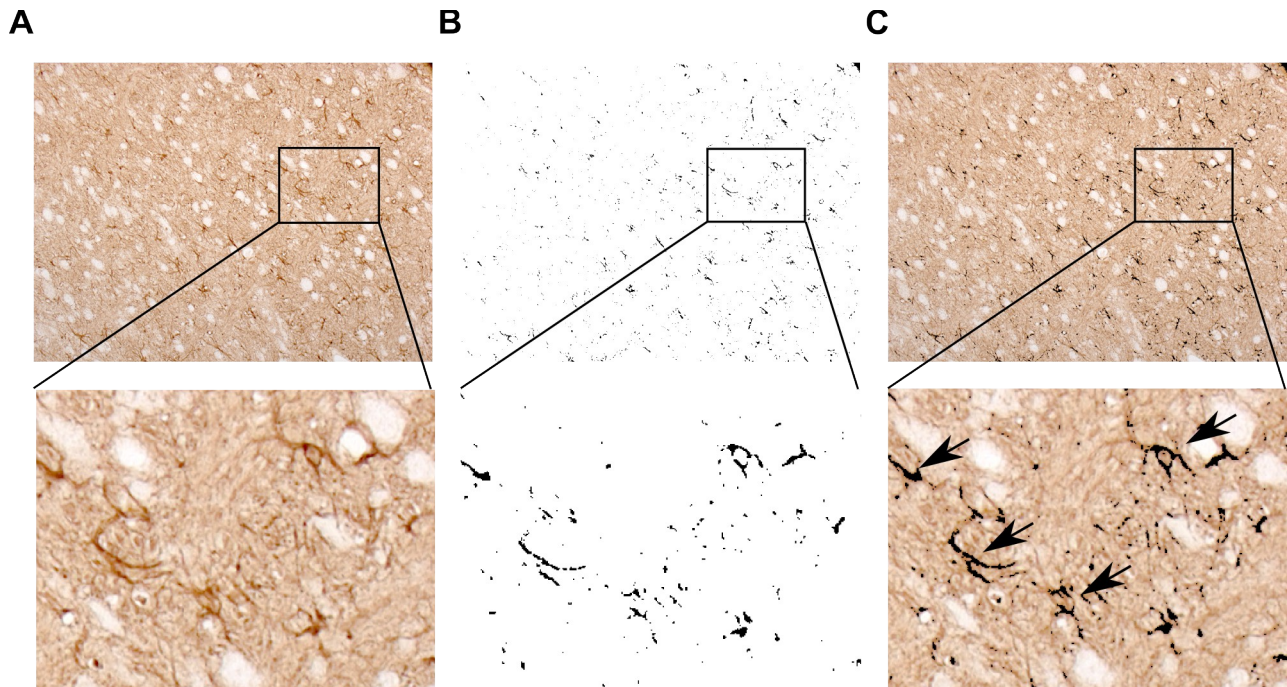
Figure 5-02: Astrocytes counting example

A) Representative example of astrocytes staining using GFAP antibody. B) Threshold output used to highlight the most significant staining (in black). Output will be used to define more clearly and in a more reproductive manner single positive events. C) Macro output highlighting most relevant staining. Output files simplify the determination of positive cells, improving the reproducibility of immunopositive event counting. Output files also allow for the measurement of staining area and staining intensity.

In this example, the major methodological weakness is the reproducibility of the manual determination of astrocytes. A more reproducible procedure based on the amount and area stained per slide is proposed in the following macro. To automatize this analysis, a repertory containing pictures to investigate is defined, pictures are then converted in gray scales and mean of gray scale is measured. Background is reduced using a restrictive threshold (Yen method) and the area stained is measured for each image.

```
// macro to quantify staining intensity and area stained
// save the working directory, select pictures and variable to measure
requires("1.38o");
    dir = getDirectory("Choose directory");
    list = getFileList(dir);
    setBatchMode(true);
    run("Set Measurements...", "area area_fraction mean standard min max limit
```

```
display redirect=None");
      run("Clear Results")

for (i=0; i<list.length; i++) {           // open picture per picture
      showProgress(i, list.length);
      open(dir+list[i]);

// ImageJ consider signal as white, therefore pictures need to be inverted
      rename("all_"+list[i]);
      run("16-bit");
      run("Invert");

// staining intensity determined by mean of scale of gray within the picture
      run("Measure");

// staining area represented by the variable area
      rename("threshold_"+list[i]);
      setAutoThreshold("Yen dark");
      run("Measure");
      close();
}

selectWindow("Results");
saveAs("Results", dir+"summary.txt");
```

3) *Proteinase K resistant alpha-synuclein automatized*

In the previous example, the estimation of astrocyte number via an algorithm is a complex task, because of the specific shape of astrocytes. However, other events (such as estimation of total cell number, aggregate number or positive cell body number) are easier to detect and therefore to automatize. In this example, we will use a macro for counting the number of cells positive for proteinase K resistant alpha-synuclein staining. Similar to the previous example, a macro will be applied on all pictures present in a specified repertory. The macro first imports pictures (Fig. 5-03A), converts them into gray scale and measures the mean of the staining intensity. Then, a restrictive threshold is applied on the pictures (output shown in Fig. 5-03B) to measure the stained area and to perform particle analysis using particle shape and size to estimate the number of stained cells.

To determine the relevant size of particles, a representative picture was opened and the size of the smallest and largest event was measured in pixels using area measurement (represented as circles in Fig. 5-03B).

```
// macro to quantify staining intensity and to quantify area stained
// save working directory, select pictures and variable to measure
requires("1.38o");
      dir = getDirectory("Choose directory");
      list = getFileList(dir);
      setBatchMode(true);
      run("Set Measurements...", "area area_fraction mean standard min max limit
display redirect=None");
      run("Clear Results")
for (i=0; i<list.length; i++) {                  // open picture per picture
```

| Appendix B: Image analysis

```
        showProgress(i, list.length);
        open(dir+list[i]);
        rename("all-"+list[i]);
        run("16-bit");
        run("Invert");
        run("Measure");
        rename("threshold-"+list[i]);
        setAutoThreshold("Yen dark");
        run("Convert to Mask");
        run("Measure");
        run("Fill Holes");        // filling holes (make particle detection sensitive)

// generation of particles
        run("Analyze Particles...", "size=250-5000 circularity=0.20-1.00 summarize");
        close();
}

// save staining mean ans particle analysis in two different text files
selectWindow("Summary");
saveAs("Text", dir+"summary.txt");                // mean staining intensity
selectWindow("Results");
saveAs("Results", dir+"results.txt");             // particle analysis
```
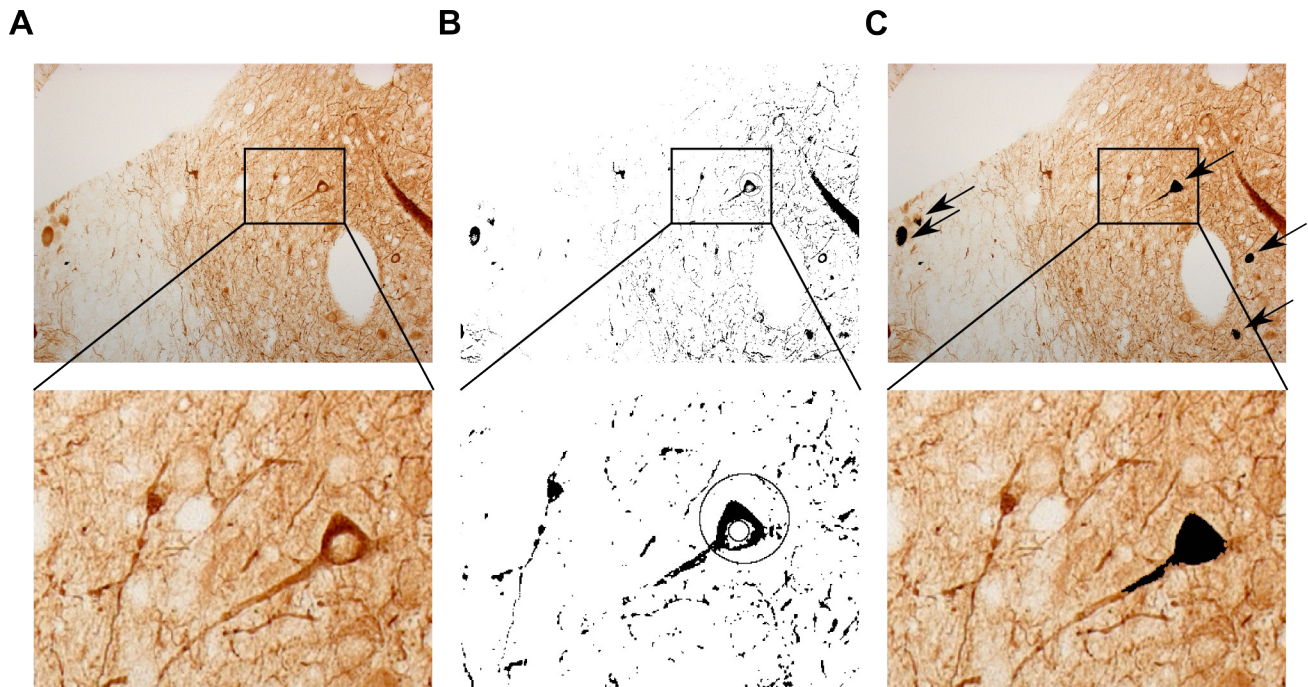

Figure 5-03: Proteinase K resistant alpha-synuclein example

A) Representative example of cells presenting proteinase K resistant a-syn staining. B) Output of restrictive thresholding (in black). The small and the large circles represent 250 and 5000 square pixels respectively. C) Validation of the particle counting, particles were counted (represented in black) and further characterized by the macro (area, number).

Acknowledgments

| Acknowledgments